

Damage Progression Effect in Subsea Pipelines Under Trawl Gear Impact

by

© Farhad Davaripour, B.Sc., M.Sc.

A thesis submitted to the School of Graduate Studies
in partial fulfillment of the requirements for the degree of

Doctor of Philosophy

Faculty of Engineering and Applied Science

Memorial University of Newfoundland

October 2020

St. John's

Newfoundland and Labrador

Canada

Abstract

The structural behaviour of pipelines is considerably dependent on the loading condition. The common industry practice for the assessment of a pipeline against an accidental event is to design the pipe against an interference load applied laterally and in the perpendicular direction. As such, the potential plastic damage is imposed at only one location and normal to the pipeline. However, there are accidental scenarios where the resulting damage could progress along the pipe. In this regard, recent studies showed a potential significant drop in the structural resistance of a plate when the interaction between the plate and the indenter translates the resulting plastic damage along the structure. As such, it is reasonable to investigate the potential similar considerable effect of damage progression for pipelines. Accordingly, a series of physical tests using a novel test apparatus was employed in the present thesis to identify, introduce, and investigate the damage progression effect in pipes. The investigation was conducted with the focus on the interference between the bottom trawl gear and subsea pipelines. The test results showed that the structural resistance of a pipe could drop significantly, where the plastic damage imposed on a pipe is translated and induced longitudinally along the pipe. Furthermore, using numerical simulations, the importance of the damage progression effect on the mechanical behaviour of subsea pipelines subject to diagonal trawl impact or subsequent trawl impact was demonstrated. In conclusion, the present thesis introduced and investigated a new mechanical behaviour in subsea pipelines, which should be considered in the assessment of failure limit states in pipes, against the bottom

trawl impact or any accidental events where the progression of plastic damage along the pipe is likely.

To my beloved family:

Elahe Nezhadhossein, Mohammad Hossein Davaripour, Maryam Khalili

Sajad Davaripour, Parya Davaripour

Acknowledgments

I would like to express my sincere gratitude and deepest appreciation to my parents and my lovely wife for their support to accomplish this work.

Dr. Bruce, Quinton – my graduate supervisor. I am extremely grateful to you for your mentorship and outstanding support throughout my program. I would like to extend my deep thankfulness to you for being a great supervisor. I appreciate your kindness, respect, and morals.

Dr. Kenton Pike – my graduate co-supervisor. I would like to express my respect and gratitude to you for your valuable support during my Ph.D. program and internship at TechnipFMC. Your expertise and kindness helped me gain the most from the industry and apply this knowledge in my Ph.D. work.

Dr. Stephen Bruneau – my committee member. I would like to express my gratitude to you for valuable discussions and recommendations. Your outstanding kindness and morals are greatly appreciated.

Mr. Sthéfano Lande Andrade and Dr. Ahmed Elruby – my research colleagues. I am grateful for your assistance in the preparation of the physical tests. Your help and comments are greatly appreciated.

Examination committee members – I do appreciate your time and effort for reviewing this thesis.

Engineering Graduate Studies Office Staff – Thank you for your continuous help and patience.

Technical Services – Billy Bidgood, David Snook, Brad Shore, John Joseph Stamp, and everyone else who worked on fabricating test apparatus. Your talent and expertise facilitated my work and made this thesis possible.

Technical Staff – Matthew Curtis, Craig Mitchell, Trevor S Clark. Thank you for your expertise, patience, and willingness to help.

I would also like to express my gratitude for the financial support provided by the Natural Sciences and Engineering Research Council (NSERC) Discovery Grant program, as well as the Mitacs Accelerate Program.

Table of Contents

Abstract	ii
Acknowledgments.....	v
Table of Contents	vii
List of Tables	xii
List of Figures	xiv
List of Terms.....	xxvii
List of Nomenclature and Acronyms	xxxi
1 CHAPTER 1.....	1
1.1 Introduction	2
1.1.1 Background and Research Motivation.....	5
1.1.2 Research Objectives and Significance	17
1.1.3 Notes on the Research Scope.....	22
1.1.4 Thesis Outline	24
1.2 Co-Authorship Statement.....	26
1.2.1 Chapter 2 – Article No. 01 (International Pipeline Conference 2018)	26
1.2.2 Chapter 3 – Article No. 02 (Applied Ocean Research 2020)	27
1.2.3 Chapter 4 – Article No. 03 (Offshore Pipeline Conference 2020)	28
1.2.4 Chapter 5 – Article No. 04 (Applied Ocean Research 2020)	29
1.2.5 Chapter 6 – Article No. 05 (Ocean Engineering Journal 2020).....	30
1.2.6 Chapter 7 – Article No. 06 (Journal of Applied Mechanics 2020).....	32
2 CHAPTER 2.....	34
2.1 Introduction	37
2.2 Moving (Sliding) Load Versus Perpendicular Load	40
2.2.1 Response of a Cylinder Under a Perpendicular and Moving Load	42
2.3 Methodology	45
2.3.1 Time Integration Scheme for the Finite Element Analysis.....	45
2.3.2 Loading Condition	45

2.3.3	Rupture-Type Versus Non-Rupture Type Moving Loads	46
2.4	Numerical Simulation	47
2.4.1	Benchmarking	50
2.4.2	Mesh Convergence Analysis.....	51
2.5	Results and Discussion.....	53
2.5.1	Damage Progression Effect.....	53
2.5.2	Effective Stress Distribution	54
2.5.3	Sensitivity Study	55
2.6	Conclusions	58
3	CHAPTER 3.....	63
3.1	Introduction	66
3.1.1	Literature Review.....	66
3.1.2	Objectives	70
3.2	Methodology	72
3.2.1	Analytical Method	72
3.2.2	Numerical Simulation	73
3.2.3	Boundary Condition Effect	80
3.2.4	Input Parameters	80
3.3	Benchmarking	83
3.3.1	BSM Model.....	83
3.3.2	Hybrid Model.....	84
3.4	Mesh Convergence Analysis.....	97
3.4.1	BSM Model.....	97
3.4.2	Hybrid Model.....	98
3.5	Results and Discussion.....	100
3.5.1	Sensitivity Analyses.....	103
3.6	Summary and Conclusions.....	109
4	CHAPTER 4.....	116
4.1	Introduction	119

4.1.1	Literature Review.....	119
4.1.2	Beam and Spring-Mass (BSM) Model	123
4.2	Hybrid Shell-Beam model.....	125
4.2.1	Material Model.....	126
4.2.2	Pipe Soil Interaction.....	127
4.2.3	Trawl board.....	128
4.2.4	Loading Condition	129
4.2.5	Benchmarking	130
4.2.6	Mesh Convergence Analysis.....	132
4.3	Results and Discussion.....	134
4.3.1	Sensitivity Analyses (Pipe Diameter)	135
4.4	Summary and Conclusions.....	137
5	CHAPTER 5.....	140
5.1	Introduction	143
5.1.1	Beam and Spring-Mass (BSM) Model	147
5.1.2	Objectives	149
5.1.3	Notes on the Scope.....	149
5.2	Experimental Investigation	152
5.2.1	Methodology	152
5.2.2	Results.....	160
5.2.3	Experiment Summary and Discussion	162
5.3	Numerical Simulation	164
5.3.1	Methodology	164
5.3.2	Benchmarking	169
5.3.3	Results and Discussion	181
5.4	Conclusions	184
6	CHAPTER 6.....	190
6.1	Introduction	193
6.1.1	Literature Review.....	194

6.1.2	Notes on the Research Scope	199
6.2	Experimental Investigation	201
6.2.1	Methodology	201
6.2.2	Result and Discussion	214
6.3	Numerical Investigations.....	231
6.3.1	Element Type	231
6.3.2	Load Path	232
6.3.3	Boundary Conditions	232
6.3.4	Interaction Properties	235
6.3.5	Mesh Convergence Analysis.....	235
6.3.6	Results.....	236
6.3.7	Repeated Trawl Impacts	238
6.3.8	Overtrawlability Assessment	246
6.4	Conclusions	252
7	CHAPTER 7.....	259
7.1	Introduction	262
7.1.1	Literature Review.....	263
7.1.2	Notes on the Research Scope	268
7.2	Physical Test	270
7.2.1	Methodology	270
7.2.2	Results.....	282
7.2.3	Summary	292
7.3	Finite Element Analysis	294
7.3.1	Element Type	294
7.3.2	Boundary Condition (BC).....	296
7.3.3	Load Path	297
7.3.4	Interaction Properties	298
7.3.5	Mesh Convergence Analysis.....	298
7.3.6	Sensitivity Case.....	299

7.3.7	Results.....	300
7.4	Summary and Conclusions.....	303
8	Summary and Conclusions.....	310
9	Future Work	318
	Reference	321
	Appendix - Static Analysis	328

List of Tables

Table 1-1 Individual Author Contribution (Paper No. 1 - IPC 2018).....	27
Table 1-2 Individual Author Contribution (Paper No. 2 – Applied Ocean Research 2020)	27
Table 1-3 Individual Author Contribution (Paper No. 3 – OPT 2020).....	29
Table 1-4 Individual Author Contribution (Paper No. 4 – Applied Ocean Research 2020)	30
Table 1-5 Individual Author Contribution (Paper No. 5 – Ocean Engineering Journal 2020)	31
Table 1-6 Individual Author Contribution (Paper No. 5 – Journal of Applied Mechanics 2020)	32
Table 2-1 Material Model Inputs for the Cylindrical Shell and the Tube-Shaped Indenter	48
Table 3-1. The Input Parameters for the Pipe, Trawl Board, and Soil	81
Table 3-2 Physical and Mechanical Properties of the Cylindrical Specimen	95
Table 4-1 Physical Properties of the SPS02 Specimen in (Zheng, 2014).....	126
Table 5-1 Physical and Mechanical Properties of the Cylindrical Specimen	156
Table 5-2. The Input Parameters for the Pipe, Trawl Board, and Soil	168
Table 5-3 Physical and Mechanical Properties of the SPS02 Specimen in (Zheng, 2014)	171
Table 6-1 Physical and Mechanical Properties of The Cylindrical Specimen.....	206
Table 6-2 Test Matrix	213

Table 6-3 The Input Parameters for the Pipe, Trawl Board, and Soil	246
Table 7-1 Physical and Mechanical Properties of The Cylindrical Specimen.....	274
Table 7-2 Test Variables and Corresponding Instruments	280

List of Figures

Figure 2-1 Schematic View of a Perpendicular Load Path (a) Versus a Moving Load Path (b).....	40
Figure 2-2 Deformation Modes of a Cylinder Under a Perpendicular Load: Crumpling Mode (a), a Combination of Crumpling and Bending Mode (b), and Structural Collapse Mode (c) (Edited and Redrawn from Thomas et al. (1976))	43
Figure 2-3 Engineering and True Stress-Strain Response for the API N80 Steel at Room Temperature	48
Figure 2-4 Numerical Model Geometries	50
Figure 2-5 Contact Force in the Wake of the Indentation Versus Dent Depth.....	51
Figure 2-6 Resultant Force Versus Resultant Displacement Using Varied Mesh Sizes Including 1.5, 2.0, and 2.5 mm	52
Figure 2-7 Resultant Force Versus Time During Perpendicular and Moving Loading Steps	53
Figure 2-8 Equivalent Stress Contour Plot of a Cylinder at the Region of Indentation, Subject to a Perpendicular Load (a), and a Moving Load (b).....	54
Figure 2-9 Resultant Force Versus Resultant Displacement Under Varied Indentation Levels, including 0.15625, 0.3125, 0.625, 1.25, and 2.5 mm.....	56
Figure 2-10 Damage Progression Effect Versus Normalized Indentation Level	57
Figure 3-1. Schematic View of the BSM Model	74
Figure 3-2 A Schematic View of the Hybrid Shell-Beam Model.....	75
Figure 3-3 Engineering and True Stress-Strain Curve of the Specimen in Zheng (2013).81	

Figure 3-4 Benchmarking the BSM Model: The Impact Force Resisted by the Pipe-Wall Thickness Versus Time	84
Figure 3-5 The region of the Hybrid Model Where the Benchmarking is Carried Out.....	86
Figure 3-6 Boundary Condition of the Physical Tests Employed to Benchmark the Hybrid Model	86
Figure 3-7 Benchmarking the Hybrid Model Against a Quasi-static Test by Zheng (2014): Vertical Load Resisted by the Specimen Versus Vertical Displacement of the Indenter..	88
Figure 3-8 Benchmarking the Hybrid Model Against an Impact Test by Zheng (2014): Vertical Load Resisted by the Specimen Versus Vertical Displacement of the Indenter..	90
Figure 3-9 Numerical Model of the Impact Test Conducted by Zheng (2014)	92
Figure 3-10 A View of the Test Apparatus of the Present Study Physical Test.....	92
Figure 3-11 Main Components of the Test Apparatus in the Present Study Physical Test	93
Figure 3-12 A Schematic View of the Boundary Condition Used in the Present Study Physical test	94
Figure 3-13 Detailed Geometries of the Cylindrical Specimen in the Physical Test of the Present Work.....	95
Figure 3-14 Engineering Stress-Strain Curve of the Cylindrical Specimen in the Physical Test of the Present Work.....	95
Figure 3-15 Benchmarking the Hybrid Model Against the Physical Test of the Present Study: Vertical Load Resisted by the Specimen Against the 35 mm Imposed Perpendicular Indentation	96

Figure 3-16 Mesh Convergence Analyses for the BSM Model: 250, 125, and 62.5 mm Element Size	98
Figure 3-17 Mesh Convergence Analysis for the Hybrid Model: Shell Elements	98
Figure 3-18 Mesh Convergence Analysis for the Hybrid Model: Beam Elements	99
Figure 3-19 Total Impact Load Resisted by the Pipe in the Hybrid Model Versus the Impact Load Resisted by the Pipe Wall in the BSM Model	100
Figure 3-20 The Impact Load Resisted by the Pipe – the Analytical Method Versus the Finite Element Method (Using the Hybrid Model).....	101
Figure 3-21 The Dent Depth Imposed on the Pipe, the Analytical Versus Numerical Method (Hybrid and BSM Models)	102
Figure 3-22 An Example of Using Butterworth Filter Function in Abaqus	104
Figure 3-23 Maximum Total Resulting Dent Depth Obtained from the Hybrid Model Versus the BSM Model for 5, 10, and 14-inch Pipe Sizes	105
Figure 3-24 Sensitivity Analysis Results: Indenter Radius: 30, 25, and 20 mm	106
Figure 3-25 Sensitivity Analysis Results: Soil Friction Coefficient.....	107
Figure 3-26 Sensitivity Analysis Results: Strain Rate Effect	108
Figure 4-1 Schematic View of Case-1: a Pipe under a Non-Perpendicular Impact, and Case-2: a Pipe Subjected to Only the Normal Component of the Non-Perpendicular Trawl Impact	123
Figure 4-2. Schematic View of the BSM Model (Edited from Davaripour et al. (2020a))	124

Figure 4-3 A Schematic View of the Hybrid Model (Edited from Davaripour et al. (2020a))	126
Figure 4-4 Engineering Stress-Strain Curve from (Zheng, 2014)	127
Figure 4-5 Loading Conditions: Case-1 with Non-Perpendicular Trawling Impact; Case-2 with Only the Normal Component of the Non-Perpendicular Trawling Impact	129
Figure 4-6 Boundary Conditions Used to Benchmark the Hybrid Numerical Simulation edited (Davaripour et al., 2020a)	131
Figure 4-7 Vertical Load-Displacement Curve; Experimental Result Versus Numerical Prediction (Davaripour et al., 2020a)	132
Figure 4-8 Mesh Convergence Analysis for the Hybrid Model: Beam Elements (Davaripour et al., 2020a)	133
Figure 4-9 Mesh Convergence Analysis for the Hybrid Model: Shell Elements (Davaripour et al., 2020a)	133
Figure 4-10 Dent Depth in a 5-inch Diameter Pipe for Case-1 and Case-2	135
Figure 4-11 Dent Depth in a 14-inch Diameter Pipe for Case-1 and Case-2	136
Figure 5-1 A Schematic View of the BSM Model (Edited from Davaripour et al. (2020a))	148
Figure 5-2 A Schematic View of the Test Apparatus	153
Figure 5-3 Components of the Test Apparatus in the Vertical Load Path (Edited from Davaripour et al. (2020b))	154
Figure 5-4 A Schematic View of the Test Setup (Colored in Red) Connected to the Carriage	155

Figure 5-5 Engineering Stress-Strain Curve for the Cylindrical Specimen (Davaripour et al., 2020a).....	156
Figure 5-6 A View of the Saddle-Shaped Support	157
Figure 5-7 The Connection Between the I-beam with a Stiffener Inside the Carriage....	157
Figure 5-8 Schematic View of the Mount.....	158
Figure 5-9 Solid Cylindrical Indenter	158
Figure 5-10 Boundary Condition Employed in the Physical Test	159
Figure 5-11 Loading Condition of the Present Study Physical Test.....	160
Figure 5-12 Test Procedure: 1) Prior to the Indentation, b) End of Phase 1, c) End of phase 2.....	160
Figure 5-13 Scanned View of the Deformed Cylindrical Specimen a) Isotropic View, b) Z-Y View, c) Z-X View.....	161
Figure 5-14 Vertical Load Applied by the Indenter to the Specimen Versus Time (Left); and Vertical Displacement of the Indenter (or Resulting Dent Size Imposed to the Pipe) Versus Time (Right)	162
Figure 5-15 A Schematic View of the Hybrid Shell-Beam Model from (Edited from Davaripour et al. (2020a)).....	165
Figure 5-16 Loading Conditions Including Case-1 with a 30 Degree Diagonal Trawl Impact; Case-2 with Only the Normal Component of the diagonal Trawl Impact.....	168
Figure 5-17 Boundary Conditions Used to Benchmark the Hybrid Model (Davaripour et al., 2020a).....	170
Figure 5-18 Engineering and True Stress-Strain Curve from (Zheng, 2014)	172

Figure 5-19 Vertical Load-Displacement Result: Experimental Result Versus Numerical Prediction from (Davaripour et al., 2020a).....	173
Figure 5-20 The Vertical Load Resisted by the Specimen Against the Impact Versus Time; Numerical Versus Experimental Results (Davaripour et al., 2020a).....	174
Figure 5-21 Numerical Simulation of the Mount	176
Figure 5-22 Force-Displacement Curve of the Mount Being Pulled at the Center of the Tied Nodes	177
Figure 5-23 Axial Connector Used to Represent the Stiffness Provided by the Mounts	177
Figure 5-24 The Vertical Displacement of the Indenter (or Dent-Size Imposed on the Specimen) Versus Resultant Displacement of the Indenter; Numerical Versus Experimental Result	178
Figure 5-25 A Comparison Between the Scanned View of the Deformed Specimen and the Numerical Prediction (a), an Isotropic View of the Numerical Model (b).....	179
Figure 5-26 Mesh Convergence Analysis for the Hybrid Model: Shell Elements (Davaripour et al., 2020a)	180
Figure 5-27 Mesh Convergence Analysis for the Hybrid Model: Beam Elements (Davaripour et al., 2020a)	180
Figure 5-28 Dent Depth in a 5-inch Diameter Pipe for Case-1 and Case-2	182
Figure 5-29 Dent Depth in a 14-inch Diameter Pipe for Case-1 and Case-2	183
Figure 6-1 An Overall View of the Test Apparatus.....	202
Figure 6-2 Components of the Test Apparatus in the Vertical Load Path.....	203
Figure 6-3 Components of the Test Apparatus Along the Horizontal Load Path.....	204

Figure 6-4 An Overall View of the Test Setup: Isotropic View (a), YZ-View (b), and XZ-View (c)	205
Figure 6-5 Engineering Stress-Strain Curve for the Cylindrical Specimen (Davaripour et al., 2020a).....	206
Figure 6-6 Deformable and Non-Deformable Parts of the Cylindrical Specimen (Davaripour et al., 2020a)	207
Figure 6-7 Saddle-shaped Support (a), and the 1 inch Plate (b) (Partly Edited from Davaripour et al. (2020c)).....	208
Figure 6-8 The Connection Between the I-Beam with a Stiffener Inside the Carriage (Edited from Davaripour et al. (2020c))	208
Figure 6-9 Schematic View of the Mount (Partly Edited from Davaripour et al. (2020c))	209
Figure 6-10 Solid Tube-Shaped Indenters: Frictionless Indenter (a), and Friction-Included Indenter (b) (Partly Edited from Davaripour et al. (2020c)).....	210
Figure 6-11 Boundary Conditions Employed in the Laboratory Tests	211
Figure 6-12 Loading Condition Including Phase 1 and 2 (Edited from Davaripour et al. (2020c)).....	212
Figure 6-13 Test Procedure: 1) Before the Indentation, b) End of Phase 1, c) End of Phase 2 (Edited from Davaripour et al. (2020c))	213
Figure 6-14 A View of the Deformed Shape of the Specimen in Test 1	215

Figure 6-15 Results of Test 1: Vertical Load Resisted by the Specimen Against the Applied Indentation Versus Time (Left); Vertical Displacement of the Indenter (or the Resulting Dent Depth on the Specimen) Versus Time (Right).....	216
Figure 6-16 Results of Test 1: the Horizontal Load as Well as the Resultant Load Imposed to the Specimen Versus Time	217
Figure 6-17 Test 2: Deformed Shape of the Cylindrical Specimen After Test 2; Views of the Laboratory Test (a and b); Scanned Views of a Section Cut of the Deformed Specimen (c, d, and e).....	218
Figure 6-18 Results of Test 2: Vertical Load Resisted by the Specimen Against the Applied Indentation Versus Time (Left); Vertical Displacement of the Indenter Versus Time (Right)	219
Figure 6-19 Results of Test 2: Resultant and Horizontal Load Imposed to the Specimen Versus Time	220
Figure 6-20 Results of Test 1 and 2: Vertical Load as well as Horizontal Load Resisted by the Specimen Against the Applied Indentation Versus Time	221
Figure 6-21 Results of Test 1 and 2: Resultant Load Resisted by the Specimen Against the Applied Indentation Versus Time	221
Figure 6-22 Vertical Load (Test 1) and Horizontal Load (Test 1&2) versus Time (Left); Friction Coefficient Versus Time During Test 1 (Right).....	222
Figure 6-23 Results of Test 3: Vertical Load Applied by the Indenter Against the Specimen Versus Time (Left); Vertical Displacement of the Indenter Versus Time (Right) (Davaripour et al., 2020c)	224

Figure 6-24 Results of Test 3: Horizontal Load Imposed to the Specimen Versus Time	225
Figure 6-25 Deformed Shape of the Specimen After Test 4	226
Figure 6-26 Scanned Views of a Section-Cut of the Deformed Specimen in Test 4.....	227
Figure 6-27 Results of Test 4: the Vertical Load Resisted by Specimen Versus Time (Left); Vertical Displacement of the Indenter Versus Time (Right)	228
Figure 6-28 Results of Test 4: Resultant Load as well as the Horizontal Load Applied to the Specimen Versus Time	228
Figure 6-29 Vertical Displacements of the Top and Bottom Points of the Mid-Pipe as well as the Resulting Dent Depth Imposed on the Specimen during Phase 1 of the Loading.	229
Figure 6-30 Results of Test 2 and 4: the Vertical Load Resisted by Specimen Versus Time	230
Figure 6-31 Load Path During Phase 1 and 2 in Test 3 (Edited from Davaripour et al. (2020c)).....	232
Figure 6-32 Boundary Conditions Employed in Test 3	233
Figure 6-33 Numerical Simulation of the Mount (Partly Edited from Davaripour et al. (2020c)).....	234
Figure 6-34 Load-Displacement Curve of the Mount (Edited from Davaripour et al. (2020c)).....	234
Figure 6-35 Axial Connectors employed to Represent the Stiffness Provided by the Mounts (Edited from Davaripour et al. (2020c))	235
Figure 6-36 Mesh Convergence Analyses Including Three Mesh Sizes: 3, 5, and 6 mm	236

Figure 6-37 The Vertical Displacement of the Indenter (or Imposed Dent Depth on the Specimen) Versus Resultant Displacement of the Indenter; Numerical Versus Experimental Result (Edited from Davaripour et al. (2020c))	237
Figure 6-38 Sensitivity Studies: Friction Coefficient (Specimen Against the Saddle-shaped Support): 0.0, 0.3, 0.5	238
Figure 6-39 Schematic Views of the Deformed Pipe under Repeated Indentations at Adjacent Locations	239
Figure 6-40 The Deformed Shape of the Specimen After 11 Indentations	240
Figure 6-41 Numerical Results Versus Physical Data of Test 3: Vertical Displacement Versus Horizontal Position of the Indenter Relative the Pipe Middle Length	240
Figure 6-42 Plastic Equivalent Stress Contour Under Indentation Number 1 and 3	244
Figure 6-43 Plastic Equivalent Stress Contour of a Ring under a Lateral Indentation	244
Figure 6-44 Load-Displacement Curve of a Ring under the Lateral Indentation	245
Figure 6-45 Schematic View of the BSM Model (Edited from Davaripour et al. (2020a))	249
Figure 6-46 Benchmarking the BSM Model (Davaripour et al., 2020a)	251
Figure 6-47 Maximum Trawl Load Imposed on the Pipeline of the Present Study – Finite Element Result using the BSM Model.....	251
Figure 7-1 An Overall View of the Test Apparatus.....	271
Figure 7-2 Components of the Test Apparatus (Partly Edited from Davaripour et al. (2020c)).....	272

Figure 7-3 An Overall View of the Test Setup Bolted to the Carriage: Isotropic View (a), YZ-View (b), and XZ-View (c) (Partly Edited from Davaripour et al. (2020c))	273
Figure 7-4 Engineering and True Stress-Strain Curves for the Carrier Pipe (Partly Edited from Davaripour et al. (2020c))	274
Figure 7-5 A Schematic View of the PiP Specimen Components.....	275
Figure 7-6 A Schematic View of the Inner Pipe Assembly Including the Inner Pipe and Bell-Shaped End Connections Which is Mounted by the Ball Supports.....	275
Figure 7-7 Bell-Shaped End Connections and Ball Supports Used to Centralize the Inner Pipe Inside the Carrier Pipe	276
Figure 7-8 Ball Support (Left), Assembly (Middle), and Bell-Shaped End Connection (Right).....	276
Figure 7-9 A Schematic View of the Mount (Partly Edited from Davaripour et al. (2020c))	278
Figure 7-10 The Solid Cylindrical Indenter (Davaripour et al., 2020c)	278
Figure 7-11 Boundary Conditions Employed for Carrier and Inner Pipes	279
Figure 7-12 Loading Condition Including Phase 1 and 2	281
Figure 7-13 Test Procedure: 1) Before the Indentation, b) End of Phase 1, c) End of Phase 2.....	281
Figure 7-14 A View of the Deformed Shape of the PiP Specimen After the Test	283
Figure 7-15 Scanned Views of the Deformed PiP Specimen Including the Isotropic View (a), View of the Cross-Section Where Phase 1 ends (b), and Elevation View (c).....	284

Figure 7-16 Scanned Views of the Deformed Inner Pipe Including Isotropic View (a), a View of the Cross-Section (b), Elevation View (c), View from the Top (d).....	285
Figure 7-17 Load Displacement Curve During the First Phase of Physical Test on the PiP Specimen.....	286
Figure 7-18 Vertical Load Resisted by PiP Specimen Versus Time (Left); Vertical Displacement of the Indenter Versus Time (Right).....	288
Figure 7-19 Resultant Load as well as Horizontal Load Imposed to the PiP Specimen .	288
Figure 7-20 Vertical Displacement of the PiP Specimen in the Middle at the Top and Bottom Points as Well as the Induced Dent Depth on the Specimen	289
Figure 7-21 Vertical Load Versus Vertical Displacement of the SWP and PiP Specimens in the Present Study, and Previous Works by Davaripour et al. (2020d) and Zheng et al. (2013).....	291
Figure 7-22 Vertical Load Imposed to the PiP (Present Study) and SWP (Davaripour et al., 2020d) specimens Versus the Resultant Displacement of the Indenter	292
Figure 7-23 An Isotropic View of the Numerical Model (a), Cut-away View of The Model (b), and a View of the End Connection and Ball Support (c)	295
Figure 7-24 Boundary Conditions Employed for the PiP Specimen	296
Figure 7-25 Simplified Representation of End Mounts in the Finite Element Model.....	297
Figure 7-26 Mesh Convergence Analyses Including Two Mesh Sizes for the Carrier and Inner Pipes: 3, 5, mm	299
Figure 7-27 Sensitivity Study on the Effect of Friction Coefficient in the Contact Regions Type-b and c	300

Figure 7-28 Vertical Load Imposed to the PiP Specimen: Test Data Versus Numerical Prediction	302
Figure 7-29 Vertical Load Imposed on the PiP Specimen Versus Vertical Displacement of the Indenter: Test Data Versus Numerical Prediction (Under 1, 100, and 200 KN Axial Load)	303
Figure 9-1 A View of the Connection Between the Swing-arm and Indenter.....	328
Figure 9-2 Static Analysis of the Load Transferred Along the Indenter and the Swing-Arm	329

List of Terms

BSM model	The beam and spring-mass (BSM) model involves beam elements to model the pipe, point masses to represent the mass of the pipe and the indenter, and springs to represent the stiffness of the pipe shell and trawl board.
Buckle propagation	Buckle propagation is the propagation of the local buckle along the pipe due to the external pressure.
Crumpling deformation mode	The crumpling deformation mode involves only local deformation of the pipe without any global/bending pipe response.
Damage progression effect	This term, Damage Progression Effect, is used interchangeably with the term Moving Load Effect throughout the present thesis. It refers to the effect of damage progression along the structure, on the mechanical behaviour of the structure. This effect is presented in percentage and shows the drop in the vertical resistance of the structure against the imposed indentation. The vertical resistance refers to the structural resistance mobilized in the direction normal to the undeformed shape of the structure.
Hybrid model	The hybrid model refers to the hybrid shell beam model, which is an improved version of the BSM model. In the hybrid model, a full model of the pipe with shell elements are used in the region of interaction between the indenter and the pipe. Furthermore, instead of using point load contact in the BSM model, the interaction between the indenter and the pipe is

modelled via a surface to surface contact between the pipe with shell elements and a rigid object with solid elements.

Interference load	The interference load refers to the loads applied by a third party activity to a subsea pipeline (i.e., trawl interference load).
Knife-edge indenter	The knife-edge indenter refers to a rigid object which has a cylindrical front face with a sharp radius in the range of 10 to 25 mm.
Leading side	In accidental events where a subsea pipeline is subject to a lateral impact by a third party, the interference load could impose damage on the pipe and translate and induce the resulting damage longitudinally along the pipe. Accordingly, the leading side refers to the region on a pipe ahead of the indenter, while the indenter translates along the pipe.
Mechanical damage	The mechanical damage refers to the localized structural dent in a pipe which is induced by an interference load.
Moving load effect	The moving load effect is the same as the damage progression effect and refers to the effect of damage progression along the structure, on the mechanical behaviour of the structure.
Non-perpendicular trawl impact	Where the direction of the bottom trawl impact is not perpendicular to the pipe, the impact is termed as the non-perpendicular trawl impact.
Non-rupture type load	The non-rupture type load refers to an interference load by a third party, which could induce elastic and/or plastic

deformation in a pipeline to the extent which does not lead to rupture initiation.

Normal direction	The direction perpendicular to the pipe
Path dependency	Path dependency refers to the effects of the plastic deformation, imposed on the pipe at the previous time increment, on the current response of the pipe.
Perpendicular step	The perpendicular step is where a lateral load is imposed on only one location and normal to the pipe.
Pipe shell stiffness	Pipe shell stiffness refers to the local stiffness of a pipe or the resistance provided by the pipe's wall thickness.
Plastic damage	Permanent local deformation in a pipe
Plastic deformation	Permanent deformation in a pipe
Rupture-type load	Rupture-type load refers to an interference load by a third party, which induces rupture in a structure.
Small-sized pipe	Any pipe diameter less than 10 inches is termed as the small-sized pipe.
Stress triaxiality	The ratio of the hydrostatic pressure over the von-Mises equivalent stress is defined as the stress triaxiality.
Structural capacity	The structural capacity refers to the resistance of a structure against an interference load applied in the lateral direction.
Trailing side	In accidental events where a subsea pipeline is subject to a lateral impact by a third party, the interference load could

impose damage on the pipe and translate and induce the resulting damage longitudinally along the pipe. Accordingly, the trailing side refers to the region on a pipe behind the indenter, while the indenter translates along the pipe.

Trawl impact The trawl impact refers to the initial phase during the interaction between trawl gear and pipeline, which lasts for several hundredths of a second, and the pipe's response is mainly local.

Trawl pull-over The trawl pull-over is the second phase during the interaction between fishing gear and a pipeline, where the pipe is dragged by the trawl board. The dominant pipe's response during this phase is the global/bending deformation.

List of Nomenclature and Acronyms

BC	Boundary condition
BSM	Beam and spring-mass
D	Steel pipe nominal outer diameter
DC	Displacement controlled
DNV	Det Norske Veritas
DOF	Degree of Freedom
E	Young's modulus
FEA	Finite element analysis
FI	Friction included (indenter)
FL	Frictionless (indenter)
f_y	Yield strength of the material
f_u	Ultimate strength of the material
$H_{p,c}$	Permanent dent depth
H_t	Total dent depth (elastic and plastic)
k_a	Out-of-plane stiffness of a trawl board
k_{pb}	Effective bending stiffness of a pipe in impact calculation (time-dependent)
k_{ps}	Effective soil stiffness applied to a pipe in impact calculation (time-dependent)
k_s	Local shell stiffness of steel pipe
kt	In-plane stiffness of a trawl board
LC	Load-controlled
$LVDT$	Linear Variable Spatial Transducer
m_a	Hydrodynamic added mass of a trawl board
m_t	Steel mass of trawl board
NA	Not applicable
No	Number

<i>NSERC</i>	Natural Sciences and Engineering Research Council
<i>PiP</i>	Pipe in pipe
<i>Sec</i>	Second
<i>SWP</i>	Single-walled pipe
t	Pipe wall thickness (steel), $t = t_{nom} - t_{corr}$
t_{corr}	Corrosion allowance thickness
V	Tow velocity of a trawler which is considered the same with the velocity of the trawl gear

1 CHAPTER 1

1.1 Introduction

Leis et al. (1998) showed that the severity of the localized damage in a pipeline, where the pipe is subject to a lateral interference load, is considerably dependent on the pipe-soil interaction, line pressure, axial force, and load magnitude and orientation. Regarding the last factor (load orientation), the common industry practice to design a pipeline against an accidental event (i.e., trawl gear interference with a subsea pipeline) is to consider a scenario where the lateral interference load is imposed to the pipe in the perpendicular direction. Accordingly, the resulting damage on the pipe is induced at only one location, and the potential considerable effects of damage progression are neglected. The term damage progression refers to the translation of plastic damage along the pipe.

According to the recent studies on ship hull structures, the structural resistance mobilized in the case of a damage progression could be significantly lower than the case where the imposed load is perpendicular to the plate, and the resulting damage is imposed at only one location. Therefore, it is reasonable to study the potential similar considerable effect of damage progression in subsea pipelines in accidental scenarios where the pipe is subject to a substantial lateral impact load. An application of the damage progression effect in pipes could be a scenario where a subsea pipeline is subject to a diagonal interference load, and the tangential component of the diagonal load translates and induces the resulting plastic damage along the pipe and lowers the structural resistance of the pipe

In order to protect the structural integrity of subsea pipelines against accidental events, the assessment of the risk presented by fishing activity in oil and gas offshore areas is critical. To mitigate this risk, flowlines are often protected using trenching/burial, and/or rock dump. However, these mitigation strategies lead to a significant extra cost to the project. Hence, it is necessary to assess the flowline overtrawlability to achieve a technically feasible pipe design and improve project economics. In this respect, previous studies showed that in general, there is less concern regarding the overtrawlability of large diameter pipelines, i.e., larger than 16 inches (Fyrileiv and Spiten, 2004; Horenberg and Koninklijke, 1987; Zheng, 2014), and the small-diameter pipelines are the ones that require a robust overtrawlability assessment. However, there is a very limited study on the overtrawlability assessment of small-sized flowlines.

In recent years, pipe in pipe (PiP) systems have been employed in an increasing number of subsea projects due to the benefits associated with thermal insulation. As there is no leakage associated risk for the carrier pipe, the denting criterion could be relaxed compared to the case of a single-walled pipe (SWP) (Konuk et al., 2005). However, the assessment of PiP solutions has traditionally been performed the same as SWPs, which leads to an over-conservative PiP design.

In order to address the above-mentioned gaps, the present study initiated a research project, which involves a series of experimental and numerical investigations on small-diameter SWP and PiP systems. The scope of the present thesis could be applied to any accidental scenario where a cylindrical structure is subject to substantial interference load in the lateral direction. However, the focus of the present study is to assess the mechanical behaviour of subsea pipelines against the bottom trawl impact. In this regard, DNV-RP-F111 (2014): “Interference Between Trawl Gear and Flowlines” is the current industry recommended practice to design a pipeline against trawl gear impact.

According to DNV-RP-F111 (2014), trawl gear interaction with a pipeline can be decoupled into three phases, including impact, pull-over, and hooking. The initial impact phase occurs in some hundredths of a second. As such, the kinetic energy is mostly absorbed by the pipe-wall as well as the protective coating. In other words, during the initial impact phase, the global pipeline deformation and pipe-soil interaction are insignificant. The scope of the present study only covers the initial trawl impact phase. In this regard, throughout this thesis, the trawl impact refers to the load applied during the initial impact phase.

1.1.1 Background and Research Motivation

1.1.1.1 Single-Walled Pipe (SWP)

The common engineering practice to assess a pipeline against an impact event is to examine a case where the pipe is subject to a lateral interference load which is imposed perpendicular to the pipe. In the case of the bottom trawl impact with a subsea pipeline, the edge of the trawl gear is relatively sharp and could be represented with a cylindrical surface with a small radius (in the range of 10 to 25 mm) (DNV-RP-F111, 2014); the indenter with the sharp tip is termed as the knife-edge indenter. In this regard, the structural behaviour of a pipe under a perpendicular indentation by a knife-edge indenter has been the subject of several studies, i.e., (Shen and Jones, 1991; Zheng et al., 2013).

Shen and Jones (1991) showed that the dynamic effect of an impact event could be replicated using quasi-static analyses if the indenter is sufficiently heavy and moves at slow speed. The finding of Shen and Jones (1991) is examined by Zheng et al. (2013) for trawl gear interference with a subsea pipeline, where the authors showed that a pipe response under impact and quasi-static analyses are within the same range. This conclusion is employed in the present work. Accordingly, the physical tests, as well as numerical simulations in the present thesis, are conducted under the quasi-static condition.

With respect to the deformation modes of a pipe under a perpendicular impact, Wierzbicki and Suh (1988) proposed an analytical model assuming the impact load is absorbed by the pure crumpling (local) behaviour of the pipe. Thomas et al. (1976) performed lab-scale tests on a pipe with simply supported boundary condition (BC) and showed three separate modes of deformation for a pipe under a transverse quasi-static indentation, including 1) pure crumpling mode, 2) combination of crumpling and bending mode, 3) structural collapse. Ellinas and Walker (1983) presented a semi-empirical model partially based on the experimental data reported in (Thomas et al., 1976). The authors assumed that the pipe's structural response could be decoupled into two separate phases, including the local deformation and then the global deformation. However, Zheng et al. (2012) conducted experimental and numerical investigations and concluded that from the very beginning of the impact event, the pipe has both local and global modes of deformations. The local deformation grows faster at the beginning. Then the global deformation increases as the cross-sectional deformation lowers the bending stiffness of the pipe (Zheng et al., 2012).

Several physical tests have been conducted in previous studies to examine the mechanical behaviour of a pipe subject to a knife-edge indenter. Thomas (1976) conducted a series of quasi-static tests on a simply supported pipe, which was transversely indented by a knife-shaped indenter. Due to the very short span of the pipe, the structural response was mainly within the crumpling mode of deformation. Soreide and Amdahl (1982) did

physical tests and investigated the structural response of a tube under the fully clamped BC. The authors did physical tests under both quasi-static and impact conditions, with the indentation rate set to 0.15 and 54 mm/sec, respectively.

With respect to the pipe's behaviour under a rupture type interference load, Jones and Birc (1996) did a series of impact tests on a 54 fully clamped pipes under a wedge-shaped indenter with a velocity up to 13.6 m/sec. While the tests were designed to be performed under the fully clamped boundary condition, at the large deformation, the pipe ends slightly deformed. The authors investigated the effect of the magnitude of the impact energy on the failure mode and the loss of internal pressure in the pipe. Chen and Shen (1998) performed a comprehensive experimental study on 226 fully clamped specimens subject to transverse impact by a wedge-shaped indenter. The authors investigated the threshold value of the impact energy, which causes the initiation of the material rupture in the pipe using different pipe geometries, internal pressure value, and impact positions. They concluded that the material rupture only occurs in the form of tensile tearing failure mode in the proximity of or at the supports.

Regarding the effect of pipe-soil interaction on the mechanical behaviour of a pipe during an impact event, Leis et al. (1998) investigated the thin-walled high-pressure pipelines under an interference load. The authors demonstrated that four factors have a strong effect on the localized structural damage in the pipe where the pipe is impacted laterally by a

third-party load, including 1) pipe-soil interaction, 2) line pressure, 3) axial force, and 4) the orientation and magnitude of the interference load. Ng and Shen (2006) presented the inelastic structural response of pressurized pipes using 52 physical impact tests on mild steel pipes. The authors examined the failure of the pipes, considering the interaction between the pipe and foundation. They concluded that incorporating the foundation in the physical tests significantly reduces the effect of the internal pressure on the critical impact energy; the critical impact energy refers to the mean of the lowest impact energy which causes rupture, and the highest impact energy which does not. During the interference between a subsea pipe and trawl gear, unless if the pipeline is buried, the pipe-soil interaction is insignificant, as the impact direction is along the seabed.

Palmer et al. (2006) investigated the response of an unpressurized pipe resting on sand and impacted by another pipeline. The authors showed that due to the dropped object impact, the main damage was imposed on the concrete coating, and the deformation of the pipelines was minimal. Furthermore, they showed that due to the pipe-soil interaction, the resulting damage on the pipe was significantly reduced, compared to the case where the pipe was resting on a steel support. Alexander (2007) presented the results of the experimental and numerical investigation with an attempt to provide a general insight regarding the major defect classifications in a subsea pipeline as well as methodologies to examine these defects. The author studied several dropped object events on a 12-inch diameter pipe (resting on steel or sand supports), including the one with the indenter mass

equal to 10900 kg falling from 9.1 m height, which leads to an impact velocity much greater than common trawling impact events.

With respect to the pipe's behaviour under combined loading, SUH (1987) presented closed-form solutions for pipe with varied boundary conditions subject to combined loading. The author investigated the pipe's response under the interaction of lateral load, axial force, and bending moments, and concluded that the lateral resistance of the pipe could drop dramatically where the pipe is subject to axial compression. In other words, the pipe could tolerate considerably less stable dent size where it is subject to an axial compression force. In the opposite, where the pipe is subject to axial tension load, the local resistance of the pipe against the lateral indentation increases.

In the common engineering practice for designing a structure against a substantial lateral impact, the interference load is applied perpendicularly to the structure. Hence, the potential damage is imposed at only one location on the structure. However, recent studies showed that the loading condition, which leads to the progression of plastic damage along the structure, could induce more severe damage to the structure, i.e., (Quinton, 2015, 2008; B. W. T. Quinton et al., 2017). Quinton (2015) investigated the progression of damage in a ship hull structure against the moving ice load, using numerical and experimental methods. The author showed that the structural resistance of a plate could drop significantly where the load slides along the structure versus the case

where the same load is imposed at only one location on the structure. Accordingly, there is potentially a similar considerable effect in pipelines where the indenter imposes plastic damage and translates and induces the damage along the pipe. An application of the damage progression effect could be a scenario where a subsea pipeline is subject to a diagonal interference load, and the tangential component of the diagonal load translates and induces the resulting plastic damage along the pipe and lowers the structural resistance of the pipe. In this regard, to the knowledge of the author, the effect of damage progression in pipelines has not been investigated in any previous studies.

The mechanical behaviour of a pipe during the damage progression by a lateral interference impact has some similarities to the buckle propagation phenomenon in subsea pipelines. The buckle propagation refers to the longitudinal propagation of the local buckle (plastic damage) along the subsea pipeline due to the external pressure, which has been investigated in the last few decades, i.e., (Hahn et al., 1993; Kyriakides, 1994; Liang et al., 2019). In this regard, it was shown that the pressure required to buckle a pipeline is more than the pressure needed to propagate the buckle, i.e., (Chater and Hutchinson, 1984). Therefore, pipelines have less structural resistance when the local buckle propagates along the pipe versus the case where the local buckle is initiated at only one location. This provides additional evidence regarding the potential considerable damage progression effect in subsea pipelines where the pipe is subject to a lateral load by a third party (i.e., bottom fishing gear), which applies plastic damage to the pipe and

translates and induces the imposed damage along the pipe. The goal of the present thesis is to address this phenomenon in SWP and PiP systems.

1.1.1.2 Pipe in Pipe (PiP) Systems

The structural components of a PiP product include the carrier pipe and the internal flowline. The carrier pipe is the outer pipe that provides structural protection. The inner pipe which carries the fluid is centralized inside the carrier pipe using spacers. In between these two pipes, there is a space for insulation material, which provides a substantial advantage for maintaining high thermal insulation (Zheng, 2014). As there is no leakage associated risk for the carrier pipe, the denting criterion could be relaxed compared to the case of an SWP (Konuk et al., 2005). However, the assessment of PiP solutions has traditionally been performed the same as SWPs (i.e., for overtrawlability assessment of subsea pipelines as recommended in DNV-RP-F111 (2014)), which leads to an over-conservative PiP design.

Sriskandarajah et al. (1999) provided an overall view on the interaction between trawl gear and PiP systems. The authors stated that the higher mass of the PiP versus the SWP system leads to absorbing more kinetic energy and, consequently, more dent size during the trawl impact. However, the carrier pipe could bear more dent depth as it does not contain hydrocarbon. As such, the employment of the SWP's conventional design method for the PiP systems leads to an over-conservative solution.

Zheng et al. (J. Zheng et al., 2014; 2013, 2012) performed numerical investigations, as well as a series of physical tests on PiP specimens subject to quasi-static and dynamic transverse indentation to provide further insight regarding the structural resistance of the PiP systems against the indentation by a knife-edge shaped object. The authors showed that the PiP specimen provides a significant additional structural capacity compared to the case of an SWP pipe. Zheng et al. (2014) examined the effect of internal and external pressure on the denting process in a pipeline and concluded that buckle propagation occurs more likely in SWPs versus PiPs. Wang et al. (2014) investigated the response of a PiP system subject to a dropped object impact, where the space between the inner pipe and the carrier pipe is filled with ultralight cement composite. The authors concluded that the presence of the composite enhances the PiP resistance against the development of the local damage. Additionally, the inner pipe contributes to the confinement of the composite material and improves the PiP response.

Furthermore, in the last two decades, the pipeline bundle technology, which is a subcategory of PiP systems, has been employed in the pipeline industry. Song et al. (2009) provided an overall review on the bundle technology, which is a cost-efficient option for projects which require multiple lines and high thermal insulation. The bundle comprises three main structural components, including the outer pipe for the mechanical protection, multiple internal flowlines for carrying the hydrocarbons, and sleeve pipes for

several purposes, such as providing additional buoyancy and structural strength. Also, the bundle is either a) open where the individual pipe and cables are strapped together, or b) closed where all the lines are protected inside an outer pipe.

Despite the present gaps regarding the structural behaviour of a PiP system, there are a very limited number of studies allocated to assess the mechanical behaviour of PiP products. As such, the behaviour of a small-diameter PiP solution under a knife-edge indenter is within the scope of the present research project with the focus on studying the effect of damage progression on the PiP behaviour. While the findings of the present work could be applied to any impact scenarios, the focus is the application of damage progression effect on subsea pipelines, where the pipe is subject to fishing gear interference.

1.1.1.3 Trawl Gear Interference

Fishing activity in oil and gas offshore areas is inevitable. This presents a risk to the structural integrity of flowlines due to the trawl gear impact. To mitigate this risk, flowlines are often protected using trenching and/or rock dump. However, these mitigation strategies lead to a considerable extra cost to the project. Hence, it is necessary to assess the flowlines against the trawl interference load to achieve an overtrawable pipe design and yet improve the project economics.

DNV-RP-F111 (2014): “Interference Between Trawl Gear and Flowlines” is the current industry recommended practice to design a pipeline against trawl gear impact. According to DNV-RP-F111 (2014), trawl gear interaction with a pipeline can be decoupled into three phases, including initial impact, pull-over, and hooking. The initial impact phase occurs in some hundredths of a second (DNV-RP-F111, 2014). As such, the kinetic energy is mostly absorbed by the pipe-wall as well as the protective coating. In other words, during the initial impact phase, the global pipeline deformation and pipe-soil interaction are insignificant. The present study only covers the initial trawl impact phase. As such, throughout this thesis, the trawl impact refers to the load applied during the initial impact phase.

Trawl types are categorized into two groups based on how the net is kept open during trawling, including a) otter trawls using trawl boards, and b) beam trawls using a transverse beam. The beam trawl type is mostly used in shallow waters (Bai and Bai, 2005). The present work only considers the interaction between a flowline and a trawl board, which is the most popular trawl type in the North Sea and the Norwegian Sea (Zheng, 2014).

In recent years, twin otter trawling has been employed to optimize the fishing catch and cost. In this respect, fuel consumption is one of the main costs, which could reduce by nearly one third, where twin trawling is used (Fyrileiv et al., 2006). In the twin trawling

method, a clump weight is employed in the middle of the trawl boards to keep the net down. As clump weight has 20-40% higher weight compared to a single trawl board (DNV-RP-F111, 2014), it could apply a considerable impact load to a flowline.

For the overtrawlability assessment of subsea pipelines where fishing data is not available, the typical fishing gear parameters could be employed from, i.e., (DNV-RP-F111, 2014; Trevor Jee Associates, 1999). However, a more detailed assessment may be required as due to the development in the fishing industry, the gear data is continuously changing (i.e., the velocity of a trawl board has increased to 4 m/sec (Emesum, 2013)).

DNV-RP-F111 (2014) proposes two methods to assess the structural response of a flowline under the impact phase, including the analytical and the numerical method. The first method is conservative as it assumes all the impact energy is absorbed through local flowline indentation. The latter method employs a beam and spring-mass (BSM) model that accounts for the stiffness of the concrete coating and insulation protection, as well as the energy dissipation during the global flowline deformation and pipe-soil interaction.

As reported in DNV-RP-F111 (2014), the DNV recommendation is only applicable for pipe diameters larger than 10 inches. However, smaller pipelines are commonly used in offshore projects. As such, there is a clear gap regarding the overtrawlability assessment of small pipe sizes. Accordingly, the applicability of the BSM model should be extended

to include the overtrawlability assessment of smaller pipe sizes, using a more advanced numerical model, i.e., a hybrid shell beam model, which is within the scope of the present study.

Using the BSM model to examine a perpendicular trawl impact on a pipeline, first, the impact velocity is applied to a point mass associated with the trawl board, as well as a point mass, which represents the hydrodynamic added mass. Then, the resulting kinetic energy is transferred to the pipe via springs, which represent the in-plane and out of plane stiffnesses of the trawl board.

For a non-perpendicular trawl impact, the impact velocity is decoupled to the normal and tangential components; the first component follows the above steps, and the latter component is disregarded, as the tangential component could not be incorporated in the BSM model. However, the tangential component of a diagonal impact could translate and induce the imposed damage (if any) along the pipe. In this regard, Quinton (2015) showed that the resistance of a ship hull structure under a lateral sliding interference load could drop significantly, where the plastic damage imposed on the structure translates longitudinally along the structure. As the BSM model does not consider the effect of damage progression (flowline is modelled with 1-D beam elements), using the BSM model could underestimate the resulting dent depth on the pipe, where the pipe is subject to a diagonal trawl impact. Accordingly, there is a gap regarding the effect of damage

progression in subsea pipelines where the pipe is subject to a non-perpendicular trawl impact, which could be accounted for, i.e., using a hybrid shell-beam model. Addressing this gap is within the scope of the present thesis.

According to DNV-RP-F111 (2014), the overtrawlability assessment of subsea pipelines requires the consideration of the subsequent trawl pull-over load and the resulting accumulation of plastic strain on the pipe. The number of subsequent trawl interactions is dependent on the trawl frequency in the field. However, if no specific data is available, DNV-RP-F111 (2014) recommends considering the effect of four subsequent pull-over loads at the same location. Likewise, the subsequent initial trawl impact should be considered where applicable. In this regard, if the repeated trawl impacts occur at neighbouring locations on a pipe, it can lead to the progression of damage. Accordingly, the potential significant drop in the structural resistance of a pipeline under subsequent trawl impact at adjacent locations on a pipe is another gap in DNV-RP-F111 (2014), which is investigated in the present thesis.

1.1.2 Research Objectives and Significance

The scope of the present work could be applied to any type of cylindrical structure (i.e., jacket leg, subsea riser, subsea pipeline, etc.) subjected to a lateral interference load, which could impose plastic damage to the structure and translate and induce the resulting damage along the structure. However, the focus of the present scope is to assess the

mechanical behaviour of a subsea pipeline, where the pipe is subject to a bottom trawl impact.

The present research project is performed to obtain the following objectives:

- Investigate the structural behaviour of small-sized SWPs (with a diameter of 5 inches) where the pipe is subject to a perpendicular indentation.
- Investigate the damage progression effect in an SWP, where the plastic damage imposed on the pipe is pushed longitudinally along the pipe.
- Investigate the structural behaviour of a small diameter PiP specimen (5-inch diameter carrier pipe and 3-inch diameter inner pipe) subject to a perpendicular indentation.
- Assess the effect of damage progression on the structural behaviour of a small-sized PiP product.
- Examine the effect of combined loading (lateral load and axial force) on the mechanical behaviour of a PiP system.
- Provide suitable laboratory data to validate the accuracy of numerical models.
- Identify and investigate the damage progression associated gaps with respect to small-diameter pipelines in DNV-RP-F111 (2014) design guideline, which includes:

- Extending the applicability of the BSM model for small pipe sizes by developing an advanced finite element model (i.e., hybrid shell-beam model).
- Investigating the response of small-sized pipelines impacted by the bottom trawl gear, using the finite element method (via the BSM and hybrid models) as well as the analytical method.
- Assessing the potential damage progression effect induced in a subsea pipeline due to a non-perpendicular trawl impact, using the hybrid shell-beam model.
- Investigating the potential damage progression effect induced in a subsea pipeline where the pipe is subject to subsequent trawl impacts at adjacent locations.

The present research project provides a significant engineering contribution by introducing and investigating the pipe's mechanical behaviour, where the pipe is subject to a longitudinal progression of plastic damage. In this respect, the importance of the present thesis is to:

- Introduce the damage progression effect in cylindrical structures.
- Adapt the methodology proposed by Quinton (2015) for plates, to investigate the damage progression effect in pipelines.

- Identify the sources causing the damage progression effect in subsea pipelines, using finite element analyses.
- Conceptualize and design test components to perform a series of physical experiments on a small-sized pipe; in order to study the damage progression effect. The test components are designed to modify the apparatus devised and employed by Quinton (2015) to study the structural response of ship hull structures under sliding loads.
- Perform project administration, conduct the physical tests, and obtain and interpret the test data, including high resolution scanned views of deformed pipes.
- Identify several gaps in the current industry recommended practice (DNV-RP-F111, 2014), with respect to the damage progression effect in small-diameter subsea pipelines:
 - Extend the applicability of the BSM model for small pipe sizes.
 - Propose a new finite element model (the hybrid shell-beam model) to assess the overtrawlability of small pipe sizes and account for the damage progression effect in the pipeline assessment.
 - Highlight the conservatism in overtrawlability assessment of small pipe sizes where the analytical method recommended in DNV-RP-F111 (2014) is employed.

- Identify and investigate the damage progression effect in subsea pipelines, where the pipe is subject to non-perpendicular trawl impacts or repeated trawl impacts at adjacent locations.
- Conceptualize and design a novel PiP system to allow for investigating the damage progression effect in small-diameter PiP products.
- Highlight the effect of damage progression in PiP systems.
- Show the effect of combined loading (axial force and lateral load) on the PiP solution's load-carrying capacity.

1.1.3 Notes on the Research Scope

The present study performs a series of physical tests on a small-diameter pipe. The main objective of performing the physical tests is to provide evidence regarding the effect of damage progression on the plastic capacity of a pipeline, which dictates the test condition. Furthermore, another major research objective of the present study is to identify and introduce applications of damage progression effect in the pipeline industry, particularly in the event of the trawl gear interference with subsea pipelines. As such, the recommendations of DNV-RP-F111 is considered in the design of the physical test components. However, the test setup does not fully represent a scenario of a trawl interference event with a subsea pipeline. Nevertheless, considering the following points, the physical test results could be employed to validate numerical models for a detailed investigation of the trawl impact on a subsea pipeline:

- The dynamic effect of a trawl impact event could be replicated by an equivalent quasi-static analysis, as reported in Shen and Jones (1991). Also, the finding of Shen and Jones (1991) was examined by Zheng et al. (2013) for trawl gear interference with a subsea pipeline, and the authors showed that a pipe response under impact and quasi-static analyses are within the same range. This conclusion was employed as one of the bases of the present work. Accordingly, the physical tests, as well as the majority of numerical simulations in the present thesis, are conducted under the quasi-static condition.

- The direction of the trawl impact is parallel to the seabed, and the pipe-soil interaction is negligible during the trawl interference event (Zheng et al., 2012). As such, the pipe-soil interaction is not incorporated in the physical test.
- The initial phase of the trawl impact (which is the focus of the present scope) occurs in some hundredths of a second (DNV-RP-F111, 2014), and hence the global deformation of the pipe is negligible. As such, the lateral deformation of the specimen in the majority of tests is restrained. Also, throughout the present thesis, the “trawl gear impact” or “overtrawlability assessment of pipelines” only refers to the initial phase of the trawl gear interference event.

Furthermore, the physical tests in the present study employ a two-phase loading condition to investigate the pipe’s response, where in phase 1, the pipe is subject to a perpendicular indentation, and in phase 2, the resulting damage in phase 1 translates and induces along the pipe. In this regard, the first phase partially represents the fishing gear impact on a subsea pipeline (considering the above-mentioned points). However, the second phase was employed (only) to highlight the effect of damage progression on the load-carrying capacity of the pipe, and may not represent any particular scenario in the pipeline industry.

1.1.4 Thesis Outline

The present thesis consists of nine chapters described as follows:

- Chapter 1 presents the background, motivation, scope of the research, objectives, and significance of the current thesis, as well as the co-authorship contribution for the publications presented in Chapters 2 to 7.
- Chapter 2 presents a comprehensive numerical study to introduce the damage progression effect in cylindrical structures.
- Chapter 3 presents an advanced hybrid shell-beam model to be used for the overtrawlability assessment of small-sized subsea pipelines. Also, the results of a physical test conducted in the present research are provided and used to validate the accuracy of the hybrid model.
- Chapter 4 employs the hybrid model developed in Chapter 3 and shows the potential significant drop in the structural resistance of a subsea pipeline where the pipe is subject to a non-perpendicular trawl impact.
- Chapter 5 extends the findings in Chapter 4 by providing test data obtained during the lab-scale tests.
- Chapter 6 presents another application of the damage progression effect where a subsea pipeline is subject to subsequent trawl impacts at adjacent locations. The data recorded during several physical tests are also provided in this chapter.
- Chapter 7 presents a novel investigation on the mechanical behaviour of a PiP system with respect to the damage progression effect as well as combined loading.

The results of the physical test conducted in the present work on a PiP specimen is provided in this chapter.

- Chapter 8 presents the summary and conclusion of the present work.
- Chapter 9 provides recommendations for future studies to extend the findings of the present thesis.

1.2 Co-Authorship Statement

I (Farhad Davaripour) hold the principle author status for all the manuscript chapters (Chapter 2 to 7) in the present thesis.

- Chapter 2 was co-authored by my Ph.D. supervisor Dr. Bruce W.T. Quinton.
- Chapter 3 was co-authored by my Ph.D. Co-supervisor, Dr. Kenton Pike, Ph.D. supervisor Dr. Bruce W.T. Quinton, and industry supervisor, Dr. Richard Persaud.
- Chapters 4 to 7 were co-authored by my Ph.D. supervisor Dr. Bruce W.T. Quinton, and Ph.D. Co-supervisor, Dr. Kenton Pike.

The contributions provided by the co-authors facilitated and enhanced the development of the manuscript chapters. Accordingly, each co-author's contribution is presented in this Section.

1.2.1 Chapter 2 – Article No. 01 (International Pipeline Conference 2018)

Davaripour, F., Quinton, B.W.T., 2018. An Investigation of the Load Carrying Capacity of Pipelines Under Accidental and Longitudinal Moving (Sliding) Loads, in: International Pipeline Conference (IPC).

The individual author contribution is presented in Table 1-1:

Table 1-1 Individual Author Contribution (Paper No. 1 - IPC 2018)

Farhad Davaripour:	Software (LS-Dyna software package), Validation (against the previous study physical test), Formal analysis, Investigation, Data Curation, Writing - Original Draft, Visualization, Project administration
Bruce Quinton:	Writing - Review & Editing, Supervision (leadership and oversight), Acquisition financial support for the project
Farhad Davaripour, and Bruce Quinton:	Conceptualization, Methodology
Bruce Quinton, and Farhad Davaripour	Resources

1.2.2 Chapter 3 – Article No. 02 (Applied Ocean Research 2020)

Davaripour, F., Pike, K., Quinton, B.W.T., Persaud, R., 2020a. An Assessment on the Overtrawlability of Small Pipe Sizes Using a Hybrid Shell- Beam Model: an Alternative to the DNV-RP-F111 Model (Revision Requested). Appl. Ocean Res.

The individual author contribution is presented in Table 1-2:

Table 1-2 Individual Author Contribution (Paper No. 2 – Applied Ocean Research 2020)

Farhad Davaripour:	Conceptualization (identifying the gap in the DNV-RP-F111 design guideline), Methodology (designing a numerical
--------------------	---

	method to address the gap), Software (Abaqus software package), Investigation, Formal analysis, Investigation, Data Curation, Writing - Original Draft, Visualization, Project administration
Bruce Quinton:	Supervision and leadership to conduct a physical test to be used for the validation of the numerical model
Bruce Quinton, and Kenton Pike:	Acquisition financial support for the project - NSERC (Bruce Quinton), and Mitacs Accelerate Program (Bruce Quinton, and Kenton Pike)
Farhad Davaripour, and Richard Persaud:	Validation against the previous study physical tests
Bruce Quinton, Kenton Pike, and Farhad Davaripour	Resources
Kenton Pike, Bruce Quinton, and Richard Persaud:	Writing - Review & Editing, Supervision (leadership and oversight

1.2.3 Chapter 4 – Article No. 03 (Offshore Pipeline Conference 2020)

Davaripour, F., Quinton, B., Pike, K., 2020a. A Numerical Investigation on a Pipe Subject to a Non- Perpendicular Trawl Impact Using a Hybrid Shell-Beam Model, in: Offshore Pipeline Conference (OPT 2020). Amsterdam.

The individual author contribution is presented in Table 1-3:

Table 1-3 Individual Author Contribution (Paper No. 3 – OPT 2020)

Farhad Davaripour:	Conceptualization (identifying a gap in the DNV-RP-F111 design guideline), Methodology (employing the numerical method presented in Chapter 3 to address the gap), Software (Abaqus software package), Formal analysis, Investigation, Data Curation, Writing - Original Draft, Visualization, Project administration
Bruce Quinton, and Kenton Pike:	Acquisition financial support for the project - NSERC (Bruce Quinton), and Mitacs Accelerate Program (Bruce Quinton, and Kenton Pike), Writing - Review & Editing, Supervision (leadership and oversight)
Bruce Quinton, Kenton Pike, and Farhad Davaripour	Resources

1.2.4 Chapter 5 – Article No. 04 (Applied Ocean Research 2020)

Davaripour, F., Quinton, B., Pike, K., 2020c. An Assessment on a Subsea Pipeline Subject to a Diagonal Trawl Impact (Under Review). Appl. Ocean Res.

The individual author contribution is presented in Table 1-4:

Table 1-4 Individual Author Contribution (Paper No. 4 – Applied Ocean Research 2020)

Farhad Davaripour:	Conceptualization (identifying a gap in the current design guideline), Methodology (developing a numerical method to investigate and address the gap), Software (Abaqus software package), Formal analysis, Investigation, Data Curation, Writing - Original Draft, Visualization, Project administration
Bruce Quinton:	Supervision and leadership to conduct a physical test presented in the article and employed for validating the numerical model
Bruce Quinton, and Kenton Pike:	Acquisition financial support for the project - NSERC (Bruce Quinton), and Mitacs Accelerate Program (Bruce Quinton, and Kenton Pike), Writing - Review & Editing, Supervision (leadership and oversight)
Bruce Quinton, Kenton Pike, and Farhad Davaripour	Resources

1.2.5 Chapter 6 – Article No. 05 (Ocean Engineering Journal 2020)

Davaripour, F., Quinton, B.W.T., C, K.P., 2020b. Effect of Damage Progression on the Plastic Capacity of a Subsea Pipeline (Under Review). Ocean Engineering Journal.

The individual author contribution is presented in Table 1-5:

Table 1-5 Individual Author Contribution (Paper No. 5 – Ocean Engineering Journal 2020)	
Farhad Davaripour:	Conceptualization (identifying a gap in DNV-RP-F111), Methodology (developing a numerical model to introduce and investigate an application of the damage progression effect in subsea pipelines), Software (Abaqus software package), Formal analysis, Investigation, Data Curation, Writing - Original Draft, Visualization, Project administration
Farhad Davaripour, and Bruce Quinton	Conceptualization (introducing the progression of damage in a structure under repeated perpendicular indentations at the adjacent locations on the structure)
Bruce Quinton:	Supervision and leadership to conduct the physical tests presented in the article and used for validating the numerical model
Bruce Quinton, Kenton Pike, and Farhad Davaripour	Resources
Bruce Quinton, and Kenton Pike:	Acquisition financial support for the project - NSERC (Bruce Quinton), and Mitacs Accelerate Program (Bruce Quinton, and Kenton Pike), Writing - Review & Editing, Supervision (leadership and oversight)

1.2.6 Chapter 7 – Article No. 06 (Journal of Applied Mechanics 2020)

Davaripour, F., Quinton, B.W.T., C, K.P., 2020b. An Assessment on the Plastic Capacity of Pipe in Pipe Systems under Damage Progression Effect (First Draft Completed). Journal of Applied Mechanics.

The individual author contribution is presented in Table 1-6:

Table 1-6 Individual Author Contribution (Paper No. 5 – Journal of Applied Mechanics 2020)

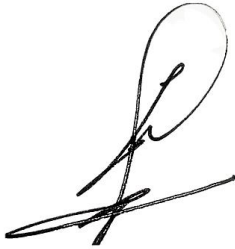
Farhad Davaripour:	Conceptualization, Methodology (devising test components for a pipe in pipe solution to allow for the investigation of the damage progression effect), Software (LS-Dyna software package), Formal analysis, Investigation, Data Curation, Writing - Original Draft, Visualization, Project administration
Bruce Quinton:	Supervision and leadership to conduct the physical test presented in the article and used for validating the numerical model
Bruce Quinton, and Kenton Pike:	Acquisition financial support for the project - NSERC (Bruce Quinton), and Mitacs Accelerate Program (Bruce Quinton, and Kenton Pike)
Bruce Quinton, Kenton Pike, and Farhad Davaripour:	Resources

Bruce Quinton, and
Kenton Pike:

Writing - Review & Editing, Supervision (leadership and oversight)

Farhad Davaripour

Date: August 2020

A handwritten signature in black ink, consisting of a large, stylized loop at the top and several horizontal strokes below it.

2 CHAPTER 2

AN INVESTIGATION OF THE LOAD CARRYING CAPACITY OF PIPELINES UNDER ACCIDENTAL AND LONGITUDINAL MOVING (SLIDING) LOADS¹

Abstract

In accidental scenarios on subsea pipeline systems, like the interference between trawl gear and a subsea pipeline, accidental loads are commonly considered as perpendicular loads that act only normal to the pipe at one location. Hence, the potential considerable effects of damage progression (i.e., under sliding loads) are neglected. In this regard, recent works on ship hull structures showed that the structural resistance mobilized against the sliding loads could be significantly lower than against the perpendicular loads of similar magnitude, when the loads incite plastic damage. As such, it is reasonable to study the novel topic of the effects of damage progression on the load-carrying capacity of pipelines. This paper employs finite element analyses to investigate the effect of damage progression on the plastic capacity of the pipe. The LS-Dyna software package with the explicit time-integration scheme is employed in the numerical simulations. The findings of the present work demonstrate that due to the progression of plastic damage,

¹ This paper was presented and published at the IPC-2018 conference in Calgary, Canada. Some modifications (mainly editorial) are applied to the material of this paper, in order to maintain consistency throughout the thesis.

the load-carrying capacity of the pipe could decrease significantly when the interference load applies plastic damage to the pipe.

Keywords: Moving load, Damage progression, Pipeline, Finite element analysis

2.1 Introduction

The load-carrying capacity of any structure is not a single value but is dependent on many variables, including the loading and boundary conditions. A single structure may have different load-carrying capacities against a perpendicular versus a moving (sliding) load. Based on the current regulation for submarine pipeline systems (DNV-OS-F101, 2013), “the design against accidental loads may be performed by direct calculation of the effects imposed by the loads on the structure, or indirectly, by design of the structure as tolerable to accidents”. In common engineering problems, these calculations against accidental loads are done based on perpendicular loads. Whereas, in load scenarios like the interference between trawl gear and a subsea pipeline, loads are often applied in a way that would be better modelled as accidental moving loads. For this discussion, moving loads are loads that act not only normal to the cylinder but at the same time translate laterally along the cylinder. The term “moving load” does not refer to the magnitude of the load; it refers to the location with respect to time.

The load-carrying capacity of a structure may be dependent on the load path if the load results in plastic deformation (or plastic damage) on the structure. The path-dependent behaviour of a structure subject to a moving load refers to the present effects of plastic strains imposed by a moving load at an earlier time. In other words, the history of plastic damage to a structure affects the behaviour of the structure at any given time.

There are multiple studies on moving load problems, where a moving load applies path-dependent behaviour to a structure. Parkes (1958) was one of the pioneers in studying the plastic behaviour of a beam subject to a moving load. He recommended a solution for a travelling mass on a massless rigid plastic beam. Symonds and Neal (1960) extended the Parkes's results by including mass to the rigid plastic beam. Toridis and Wen (1966) presented an analytical solution for the dynamic response of an elasto-plastic beam subject to a moving load. The authors modelled the beam with a series of massless rigid panels connected via flexible joints with a point mass. Frýba (1999) provided analytical solutions for many examples of simple moving load problems. He presented a solution for a case of the rigid plastic beam subject to a moving load with a stationary plastic hinge in the middle of the beam.

In recent years, several works have examined the plastic capacity of ship hull structures during grounding on soft-bottom events or collisions with moving ice loads, where the moving load imposes plastic damage on the structure that does not cause tearing (Hong, 2008; Quinton, 2008). The plastic capacity refers to the load-carrying capacity of the structure against the lateral indentation, where the lateral load imposes plastic damage on the structure. Quinton (2008) defined the term moving load effect as the phenomenon of the reduced plastic capacity of a grillage structure, where a substantial moving load induces and translates plastic damage along the structure. This reduction is defined with respect to the change in the hull's response during two load cases, including case-1, where

the grillage is subject to a perpendicular indentation, and case-2, where the resulting dent depth in case 1 is translated along the carriage. The present paper extends the study conducted by Quinton (2008) on a cylindrical structure. Also, the term damage progression effect is used interchangeably with the moving load effect throughout the present paper.

The present work investigates the progression of plastic damage on the load-carrying capacity of a cylindrical structure, where the moving load only imposes local deformation (not bending/global deformation) on the cylinder, and the resulting damage does not cause tearing on the cylinder. Throughout the present study, the effect of dent size on the damage progression effect is studied. Furthermore, the source of this effect is investigated with respect to the equivalent stress distribution in a cylinder during the progression of plastic damage.

2.2 Moving (Sliding) Load Versus Perpendicular Load

A Perpendicular load refers to a load that acts only normal to a cylindrical structure at one location. It may vary in magnitude, but does not translate along the cylinder. A moving load is a load that may vary in magnitude and lateral position, i.e. it acts not only normal to a cylinder but at the same time translates laterally along the cylinder. As a general definition of a moving load acting on a cylinder, the load has two components: one normal and another lateral to the cylinder. Figure 2-1 demonstrates a schematic view of a cylinder under a perpendicular load (a) and under a moving load (b). However, the present work only examines a particular definition of a moving load where the load is perpendicular to a cylinder and slides along the cylinder, as presented in Section 2.3.2.

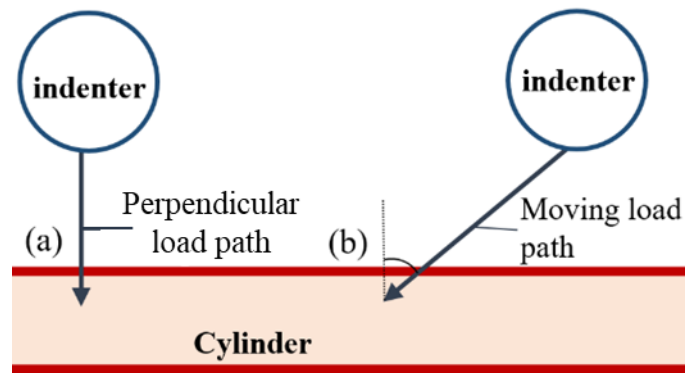


Figure 2-1 Schematic View of a Perpendicular Load Path (a) Versus a Moving Load Path (b)

Considering the progression of plastic damage along a cylinder, where the cylinder is subject to a substantial moving load, the part of the cylinder behind the moving load is termed as the trailing side, and the part ahead of the moving load is termed as the leading

side. As shown in Quinton et al. (2010), under a perpendicular load, the stress contour is symmetrical (unless prevented by some geometric conditions). However, when the resulting damage progresses along the structure, the trailing side has less contribution in the load-carrying capacity of the grillage compared to the leading side. In this regard, the authors stated that the membrane stress, bending moment, and through-thickness shear responses are smaller on the trailing side of the structure compared to the leading side, which is considered as the main source of the damage progression effect.

Quinton (2008) conducted numerical investigations and demonstrated that the lateral motion of an applied indentation would lower the structural capacity of a ship hull if the indentation causes plastic damage to the structure. This finding was later verified via experimental tests by Quinton (2015; 2017). Quinton (2008) stated that in the case of a hull structure subject to a moving load inciting only elastic behaviour, the load-carrying capacity of the structure is similar to the one subject to a perpendicular load of equal magnitude. In addition, the author showed that the damage progression effect in a hull structure is negligible when a moving load incites minimal localized plastic damage. The moving load examined in Quinton (2008) refers to a perpendicular load that slides on the carriage.

2.2.1 Response of a Cylinder Under a Perpendicular and Moving Load

Understanding the response of a cylinder under a perpendicular load is crucial to get a better insight regarding the damage progression effect. In this regard, Thomas and co-workers (1976) did a series of tests on a simply-supported thin-walled cylinder subject to a perpendicular indentation. In the experiments conducted by Thomas et al. (1976), as shown in Figure 2-2, the deformation modes are categorized into three levels, including (a) the pure crumpling mode, which is a nonlinear plastic response; (b) the combination of crumpling and bending mode, where during this phase, the bending response is either elastic or plastic; (c) the structural collapse, which occurs by the formation of plastic hinges on the cylinder and in the wake of the indentation.

As stated by Thomas et al. (1976), the primary deformation mode of a cylinder subject to a perpendicular indentation starts with localized crumpling (plastic damage) at the top surface of the cylinder. During the pure crumpling deformation, the force increases rapidly until the bottom of the cylinder starts contributing to the response. Then, a combination of bending and crumpling deformations occurs, which leads to a slightly less stiff response. Finally, the cylinder collapses, followed by a drop in the force-displacement curve.

Based on the length, diameter, and thickness of a cylinder, the pure bending phase as another form of deformation should also be considered. This mode of deformation is

important in cases where bending response occurs before the crumpling phase, i.e. when the pipeline is dragged by trawl gear during the interference between trawl gear and a subsea pipeline.

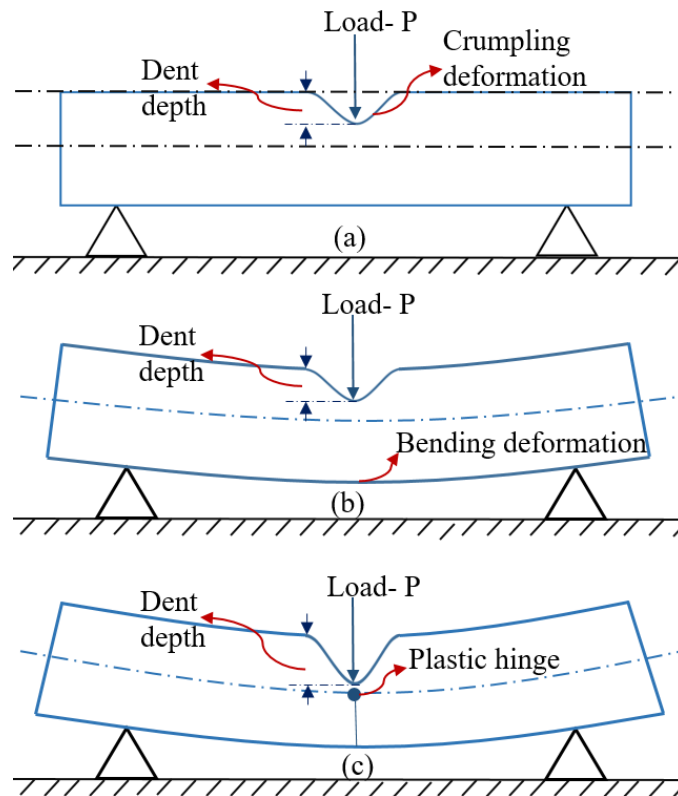


Figure 2-2 Deformation Modes of a Cylinder Under a Perpendicular Load: Crumpling Mode (a), a Combination of Crumpling and Bending Mode (b), and Structural Collapse Mode (c) (Edited and Redrawn from Thomas et al. (1976))

Similarly, deformation modes of a cylinder under a moving load could be categorized into (a) the pure crumpling mode; the present work only considers this deformation mode; (b) the pure bending mode, including elastic or plastic bending; (c) the combination of

crumpling and bending mode, including the crumpling and elastic bending or the crumpling and plastic bending; (d) the structural collapse.

2.3 Methodology

2.3.1 Time Integration Scheme for the Finite Element Analysis

As the progression of plastic damage on a cylindrical structure shows extreme nonlinearity, the solution requires a finite element (FE) code capable of modelling nonlinearities in geometry, material, and boundary conditions. In addition, the contact between an indenter and a cylinder, which is a transient behaviour, requires time integration at a small time-step. An explicit time integration code can handle all of these features and effectively find solutions for moving load problems. However, theoretically, using nonlinear implicit FE analysis may produce the same results. But in practice, due to the short time-steps required to capture unstable, transient, and nonlinear responses, as well as the difficulties in achieving convergence in each time step, the implicit code is inefficient for the application of moving load scenarios (B. Quinton et al., 2017). Accordingly, the present paper employs numerical simulation to investigate the progression of plastic damage on a cylindrical shell (geometries are shown in Figure 2-3) using explicit FE analysis with the LS-Dyna software package

2.3.2 Loading Condition

According to the main scope of the present work, which is to provide numerical evidence regarding the effect of damage progression on the plastic capacity of a pipe where the pipe is subject to a moving load, the following two steps loading condition is employed:

step 1, where the cylinder is under a perpendicular indentation, and step 2, where the vertical position of the indenter is maintained, and the indenter translates longitudinally along the cylinder. The second step represents a moving (sliding) load. Using this two steps loading condition, it is possible to examine the change in the load-carrying capacity of the cylinder by the initiation and during step 2 of loading.

2.3.3 Rupture-Type Versus Non-Rupture Type Moving Loads

To study the moving load effects on cylindrical shells, it is crucial to classify the moving loads into: first, non-rupture type moving loads, which does not cause tearing on the cylinder; second, rupture-type moving loads, which leads in tearing. This work only studies some aspects of the non-rupture type moving loads.

Regarding the rupture-type moving loads, Bao and Wierzbicki (2004) did a series of tests on aluminum alloy. The authors demonstrated that the ductile fracture is a function of stress triaxiality, in addition to the strain intensity. Further, Bai and Wierzbicki (2008) showed that for some metals, the fracture ductility is also dependent on the third deviatoric stress invariant (lode angle). Accordingly, these findings might be applicable to the case of rupture-type moving loads on cylindrical steel shells, which is not within the scope of the present paper.

2.4 Numerical Simulation

For validating the accuracy of the numerical model, experimental results presented in Ruggieri and Ferrari (2004) are employed. Accordingly, similar input parameters, as reported in Ruggieri and Ferrari (2004), are utilized in the present work. In this regard, the analyses are performed using the LS-Dyna software package for a 4 ½” O.D. (114 mm) API N80 pipe (580 MPa yield stress) with 7 mm thickness and 1 m length. Also, the analyses are conducted under the quasi-static condition. The kinetic energy is controlled to be less than 5% of the internal energy during the analyses.

The material properties of the pipe are extracted based on the true stress-strain response of the API N80 steel at room temperature, as shown in Figure 2-3. The true stress-strain response is converted from the engineering stress-strain curve, presented by Ruggieri and Ferrari (2004), using Equation 2-1 and Equation 2-2:

$$\varepsilon_{true} = \ln(1 + \varepsilon_{eng}) \quad \text{Equation 2-1}$$

$$\sigma_{true} = \sigma_{eng}(1 + \varepsilon_{eng}) \quad \text{Equation 2-2}$$

Where, σ_{true} is the true stress, ε_{true} is the true strain, σ_{eng} is the engineering stress, and ε_{eng} is the engineering strain.

In order to implement the true stress-strain curve, piecewise-linear-plasticity material in LS-Dyna software is employed. Other material input parameters are employed based on Table 2-1. Also, for the indenter, the rigid material property is implemented using the input parameters presented in Table 2-1.

Table 2-1 Material Model Inputs for the Cylindrical Shell and the Tube-Shaped Indenter

Density_ kg/m ³	Elasticity modulus_ MPa	Poisson's ratio
7850	2e5	0.3

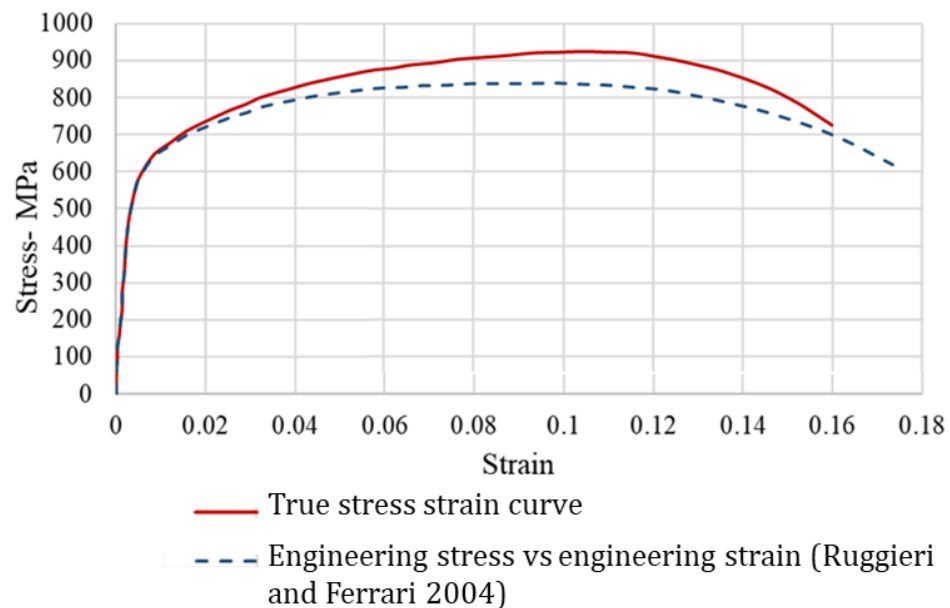


Figure 2-3 Engineering and True Stress-Strain Response for the API N80 Steel at Room Temperature

Figure 2-4 demonstrates the geometry of the model, including the cylinder and the indenter. For the purpose of benchmarking the model against the experiment conducted by Ruggieri and Ferrari (2004), all nodes at both ends of the pipe are constrained using

the Constrained-Nodal-Rigid-Body-Spc feature in LS-Dyna software; translational degrees of freedom at y and z are fixed.

This work only investigates the crumpling deformation of a cylinder under a moving load. Hence, to avoid the bending response, two new conditions are later applied to the cylinder, in addition to the previously applied boundary conditions: (a) the bottom of the pipe is fixed in y and z directions; (b) due to the translational movement of the indenter during the moving step, nodal-rigid-bodies at both ends of the beam are fixed at x-direction; the geometry of the model is shown in Figure 2-4.

Moving loads are applied in two steps: first, the indenter is pushed into the pipe for 2.5 mm; second, the indenter translates longitudinally along the pipe for 100 mm. Each of these steps is performed in 0.5 sec. The penalty contact method using the automatic-surface-to-surface feature in LS-Dyna is used during the analysis. Also, the friction coefficients between the indenter and the cylinder are assumed equal to zero to study the moving load effect without the influence of the friction. The pipe is modelled with thick shell elements with the mesh size of 2 mm on the surface, and 2.33 mm through the thickness (three mesh layers), using one point reduced integration thick-shell elements with a shear correction factor equal to $5/6$. The tube-shaped rigid indenter is modelled with solid elements with 1 mm mesh size on the surface and 1 mm mesh size through the thickness (one mesh layer).

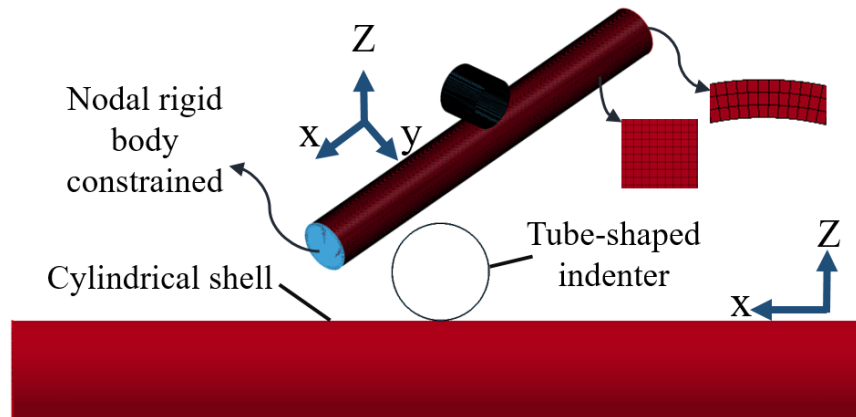


Figure 2-4 Numerical Model Geometries

2.4.1 Benchmarking

The numerical simulations are validated only for step 1 of the loading, where the cylinder is subject to the perpendicular indentation. During the moving step, stress distribution on the pipe is compared against the findings of Quinton et al. (2012).

Figure 2-5 demonstrates the contact force in the wake of the indentation versus the dent depth during the perpendicular step. The dent depth is measured based on the point with the most deformation referenced to the undamaged element of the outer surface of the pipe (the element without plastic strain), as shown in Figure 2-2.

Figure 2-5 shows that the numerical results of this work reasonably capture the behaviour of the pipe during the dent depth of 20 mm. For dent depth less than 10 mm, the prediction of this study underestimates the experimental results, which are due to the errors in the

experimental measurement for small values of dent depth, as stated by Ruggieri and Ferrari (2004). For the dent depth greater than 10 mm, the results of this work are in good agreement with the experimental results. Furthermore, the numerical prediction of this work is in an excellent agreement with the numerical results conducted by Ruggieri and Ferrari (2004).

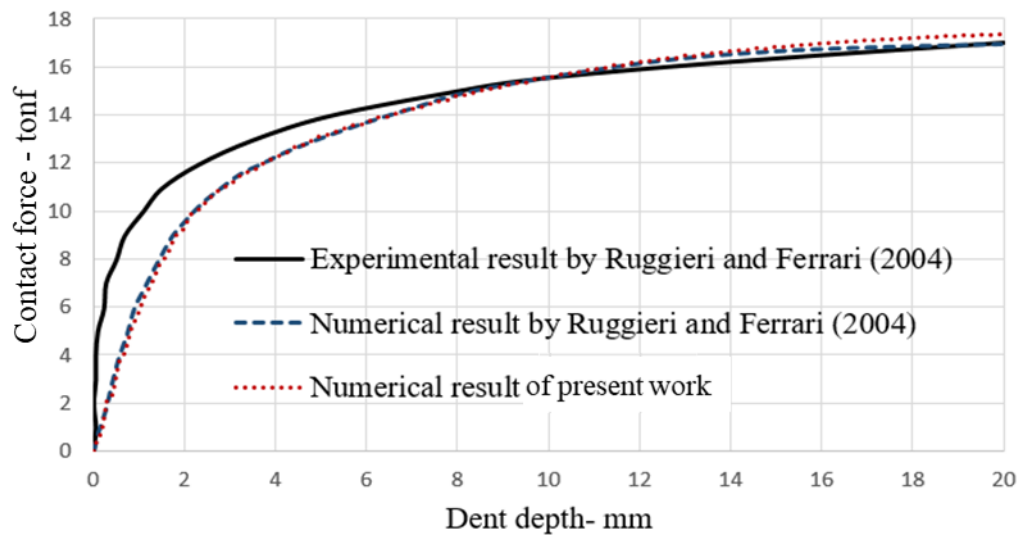


Figure 2-5 Contact Force in the Wake of the Indentation Versus Dent Depth

2.4.2 Mesh Convergence Analysis

Three mesh sizes, including 1.5 mm, 2 mm, and 2.5 mm, were examined for the surface of the cylindrical shell. For all cases, the thickness of the cylinder was meshed in three layers. Figure 2-6 shows that during the simulation, all mesh sizes converge to similar resultant forces. In the present work, the mesh size of 2 mm is selected for the analyses.

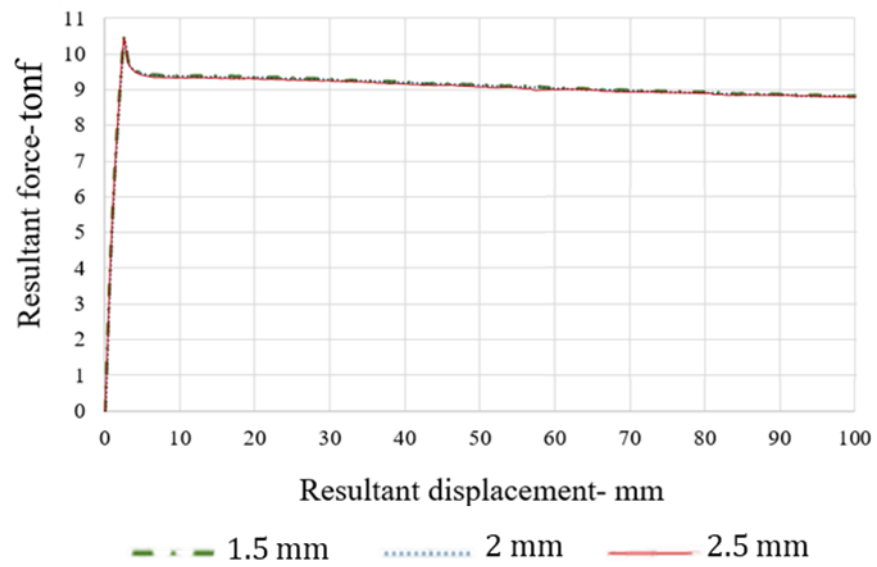


Figure 2-6 Resultant Force Versus Resultant Displacement Using Varied Mesh Sizes Including 1.5, 2.0, and 2.5 mm

2.5 Results and Discussion

2.5.1 Damage Progression Effect

Figure 2-7 shows the resultant force versus time during perpendicular and moving steps with geometries shown in Figure 2-4. The indentation at the end of the perpendicular step is 2.5 mm followed by the 10 mm lateral motion of the indenter during the moving step. Figure 2-7 shows that by the onset of the moving step, the plastic capacity of the cylinder drops significantly, almost 10%. This reduction introduces a new mechanical behaviour in cylindrical structures, where the cylinder is subject to a substantial lateral load, which slides along the cylinder.

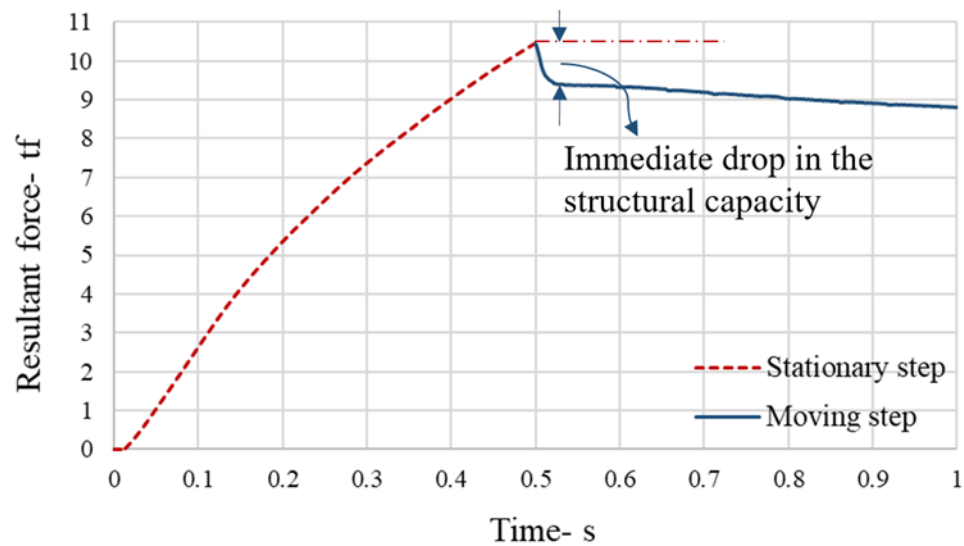


Figure 2-7 Resultant Force Versus Time During Perpendicular and Moving Loading Steps

2.5.2 Effective Stress Distribution

Figure 2-8 demonstrates the von-Mises contour plot of a cylinder during the perpendicular step (a) and moving step (b). It shows that during the perpendicular step, the response of the cylinder is symmetrical. Whereas, by the onset of the moving step, the cylinder on the trailing side of the moving load resists less than the leading side. Therefore, the response of the cylinder subject to the moving load is not symmetrical. These results are in agreement with the findings of Quinton (2012). The lower structural resistance, mobilized on the trailing side of the cylinder during the moving step, is considered as the main source of the damage progression effect.

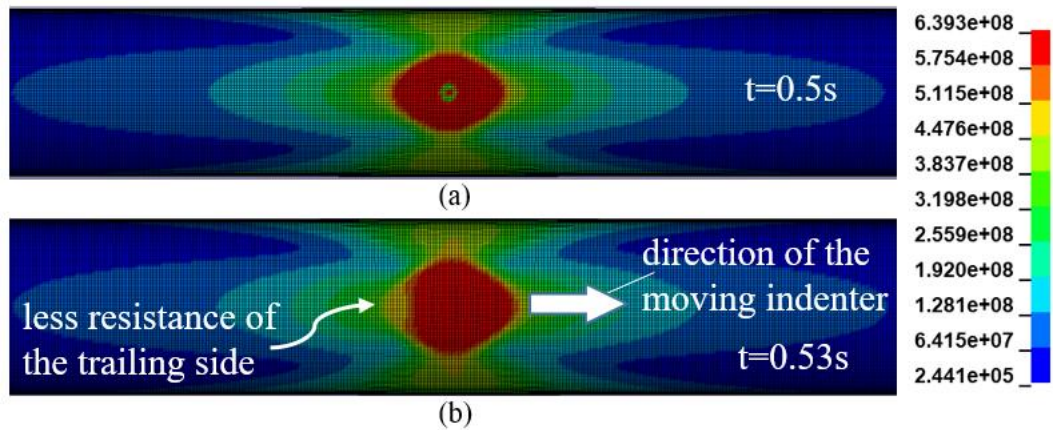


Figure 2-8 Equivalent Stress Contour Plot of a Cylinder at the Region of Indentation, Subject to a Perpendicular Load (a), and a Moving Load (b)

2.5.3 Sensitivity Study

Quinton (2015) showed that the damage progression effect occurs in a ship hull structure if a moving indenter imposes plastic damage on the structure. As such, in this section, the damage progression effect under five different indentation levels is investigated: 2.5, 1.25, 0.625, 0.3125, and 0.15625 mm; where the response of the cylinder under the indentation level of 0.15625 mm is elastic, and under 0.3125 mm is elastic with localized plastic damage.

Figure 2-9 shows the resultant force versus resultant displacement under five indentation levels. It shows that increasing the indentation level raises the resultant forces. In addition, when the cylinder's response is purely elastic (indentation level equal to 0.15625 mm), there is no damage progression effect. Furthermore, the damage progression effect under minimal localized plastic response (indentation level equal to 0.3125 mm) is insignificant. In conclusion, the damage progression effect only appears in the case where the moving load applies plastic damage to a cylinder (indentation levels equal to 2.5 and 1.25 mm). These findings are in agreement with the results of Quinton (2015).

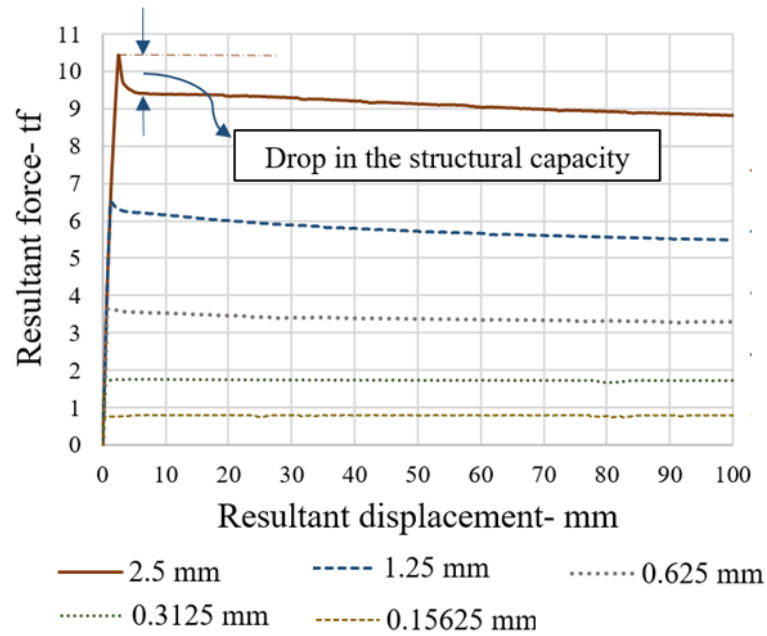


Figure 2-9 Resultant Force Versus Resultant Displacement Under Varied Indentation Levels, including 0.15625, 0.3125, 0.625, 1.25, and 2.5 mm

Figure 2-10 demonstrates the damage progression effect versus the normalized indentation (indentation/diameter, NI) for the above-mentioned indentation levels. The damage progression effect is calculated based on the peak force in the perpendicular step over the average of the residual forces during the moving step. The graph indicates three levels, including: first, a low slope for normalized indentation level $(NI) < 0.27$; then, a sharp increase for $0.27 < NI < 0.55$; finally, a medium rise for $0.55 < NI < 2.2$. An empirical equation (Equation 2-3) is extracted from the graph, which reasonably captures the results for $NI > 0.27$, for the pipe used in this study with a diameter over thickness (D/t) equal to 16.3. The validation of Equation 2-3 with respect to variables such as different D/t , internal pressure, and etc., is not within the scope of the present work.

$$y = 5.95 * \ln(x) + 8.5$$

Equation 2-3

Where y is the damage progression effect, and x is the normalized indentation, both in percent.

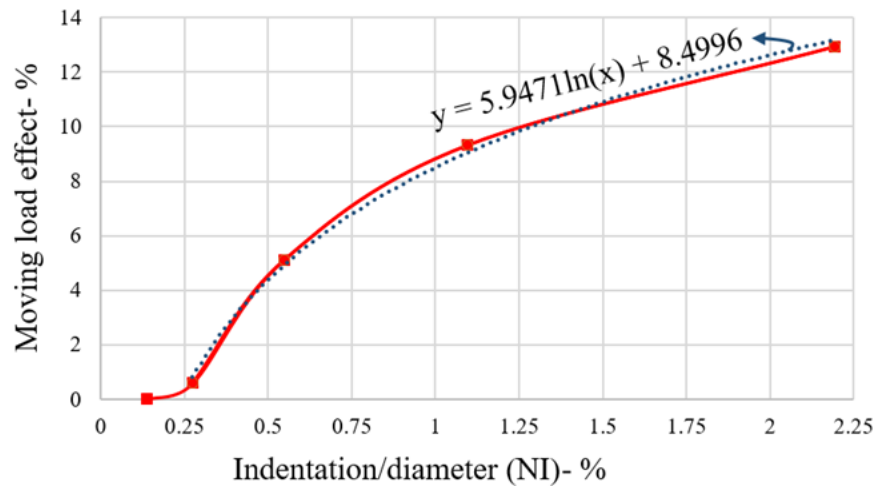


Figure 2-10 Damage Progression Effect Versus Normalized Indentation Level

2.6 Conclusions

Throughout the present study, the authors demonstrate that the progression of plastic damage along a cylindrical structure results in a lower plastic capacity of the cylinder. This reduction is in comparison with the case that the cylinder is subject to a perpendicular indentation. As a result, disregarding the damage progression effect in the assessment of cylindrical structures, subject to a substantial lateral load, could lead to a significant underestimation of the load-carrying capacity of the structure.

It was shown that the damage progression effect occurs only if the imposes plastic damage on the structure. Therefore, there is no damage progression effect during the elastic response. Furthermore, under minimum localized plastic response, the damage progression effect is negligible. In addition, this study shows that the main source of the moving load effect is due to the lesser structural contribution of the trailing side of the pipe during the moving scenario, compared to the leading side.

Future Works

This paper studied some aspects of the non-rupture type moving loads. For future works, the structural response of a cylinder under the lateral motion of an indentation causing failure (rupture-type moving load) should be investigated. Accordingly, studying the triaxiality and lode parameter of a cylindrical shell subject to a moving load is recommended.

The present work investigated the specific load cases where the cylinder is subject to a perpendicular indentation, which is then followed by the translation of the resulting damage along the cylinder. Also, as another loading scenario, the damage progression effect could be studied where the cylinder is subject to a diagonal load.

The numerical studies in the present work were conducted under the quasi-static condition. In this regard, for future works, the effect of damage progression in a cylinder subject to a lateral impact load is recommended. Furthermore, sensitivity studies on the effect variables such as D/t , internal pressure, and etc., should also be studied in future works. In this regard, the findings of the sensitivity studies should be employed to improve and validate the empirical equation (Equation 2-3) derived in the present work.

Acknowledgments

This research became possible through the funds provided by the Natural Sciences and Engineering Research Council's (NSERC) Discovery Grant program.

References

- Bai, Y., and Wierzbicki, T. (2008). “A new model of metal plasticity and fracture with pressure and Lode dependence.” *International Journal of Plasticity*, 24(6), 1071–1096.
- Bao, Y., and Wierzbicki, T. (2004). “On fracture locus in the equivalent strain and stress triaxiality space.” *International Journal of Mechanical Sciences*, 46(1), 81–98.
- DNV-OS-F101. (2013). Det Norske Veritas - DNV-OS-F101: Submarine pipeline systems.
- Fryba, L. (1999). *Vibration of solids and structures under moving loads*. Telford, London, Springer.
- Hong, L. (2008). “Simplified analysis and design of ships subjected to collision and grounding.” PhD thesis, Norwegian University of Science and Technology.
- Parkes, E. W. (1958). “How to cross an unsafe bridge.” *A Diversion in Dynamic Plasticity. Engineering*, 186, 606–608.
- Quinton, B. (2008). “Progressive damage to a Ship’s structure due to ice loading.” Master thesis, Memorial University of Newfoundland.
- Quinton, B. (2015). “Experimental and numerical investigation of moving loads on hull structures.” PhD thesis, Memorial University of Newfoundland.
- Quinton, B., Daley, C. G., and Gagnon, R. E. (2012). “Realistic moving ice loads and ship structural response.” *Proceedings of the Twenty-second International Offshore and Polar Engineering Conference*, 17–22.

- Quinton, B. W. T., Daley, C. G., and Gagnon, R. E. (2010). "Effect of Moving Ice Loads on the Plastic Capacity of a Ship's Structure." Icetech 2010. Anchorage, Alaska.
- Quinton, B. W. T., Daley, C. G., Gagnon, R. E., and Colbourne, D. . (2017a). "Experimental investigation of accidental sliding loads on the response of hull plating." 6th International Conference on Marine Structures (MARSTRUCT 2017), 8-10 May, Lisbon, Portugal.
- Quinton, B. W. T., Daley, C. G., Gagnon, R. E., and Colbourne, D. B. (2017b). "Guidelines for the nonlinear finite element analysis of hull response to moving loads on ships and offshore structures." Ships and Offshore Structures, Taylor & Francis, 12(October), S109–S114.
- Ruggieri, C., and Ferrari, J. A. (2004). "Structural Behavior of Dented Tubular Members Under Lateral Loads." Journal of Offshore Mechanics and Arctic Engineering, 126(2), 191.
- Symonds, P. S., and Neal, B. G. (1960). "Traveling loads on rigid-plastic beams." Journal of the Engineering Mechanics Division, ASCE, 86(1), 79–90.
- Thomas, S. G., Reid, S. R., and Johnson, W. (1976). "Large deformations of thin-walled circular tubes under transverse loading—I: an experimental survey of the bending of simply supported tubes under a central load." International journal of mechanical sciences, Elsevier, 18(6), 325in3327-326in6333.
- Toridis, T. G., and Wen, R. K. (1966). "Inelastic response of beams to moving loads." Journal of the Engineering Mechanics Division, ASCE, 92(6), 43–62.

3 CHAPTER 3

AN ASSESSMENT ON THE OVERTRAWLABILITY OF SMALL PIPE SIZES USING A HYBRID SHELL-BEAM MODEL: THE INITIAL TRAWL IMPACT PHASE

Abstract

Fishing activity in offshore areas associated with oil and gas development presents a risk to the structural integrity of subsea pipelines from trawl gear interactions. In this regard, DNV-RP-F111 is the industry recommended practice and proposes a beam and spring-mass (BSM) model as well as an analytical method to assess the overtrawlability of pipelines. However, the recommended practice is only applicable for pipelines with an outer diameter of more than 10-inch. Accordingly, the present paper proposes an alternative model (the hybrid shell-beam model) to extend the applicability of the BSM model for small pipe sizes. Furthermore, the BSM, analytical, and hybrid models are examined and compared for a case of 5-inch pipe diameter. Accordingly, for the 5-inch pipe, the resulting dent depth predicted by both the BSM and the hybrid model is very close; however, the BSM model is relatively non-conservative and slightly underestimates the resulting dent depth on the pipe by 6.5%, compared to the hybrid model. Furthermore, using the analytical model leads to a very conservative dent depth on the pipe, especially for small pipe sizes. In conclusion, the hybrid model is a suitable alternative to the BSM model for small pipe sizes.

Keyword: Trawl Impact, Subsea Pipeline, Hybrid Shell-Beam Model, Beam and Spring-Mass Model, DNV-RP-F111

3.1 Introduction

The accidental events which could cause damage to pipelines are either impact or pull-over/hooking (DNV-RP-F107, 2010). This paper investigates the case of a small-diameter subsea pipeline subject to an accidental impact by a trawl board using numerical simulation with the finite element method. In this regard, only the initial phase of the trawl gear impact, which occurs in some hundredths of a second, where the pipe's response is mainly local (DNV-RP-F111, 2014), is within the scope of the present work.

3.1.1 Literature Review

Fishing activities in offshore areas with oil and gas developments put the oil and gas assets, including subsea structures and flowlines, at risk of impact from trawling fishing gear. To mitigate this risk, the following strategies are often employed: rock dump, trenching/burial, and protective coating. These mitigation strategies add significant project costs and may be unnecessary in cases where either the flowline structural capacity is sufficiently high to withstand the impact load (pipeline is overtrawlable), or where the frequency of impact is sufficiently low so that the trawl gear impact could be disregarded. An assessment of flowline overtrawlability is therefore recommended, which could lead to a feasible solution and save a significant cost in the project.

The structural response of a pipe under a transverse impact has been the subject of several studies. Accordingly, many parameters, such as loading condition, impact directionality, and indenter shapes, have been investigated. In this regard, those works that studied a pipeline subject to a transverse indentation by a front round-shaped indenter are more relevant to the overtrawlability problems, e.g., (Ellinas and Walker, 1983). Ellinas and Walker (1983) presented a semi-empirical model partially based on the experimental data of Thomas et al. (1976). The authors assumed that the pipe structural response could be decoupled into two separate phases, including the purely local and the combination of local and global deformation. However, Zheng et al. (2012) conducted experimental and numerical investigations and concluded that from the very beginning of the impact, the pipe has both local and global modes of deformation. The authors stated that the local deformation grows faster at the beginning; then, global deformation increases as the change in the geometry of the pipe cross-section affects the bending stiffness of the pipe (Zheng et al., 2012).

The idealized model of the trawl impact has been investigated by several studies. Soreide and Amdahl (1982) did physical tests and investigated the structural response of a tube under the clamped boundary condition with and without axial restraints at both ends of the specimen. The authors did physical tests under both quasi-static and impact conditions, with the indentation rate set to 0.15 and 54 mm/sec, respectively. Alexander (2007) presented the results of the experimental and numerical investigation with an

attempt to provide a general insight regarding the major defect classifications in a subsea pipeline, as well as methodologies to examine these defects. The author studied several dropped object events on a 12-inch pipe, including one with the indenter mass equal to 10900 kg falling from 9.1 m height which leads to an impact velocity much greater than common trawling impact events.

Jones and Birch (1996) did a series of impact tests on 54 pressurized specimens under a wedge-shaped indentation with very high impact velocity, 13.6 m/sec. The tests were designed to be performed under the fully clamped boundary condition. The authors discussed the failure modes in the pipeline under different range of the imposed energy and internal pressure. Ng and Shen (2006) investigated the inelastic structural response of 52 pressurized mild steel pipes, using physical impact tests. The authors examined the failure of the specimens by incorporating the foundation support in the test setup. They concluded that the circumferential stress developed by the pipe foundation interaction could dramatically affect the failure threshold for pipelines. However, during the trawl impact on a subsea pipeline, unless if the pipeline is partially buried, the pipe-soil interaction is insignificant, as the impact direction is along the seabed.

Currently, DNV-RP-F111 (2014): Interference Between Trawl Gear and Flowlines is the industry recommended practice for flowline design against trawl gear interaction. Based on DNV-RP-F111(2014), the interference between trawl gear and a flowline can be

considered in three distinct phases: impact, pull-over, and hooking. The present study only examines the initial impact phase, which is a short duration interaction (i.e., some hundredths of a second) that occurs when a flowline is contacted by trawl gear. Due to the short duration, global flowline deformation and pipe-soil interaction are negligible during this phase; the initial impact is mostly withstood by the pipe-wall as well as any protective coatings. The trawl impact load throughout this paper refers to the load applied by trawl gear during the initial impact phase.

Based on how the trawl net is kept open, there are two categories of trawl types (DNV-RP-F111, 2014), including beam trawls, which use a transverse beam, and otter trawls, which use trawl boards. The first method typically occurs in shallow waters around 100 m depth (Bai and Bai, 2005). The latter trawl type is within the scope of the present study.

DNV-RP-F111 (2014) proposes two methods to assess the structural response of a flowline under the impact phase, including the analytical method and the finite element method. The first approach (termed as the simplified method in DNV-RP-F111(2014)) conservatively assumes that all the impact energy is absorbed by the pipe wall thickness. The latter approach (termed as the advanced method in DNV-RP-F111 (2014)) is based on a Beam and Spring-Mass (BSM) model. In the BSM model, the pipe is idealized with beam elements representing the global stiffness of the pipe, and a spring representing the local shell stiffness of the pipe. Furthermore, the BSM model could include the stiffness

of concrete coating and insulation protection of a flowline using springs. Also, the energy dissipation during the global flowline deformation and pipe-soil interaction could be accounted for in the BSM model in a simplified manner.

As reported in DNV-RP-F111 (2014), the DNV recommendation is only applicable for pipe sizes larger than 10-inch. However, smaller pipelines are commonly used in offshore projects. As such, the present work examines the results of the BSM and analytical model for a 5-inch pipe size against the novel model (hybrid shell-beam model), which is the improved version of the BSM model.

3.1.2 Objectives

The objectives of this paper are to (a) improve the BSM model and propose a novel and numerically efficient model (hybrid shell-beam model) to assess the overtrawlability of small pipe sizes; (b) assess the results of the analytical method and BSM model for a 5-inch pipe size against the hybrid model; (c) highlight the importance of using finite element methods (via BSM or hybrid model) to examine the overtrawlability of small pipe sizes, versus the analytical method.

Accordingly, first, the analytical method, as well as the BSM and hybrid models, are presented. Then, the BSM model is validated against the example in appendix B of DNV-RP-F111 (2014), and the hybrid shell beam model is accompanied by partial validation

against physical test data (the physical tests conducted in the present work and the previous work by Zheng et al. (2013)). Finally, the analytical and finite element methods are employed to assess the overtrawlability of a 5-inch pipe, followed by sensitivity analyses for the pipe sizes of 10 and 14-inch.

3.2 Methodology

3.2.1 Analytical Method

The analytical approach is based on the assumption that all the energy of the impact is absorbed locally by the bare pipe; correction factors are also used to account for the energy absorption by the global pipe deformation, as well as the pipe-soil interaction (DNV-RP-F111, 2014). Accordingly, the dent depth is calculated based on Equation 3-1, where the F_{sh} is obtained from Equation 3-2 and Equation 3-3 (DNV-RP-F111, 2014):

$$H_{pc} = H_t - H_e = D \cdot [F_{sh}/m_p \cdot \alpha]^{1/\beta} - [F_{sh}/(m_p \cdot 6 \cdot 10^3) \cdot \sqrt{D^3/t}] \quad \text{Equation 3-1}$$

$$F_{sh} = m_p \cdot \alpha \cdot [(E_{loc}/m_p \cdot D) * (\beta + 1)/\alpha]^{\beta/(\beta+1)} \quad \text{Equation 3-2}$$

$$E_{loc} = \max \left(\frac{E_s}{E_a} \right) \quad \text{Equation 3-3}$$

Where H_{pc} is the estimated permanent plastic dent depth; H_t is the total dent depth; H_e is the elastic dent depth; F_{sh} is the maximum impact force experienced by the pipe shell; m_p is the plastic moment capacity for a pipe (Equation 3-5); α and β are factors calculated based on separate equations (Equation 3-6 and Equation 3-7); E_{loc} is the kinetic energy; E_s is the impact energy associated with the steel mass of the trawl board; E_a is the impact energy associated with the added mass of the trawl board.

3.2.2 Numerical Simulation

The Abaqus explicit software package was used to conduct numerical studies using the finite element method. In this section, the BSM and the hybrid models are presented.

3.2.2.1 BSM Model

Figure 3-1 shows a schematic view of the BSM model, where K_{ps} is the effective soil stiffness; it is modelled using discrete springs attached to beam elements. K_{pb} is the effective stiffness of steel pipe; it is modelled using beam elements and represents the global stiffness of a pipeline. K_s is the local shell stiffness of a steel pipe; it is modelled by a nonlinear spring with the stiffness obtained from the force versus indentation behaviour given in Equation 3-4. K_t is the in-plane stiffness of the indenter. K_a is the out-of-plane stiffness of the indenter. M_p is the pipe mass. M_t is the indenter mass. M_a is the added mass.

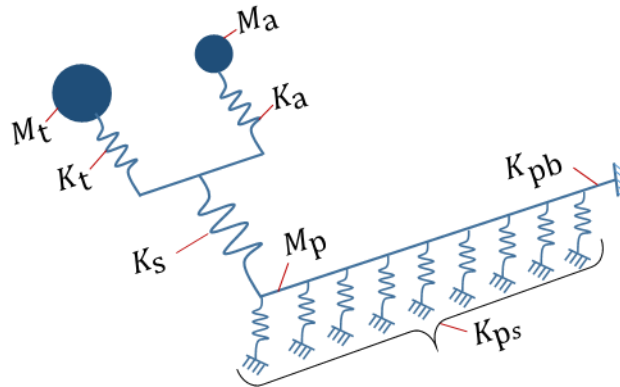


Figure 3-1. Schematic View of the BSM Model

$$f = m_p \cdot \alpha \cdot (H_t/D)^\beta \quad \text{Equation 3-4}$$

Where f is the impact force applied to the pipe shell, H_t is the total dent depth, m_p is the moment capacity of the pipeline (Equation 3-5), α and β are a function of the pipeline's geometrical and mechanical properties (Equation 3-6 and Equation 3-7), t is the nominal thickness, D is the outer diameter of a pipeline, and f_y is the yield strength (DNV-RP-F111, 2014).

$$m_p = 1/4 \cdot f_y \cdot t^2 \quad \text{Equation 3-5}$$

$$\alpha = 37 \cdot [\ln(D/t) - 1/2] \quad \text{Equation 3-6}$$

$$\beta = 0.125 \cdot [\ln(D/t) + 1] \quad \text{Equation 3-7}$$

3.2.2.1.1 Principles of Simulation

The numerical simulation using the BSM model encompasses the load path where the initial velocity is applied to m_t and m_a . Then, the resulting kinetic energy is absorbed by the deformation of the indenter (K_t and K_a), the local indentation of the pipe-wall (K_s), the global deformation of the flowline (K_{pb}), and the pipe-soil interaction (K_{ps}).

3.2.2.1.2 Pipe Shell Stiffness

The static shell stiffness of the pipe under transverse indentation can be calculated using Equation 3-4, as recommended by DNV-RP-F111 (2014), or by an independent 3-dimensional continuum finite element analysis. Equation 3-4 is used to represent the pipe shell stiffness in the present paper. In Equation 3-4, the corroded thickness may be implemented; corrosion allowance should be obtained based on (DNV-OS-F101, 2013). For the present work, the pipeline is assumed uncorroded.

3.2.2.2 Hybrid Shell-Beam Model

Figure 3-2 shows a schematic view of the hybrid shell-beam model; the proposed changes in the hybrid model compared to the BSM model are shown in the figure.

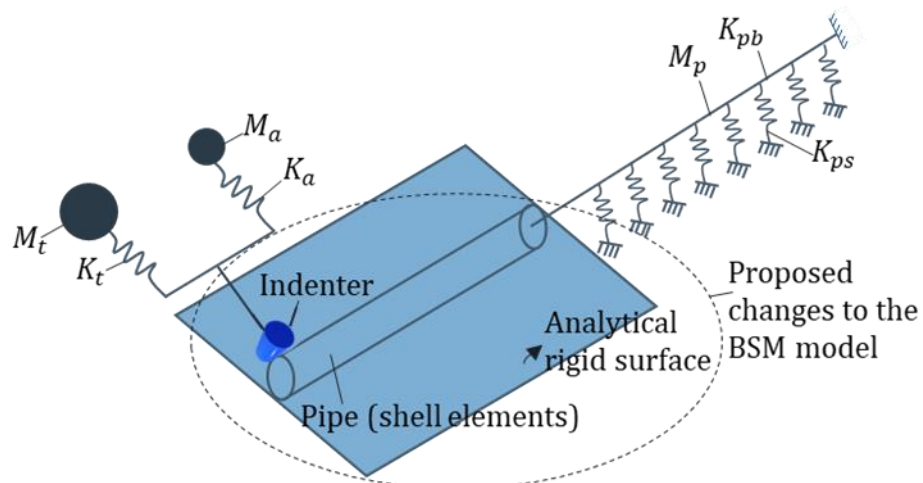


Figure 3-2 A Schematic View of the Hybrid Shell-Beam Model

The proposed changes in the hybrid model are to assess the assumptions implemented in the BSM model. Using the BSM model, the local and global stiffness of the pipeline are decoupled. However, in reality, there is a coupling effect between the local and global stiffness of the pipeline. For example, the cross-sectional ovalization in a pipe could lower the pipe's bending stiffness, which could result in increasing the pipe's global deformation. Additionally, the pipe's response during the trawl impact involves 1) mainly the local deformation mode, and 2) the combination of local and global deformation mode. However, the simplification in the BSM model could affect the transition between deformation mode 1 to mode 2. Furthermore, the path-dependent behaviour of the pipe, where the trawl impact imposes plastic damage to the pipe, could not be represented via the BSM model. For example, the effect of pipe's bending deformation on the pipe's shell stiffness could not be incorporated in the BSM model.

As such, the pipeline with beam elements at the region of interaction with the trawl board in the BSM model is replaced with the full model of the pipe with shell elements in the hybrid model. Furthermore, the point contact load in the BSM model is replaced with the surface to surface contact between the pipe with shell elements and a solid cylinder with a radius equal to 25 mm. Finally, the effect of soil support for the pipe with shell elements is represented with the surface to surface contact between the pipe and an analytical surface.

The load path mechanism in the hybrid model is similar to the BSM model, where the initial velocity is applied to the point masses, which represent the steel mass of the trawl board as well as the hydrodynamic added mass. Then, the kinetic energy is transferred to the pipeline via the springs, which represent the in-plane and out-of-plane stiffnesses of the trawl board. The applied load is transferred to the pipe through the surface to surface contact between a solid rigid cylinder, which represents the edge of the trawl board, and a full model of the pipe with shell elements. The pipe's response is first, (mainly) within the purely local mode of deformation, and then, in the combination of the local and global deformation mode. The latter deformation mode of the pipeline is partly dissipated by the pipe-soil interaction.

3.2.2.2.1 Element Type

The pipe is modelled with shell elements in the middle, using the reduced integrated shell elements (S4R) and 2.5 mm x 2.5 mm mesh size on the surface. The middle pipe is extended for 250 m from each end, using beam elements (PIPE31); the size of the beam elements in the mesh is equal to 125 mm. The kinematic coupling constraint is used to constrain the beam and shell elements in all translational and rotational degrees of freedom, where the shell elements meet the beam elements.

3.2.2.2.2 Pipe Soil Interaction

To model the pipe-soil interaction for the middle part of the pipeline, the soil is modelled using an analytical plate (Figure 3-2). General surface to surface contact is used for the interaction between the pipe (with shell elements) and soil. The interaction property comprises the normal behaviour with linear pressure-overclosure contact stiffness and the tangential behaviour with the penalty-based formulation. For the extended part with beam elements, springs are used to represent the soil stiffness in all translational degrees of freedom (Figure 3-2).

3.2.2.2.3 Trawl board

Similar to the BSM model, in order to model the trawl board, the in-plane stiffness (K_t) of the board is decoupled from the out of plane stiffness (K_a) (Figure 3-2). The first board's stiffness is modelled using the basic nonlinear-only axially-released connector, which is connected to the indenter at one end, and the other end is connected to the M_t mass (steel mass). Similarly, the K_a connector, which represents the latter board's stiffness, is connected to the indenter at one end, and the other end is connected to the M_a mass (added mass). The trawl gear is simplified as a solid tube, which is rigidly constrained with the radius equal to 25 mm, as recommended by DNV-RP-F111 (2014).

3.2.2.3 Trawl Board Stiffness

In both BSM and hybrid models, the stiffness of the pipe shell falls between the in-plane and out-of-plane stiffness of a trawl board; the in-plane stiffness is around 50 times stiffer than the out-of-plane stiffness (DNV-RP-F111, 2014). Hence, the energy applied by the in-plane steel mass is mainly absorbed by the pipe shell. However, the energy applied by the out-of-plane steel mass (added mass) is partly absorbed by the bending response of the trawl board. Trawl board stiffness is presented in Table 3-1.

3.2.2.4 Soil Stiffness

For both BSM and hybrid models, as the impact phase occurs in some hundredths of a second (DNV-RP-F111, 2014), the prominent pipe response is local, and the global pipe response is insignificant. Hence, small shear strain is expected in the surrounding soil, and a dynamic soil stiffness is used, rather than a static stiffness (Wichtmann and Triantafyllidis, 2009). The dynamic stiffness of the soil is calculated using Equation 3-8 (DNV-RP-F105, 2006):

$$K_v = C_v / (1 - \nu) \cdot (2/3 * \rho_s / \rho) D^{0.5} \quad \text{Equation 3-8}$$

Where K_v is the vertical soil stiffness; C_v is the coefficient for vertical soil stiffness (DNV-RP-F105, 2006); ρ_s / ρ is the specific mass ratio between the flowline mass and

the displaced water mass; added mass is not considered in the computation, and the above expression is only valid for $1.2 < \rho_s/\rho < 2.0$; ν is the Poisson's ratio of the soil obtained from DNV-RP-F105 (2006). For the lateral and axial soil resistance, a simple constant friction coefficient is used to model the pipe-soil interface friction during the lateral/axial deflection of a flowline. Soil properties are presented in Table 3-1.

3.2.3 Boundary Condition Effect

In both BSM and hybrid models, to eliminate boundary condition effects, a sufficient length of the flowline should be modelled. Accordingly, the ratio of the length over the diameter of the pipeline is set to more than 100, as recommended by DNV-RP-F111 (2014).

3.2.4 Input Parameters

In both analytical and finite element methods, the physical and mechanical properties for the pipe are selected based on the work done by Zheng (2014; 2013). The author performed experimental studies to investigate the structural response of a pipe subject to a transverse knife-shaped indentation; the physical properties of the pipe are summarized in Table 3-1. Also, Figure 3-3 shows the engineering stress-strain curve reported by Zheng (2013), as well as the true stress-strain curve.

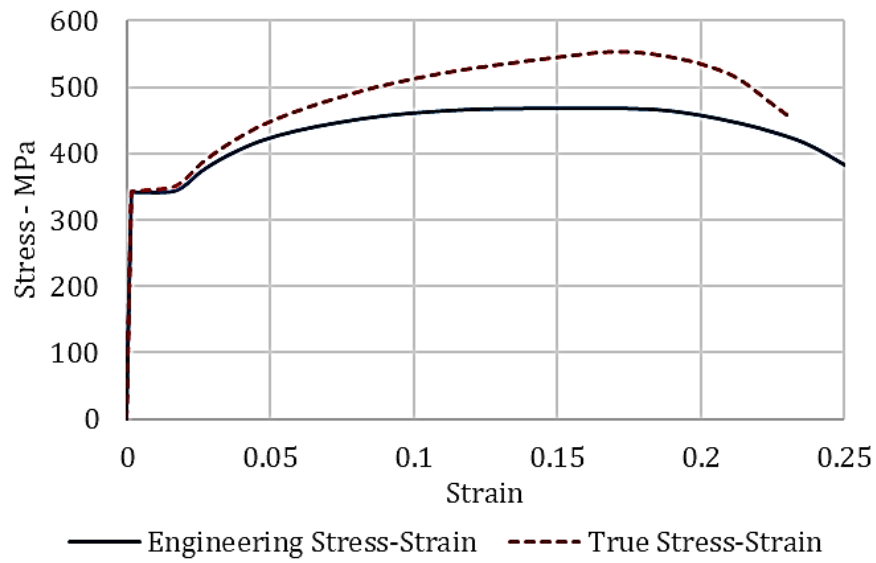


Figure 3-3 Engineering and True Stress-Strain Curve of the Specimen in Zheng (2013)

The input parameters for the pipe, trawl boards, and soil are presented in Table 3-1. Furthermore, the following parameters are not included in the analyses of the present work, including non-structural weight, metocean forces, buoyancy force, hydrostatic pressure, internal pressure, strain rate effect, and thermal expansion force.

Table 3-1. The Input Parameters for the Pipe, Trawl Board, and Soil

Pipeline	Value	Units	Trawl board	Value	Units
Outside diameter	141.3	mm	Trawl board steel mass	4000	kg
Nominal thickness	6.55	mm	Added mass	8560	kg
Reduction factor for impact energy associated with steel mass	0.5		Tow velocity of a trawler	2.6	m/s
Reduction factor based on pipe size and soil type	0.1		In-plane board stiffness	500E6	N/m

Coefficient of the effect of span height on impact velocity	0.85		Out-of-plane (bending) board stiffness	10E6	N/m
Material strength factor	1		Half the trawl board height	1.75	m
Span height	0	m	Soil	Value	Units
			Soil Type	Medium sand	
			Friction coefficient for the lateral/axial direction	0.6	

Note: Span height refers to the vertical distance between the bottom of the pipe and the seabed.

3.3 Benchmarking

3.3.1 BSM Model

The BSM model is validated against the example in Appendix B of DNV-RP-F111 (2014). Figure 3-4 shows a comparison between the local impact load obtained from the analysis of the present study against the data presented in Appendix B of DNV-RP-F111 (2014). The result of the present work using an implicit time integration method is also provided as a sensitivity case. As shown in Figure 3-4, the data compares very well. The oscillation in the tail of the curve ($t > 0.03$) is mainly due to using the dynamic explicit approach. Using the dynamic implicit method eliminates the oscillation.

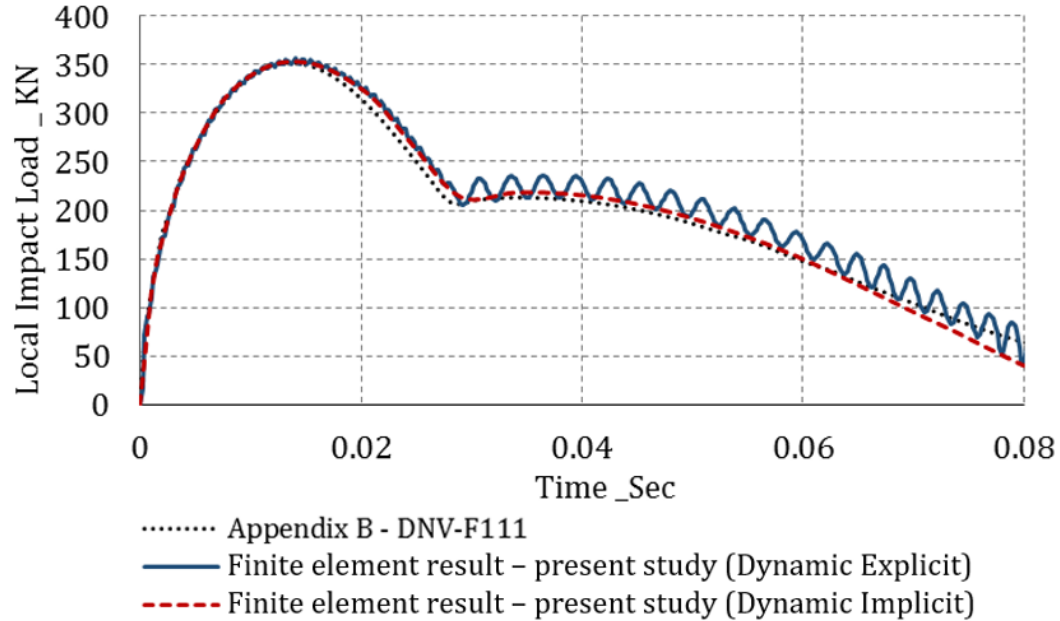


Figure 3-4 Benchmarking the BSM Model: The Impact Force Resisted by the Pipe-Wall Thickness Versus Time

3.3.2 Hybrid Model

The validation of the hybrid shell beam model is carried out considering the following points:

- Deformation mode of the pipe: The initial phase of the trawl gear interference with a subsea pipeline, which is the main focus of the current scope, occurs in some hundredths of a second (DNV-RP-F111, 2014). As such, during the initial trawl impact, the pipe's response is mostly local, and the global deformation of the pipe is insignificant.
- Pipe-soil interaction: As a result of physical tests reported by Ng and Shen (2006), during an impact event on a pipeline, the developed circumferential stress due to the pipe-soil interaction could significantly affect the pipe's structural response. However, this effect during the initial trawl impact is insignificant, as the impact direction is along the seabed (Zheng et al., 2012).
- Reproducing an impact event via a quasi-static analysis: Shen and Jones (1991) examined a clamped beam under a transverse load and showed that an indentation on a pipe, which is applied by a relatively slow and heavy indenter, could be modelled using a quasi-static approach. Additionally, Zheng (2014) did experimental and numerical investigations on a pipe under a lateral indentation and

reached to the comparable outcomes. According to DNV-RP-F111 (2014), in scenarios of the interaction between otter trawl gear and a flowline, trawl boards have a mass of several tons and moves relatively slowly. Hence, the trawling impact scenarios could be modelled using the quasi-static condition.

- The idealization of a trawl board: In the interference between trawl gear and pipeline, the edge of the trawl gear could be represented by a solid cylinder with a small radius in the range of 10 to 25 mm, as recommended in DNV-RP-F111 (2014). As such, in order to validate the accuracy of the hybrid shell-beam model, those physical studies should be employed, which examined the lateral indentation of a pipe via a wedge-shaped or knife-shaped indenter (with the relatively sharp edge), i.e., Zheng (2014).

In order to validate the accuracy of the hybrid model, the region depicted in Figure 3-5 is used to partly represent the hybrid model, as a) the global deformation of a subsea pipeline, as well as pipe-soil interaction, are insignificant during the initial phase of the trawl impact event, and b) to the knowledge of the authors, there is no publicly available experimental data (of a submerged pipe laid on soil and impacted by a trawl board) to directly validate the accuracy of the hybrid shell-beam model. In this regard, the relevant physical studies are employed, including the previous study physical tests (a quasi-static test and an impact test conducted by Zheng (2014)), as well as the present study physical test (a quasi-static test). These tests were conducted on a 5-inch pipe, which was subject

to a lateral indentation by an indenter with a sharp edge. Figure 3-6 shows the boundary conditions of the physical tests. In summary, the tests conducted by Zheng (2014), as well as the present study, are employed to demonstrate the accuracy of the numerical model, which partly represents the hybrid shell-beam model.

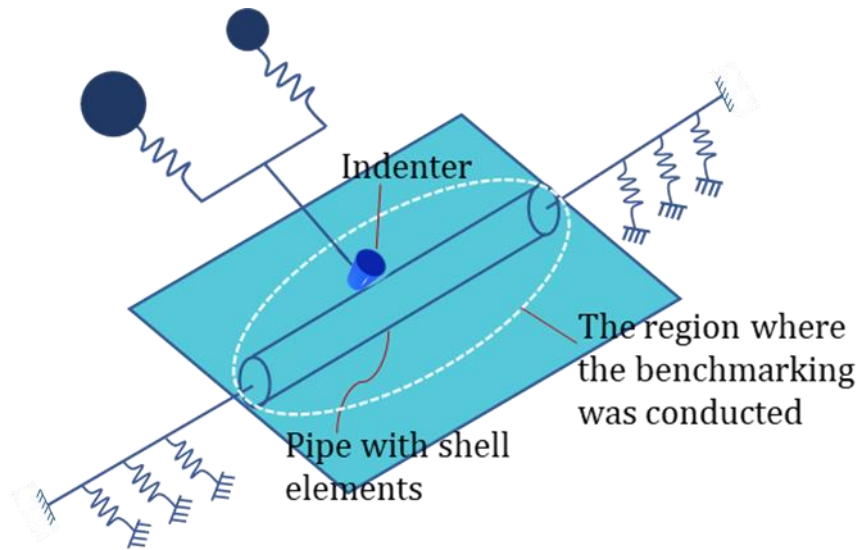


Figure 3-5 The region of the Hybrid Model Where the Benchmarking is Carried Out

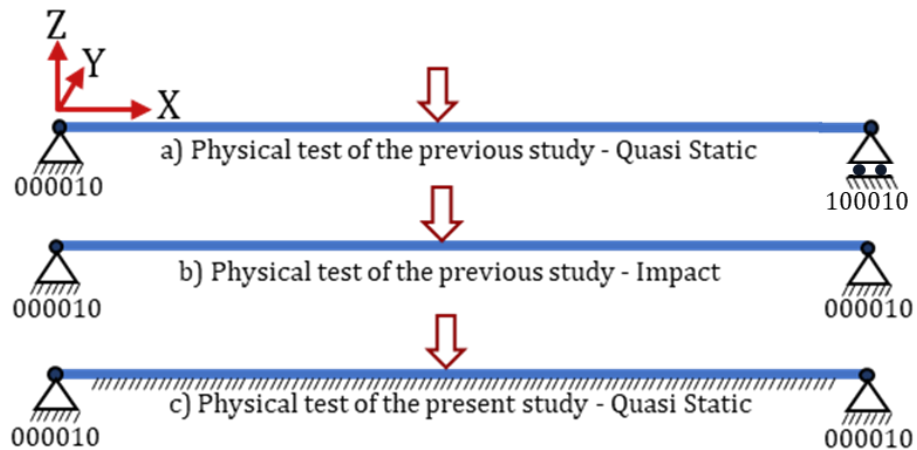


Figure 3-6 Boundary Condition of the Physical Tests Employed to Benchmark the Hybrid Model

3.3.2.1 Verification Against the Previous Study Physical Test

The hybrid model is validated against the work conducted by Zheng (2014). The author performed experimental investigations to study the structural response of a pipe subject to an indentation, via a rounded frontal shape indenter. Zheng (2014) did two series of tests, one under the quasi-static condition and another under impact condition (dropped object). Accordingly, one quasi-static test and one impact test are used to partially validate the accuracy of the hybrid model (only the interaction between the indenter and the pipeline in the middle).

3.3.2.1.1 Quasi-Static Test

The quasi-static test conducted by Zheng (2014) is used to benchmark the hybrid model. The pipe is 5-inch API Grade B with Schedule 40; this specimen is termed as SPS02 in Zheng (2014). The physical properties of the pipe are summarized in Table 3-1. Also, Figure 3-3 shows the engineering stress-strain curve, which is reported in Zheng (2014), as well as the true stress-strain curve. The boundary condition is simply supported, as shown in Figure 3-6.

Figure 3-7 shows the vertical load resisted by the specimen against the 100 mm imposed indentation. Accordingly, there is a very good agreement between the finite element results of the present study and the one conducted by Zheng (2014). However, both finite

element results overestimate the experimental data. This discrepancy could be associated with the potential boundary condition effect, which is not recorded during the physical test, and hence not fully represented in the finite element model.

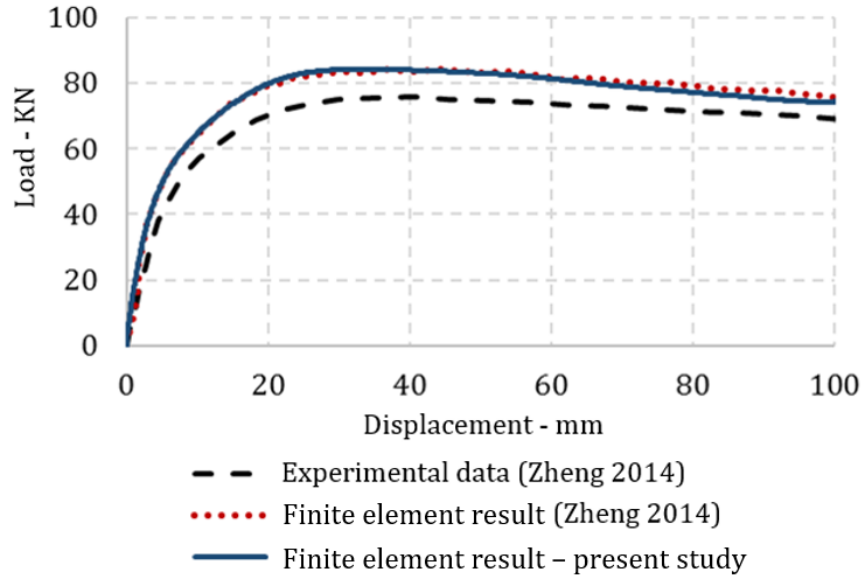


Figure 3-7 Benchmarking the Hybrid Model Against a Quasi-static Test by Zheng (2014):
Vertical Load Resisted by the Specimen Versus Vertical Displacement of the Indenter

3.3.2.1.2 Impact Test

The impact test conducted by Zheng (2014) is also used to partially validate the hybrid model. The pipe is 5-inch API Grade B with Schedule 40; this specimen is termed as I-SPS02 in Zheng (2014). The physical properties of the pipe are presented in Table 3-1. Also, Figure 3-3 shows the engineering stress-strain curve, which is reported in Zheng (2014), as well as the true stress-strain curve. The boundary condition is shown in Figure 3-6.

Figure 3-8 shows that there is a reasonable agreement between the numerical result of the present work and the one done by Zheng (2014); the finite element result of Zheng (2014) leads to a slightly better numerical prediction of the test result. However, both numerical results underestimate the experimental data. The total mass of the indenter and the steel blocks are set to 1350 kg with the initial velocity of 2.99 m/sec. As the mass of indenter could reach up to 1400 kg as reported in Zheng (2014), a sensitivity case is also conducted for the indenter's mass equal to 1400 kg. Figure 3-8 shows that the load-displacement curve obtained from the sensitivity case provides a better agreement with the test data of Zheng (2014), compared to the base case curve of the present study.

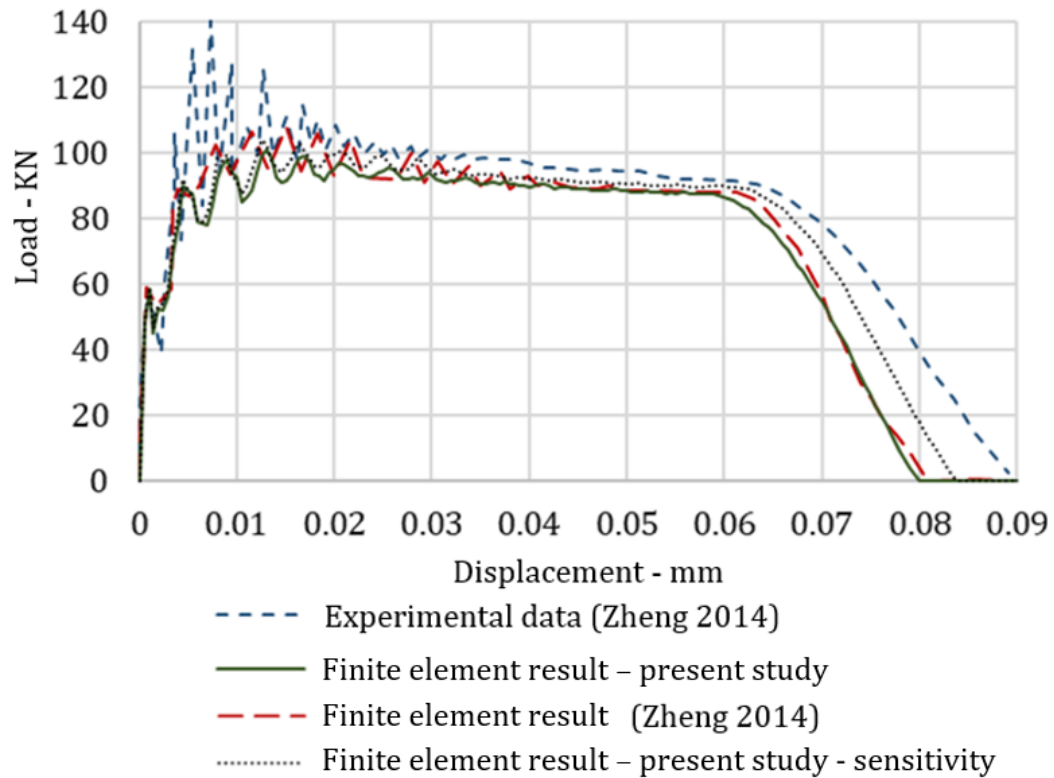


Figure 3-8 Benchmarking the Hybrid Model Against an Impact Test by Zheng (2014): Vertical Load Resisted by the Specimen Versus Vertical Displacement of the Indenter

Based on parametric studies, the following points are considered for the analysis, including (a) the rotation axis of the supports at two ends of the pipe should be chosen at the bottom center of the support (Figure 3-9), which is aligned with the description presented in Zheng (2014); (b) the length of interaction between pipe and supports (Figure 3-9) is set to 62.5% of the support width; the support width is 50 mm; also, the pressure applied by omega clamps (Figure 3-9) to the pipe ends are incorporated having 5 mm penetration of the clamps into the pipe ends; (c) No separation is allowed between the end supports and the pipe during the interaction; (d) indenter, as well as steel blocks,

are modelled in full size (Figure 3-9). Steel blocks are modelled separately, and surface to surface contact is used between them, which slightly changed the distribution of the kinetic energy during the simulation, and enhanced the numerical results.

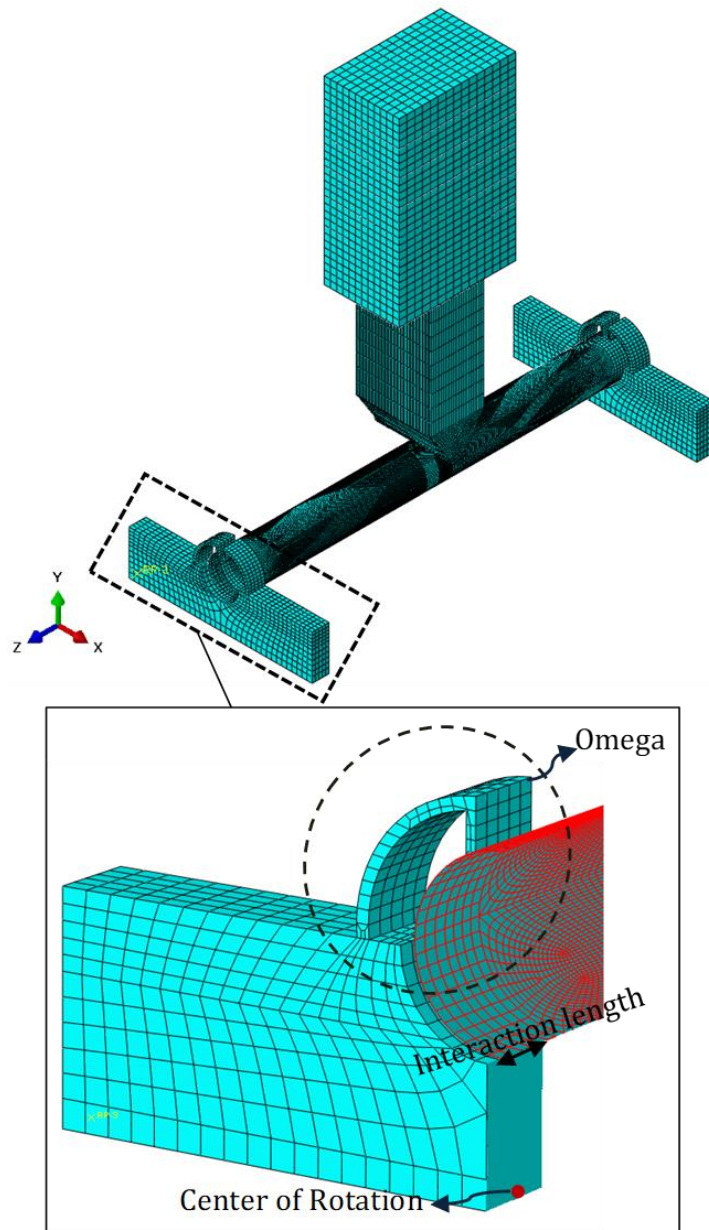


Figure 3-9 Numerical Model of the Impact Test Conducted by Zheng (2014)

3.3.2.2 Verification Against the Present Study Physical Test

A quasi-static test was carried out on a 5-inch steel pipe, schedule 40, under a 35 mm perpendicular indentation. The test apparatus, located at the Memorial University of Newfoundland, was used to conduct the test. Figure 3-10 shows a view of the test apparatus.

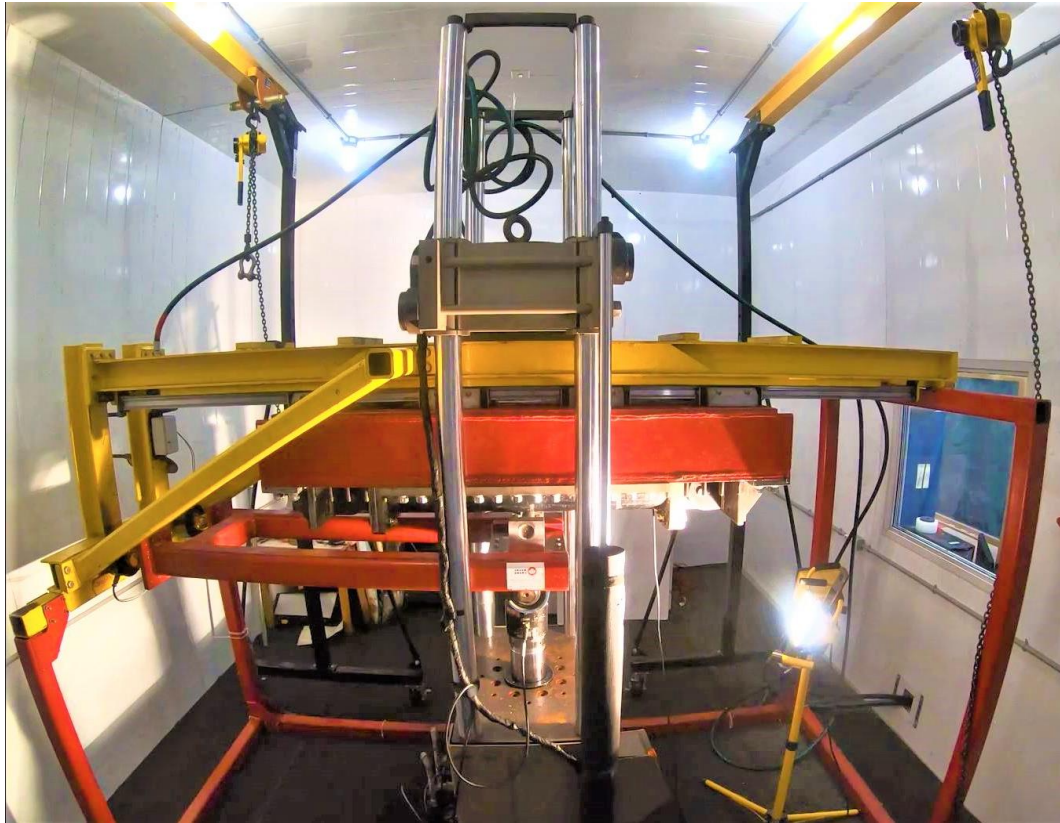


Figure 3-10 A View of the Test Apparatus of the Present Study Physical Test

Figure 3-11 shows the main components involved in the test, including MTS hydraulic ram, swing arm, indenter, test setup, and carriage. The outer radius of the tube-shaped indenter is 25 mm, as recommended in DNV-RP-F111 (2014). The indentation was conducted in the following steps: first, the vertical MTS hydraulic ram translates the tube-shaped indenter vertically. Second, the swing-arm rotates and provides contact between the indenter and the cylindrical specimen. Then, the indentation initiates on the pipe, which is supported by the carriage.

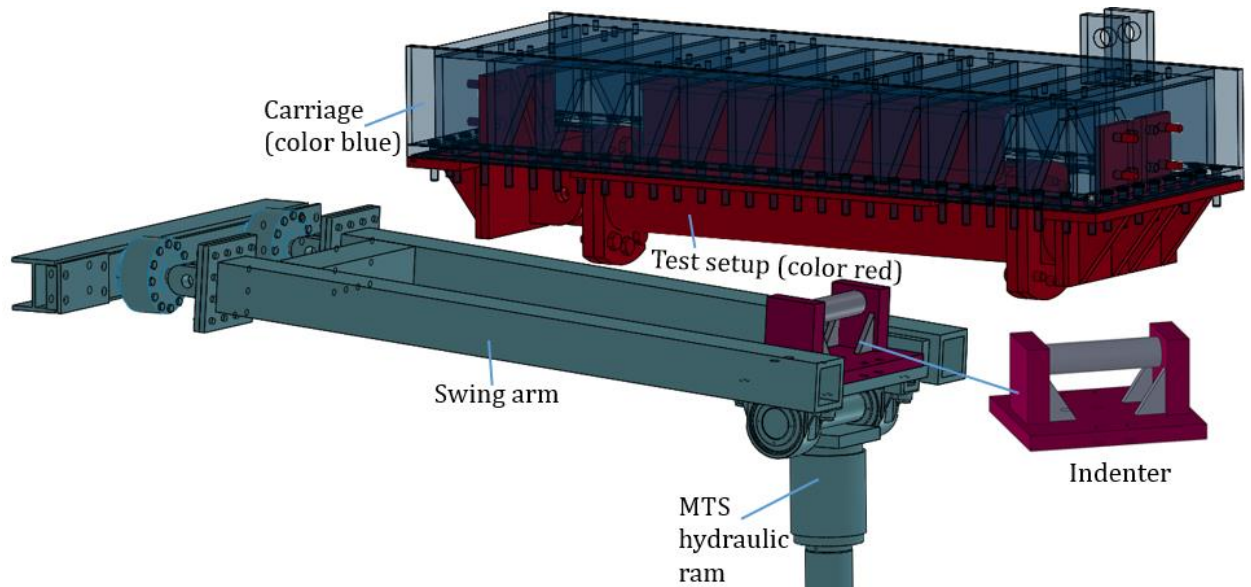


Figure 3-11 Main Components of the Test Apparatus in the Present Study Physical Test

Figure 3-12 shows the schematic view of the specimen restrained at the top and both ends; the global deformation of the pipe is restrained at the top with a saddle-shaped support which provides 60 degrees circumferential contact with the pipe, and involves a curve with the same radius as the pipe, as recommended in DNV-RP-F111 (2014). The friction

coefficient between the indenter and the specimen is set to ~ 0.3 , according to the recorded test data. Furthermore, using sensitivity studies, the stiffness of the boundary conditions at the top and two ends are set to $3\text{E}9 \text{ N/m}$ and $1.4\text{E}9 \text{ N/m}$, respectively; the end restraints are modelled with axial connectors. Also, Figure 3-13 shows the middle deformable region and relatively rigid regions (compared to the cylindrical part in the middle) of the specimen; where the latter regions are rigidly constrained during the numerical analysis.

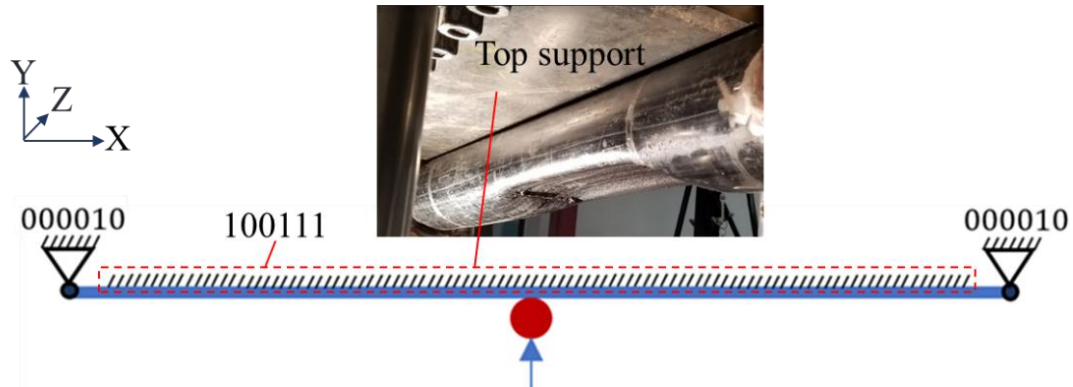


Figure 3-12 A Schematic View of the Boundary Condition Used in the Present Study Physical test

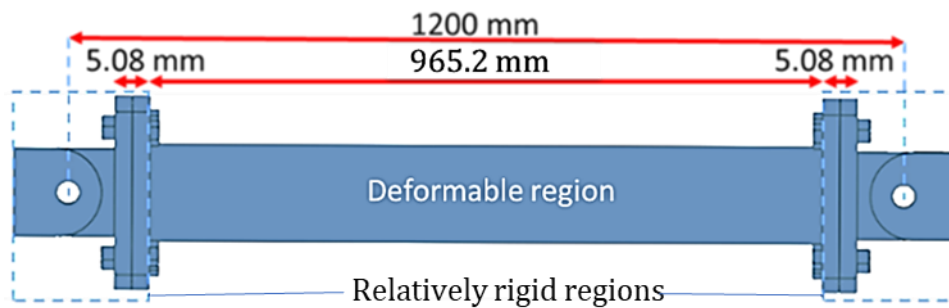


Figure 3-13 Detailed Geometries of the Cylindrical Specimen in the Physical Test of the Present Work

Figure 3-14 shows the engineering stress-strain curve obtained and averaged from standard tensile tests. Accordingly, the analysis is performed by implementing the stress-strain curve in a multilinear elastoplastic material model in Abaqus. The physical and mechanical properties of the pipe are summarized in Table 3-2.

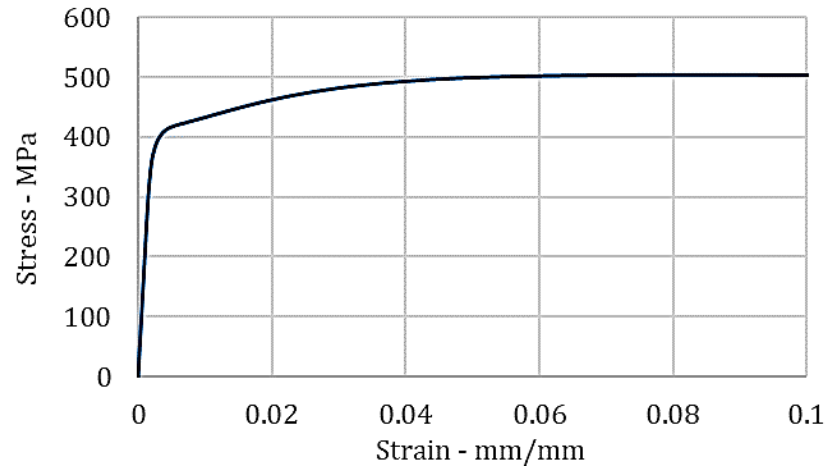


Figure 3-14 Engineering Stress-Strain Curve of the Cylindrical Specimen in the Physical Test of the Present Work

Table 3-2 Physical and Mechanical Properties of the Cylindrical Specimen

Physical properties		
D (mm)	t (mm)	L (mm)
140.97	6.1468	1200
Mechanical properties		
E (MPa)	f _y (MPa)	f _u (MPa)
201404	412.26	503.56

Figure 3-15 shows the experimental result, as well as numerical prediction of the load resisted by the specimen, against the 35 mm imposed indentation. A very good agreement can be observed between the experimental data and the model prediction, except at the beginning of the curve, where the finite element results overestimate the experimental data. This could be due to gaps between different components of the test apparatus, which is very hard to measure and hence are not included in the numerical model. Also, the slight oscillations in the finite element results are due to using the explicit time integration method.

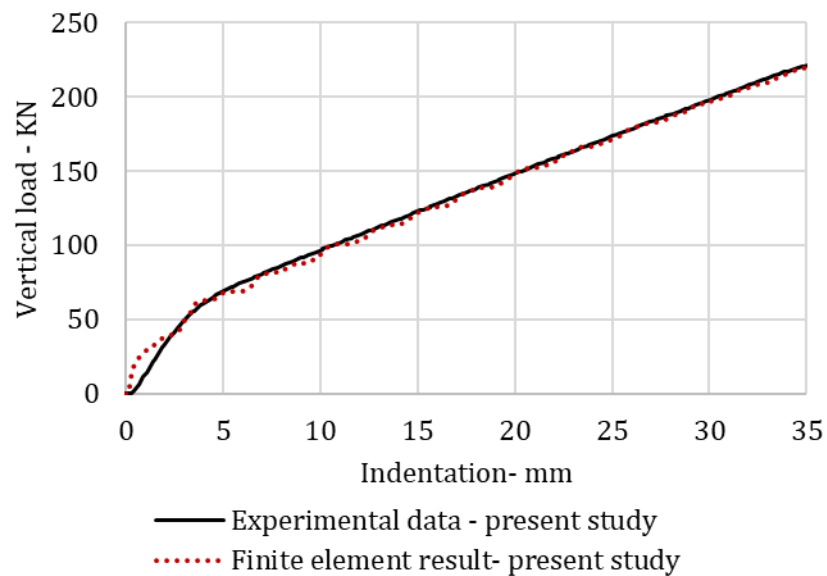


Figure 3-15 Benchmarking the Hybrid Model Against the Physical Test of the Present Study:
Vertical Load Resisted by the Specimen Against the 35 mm Imposed Perpendicular Indentation

3.4 Mesh Convergence Analysis

Mesh convergence analyses are conducted to ensure the independence of the numerical results from the sizes of the elements employed in the BSM and hybrid models. Accordingly, the following sections present the results of the mesh convergence analyses for the BSM and hybrid models.

3.4.1 BSM Model

Figure 3-16 shows the impact load resisted by the pipe shell versus time for three cases with mesh sizes equal to 250, 125, and 62.5 mm. As shown in the figure, all three cases lead to very similar load-time curves. As such, the mesh size equal to 62.5 mm is used for the analyses.

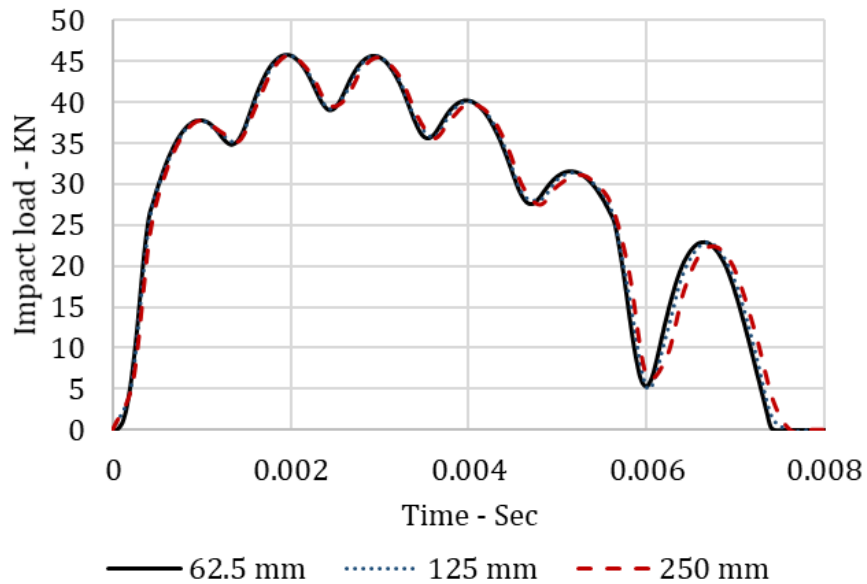


Figure 3-16 Mesh Convergence Analyses for the BSM Model: 250, 125, and 62.5 mm Element Size

3.4.2 Hybrid Model

For the mesh convergence analyses, results are filtered using the Butterworth filter function in Abaqus. Section 3.5.1 shows an example of using this function to filter the load-time curve. The mesh convergence analysis was conducted for both shell elements (four element edge lengths: 5.0, 3.75, 2.5, and 1.75 mm) and beam elements (three lengths: 250, 125, 62.5 mm). The analysis converges for shell elements with element edge length equal to 2.5 mm (Figure 3-17), and for beam elements with edge length equal to 125 mm (Figure 3-18).

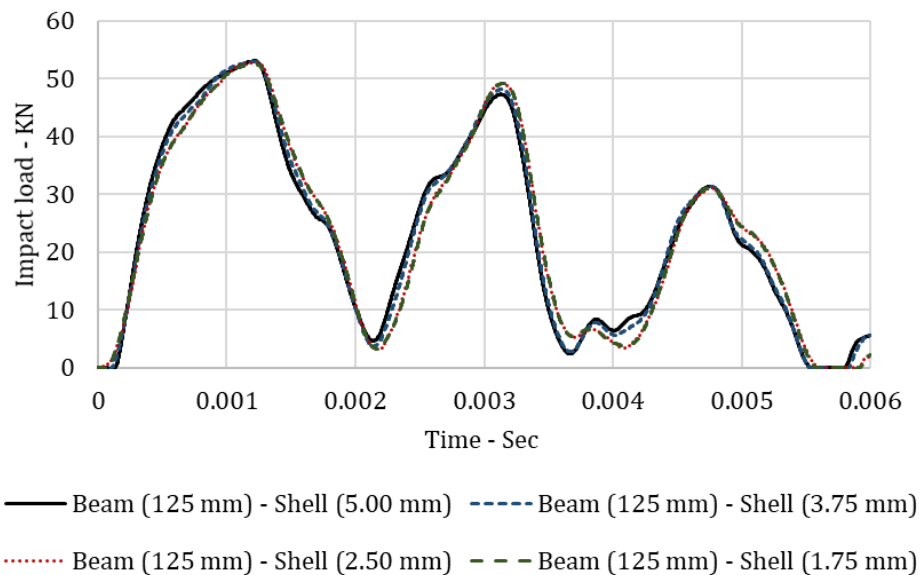


Figure 3-17 Mesh Convergence Analysis for the Hybrid Model: Shell Elements

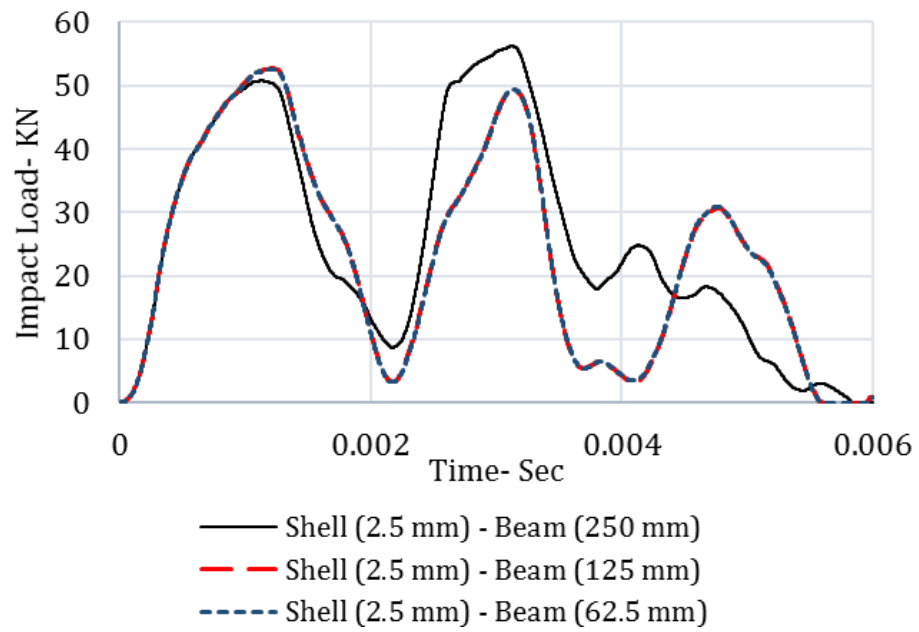


Figure 3-18 Mesh Convergence Analysis for the Hybrid Model: Beam Elements

3.5 Results and Discussion

In this section, the results of the hybrid model are compared against the BSM model, as well as the analytical method. Accordingly, Figure 3-19 shows the total impact load resisted by the pipe in the hybrid model, versus the impact load withstood by only the pipe wall thickness in the BSM model. As shown in the figure, at the beginning of the impact, while only the local shell stiffness of the pipe is involved to resist against the load, the hybrid and BSM models lead to very similar results. These findings provide further validation regarding the accuracy of the models.

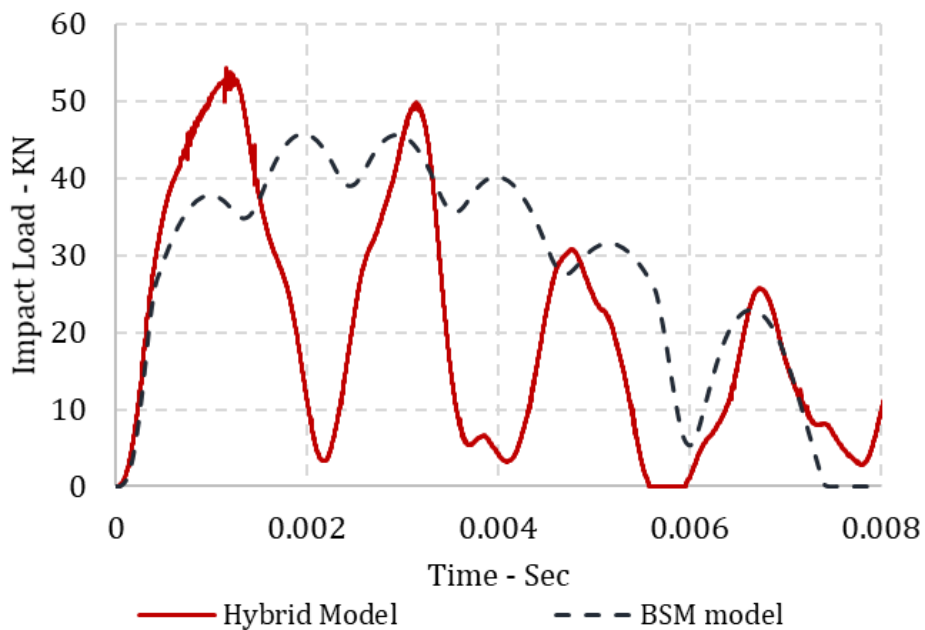


Figure 3-19 Total Impact Load Resisted by the Pipe in the Hybrid Model Versus the Impact Load Resisted by the Pipe Wall in the BSM Model

Figure 3-20 compares the impact load resisted by the pipe in the numerical method with the hybrid model versus the analytical method. Accordingly, the analytical method leads to a significantly higher impact load compared to the hybrid model. This result is in agreement with the statement of DNV-RP-F111 (2014) that the analytical method is very conservative for small pipe sizes; for thin-walled pipes with small sizes, the impact energy associated with the hydrodynamic added mass increases dramatically.

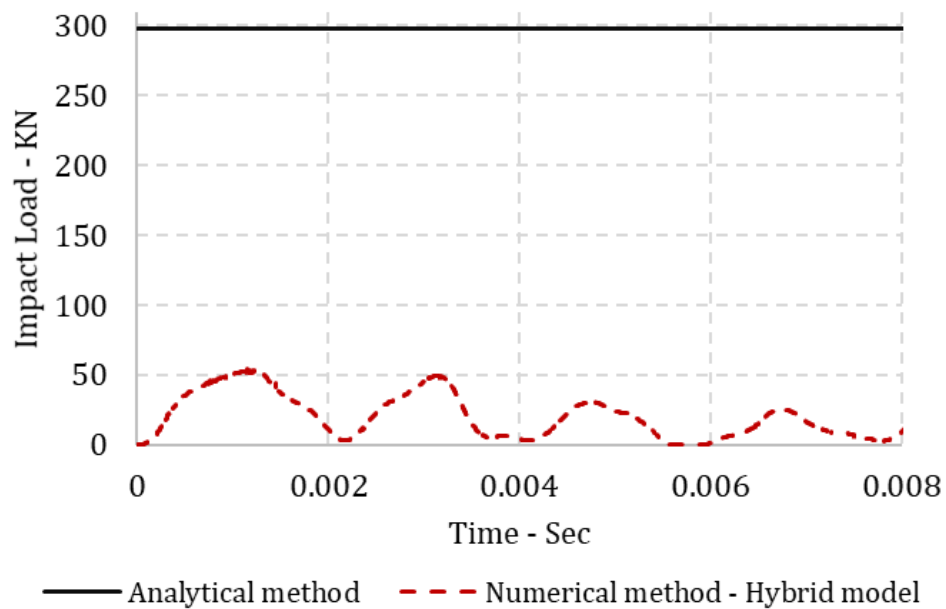


Figure 3-20 The Impact Load Resisted by the Pipe – the Analytical Method Versus the Finite Element Method (Using the Hybrid Model)

Figure 3-21 shows the resulting dent depth obtained from the analytical versus numerical method using hybrid and BSM models. As shown in the figure, the analytical method leads to a very conservative dent depth on the pipe. Furthermore, using the BSM model,

the resulting dent depth is relatively non-conservative and slightly underestimates the dent depth (by 6.5%), compared to the hybrid model. As such, while the discrepancy is insignificant, the results show that the hybrid model is a suitable alternative to the BSM model to assess the overtrawability of pipelines with small sizes.

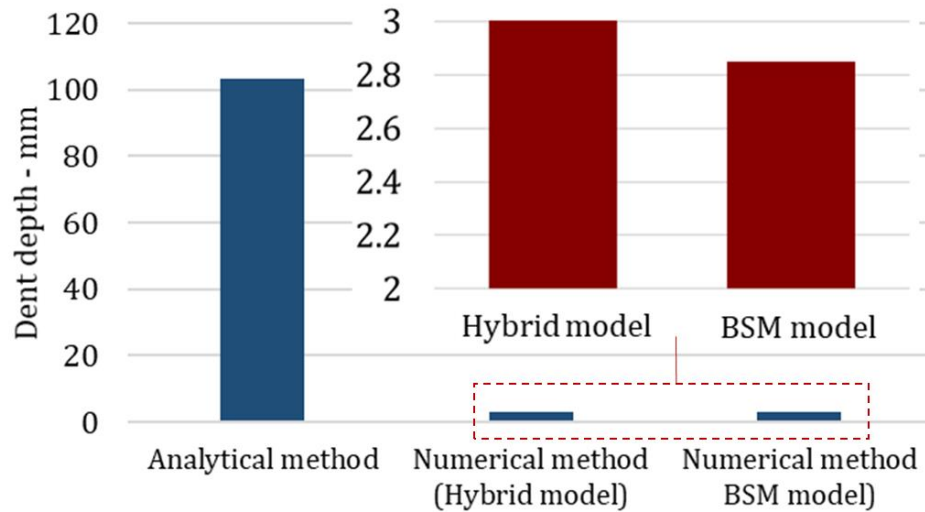


Figure 3-21 The Dent Depth Imposed on the Pipe, the Analytical Versus Numerical Method (Hybrid and BSM Models)

The discrepancy between the BSM versus hybrid model could be due to the following reasons:

- The local damage in the pipe affects the pipe's section modulus and consequently changes the global stiffness of the pipe. However, due to the idealization of the pipe in the BSM model by separating the global bending stiffness from the local shell stiffness, this coupling effect could not be considered. Additionally, as the impact occurs in some hundredths of a second, initially, only shell stiffness of the pipe

absorbs the kinetic energy of the impact (phase-a). Then, the global and local stiffnesses of the pipe resist the load (phase-b). Separating the global and local stiffness of the pipe in the BSM model could influence the transition time between phase-a to phase-b.

- The pipe response under the trawl impact is path-dependent; the effects of the local plastic damage at the current time increment affects the pipe response at the next time increment. The path-dependency could not be considered in the BSM model.
- In the BSM model, the impact load is transferred to a node. Whereas, in the hybrid model, more realistic contact occurs between the indenter and pipe shell elements.
- The shell stiffness in the BSM model is derived from Equation 3-4, which assumes the pipe as an elastic perfectly plastic material. However, in the hybrid model, the multilinear elastoplastic model is used.

3.5.1 Sensitivity Analyses

For the sensitivity analyses as well as mesh convergence analysis (in Section 3.4), results are filtered using the Butterworth filter function in Abaqus. Figure 3-22 shows an example of using this function to filter the impact load resulting from the hybrid model.

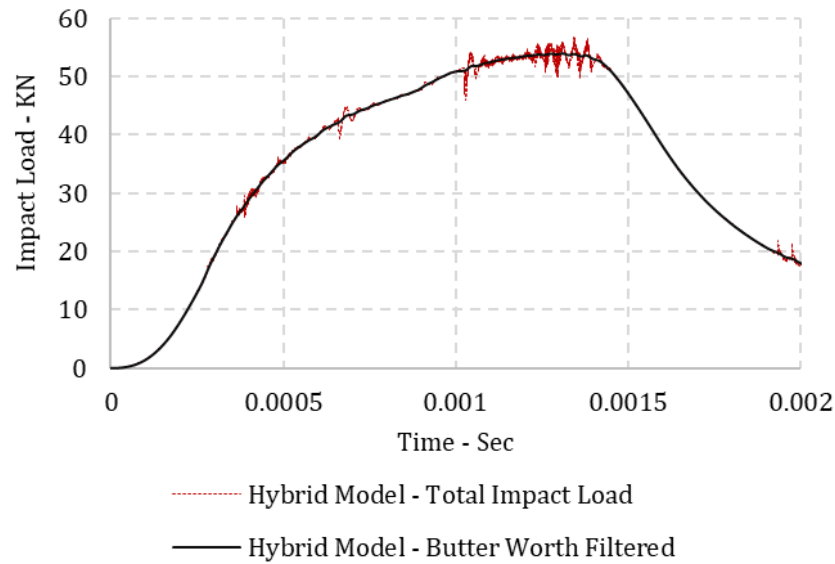


Figure 3-22 An Example of Using Butterworth Filter Function in Abaqus

3.5.1.1 Pipe Diameter

Two additional cases with a similar ratio of outer diameter over thickness equal to 21 are examined using the hybrid and BSM models, including a 10-inch pipe with 12.7 mm thickness and a 14-inch pipe with 16 mm thickness. The first case examines the results of the hybrid model versus the BSM model at the threshold where DNV-RP-F111 (2014) becomes applicable. The latter case examines the results of the hybrid versus the BSM model for medium pipe size (larger than 10-inch). It is worth noting that the validation of the hybrid model was performed only for a 5 inches pipe. As such, the accuracy of the hybrid model for sensitivity cases with 10 and 14 inches pipe diameter requires further validation, which is not within the scope of the present study.

Figure 3-23 shows the maximum total dent depth for the pipe sizes studied above. It is shown that for a 5-inch pipe, the BSM model slightly underestimates the dent depth compared to the hybrid model. However, for the 10-inch pipe, the maximum total dent depth resulting from both models is very close. Furthermore, for the 14-inch pipe, the BSM model is relatively conservative in determining the dent depth. Accordingly, the hybrid model could be a suitable alternative to the BSM model to assess the overtrawlability of small pipe sizes; also, it could reduce the conservatism when designing medium pipe sizes (larger than 10-inch) against trawl impacts.

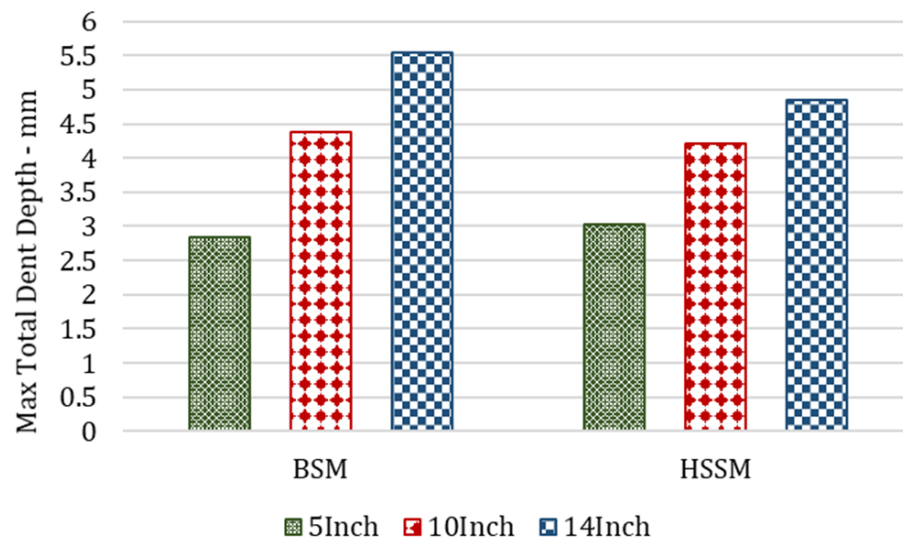


Figure 3-23 Maximum Total Resulting Dent Depth Obtained from the Hybrid Model Versus the BSM Model for 5, 10, and 14-inch Pipe Sizes

3.5.1.2 Indenter Shape

Zheng (2012) did sensitivity analyses on the indenter front radius and stated that for the radius range from 5 to 20 mm, the front radius does not have any significant influence on the impact result. Based on Figure 3-24, three radii are examined for the indenter front shape (R): 20, 25, and 30mm. A comparison between the curves shows that for R= 20 mm, the results are slightly different compared to when R= 25 or 30 mm. Whereas, using either R=25 mm or R= 30 mm leads to the same impact load.

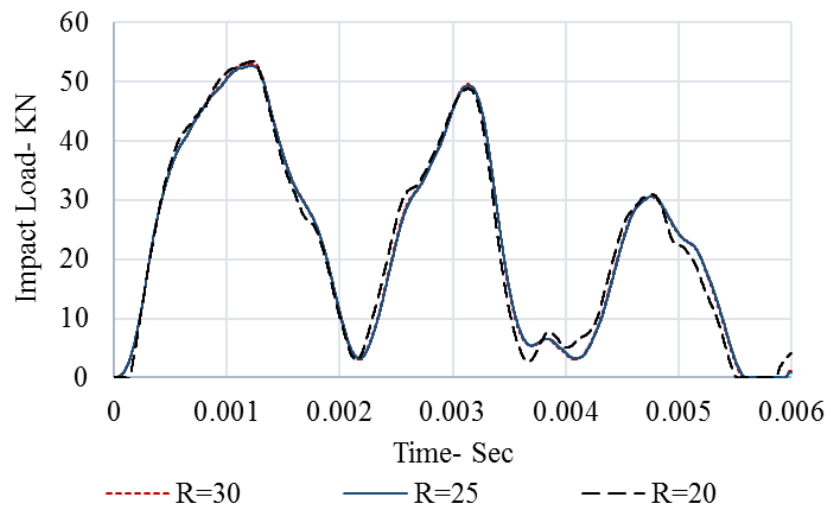


Figure 3-24 Sensitivity Analysis Results: Indenter Radius: 30, 25, and 20 mm

3.5.1.3 Soil Stiffness

As the pipeline laid on the seabed and the trawling impact is parallel to the seabed, soil stiffness has a negligible effect on the impact force, as well as the resulting dent depth in

the pipeline. Figure 3-25 shows the load-time curve using two soil friction coefficients (Mu=0.6 and 1.0). The results show that the variation of soil friction coefficient has no effect on the impact load.

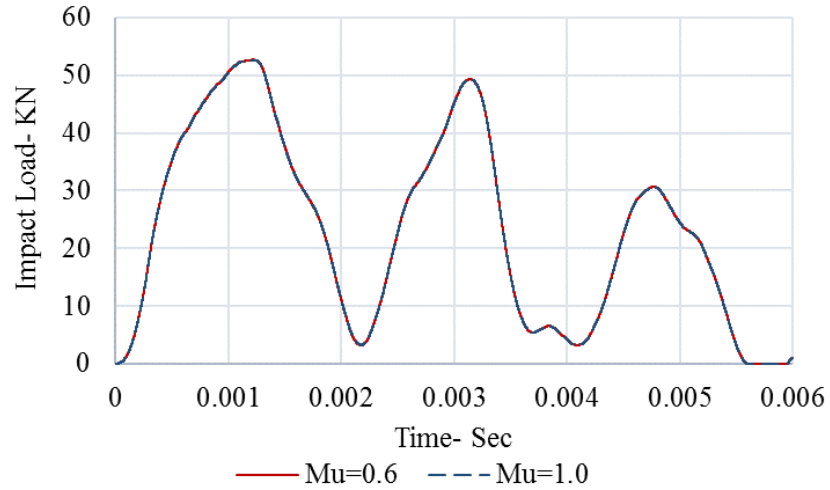


Figure 3-25 Sensitivity Analysis Results: Soil Friction Coefficient

3.5.1.4 Strain Rate Effect

The Cowper-Symonds constitutive equation (Equation 3-9) is used to examine the influence of the strain rate on the impact force:

$$\sigma_0 = \sigma_0 [1 + (\dot{\epsilon}/Q)]^{1/q} \quad \text{Equation 3-9}$$

Where σ_0 is the static yield stress, and $\dot{\sigma}_0$ is the dynamic yield stress, and Q and q are the coefficients. The two coefficients could be set to Q=40.4 /s and q=5 for mild steel (Jones, 2012).

Figure 3-26 highlights the influence of accounting for the strain rate effect in the analysis. Accordingly, as shown in the figure, the impact load increases by 12% when using the Cowper Symonds model. This effect could be incorporated into the hybrid model. However, in the BSM model, where the shell stiffness is derived from Equation 3-4, the strain rate effect could not be considered.

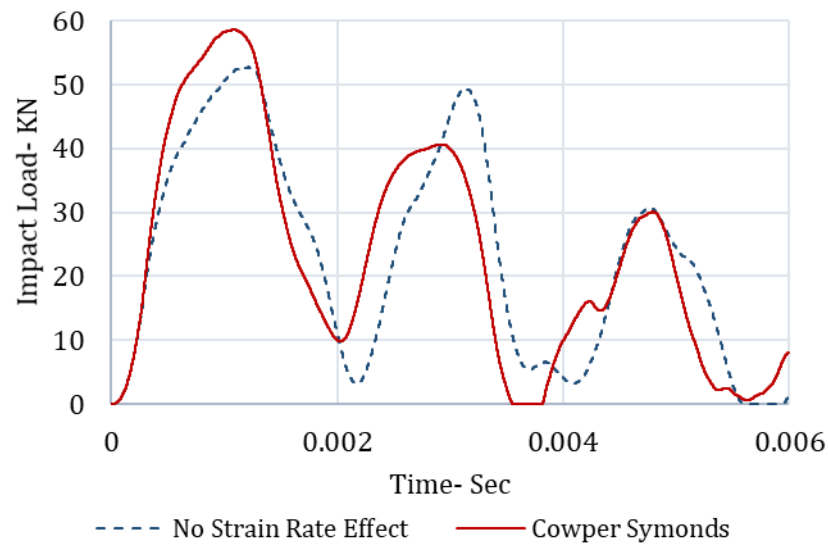


Figure 3-26 Sensitivity Analysis Results: Strain Rate Effect

3.6 Summary and Conclusions

A comparison of the results obtained from the analytical method against the finite element method showed that using the finite element approach could significantly reduce the unnecessary conservatism and improve the economy of a project. The difference between the analytical and the finite element methods is particularly significant for small pipe sizes (i.e., 5-inch).

As DNV-RP-F111 (2014) is only applicable for a pipe size larger than 10-inch, the hybrid shell beam model is developed as an alternative to predict the trawling impact on a pipeline for small pipe sizes. Using the hybrid model could be a suitable alternative to the BSM model for small pipe sizes (outer diameter less than 10-inch). Accordingly, a case was studied for a 5-inch pipe, which showed that the BSM model is relatively non-conservative and slightly underestimates the resulting dent depth on the pipe (6.5%), compared to the hybrid model.

The discrepancy between the BSM and the hybrid model could be due to the following sources:

- The shell stiffness implemented in the BSM versus the hybrid model.
- The more realistic contact representation in the hybrid model versus point contact in the BSM model.

- The coupling effect between the local and global stiffness of the pipe, which is disregarded in the BSM model.
- The difference in the transition time from phase a to b in the BSM versus the hybrid model.
- The path-dependency of the pipe response during the plastic indentation, which could not be considered in the BSM model.

Also, the additional sensitivity analyses show that the results obtained from the hybrid model are not sensitive to the soil friction coefficient. Additionally, the effect of the indenter front shape radius on the pipe response is negligible. Moreover, using the Cowper-Symonds strain rate model could increase the pipe response by 12%. Furthermore, for medium diameter pipelines (10 and 14 inches pipe), the prediction of both hybrid and BSM models are comparable. However, the hybrid model leads to slightly less resulting dent depth on the pipe.

Future Work

The findings of the present work correspond to a very specific trawling interference event where the pipe-soil interaction is negligible. In this regard, a comprehensive sensitivity study should be performed to fully understand the effect of pipe-soil interaction on the pipe's response during the trawl impact. Accordingly, the effect of the pipe's burial depth, pipe diameter, trawl load magnitude, and development of the soil berm along the pipe should be studied for different soil conditions. Furthermore, the pipe-soil interaction for pipe with beam elements could be modelled with the surface to surface contact between beam elements and analytical surface, which should be considered in the future works.

The Pipe in Pipe (PIP) system is being used increasingly in the flowline industry due to the thermal insulation benefits. However, the DNV-RP-F111 (2014) guideline is developed for a single-wall steel pipe and only has some suggestions for the PIP system. Accordingly, the use of the PIP system raises questions regarding the specific non-conservative regulations for designing the carrier pipe against the trawl impact. As such, the hybrid model should be extended for the PIP system.

In the event of twin bottom trawling, a clump weight is used to keep the net down, which is typically 1.2 to 1.4 times the weight of a single trawl door (DNV-RP-F111, 2014), and could apply a significant load on the flowline during the initial impact. Hence, the hybrid model should be extended to examine the interaction of a clump weight with a flowline.

The hybrid model is developed for trawling gear interference with a pipeline. However, it could be used for other impact scenarios in offshore areas to investigate a submerged pipeline subject to a transverse load applied by a knife front shaped indenter (i.e., dropped object, anchor impact, etc.).

Acknowledgment

This research became possible through the funds provided by the Natural Sciences and Engineering Research Council (NSERC), as well as the Mitacs Accelerate Program.

Reference

- Alexander, C., 2007. ASSESSING THE EFFECTS OF IMPACT FORCES ON SUBSEA FLOWLINES AND PIPELINES, in: The 26th International Conference on Offshore Mechanics and Arctic Engineering. San Diego, California USA.
- Bai, Y., Bai, Q., 2005. Subsea Pipelines and Risers. Mater. Mech. 1–700.
<https://doi.org/10.1016/B978-008044566-3.50023-3>
- DNV-OS-F101, 2013. Det Norske Veritas - DNV-OS-F101: Submarine pipeline systems. <https://doi.org/DNV-OS-F101>
- DNV-RP-F105, 2006. Det Norske Veritas - Free spanning pipelines 138.
- DNV-RP-F107, 2010. Det Norske Veritas - Risk Assessment of Pipeline Protection. Mater. Technol.
- DNV-RP-F111, 2014. Det Norske Veritas - Interference Between Trawl Gear and Pipelines.
- Ellinas, C.P., Walker, A.C., 1983. Damage on offshore tubular bracing members, IABSE reports = Rapports AIPC = IVBH Berichte.
<https://doi.org/http://doi.org/10.5169/seals-32425>
- Jones, N., 2012. Structural impact. Cambridge University Press.
- Jones, N., Birch, R.S., 1996. Influence of internal pressure on the impact behavior of steel pipelines. J. Press. Vessel Technol. Trans. ASME 118, 464–471.
<https://doi.org/10.1115/1.2842215>
- Ng, C.S., Shen, W.Q., 2006. Effect of lateral impact loads on failure of pressurized

- pipelines supported by foundation. *Proc. Inst. Mech. Eng. Part E J. Process Mech. Eng.* 220, 193–206. <https://doi.org/10.1243/0954408JPME97>
- Shen, W.Q., Jones, N., 1991. A comment on the low speed impact of a clamped beam by a heavy striker. *J. Struct. Mech.* 19, 527–549.
- Soreide, T.H., Moan, T., Amdahl, J., Taby, J., 1982. Analysis of Ship/Platform Impacts. *Behav. Off-Shore Struct.* 2, 257–278.
- Thomas, S.G., Reid, S.R., Johnson, W., 1976. Large deformations of thin-walled circular tubes under transverse loading—I: an experimental survey of the bending of simply supported tubes under a central load. *Int. J. Mech. Sci.* 18, 325–333.
- Wichtmann, T., Triantafyllidis, T., 2009. On the correlation of “static” and “dynamic” stiffness moduli of non-cohesive soils. *Bautechnik* 86, 28–39. <https://doi.org/10.1002/bate.200910039>
- Zheng, J., 2014. Overtrawlability and Mechanical Damage of Pipe-in-Pipe, PhD thesis. NATIONAL UNIVERSITY OF SINGAPORE.
- Zheng, J., Palmer, A., Brunning, P., 2013. Overtrawlability and Mechanical Damage of Pipe-in-Pipe. *J. Appl. Mech.* 81, 031006. <https://doi.org/10.1115/1.4024877>
- Zheng, J., Palmer, A., Lipski, W., Brunning, P., 2012. Impact Damage on Pipe-in-Pipe Systems, in: *International Offshore and Polar Engineering Conference*. Rhodes, Greece, pp. 152–157.

4 CHAPTER 4

A NUMERICAL INVESTIGATION ON A PIPE SUBJECT TO A NON-PERPENDICULAR TRAWL IMPACT USING A HYBRID SHELL-BEAM MODEL ²

Abstract

Fishing activity in offshore areas associated with oil and gas development is unavoidable. This presents a risk to the structural integrity of flowlines from trawl gear impact. Accordingly, DNV-RP-F111 recommends a beam and spring-mass (BSM) model to assess the overtrawlability of pipelines. Using the BSM model to examine a non-perpendicular trawl impact considers only the normal component of the impact; the tangential component of the non-perpendicular trawl impact is disregarded in the BSM model; this could lead to an underestimation of the pipe structural response. Accordingly, a hybrid shell-beam model is introduced to examine two cases, including 1) a pipe subjected to a non-perpendicular trawl impact, and 2) the case where only the normal component of the non-perpendicular trawl impact is considered. The results of this work for two pipe sizes, 5 and 14-inch diameter pipes, show that the dent depth in the pipe in case-1 exceeds the one in case-2 by 20 percent. It is concluded that the dent size in a pipe subject to a diagonal impact is dependent on both normal and tangential components of

² This paper was presented at the OPT-2020 conference in Amsterdam, Netherland. Editorial modifications are applied to the material of this paper, in order to maintain consistency throughout the thesis.

the impact. Accordingly, the hybrid shell-beam model enhances the capabilities of the BSM model, as the full non-perpendicular impact could be incorporated in the hybrid model.

Keywords: Non-perpendicular trawl impact, DNV-RP-F111, Beam and spring model, Hybrid shell-beam model, Damage propagation.

4.1 Introduction

DNV-RP-F107 (2010) categorizes the accidental events which could damage pipelines into impact or pull-over. In this regard, the interference of fishing gear with a pipe is an example that encompasses both impact and pull-over load (DNV-RP-F111, 2014). In this work, a numerical approach is employed to investigate an accidental trawling impact on a pipe, where the direction of the impact is not perpendicular to the pipe.

4.1.1 Literature Review

Oil and gas offshore areas are inevitably prone to fishing activity; this endangers the structural integrity of subsea structures when impacted by trawl fishing gear (e.g. the interference between trawl gear and pipelines). The common strategy to mitigate this risk is to trench the pipeline or cover it with a rock berm. However, the mitigation methods in offshore areas accompany a significant cost, which may not always be necessary, e.g. if the pipeline has a sufficiently high structural capacity or the likelihood of the trawl impact is negligible. As such, assessing the overtrawlability of pipelines not only results in a technically feasible pipe design but also could save a considerable unnecessary cost in a project.

The current industry practice to design a pipeline against trawl gear interference is the recommended practice by Det Norske Veritas: DNV-RP-F111 (2014). According to this

recommended practice, the trawling interference with a pipeline could include three phases: 1) the trawl gear impact, which occurs in some hundredths of a second; 2) the trawl pull-over load, which drags the pipeline; 3) the hooking phase, which is a rare phenomenon. During the initial phase, which is the focus of this paper, the global deformation of a pipe and consequently, the pipe-soil interaction is insignificant. Therefore, the impact is mainly resisted by the pipe wall thickness as well as a protective coating (if any).

There are two main methods to keep the trawl net open while fishing: beam trawls, this method uses a transverse beam; and otter trawls, which use trawl boards. The first trawl type is used mostly in shallow offshore areas (Bai and Bai, 2005); the latter trawl type is examined in this paper.

An analytical approach is proposed by DNV-RP-F111 (2014) to examine subsea pipelines against trawling interference. However, this method is conservative, particularly for small pipe sizes, as it assumes all the impact is resisted only by the pipe wall thickness. As an alternative method, a numerical approach is proposed, which leads to a more technically feasible pipe design; this method presents a beam and spring-mass (BSM) model, which considers several sources of energy dissipation, such as the pipe's global deformation and pipe-soil interaction.

Using the BSM model for the perpendicular trawl impact, the impact velocity is applied to a point mass associated with the trawl board; the velocity is also applied to another point mass, which represents the hydrodynamic added mass. The resulting kinetic energy is then transferred to the pipe via springs, which represent the trawl board. For a non-perpendicular trawl impact, the impact velocity is decoupled to a normal and tangential component relative to the pipeline; the tangential component is ignored, and the normal component is used in the BSM model.

The trawl impact presents a path-dependent response in the pipe if the impact induces plastic damage in the pipe. For path-dependent events, the structural behaviour at each time increment is influenced by the structural response at the previous time increment. In this regard, Quinton (2015, 2008) investigated the path-dependent interaction between ship hull structure and a moving ice load, using numerical and experimental methods. The authors concluded that the progression of the damage applied to the ship hull decreases the load-carrying capacity of the hull structure, compared to the scenario where the indentation is only perpendicular to the ship hull. The author termed this reduction as the moving load effect. Davaripour and Quinton (2018) used a numerical approach to investigate the effect of damage progression on the plastic capacity of pipes. It was concluded that the progression of plastic damage along a pipe may result in a significant decrease in the pipe's load-carrying capacity. This damage progression effect

is investigated in the present work in a scenario of a pipeline subject to a substantial lateral load.

In a non-perpendicular trawl interference with a pipeline, the tangential component of the trawl impact could result in the damage progression effect. Therefore, as the damage progression could not be considered in the BSM model, the diagonal trawl impact on a subsea pipeline should be investigated using a more realistic numerical model. Accordingly, the hybrid shell beam model, which was introduced in Davaripour et al. (2020a), is employed to investigate a scenario where the non-perpendicular trawl impact is applied to the pipe (Figure 4-1-a) versus when only the normal component of the diagonal trawl impact is applied to the pipe (Figure 4-1-b). These load cases are considered to examine the gap in the BSM model where the trawl impact is non-perpendicular, as the full diagonal impact could not be incorporated in the BSM model. In other words, using the BSM model, a diagonal trawl impact (case-1) is analyzed by considering only the normal component of the impact (case-2).

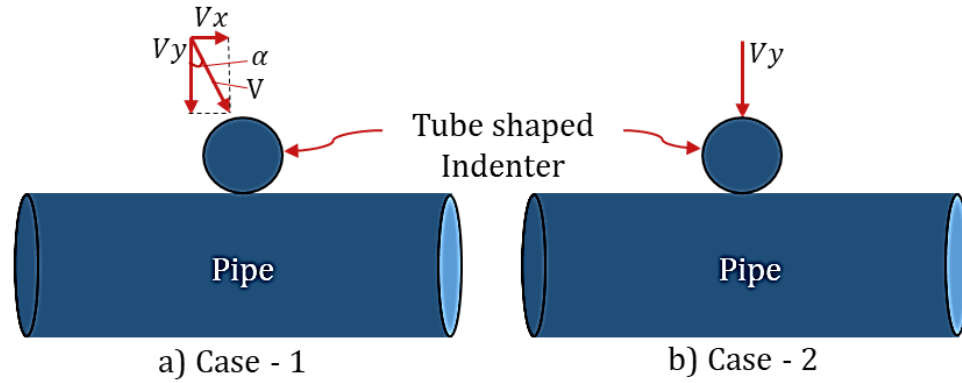


Figure 4-1 Schematic View of Case-1: a Pipe under a Non-Perpendicular Impact, and Case-2: a Pipe Subjected to Only the Normal Component of the Non-Perpendicular Trawl Impact

In this paper, first the BSM model is introduced; then, the hybrid model (an enhanced version of the BSM model) is presented, along with partial validation against physical test data. Finally, the relative damage using the hybrid model for two cases in Figure 4-1 is investigated for 5 and 14-inch diameter pipes.

4.1.2 Beam and Spring-Mass (BSM) Model

Figure 4-2 shows a schematic view of the BSM model, where:

- K_{ps} is the effective soil stiffness.
- K_{pb} is the effective stiffness of steel pipe.
- K_s is the local shell stiffness of a steel pipe, which is modelled by a spring with the stiffness derived from the load-displacement curve presented in Equation 4-1.
- K_t is the in-plane stiffness of the indenter.
- K_a is the out-of-plane stiffness of the indenter.

- M_p is the pipe mas.
- M_t is the indenter mass.
- M_a is the added mass.

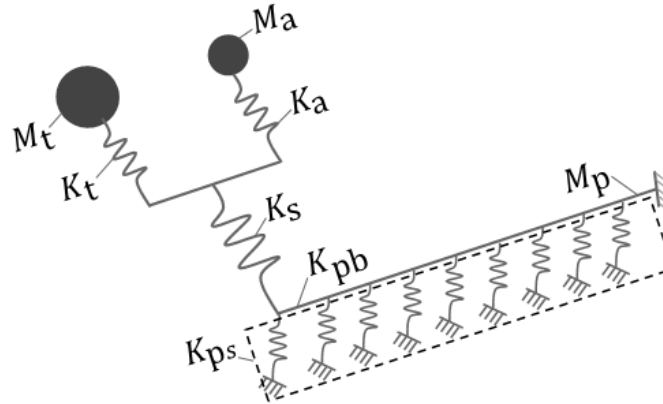


Figure 4-2. Schematic View of the BSM Model (Edited from Davaripour et al. (2020a))

$$f = m_p \cdot \alpha \cdot \left(\frac{H_t}{D} \right)^\beta \quad \text{Equation 4-1}$$

Where f is the impact force resisted by the pipe wall thickness, H_t is the total dent depth (elastic and permanent dent depth), m_p is the moment capacity of a pipeline (Equation 4-2), α and β are a function of pipeline's geometrical and mechanical properties (Equation 4-3 and Equation 4-4), t is the nominal thickness, and D is the outer diameter of a pipeline (DNV-RP-F111, 2014).

$$m_p = \frac{1}{4} \cdot f_y \cdot t^2 \quad \text{Equation 4-2}$$

$$\alpha = 37 \cdot \left[\ln\left(\frac{D}{t}\right) - \frac{1}{2} \right] \quad \text{Equation 4-3}$$

$$\beta = 0.125 \cdot \left[\ln\left(\frac{D}{t}\right) + 1 \right] \quad \text{Equation 4-4}$$

4.2 Hybrid Shell-Beam model

In this section, the hybrid shell beam model, which was introduced in Davaripour et al. (2020a), is presented. A schematic view of the model is shown in Figure 4-3; where:

- _ The middle part of the pipe is replaced with reduced integrated shell elements with 2.5 mm x 2.5 mm mesh size.
- _ A tube-shaped indenter with a radius equal to 25 mm is added, which represents the geometrical front shape of the trawl board.
- _ The middle part is extended for 250 m on each side using PIPE31 type beam elements with 125 mm mesh size.
- _ Kinematic coupling constraint is used to constrain the middle part at the ends to adjacent beam elements.

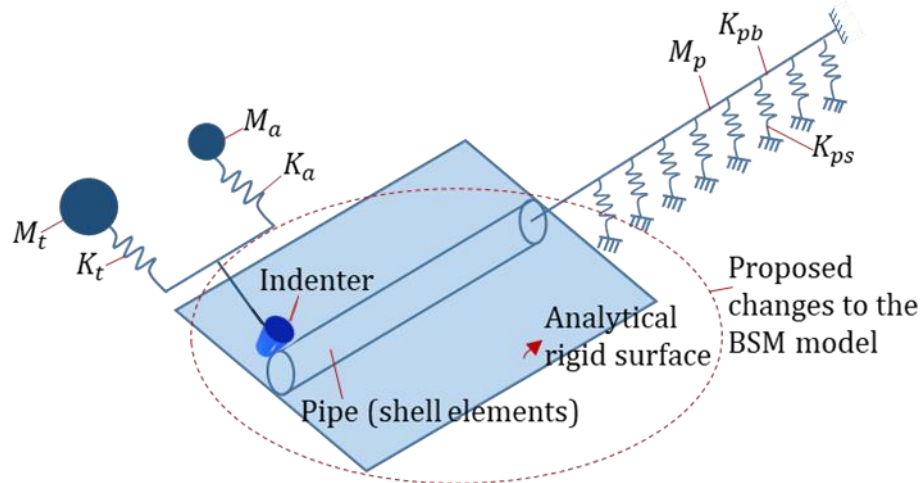


Figure 4-3 A Schematic View of the Hybrid Model (Edited from Davaripour et al. (2020a))

4.2.1 Material Model

In order to benchmark the hybrid model against publicly available physical data, the physical and mechanical properties of the pipe used in the hybrid model are selected the same as those used in the work conducted by Zheng (2014). Accordingly, specimen number SPS02 in (Zheng, 2014), which is a 5-inch diameter pipe schedule 40, is used to validate the hybrid model (Table 4-1). The engineering stress-strain curve, which is reported by Zheng (2014), is shown in Figure 4-4; this curve is converted into the true stress strain curve which is then implemented in the numerical model.

Table 4-1 Physical Properties of the SPS02 Specimen in (Zheng, 2014)

Outside diameter (mm)	Nominal thickness (mm)	Length (mm)
141.3	6.55	1500

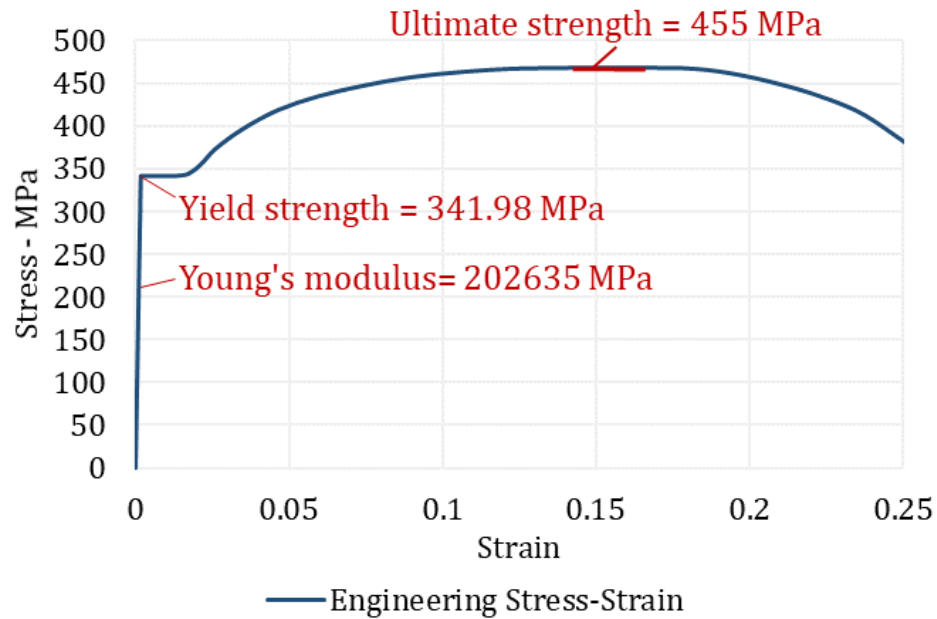


Figure 4-4 Engineering Stress-Strain Curve from (Zheng, 2014)

4.2.2 Pipe Soil Interaction

The pipe-soil interaction for the middle part of the pipeline with shell elements is modelled using the general contact between the pipe and an analytical rigid plate (Figure 4-3); the penalty friction formulation and linear pressure-overclosure are employed as the tangential behaviour and normal behaviour, respectively. For the extended parts of the pipeline with beam elements, the pipe-soil interaction is modelled using springs in all translational degrees of freedom (Figure 4-3). The vertical soil stiffness is derived based on Equation 4-5 (DNV-RP-F105, 2006). Also, for the lateral and axial pipe-soil interaction, a constant friction coefficient equal to 0.6 is employed.

$$K_v = \frac{C_v}{1 - \nu} \cdot \left(\frac{2}{3} * \frac{\rho_s}{\rho} \right) D^{0.5} \quad \text{Equation 4-5}$$

Where:

K_v is the vertical soil stiffness.

C_v is the coefficient for vertical soil stiffness.

$\frac{\rho_s}{\rho}$ is the specific mass ratio between the flowline mass and the displaced

water mass.

4.2.3 Trawl board

As shown in Figure 4-3, the stiffness of the trawl board is decoupled into the out-of-plane stiffness, which is associated with the hydrodynamic added mass, and the in-plane stiffness, which is associated with the trawl board steel mass. These stiffnesses are modelled using basic nonlinear connectors, which only move along the axial direction. Additionally, a rigid tube-shaped geometry is modelled to represent the front shape of the trawl board. The in-plane and out-of-plane stiffness of the trawl board are set to 500 and 10 MN/m. Also, the steel mass and hydrodynamic added mass are set to 4000 and 8560 kg.

4.2.4 Loading Condition

Two cases are examined and compared to investigate if the pipe response under the non-perpendicular trawl impact could be simplified by modelling only the normal component of the trawl impact: case-1) 30-degree impact angle with 2.6 m/sec impact velocity (Figure 4-5-a); case-2) only the normal component of the non-perpendicular impact (Figure 4-5-b). The analyses are performed using Abaqus explicit; the explicit time integration method is the best fit short duration impact events.

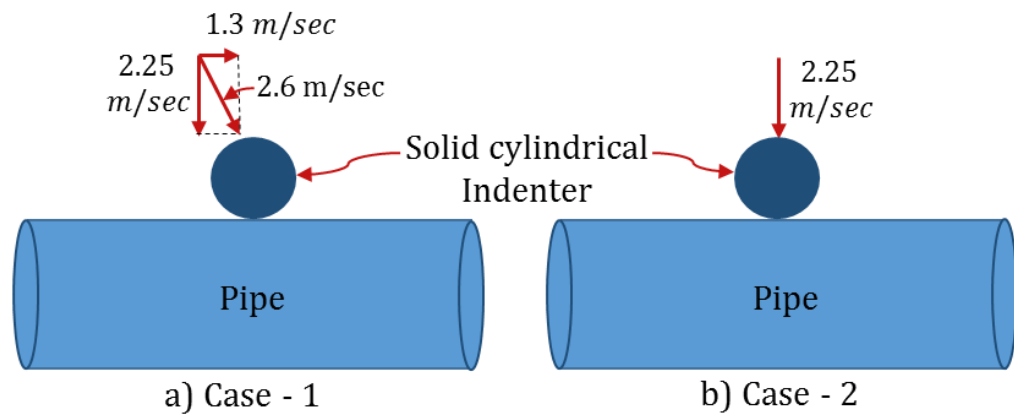


Figure 4-5 Loading Conditions: Case-1 with Non-Perpendicular Trawling Impact; Case-2 with Only the Normal Component of the Non-Perpendicular Trawling Impact

4.2.4.1 A Note on the Loading Condition

The loading condition, which was presented in Figure 4-5, does not correspond to two separate scenarios where a trawl board hits a subsea pipeline at two different angles. It

does correspond to one scenario of a subsea pipeline subject to a diagonal trawl impact at 30 degrees angle, where the following two conditions are considered in the analysis:

- Incorporating the full diagonal trawl impact
- Incorporating only the normal component of the trawl impact

The main motivation for this case study is to examine the applicability of the BSM model for the overtrawlability of a subsea pipeline where the pipe is subject to a diagonal trawl impact; as the BSM model could not incorporate the tangential component of a diagonal trawl impact.

4.2.5 Benchmarking

To the knowledge of the authors, partly due to the complex boundary conditions of a submerged pipeline laid on the seabed and impacted by a trawl board, there is no publicly available large-scale physical data that can be used to benchmark the hybrid model. Therefore, partial validation of the model, in comparing the local pipe response due to indenter (15 mm radius) impact, was conducted.

Zheng (2014) conducted experimental and numerical investigations on a pipe subject to a transverse indentation and concluded that for trawl gear interference with a pipeline, the quasi-static analysis could be used to predict the pipe structural behaviour. As such, the quasi-static test conducted by Zheng (2014) on a 5-inch diameter pipe schedule 40

(test number SPS02) is employed to validate the accuracy of the hybrid model; in this test, the indentation was performed using an indenter with a knife front shaped geometry with a radius equal to 15 mm. Figure 4-6 shows the boundary condition of the physical test. The hybrid model is adapted accordingly to be benchmarked against the test data.



Figure 4-6 Boundary Conditions Used to Benchmark the Hybrid Numerical Simulation edited (Davaripour et al., 2020a)

Figure 4-7 shows the load-displacement curve predicted by the numerical models versus the experimental data. Accordingly, the numerical result of this work is in a great agreement with the one conducted by Zheng (2014). However, both finite element models overpredict the experimental data. This discrepancy could be due to the idealization of the boundary conditions in the finite element model.

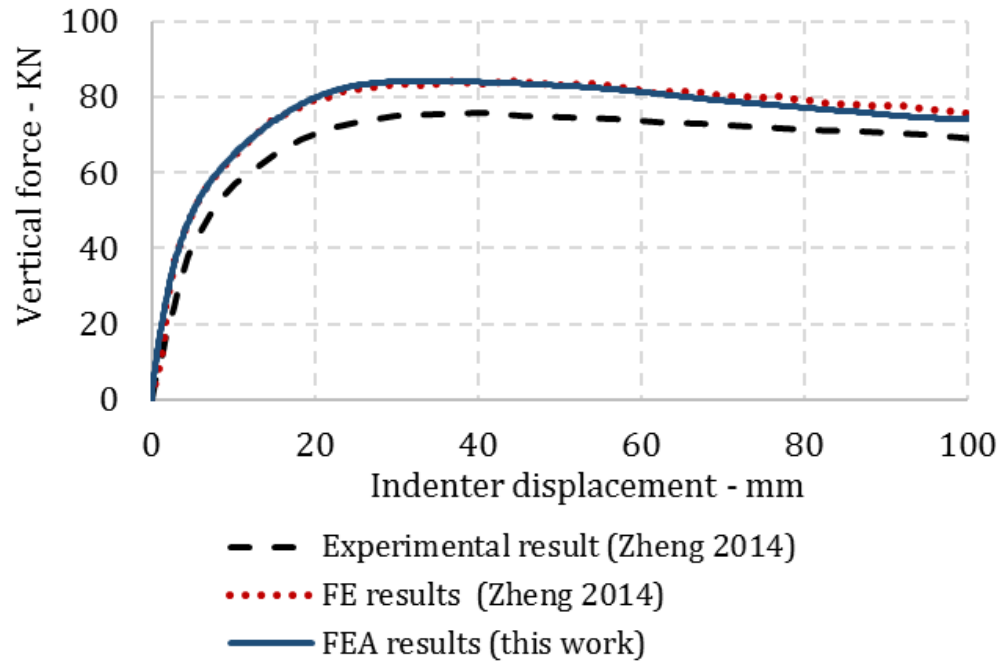


Figure 4-7 Vertical Load-Displacement Curve; Experimental Result Versus Numerical Prediction (Davaripour et al., 2020a)

4.2.6 Mesh Convergence Analysis

Mesh convergence analyses are conducted for both beam and shell elements independently. For beam elements, three edge lengths are used, including 250, 125, 62.5 mm; the analyses converged at 125 mm edge length (Figure 4-8). Similarly, for shell elements, four element lengths are employed, including 5.0, 3.75, 2.5, and 1.75 mm; the analyses converged at 2.5 mm element length (Figure 4-9).

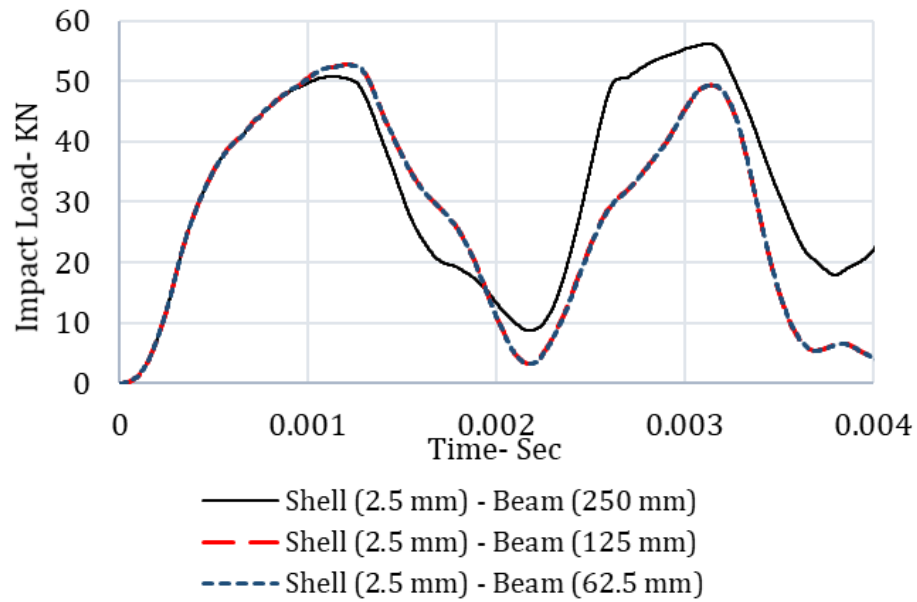


Figure 4-8 Mesh Convergence Analysis for the Hybrid Model: Beam Elements (Davaripour et al., 2020a)

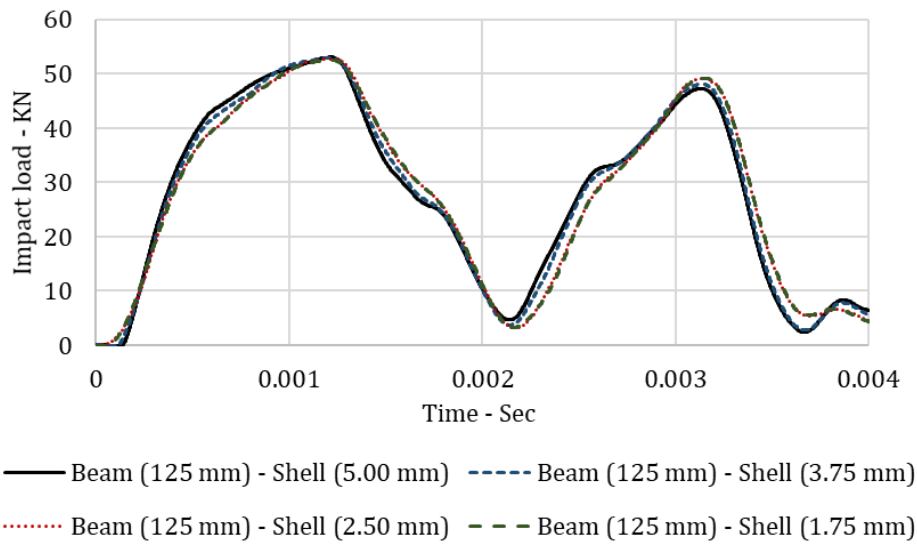


Figure 4-9 Mesh Convergence Analysis for the Hybrid Model: Shell Elements (Davaripour et al., 2020a)

4.3 Results and Discussion

Two scenarios of a pipeline subjected to a non-perpendicular trawl impact are investigated, including case-1) a non-perpendicular trawl impact with 2.6 m/sec impact velocity and 30 deg impact angle (Figure 4-5-a); case-2) only the normal component of the non-perpendicular trawl impact with 30 deg angle and impact velocity of 2.6 m/sec (Figure 4-5-b).

Figure 4-10 shows the dent depth in a pipeline resulting from case-1 and 2; the dent depth in case-1 exceeds the one in case-2 by 20 percent, at the steady-state part of the curves. While both scenarios have the same normal impact component, the discrepancy is due to the tangential component of the trawl impact, which is ignored in case-2. Considering that the tangential component of the non-perpendicular trawl impact pushes the plastic damage along the pipe, the result of this work is in agreement with the finding of Davaripour and Quinton (2018) that the progression of plastic damage along a cylinder could decrease its structural resistance.

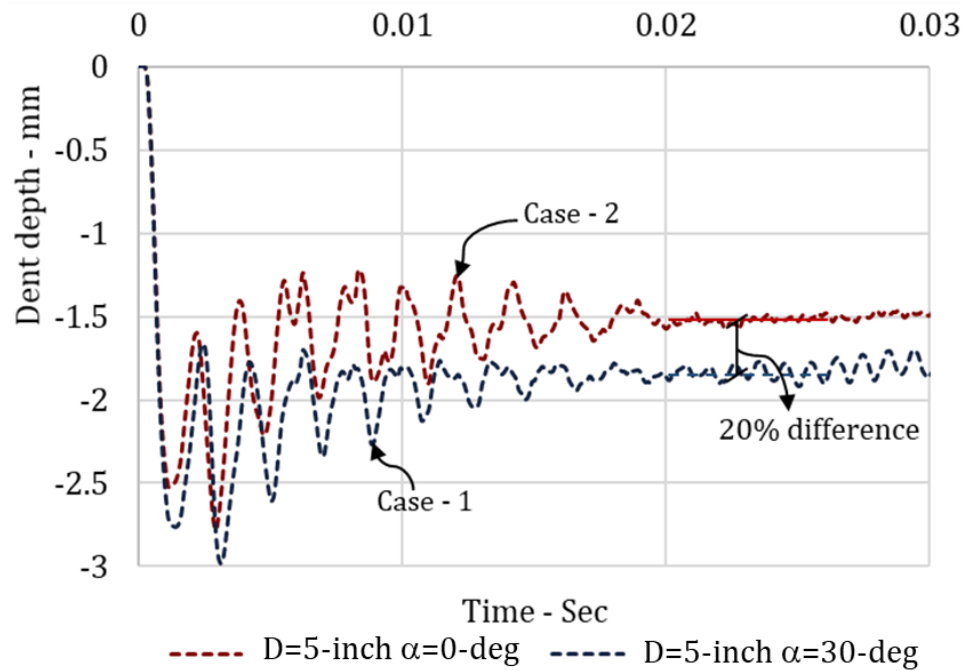


Figure 4-10 Dent Depth in a 5-inch Diameter Pipe for Case-1 and Case-2

4.3.1 Sensitivity Analyses (Pipe Diameter)

Numerical analyses are also conducted on a 14-inch diameter pipe with the wall thickness equal to 16 mm, under both case-1 and 2 scenarios. Accordingly, the dent depth in a pipeline under the trawl impact of case-1 exceeds the one from case-2 by 20 percent, at the steady-state part of the curve (Figure 4-11); this result is similar to the one obtained from the 5-inch diameter pipe.

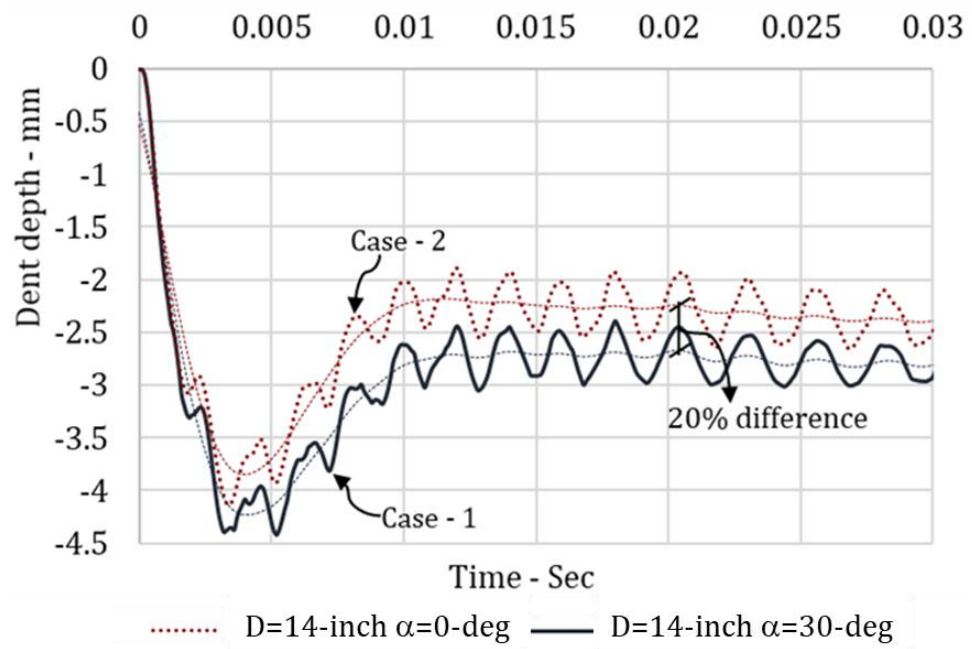


Figure 4-11 Dent Depth in a 14-inch Diameter Pipe for Case-1 and Case-2

4.4 Summary and Conclusions

Using the BSM model for a non-perpendicular trawl impact, the tangential component of the trawl impact is disregarded, and only the normal component of the impact is considered. However, the tangential component of the non-perpendicular trawl impact could push the applied damage along the pipe. In this regard, the findings of the previous work by Davaripour and Quinton (2018) showed that the progression of an indentation along a cylinder could decrease its structural resistance. Accordingly, a hybrid shell-beam model is introduced and employed to examine two scenarios including case-1) non-perpendicular trawl impact with 2.6 m/sec impact velocity and 30 deg impact angle; case-2) only the normal component of the non-perpendicular trawl impact with 30 deg angle and impact velocity of 2.6 m/sec. As a result of the numerical investigation, it is shown that the dent depth resulting from case-1 exceeds the one from case-2 by 20 percent for both 5 and 14-inch pipe sizes.

The numerical findings of this work show that in an event where a pipe is subject to a non-perpendicular trawl impact, the imposed damage size in the pipe is dependent on both normal and tangential component of the impact; in other words, the tangential component of the non-perpendicular impact could not be disregarded. Accordingly, the hybrid shell-beam model, which incorporates the full diagonal impact (not only the normal component of the impact), could enhance the capability of the BSM model.

Future Work

The shell stiffness in the BSM model is derived from an empirical equation (Equation 4-1), which predicts the pipe's response under a perpendicular indentation. A new empirical equation should be proposed to account for a non-perpendicular indentation on a pipe. The shell stiffness in the BSM model should be obtained based on this equation to account for the damage progression effect; when assessing a scenario of a pipe subject to a diagonal trawl impact.

A series of physical tests should be conducted to investigate the pipe response subject to a non-perpendicular indentation. The outcome of these tests will present further insight into the path-dependent behaviour of a pipe when the applied damage is translated along the pipe.

Acknowledgment

This research became possible through the funds provided by the Natural Sciences and Engineering Research Council's (NSERC) Discovery Grant program, as well as the Mitacs Accelerate Program. The authors sincerely appreciate the valuable comments provided by Richard Persaud from Genesis.

Reference

- Bai, Y., Bai, Q., 2005. Subsea Pipelines and Risers. *Mater. Mech.* 1–700.
<https://doi.org/10.1016/B978-008044566-3.50023-3>
- Davaripour, F., Pike, K., Quinton, B.W.T., Persaud, R., 2020a. An Assessment on the Overtrawlability of Small Pipe Sizes Using a Hybrid Shell- Beam Model : The Initial Trawl Impact Phase (Revision Requested). *Appl. Ocean Res.*
- Davaripour, F., Quinton, B.W.T., 2018. An Investigation of the Load Carrying Capacity of Pipelines Under Accidental and Longitudinal Moving (Sliding) Loads, in: *Proceedings of the 12th International Pipeline Conference IPC 2018*. pp. 1–7.
- DNV-RP-F107, 2010. Det Norske Veritas - Risk Assessment of Pipeline Protection. *Mater. Technol.*
- DNV-RP-F111, 2014. Det Norske Veritas - Interference Between Trawl Gear and Pipelines.
- Quinton, B., 2015. Experimental and numerical investigation of moving loads on hull structures. PhD thesis, Memorial University of Newfoundland.
- Quinton, B., 2008. Progressive damage to a Ship's structure due to ice loading. Master thesis, Memorial University of Newfoundland.
<https://doi.org/10.13140/RG.2.1.1395.6562>
- Zheng, J., 2014. Overtrawlability and Mechanical Damage of Pipe-in- Piped. NATIONAL UNIVERSITY OF SINGAPORE. <https://doi.org/10.1115/1.4024877>

5 CHAPTER 5

ASSESSMENT ON A SUBSEA PIPELINE SUBJECT TO A DIAGONAL TRAWL IMPACT

Abstract

In oil and gas offshore areas, flowlines in fishing waters are at risk of trawl gear impacts. In this regard, DNV-RP-F111 recommends a beam and spring-mass (BSM) model to assess the overtrawlability of subsea pipelines, and the BSM model is commonly employed to assess perpendicular trawl impacts on pipelines. However, in the case of a subsea pipeline under a non-perpendicular trawl impact, the BSM model does not incorporate the full diagonal load; the tangential component of the impact load is disregarded. Furthermore, the BSM model does not account for the progression of damage on a pipe (e.g., the plastic damage on a pipe that is imposed by a non-perpendicular trawl impact and is pushed along the pipe during the impact). Davaripour and Quinton (2018) showed that damage progression could decrease the structural resistance of a pipeline. Therefore, as the BSM model does not consider the damage progression effect, it could underestimate the resulting dent depth in a pipe. The present study uses an experimental investigation to examine the damage progression effect in a cylindrical specimen. Furthermore, using a hybrid shell-beam finite element model, an enhanced version of the BSM model, a scenario of a pipe subject to a diagonal impact is investigated. The experimental results show that the dent depth in a 5-inch diameter pipe under a perpendicular 150 KN load could increase by 52%, where the imposed damage

is pushed for 300 mm along the pipe. In addition, the results obtained from the finite element analyses show that the dent depth in 5 and 14-inch diameter pipelines increases by 20% under a diagonal trawl impact with 30 degrees from normal to the pipe, compared to applying only the normal component of the diagonal impact. In conclusion, the resulting dent size in a pipe under a diagonal trawl impact is dependent on both normal and tangential components of the impact. Furthermore, the hybrid shell-beam model could be a suitable alternative to the BSM model for scenarios where a pipe is subject to a diagonal trawl impact.

Keywords: Diagonal trawl impact, Damage progression, DNV-RP-F111, Beam and spring model, Hybrid shell-beam model.

5.1 Introduction

Fishing activity in oil and gas offshore areas is inevitable. This presents a risk to the structural integrity of flowlines due to trawl gear impact. To mitigate this risk, flowlines are often protected using trenching/burial, and/or rock dump. However, these mitigation strategies lead to a significant extra cost to the project. Hence, it is necessary to assess the flowline overtrawlability to achieve a technically feasible pipe design and improve project economics.

The structural behaviour of a pipe subject to different loading conditions has been investigated by several studies; however, among these works, the ones that examined the pipe response subject to a transverse load via a knife front-shaped indenter are more relevant to the overtrawlability problems, i.e. (Ellinas and Walker, 1983). In this regard, Ellinas and Walker (1983) and Thomas et al. (1976) assumed the deformation of pipelines could be idealized to phase-1) purely local and then phase-2) global and local deformation. Whereas, Zheng et al. (2012) stated that the bending response in a pipeline initiates slowly from the very beginning of the indentation. Then, the global deformation increases when the cross-section of the pipe changes due to the local deformation.

Jones and Birch (1996) investigated pressurized pipes under high-velocity impact tests, i.e., 13.6 m/sec. The authors assessed the failure modes of pipes using varied impact load and with the internal pressure leading to a hoop stress up to one-third of the material yield

strength. Ng and Shen (2006) investigated the effect of incorporating the foundation support in the impact test on pressurized pipes. The authors concluded that the circumferential stress developed due to the interaction between the pipe and the foundation support affects the threshold where failure occurs in the pipes. However, in trawl interference events, the impact occurs along the seabed, and the pipe-soil interaction is insignificant.

Shen and Jones (1991) did analytical studies on a clamped beam under a transverse load and concluded that the dynamic response of a pipe under a heavy indenter moving at relatively low speed could be captured using quasi-static analysis. Also, Zheng (2014) conducted experimental and numerical investigations on a pipe under a lateral indentation and reached the same conclusion. For trawl gear impact with a pipe, the indenter is several tonnes and moves at a relatively low speed. As such, the quasi-static method could be used to investigate the interference between trawl gear and pipelines.

DNV-RP-F111 (2014): “Interference Between Trawl Gear and Flowlines” is the current industry recommended practice to design a pipeline against trawl gear impact. According to DNV-RP-F111 (2014), trawl gear interaction with a pipeline can be decoupled into three phases, including impact, pull-over, and hooking. The initial impact phase, which is the focus of the present research scope, occurs in some hundredths of a second. As such, the kinetic energy is mostly absorbed by the pipe-wall as well as the protective

coating in the form of strain energy. In other words, during the initial impact phase, the global pipeline deformation and pipe-soil interaction are insignificant. In the present paper, the trawl gear impact or overtrawlability assessment of pipelines only refers to the initial phase of the trawl gear interference event.

Trawl types are categorized into two groups based on how the net is kept open during trawling, including a) otter trawls using trawl boards; b) beam trawls using a transverse beam. The beam trawl type is mostly used in shallow waters (Bai and Bai, 2005). The present work only considers the interaction between trawl boards and flowlines.

DNV-RP-F111 (2014) proposes two methods to assess the structural response of a flowline under the impact phase, including the analytical and the numerical method. The first method is conservative as it assumes all the impact energy is absorbed through local flowline indentation. The latter method employs a beam and spring-mass (BSM) model that accounts for the stiffness of the concrete coating and insulation protection, as well as the energy dissipation during the global flowline deformation (e.g., pipe-soil interaction).

Using the BSM model to examine a perpendicular trawl impact on a pipeline, first, the impact velocity is applied to a point mass associated with the trawl board, as well as a point mass which represents the hydrodynamic added mass. Then, the resulting kinetic energy is transferred to the pipe via springs which represent the in-plane and out of plane

stiffnesses of the trawl board. On the other hand, for a non-perpendicular trawl impact, the impact velocity is decoupled to the normal and tangential components; the normal component follows the above steps, and the tangential component is disregarded; the tangential component could not be incorporated in the BSM model. However, the tangential component of a diagonal impact could push the imposed damage (if any) along the pipe. In this regard, Davaripour and Quinton (2018) showed that pipe resistance could drop significantly, where the plastic damage imposed on the pipe, translates longitudinally along the pipe. As the BSM model does not consider this effect, using the BSM model could underestimate the pipe response, where the pipe is subject to a diagonal trawl impact (Davaripour et al., 2020b).

The progression of damage in a structure was studied in several recent works. Davaripour and Quinton (2018) were the first to investigate the behaviour of a cylindrical structure where the imposed damage on the pipe was pushed longitudinally along the pipe. The authors employed finite element (FE) methods and concluded that the resistance of a pipe could drop significantly where the applied plastic damage travels along the pipe; this reduction in the pipe structural response is termed as the damage progression effect throughout the present work. Similar studies are also conducted using numerical and experimental methods to investigate the damage progression effect on plates, and comparable results are provided, e.g., (Quinton, 2015, 2008).

Furthermore, several relevant works are conducted to examine the plastic behaviour of a structure where the applied load moves along the structure. Parkes (1958) investigated the plastic response of a rigid plastic beam subjected to a travelling load. Neal (1960) conducted similar research but on the mass-included rigid plastic beam. Toridis and Wen (1966) presented an analytical solution for an elasto-plastic beam under a travelling load. Frýba (1999) performed an analytical investigation on a rigid plastic beam with a stationary hinge in the middle under a concentrated travelling load.

As there is no previous physical test on the subject of the damage progression effect on pipelines, an experimental investigation is conducted in the present study, using a novel test apparatus. Furthermore, a numerical study is conducted to examine the trawl gear interference with a subsea pipeline, where the impact direction is non-perpendicular to the pipe. Accordingly, first, the BSM and hybrid shell beam models are presented; then, the hybrid model is employed to examine the scenario, where: case-1) pipe is under a diagonal impact; case-2) pipe is only subject to the normal component of the diagonal impact in case-1.

5.1.1 Beam and Spring-Mass (BSM) Model

Figure 5-1 presents a schematic view of the BSM model, where a) K_{ps} is the effective soil stiffness, which is modelled using discrete springs attached to the end of beam elements; b) K_{pb} is the effective stiffness of the steel pipe, which is modelled using beam elements,

and represents the global stiffness of a pipeline; c) K_s is the local shell stiffness of a steel pipe, which is modelled by a spring with the stiffness presented in Equation 5-1; K_s represents the indentation characteristics of a pipe-wall; d) K_t is the in-plane stiffness of the indenter; e) K_a is the out-of-plane stiffness of the indenter; f) M_p is the pipe mass; g) M_t is the indenter mass; h) M_a is the added mass.

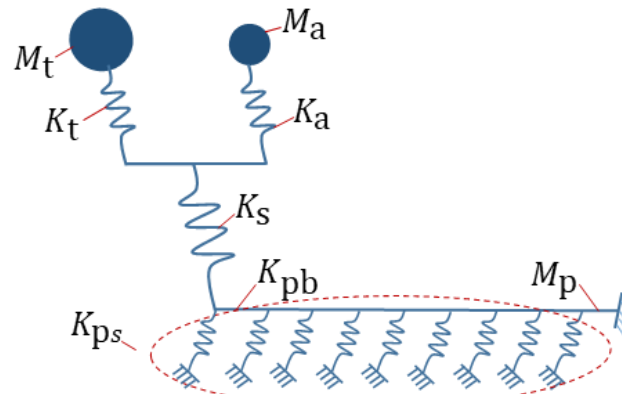


Figure 5-1 A Schematic View of the BSM Model (Edited from Davaripour et al. (2020a))

$$f = m_p \cdot \alpha \cdot (H_t/D)^\beta \quad \text{Equation 5-1}$$

Where f is the impact force resisted by the pipe wall thickness, H_t is the total dent depth (elastic and plastic dent depth), m_p is the moment capacity of a pipeline (Equation 5-2), α and β are a function of pipeline's geometrical and mechanical properties (Equation 5-3 and Equation 5-4), t is the nominal thickness, and D is the outer diameter of a pipeline (DNV-RP-F111, 2014).

$$m_p = 1/4 \cdot f_y \cdot t^2 \quad \text{Equation 5-2}$$

$$\alpha = 37 \cdot [\ln(D/t) - 1/2] \quad \text{Equation 5-3}$$

$$\beta = 0.125 \cdot [\ln(D/t) + 1] \quad \text{Equation 5-4}$$

5.1.2 Objectives

The objectives of the present study are to a) investigate the structural behaviour of a small diameter pipe when subject to a rigid cylindrical indenter; b) investigate the damage progression effect in a small diameter pipe, where the plastic damage imposed on the pipe is translated longitudinally along the pipe; d) provide suitable laboratory data to validate the accuracy of future numerical models; e) assess the structural response of a subsea pipeline subject to a non-perpendicular trawl impact using the hybrid shell-beam model. Furthermore, the results of the present study give an insight into the accuracy of the BSM model to assess the diagonal trawl gear interference with subsea pipelines.

5.1.3 Notes on the Scope

The present study presents a physical test on a small-diameter pipe to provide evidence regarding the effect of damage progression on the plastic capacity of a pipeline. This is the main objective of the present work, which dictates the physical test condition. Furthermore, this work introduces an application of the damage progression effect in the pipeline industry, where the pipe is subject to a diagonal trawl impact. In this regard, the recommendations of DNV-RP-F111 was considered in the design of the physical test

components. However, the test setup does not fully represent a scenario of a trawl interference event with a subsea pipeline. Nevertheless, considering the following points, the physical test results could be employed to validate numerical models for a detailed investigation of the trawl impact on a subsea pipeline:

- Shen and Jones (1991) showed that the dynamic effect of an impact scenario could be reproduced using an equivalent quasi-static analysis. This finding was assessed by Zheng et al. (2013) for a scenario of a subsea pipeline subject to fishing gear impact. The authors performed physical tests and showed that the pipe's response under impact event and quasi-static scenario is in the same range. As such, this finding was implemented in the present study physical test. Accordingly, the physical test of the present work was conducted under the quasi-static condition.
- The interference of trawl gear with a subsea pipeline is parallel to the seabed. As such, assuming that the pipe is laid on the seabed, the pipe-soil interaction is negligible (Zheng et al., 2012). Therefore, the interaction between pipe and soil could be disregarded in the pipe's overtrawlability assessment. As such, the present study test setup does not incorporate the pipe-soil interaction.
- The present study only considers the initial phase of trawl gear impact with a subsea pipeline where the governing pipe's response is local deformation on the pipe wall. In other words, the global deformation of the pipe is insignificant during the trawl gear impact. Therefore, in the present study test setup, the lateral deformation of the specimen is restrained.

Furthermore, the two-phase loading condition is employed for the physical test of the present study to assess the pipe's response during the progression of plastic damage, including phase 1, where the specimen is subject to a perpendicular indentation; then the resulting plastic damage in phase 1 induces and translates along the pipe in phase 2. Considering the above-mentioned points, the first phase could represent the initial phase of the trawl gear impact event. However, the second phase was aimed to only highlight the effect of damage progression on the plastic capacity of the pipe. Hence, the second phase may not correspond to any particular event in the offshore pipeline industry.

5.2 Experimental Investigation

As the damage progression effect has not been studied in a physical test, an experimental investigation was conducted using a novel test apparatus devised by Quinton (2015); the apparatus was modified to meet the recommendations provided in DNV-RP-F111 (2014). As such, the test results could partly represent trawl gear interaction with flowlines.

5.2.1 Methodology

5.2.1.1 Test Apparatus

Figure 5-2 shows an overall view of the test apparatus, which was employed to perform the load-controlled test on a cylindrical specimen. The apparatus was designed to allow for perpendicular, as well as sliding loads on the specimen.

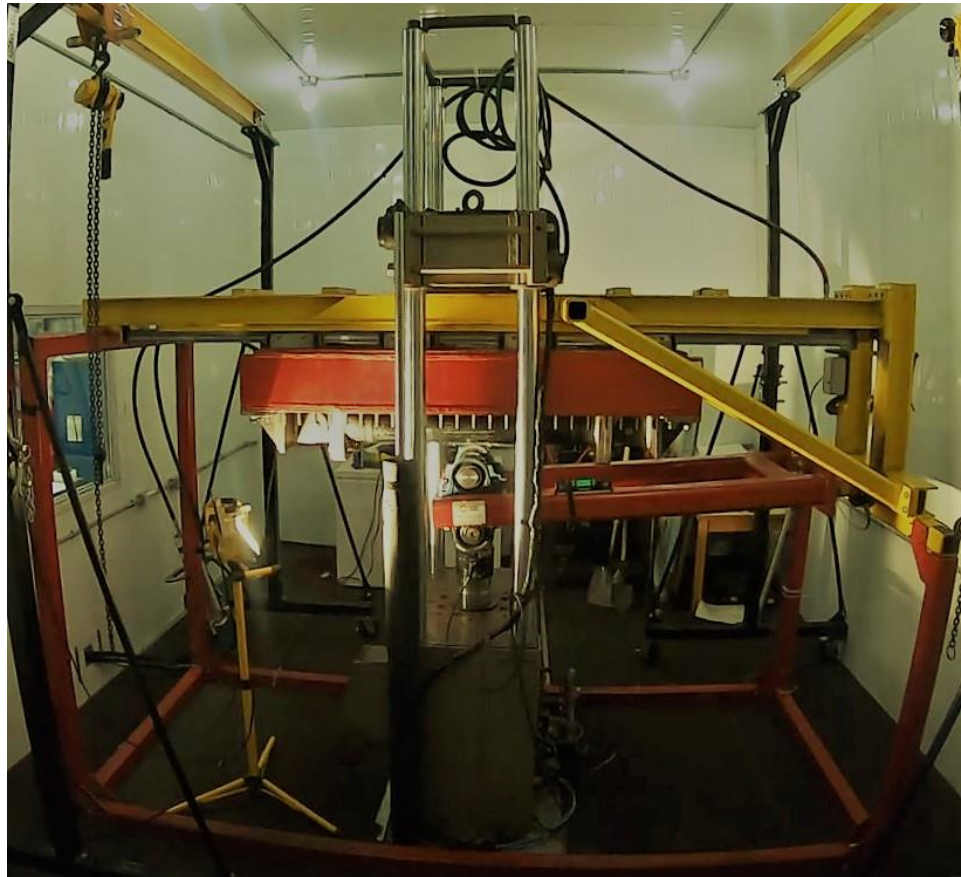


Figure 5-2 A Schematic View of the Test Apparatus

Figure 5-3 shows the components of the test apparatus involved in the vertical and horizontal load paths with the main components in the vertical direction including MTS hydraulic ram, cylindrical indenter, test specimen, and carriage, and in the horizontal direction including horizontal ram, carriage, test specimen, indenter, swing-arm, and the horizontal load cell. A vertically oriented hydraulic ram, mounted in the MTS test frame, provides the vertical load up to 500 KN. Also, in the horizontal direction, which refers to

the direction along the carriage, a horizontally oriented ram provides up to a 225 kN horizontal load.

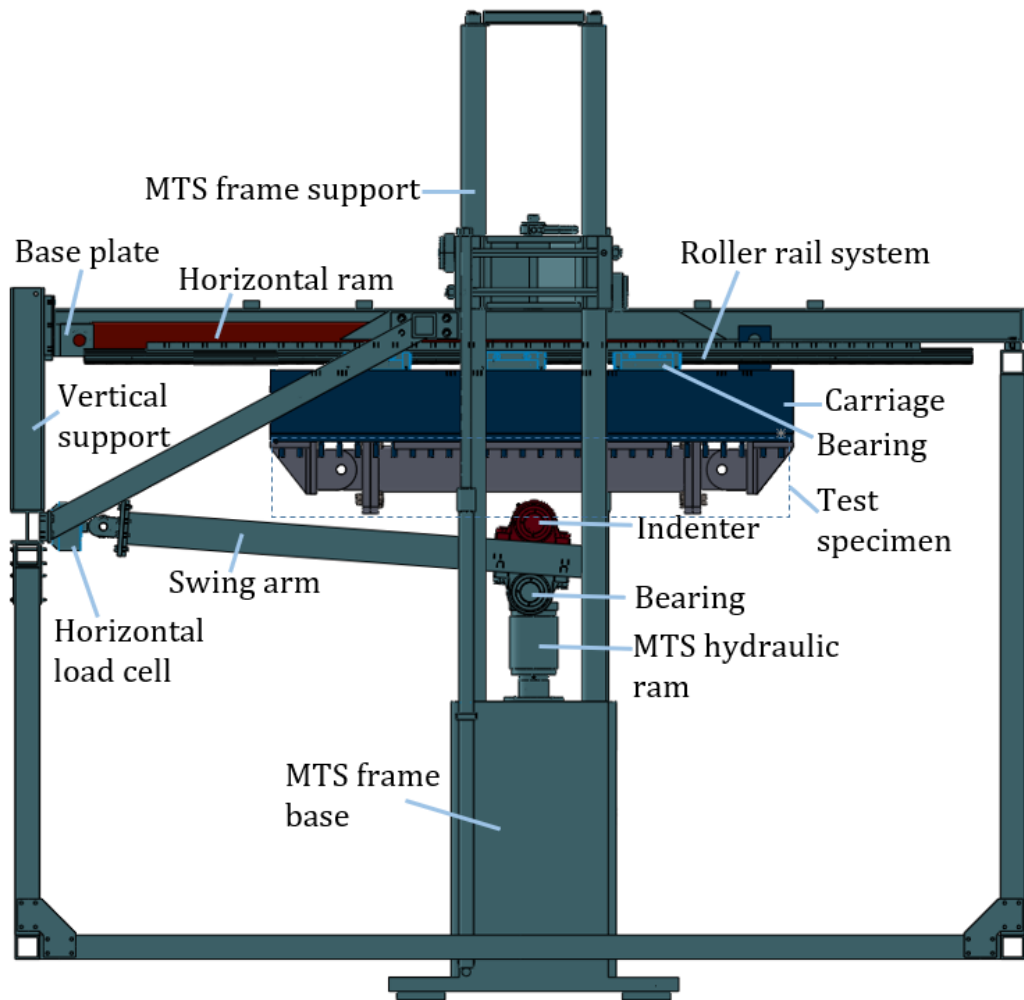


Figure 5-3 Components of the Test Apparatus in the Vertical Load Path (Edited from Davaripour et al. (2020b))

The test setup is designed according to DNV-RP-F111 (2014). Figure 5-4 shows a schematic view of the test setup, which is bolted to the carriage; it encompasses three

components, including the cylindrical specimen, the saddle-shaped support, and the mounts. The specimen is a 5-inch diameter steel tube (schedule 40); the pipe is an API grade B with the mechanical properties obtained from standard tensile coupon tests. Figure 5-5 shows the stress-strain curve averaged from the tensile test results. Also, Table 5-1 summarizes the mechanical and physical properties of the cylindrical specimen. The whole length of the specimen between the pins is 1200 mm. However, the middle deformable part by accounting for the groove welding between the specimen and the end flanges is ~ 940 mm long.

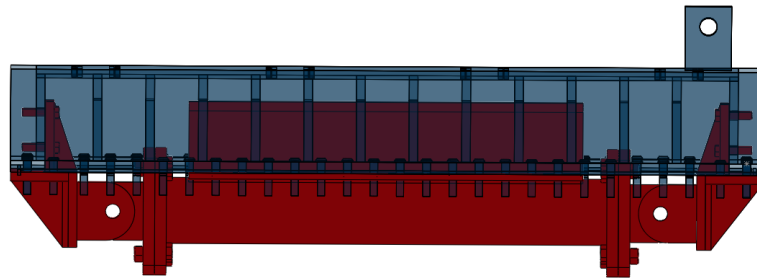


Figure 5-4 A Schematic View of the Test Setup (Colored in Red) Connected to the Carriage

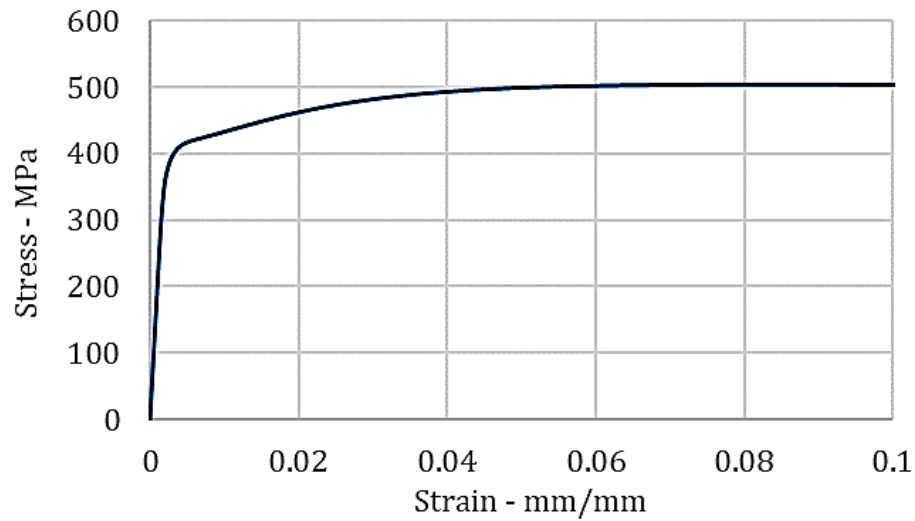


Figure 5-5 Engineering Stress-Strain Curve for the Cylindrical Specimen (Davaripour et al., 2020a)

Table 5-1 Physical and Mechanical Properties of the Cylindrical Specimen

Physical properties		
Pipe Outer Diameter_ D (mm)	Pipe Wall Thickness_ t (mm)	Pipe Length_ L (mm)
140.97	6.1468	1200
Mechanical properties		
Elastic Modulus_ E (MPa)	Yield Strength_ fy (MPa)	Ultimate Strength_ fu (MPa)
201404	412.26	503.56

Figure 5-6 shows the saddle-shaped support, which involves a plate with length and thickness equal to 863.6 and 25.4 mm, respectively; the radius of the cylindrical groove in the center of the plate is 70.65 mm (the same as the pipe diameter); the cylindrical groove in the center of the plate provides 60 degrees of circumferential contact with the pipe, as recommended by DNV-RP-F111 (2014). Also, an I-beam is welded to the plate and contacts the stiffeners inside the top of the carriage (Figure 5-7); the I-beam, along

with the bolts along the long edges of the plate, transfer the applied load from the specimen to the carriage.

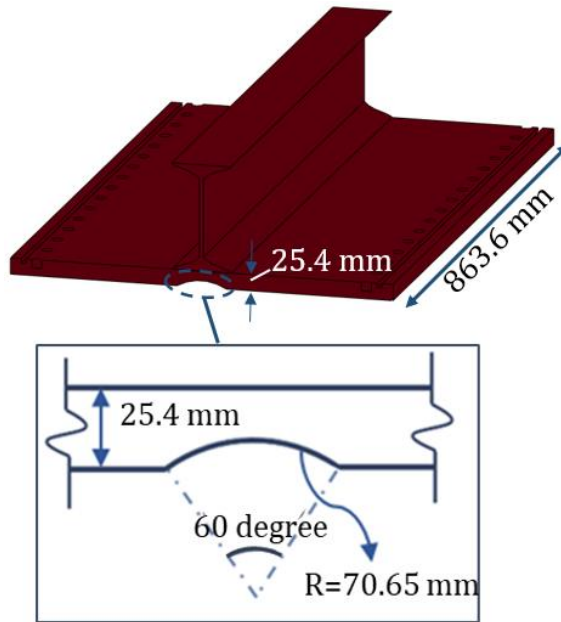


Figure 5-6 A View of the Saddle-Shaped Support

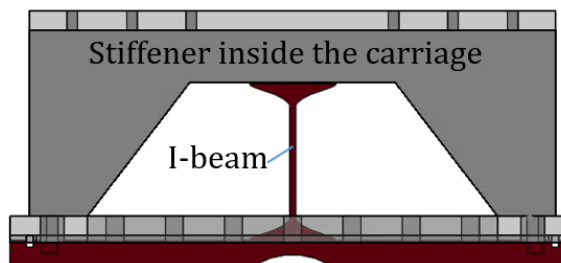


Figure 5-7 The Connection Between the I-beam with a Stiffener Inside the Carriage

Figure 5-8 shows a view of the mounts which are made of high strength steel (ASTM A514) with yield and ultimate strengths equal to 779 and 827 MPa, respectively, based

on the mill material certification. The mounts are connected to the carriage through the key stock and the bolts.

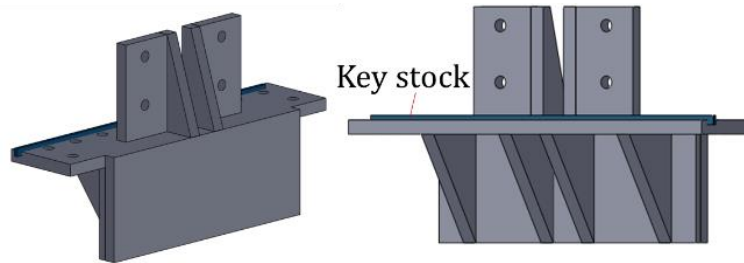


Figure 5-8 Schematic View of the Mount

Figure 5-9 shows a view of the solid cylindrical indenter, which is designed according to DNV-RP-F111 (2014). The indenter represents the trawl board and has a radius equal to 25 mm, and a length of 203 mm. In order to eliminate the influence of friction on the pipe structural response, the indenter is supported by two pillow-block bearings, where the shaft could roll while translating along the specimen. Additionally, lubrication is used in the region of contact to further decrease the friction between the indenter and the specimen.

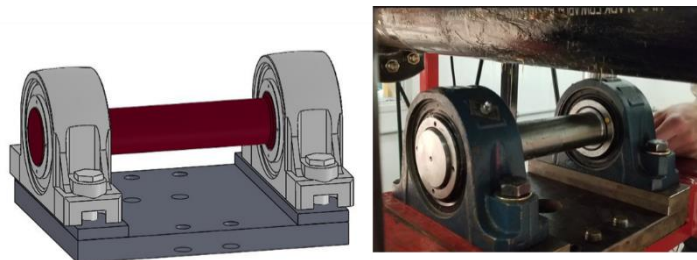


Figure 5-9 Solid Cylindrical Indenter

5.2.1.2 Boundary Conditions

Figure 5-10 shows the schematic view of the boundary conditions (BC) employed in the test setup. The indentation is absorbed only by local deformation of the pipe wall thickness; the global deformation of the pipe is restrained.

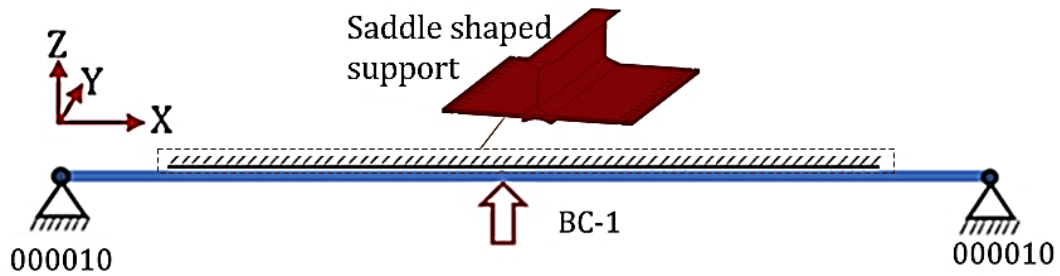


Figure 5-10 Boundary Condition Employed in the Physical Test

5.2.1.3 Test Procedure

According to the studies conducted by Shen and Jones (1991) and Zheng (2014), the overtrawlability of pipelines could be assessed using quasi-static analyses. As such, the test in the present study is performed under the quasi-static condition and in two phases, including a) Phase 1, where the vertical hydraulic ram applies 150 kN to the pipe in a load-controlled condition (3 kN/sec), as shown schematically in Figure 5-11-a; b) Phase 2, where the 150 kN vertical force remains steady, and the horizontal hydraulic ram pushes the carriage along the rail in a displacement-controlled condition (1 mm/sec), as shown schematically in Figure 5-11-b. Also, Figure 5-12 shows the deformed cylindrical

specimen prior to the indentation (Figure 5-12-a), at the end of phase 1 (Figure 5-12-b), and after the completion of phase 2 (Figure 5-12-c).

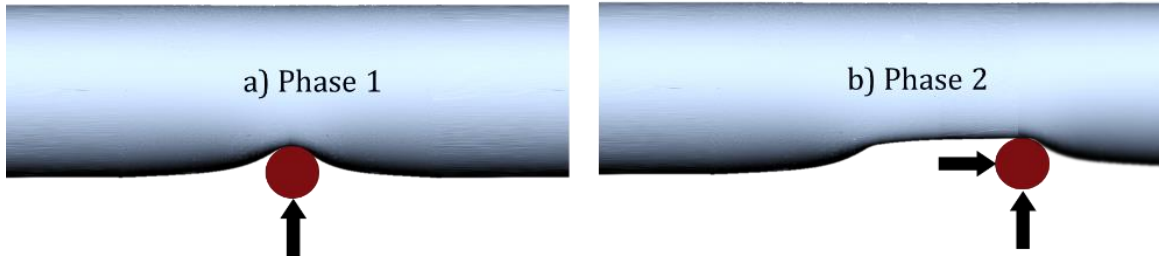


Figure 5-11 Loading Condition of the Present Study Physical Test

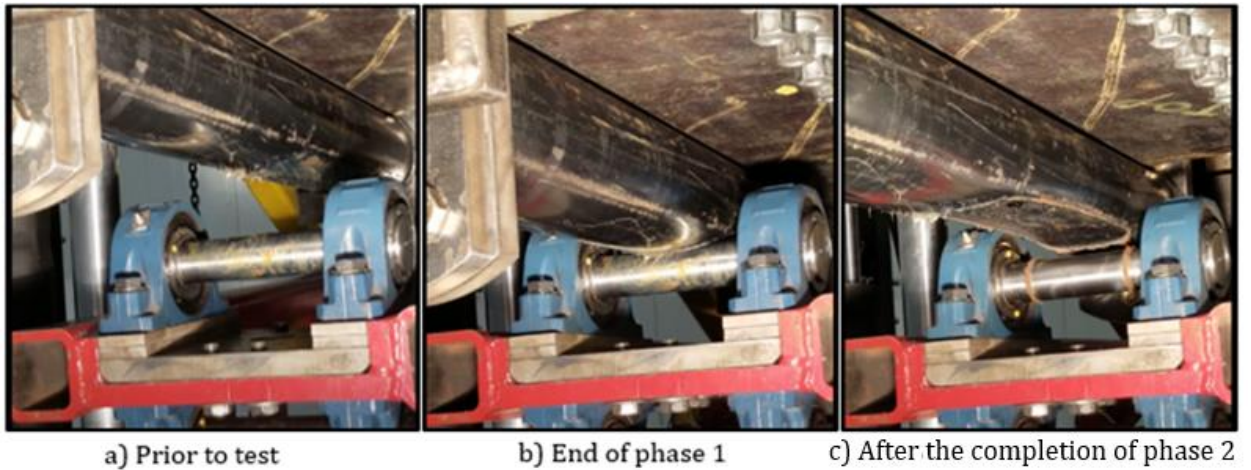


Figure 5-12 Test Procedure: 1) Prior to the Indentation, b) End of Phase 1, c) End of phase 2

5.2.2 Results

The results provided in the present study mainly involve the load-displacement curve as well as the measurement of the spatial displacement of the deformed specimen; which are obtained using the MTS test frame data acquisition system, imaging technology, and

laser scanning technology. Figure 5-13 shows the scanned view of the deformed specimen.

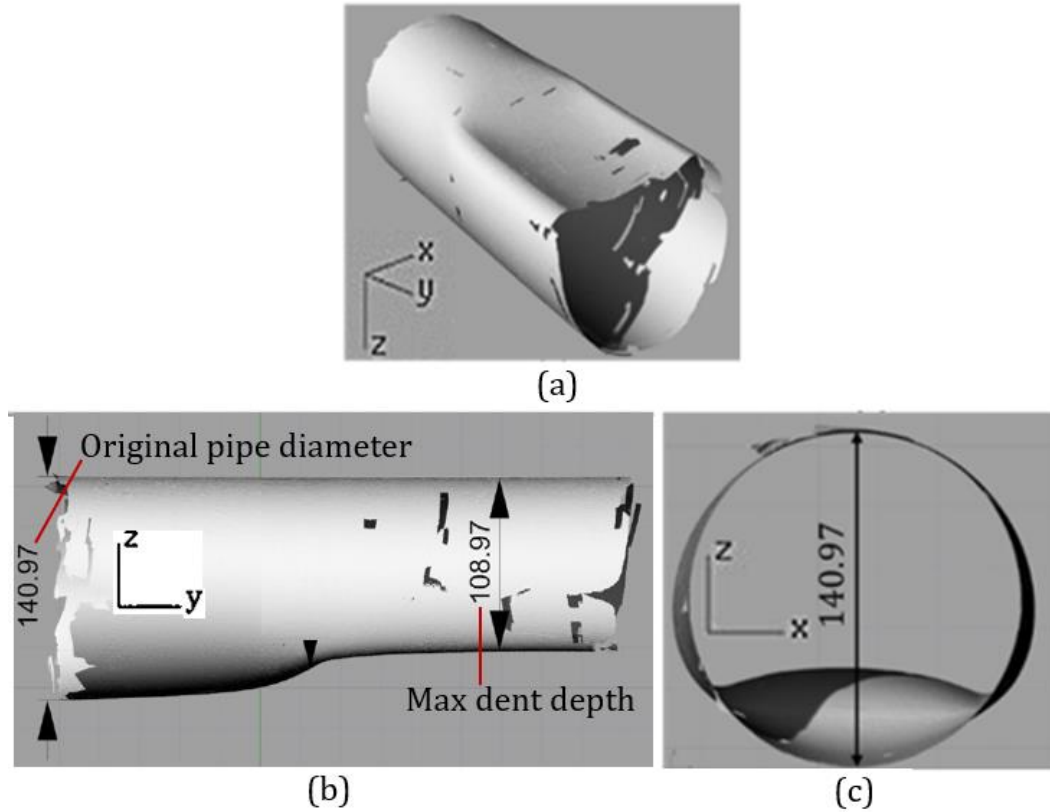


Figure 5-13 Scanned View of the Deformed Cylindrical Specimen a) Isotropic View, b) Z-Y View, c) Z-X View

Figure 5-14 shows the resulting dent depth imposed on the specimen, as well as the load applied by the indenter against the specimen versus time. As shown in the figure, during phase 1, the vertical load applied by the indenter increases to 150 kN. Consequently, the resulting dent size imposed on the specimen increases to 20.7 mm. Then, during phase 2, while the vertical load almost remains constant, the dent depth on the pipe increases by

52% and reaches 32 mm. The slight drop in the vertical load (4%) at the beginning of phase 2 is an unavoidable consequence due to the design of the test setup; without this error, the dent depth could have increased even more than 52%. At the end of phase 2, as the indenter approaches the end boundary condition, the dent depth on the pipe slightly decreases.

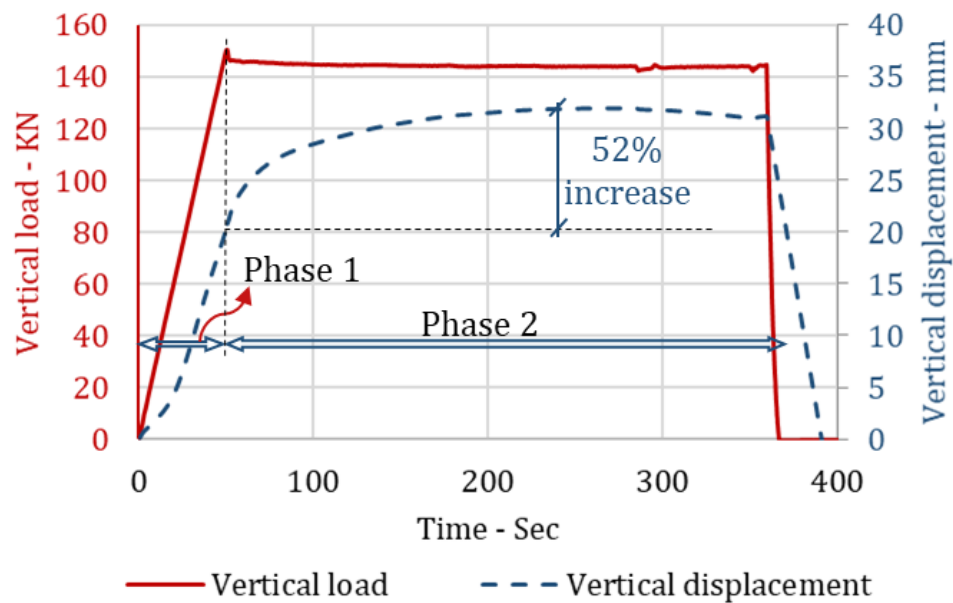


Figure 5-14 Vertical Load Applied by the Indenter to the Specimen Versus Time (Left); and Vertical Displacement of the Indenter (or Resulting Dent Size Imposed to the Pipe) Versus Time (Right)

5.2.3 Experiment Summary and Discussion

An experimental investigation was conducted on a 5-inch diameter pipe schedule 40 under a sliding load (without sliding friction) applied by a cylindrical indenter. The load path during the test includes two phases: first, the indenter applies a 150 kN load

perpendicularly against the specimen in the force-controlled condition (3 KN/sec); then, during phase-2 the applied load almost remains constant, and the indenter moves along the pipe for 300 mm in a displacement-controlled condition (1 mm/sec); due to an unavoidable error, the vertical load drops by 4%, at the beginning of phase 2, but remains constant throughout phase 2.

It was presented that during phase 2, while the vertical load remains steady, the vertical displacement of the indenter (or the resulting dent size imposed on the specimen) increases by 52%. In other words, the progression of the damage along the pipe decreases the pipe's structural resistance. Accordingly, this result provides evidence of the damage progression effect and could be employed to assess any accidental events where the progression of damage along the pipe is likely (i.e., a subsea pipeline subject to a diagonal trawl impact).

5.3 Numerical Simulation

The numerical study is conducted to examine a case of a subsea pipeline subject to a non-perpendicular trawl impact. Abaqus Explicit was used to conduct this numerical study. The hybrid shell-beam model proposed in Davaripour et al. (2020a) is validated and employed to examine a scenario where a pipeline is subject to case-a) a fully diagonal trawl impact; case b) the normal component of the diagonal impact. The comparison between the two cases provides insight as to whether the tangential component of a diagonal trawl impact load could be disregarded; the BSM model only incorporates the normal component of a non-perpendicular trawl load and ignores the tangential component.

5.3.1 Methodology

Figure 5-15 shows the schematic view of the hybrid model with parameters the same as in the BSM model, defined in section 5.1.1. As shown in Figure 5-15, the pipe is modelled with reduced integrated shell elements in the middle (S4R) with 2.5 mm x 2.5 mm mesh size. The middle pipe is extended for 250 m from each end using beam elements (PIPE31). The beam elements are 125 mm long. A kinematic coupling constraint is used to connect the beam and shell elements at both ends of the middle pipe in all translational and rotational degrees of freedom.

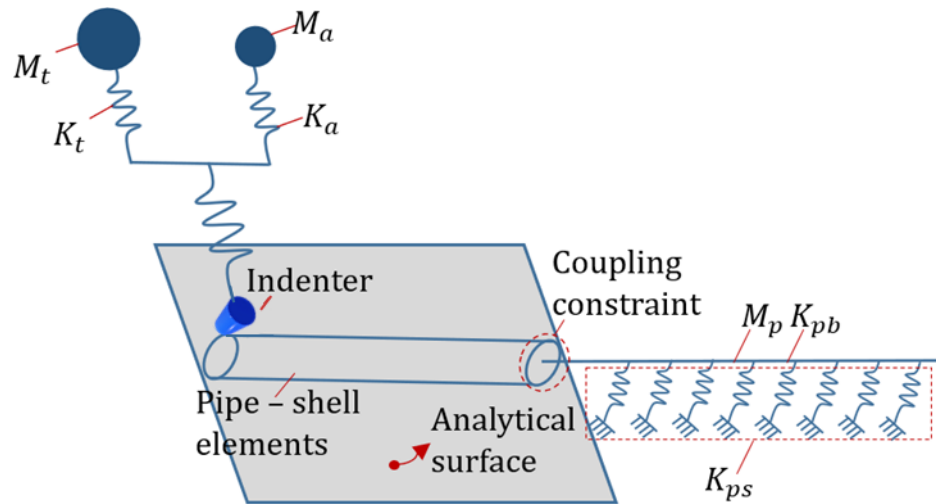


Figure 5-15 A Schematic View of the Hybrid Shell-Beam Model from (Edited from Davaripour et al. (2020a))

5.3.1.1 Pipeline

The physical and mechanical properties for the pipe are selected the same as the experiment conducted by Zheng (2014), which is presented in Section 5.3.2.1.

5.3.1.2 Pipe-Soil Interaction

To model the pipe-soil interaction for the middle part of the pipeline, the soil is modelled using an analytical plate (Figure 5-15). General surface to surface contact is used for the interaction between the pipe (i.e. shell elements) and soil. The interaction properties comprise the normal behaviour with linear pressure-overclosure stiffness and the tangential behaviour with a penalty friction formulation. For the extended part of the pipe

modelled with beam elements, springs are used to represent the soil stiffness in all translational degrees of freedom (Figure 5-15).

5.3.1.2.1 Soil Stiffness

As the impact phase occurs in some hundredths of a second (DNV-RP-F111, 2014), the prominent pipe response is local. Therefore, the shear strain in the surrounding soil is expected to be negligible; as such, dynamic soil stiffness is used instead of static soil stiffness (Wichtmann and Triantafyllidis, 2009). The dynamic effective stiffness of the pipe is calculated using Equation 5-5 (DNV-RP-F105, 2006):

$$K_v = C_v / (1 - \nu) \cdot (2/3 * \rho_s / \rho) D^{0.5} \quad \text{Equation 5-5}$$

Where K_v is the vertical soil stiffness; C_v is the coefficient for vertical soil stiffness; ρ_s / ρ is the specific mass ratio between the flowline mass and the displaced water mass; ν is the Poisson's ratio of the soil. Also, for the lateral and axial soil resistance, a simple constant friction coefficient ($\mu = 0.6$) is used to model the pipe-soil interface friction during the lateral/axial deflection of a flowline; the soil type is set to medium sand.

5.3.1.3 Trawl board

To consider the kinetic energy applied to the pipe by the displaced water, the stiffness of the trawl board is decoupled into the in-plane stiffness which is associated with the board steel mass, and the out of plane stiffness which is associated with hydrodynamic added mass. A basic axial connector is used to model the trawl board stiffness, as shown in Figure 5-15. The front shape of the indenter is modelled by a solid tube with a radius equal to 25 mm, as recommended by DNV-RP-F111 (2014).

5.3.1.4 Loading Condition

Two load cases are investigated on the pipe including case-1, where the pipe is subject to a 30-degree diagonal impact with the velocity equal to 2.6 m/sec (Figure 5-16-a); case-2, where only the normal component of the non-perpendicular impact is considered (velocity is equal to 2.25 m/sec) (Figure 5-16-b). For case-1, the indenter is free to move only along the 30-degree diagonal direction and restrained for other degrees of freedom.

Furthermore, Figure 5-16 shows one scenario of a subsea pipeline subject to a diagonal trawl impact. It does not correspond to two scenarios of a trawl gear impacting a pipe at two different angles. According to Figure 5-16, the diagonal impact could be incorporated in the analysis either by considering the full diagonal impact (case-1) or only the normal component of the diagonal impact (case-2). The main objective for the investigation of

this scenario is to assess the applicability of the BSM model for the assessment of pipelines under non-perpendicular trawl impacts; as the BSM model could only represent case-2.

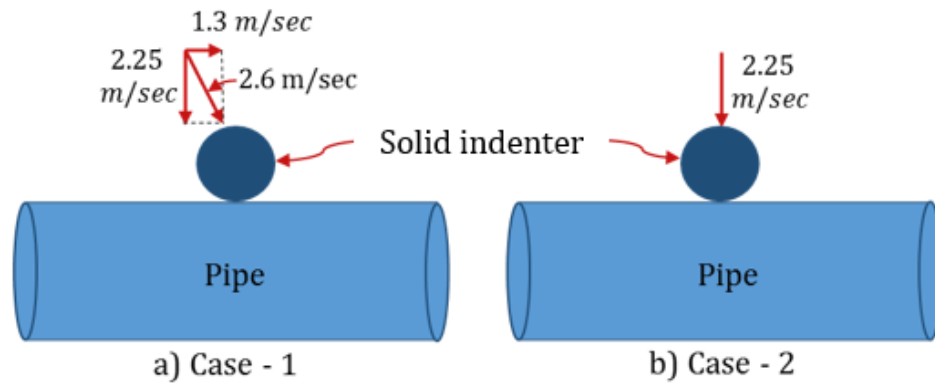


Figure 5-16 Loading Conditions Including Case-1 with a 30 Degree Diagonal Trawl Impact;
Case-2 with Only the Normal Component of the diagonal Trawl Impact

5.3.1.5 Input Parameters

The input parameters employed in the analyses are presented in Table 5-2. Furthermore, the following parameters are disregarded in the analyses of the present study, including non-structural weight, metocean forces, buoyancy force, hydrostatic pressure, internal pressure, strain rate effect, and thermal expansion force.

Table 5-2. The Input Parameters for the Pipe, Trawl Board, and Soil

Pipeline	Value	Units	Trawl board	Value	Units
Outside diameter	141.3	mm	Trawl board steel mass	4000	kg
Nominal thickness	6.55	mm	Added mass	8560	kg

Span height	0	m	Tow velocity of a trawler	2.6	m/s
Soil	Value	Units	In-plane board stiffness	500E6	N/m
Soil Type	Medium sand		Out-of-plane (bending) board stiffness	10E6	N/m
Friction coefficient for the lateral/axial direction	0.6				

Note: Span height is the vertical distance between the pipe's bottom and the seabed.

5.3.2 Benchmarking

The authors are not aware of any published test data on a submerged pipe laid on soil and impacted by a trawl board. According to DNV-RP-F111 (2014), to examine the trawl board interaction with a pipeline, trawl boards could be idealized with a knife-shaped indenter. As such, the papers where the pipe is transversely indented by a knife-shaped indenter are the most relevant to the overtrawlability problems (e.g., Zheng (2014)).

Furthermore, for trawl gear interference with a pipeline, as the direction of the trawl impact is along the seabed, the pipe-soil interaction is insignificant (Zheng et al., 2012). Additionally, Shen and Jones (1991) and then Zheng et al. (2012) concluded that for an impact scenario where the velocity of impact is relatively low and with a heavy mass, the dynamic effect of the impact could be replicated using quasi-static analyses. As such, three sets of test data of a pipe subject to a perpendicular knife-shaped indenter are employed to partly validate the hybrid model; only the interaction between the indenter and the pipe with shell elements are validated. Figure 5-17 shows the BC of the tests

employed for the benchmarking the hybrid model, including a) a quasi-static test using globally restrained BC; b) an impact test using simply supported BC; c) a quasi-static test using a pinned-pinned BC. In all three tests, a 5-inch diameter pipe is examined under a transverse load, and the indenter has a front round face with a radius equal to 25mm.

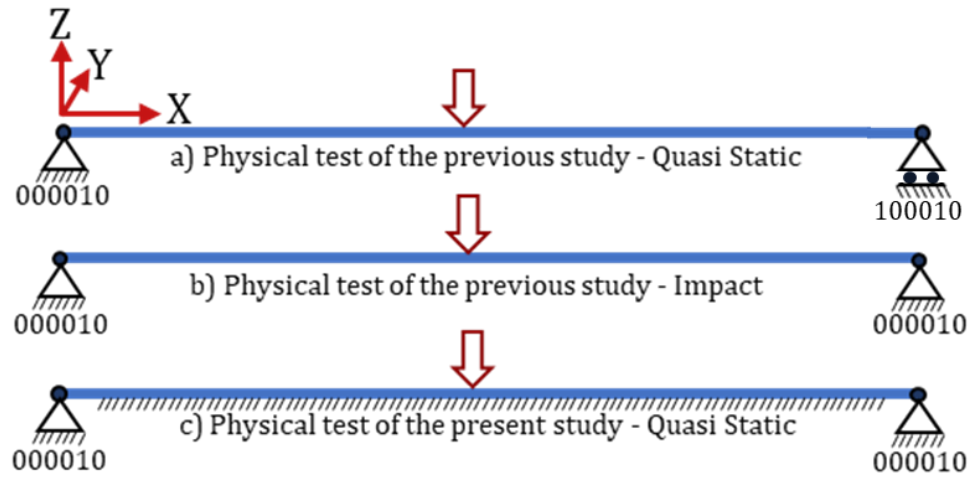


Figure 5-17 Boundary Conditions Used to Benchmark the Hybrid Model (Davaripour et al., 2020a)

5.3.2.1 Verification Using Previous Study Physical Tests

Zheng (2014) conducted two series of experiments, one under the impact (dropped object) and another under the quasi-static condition, to study the pipe response subject to a transverse indentation. The hybrid model is benchmarked against the results of two physical tests performed by Zheng (2014): one under quasi-static and another under impact loading condition. The verification of the hybrid model provided in Section 5.3.2.1 is also presented in (Davaripour et al., 2020a).

5.3.2.1.1 Quasi-Static Test

Zheng (2014) performed a series of quasi-static tests on a 5-inch diameter pipe schedule 40. The test specimen defined as SPS02 in (Zheng, 2014) is used for benchmarking the hybrid model. The physical and mechanical properties of the specimen are presented in Table 5-3. The engineering stress-strain curve reported in (Zheng, 2014), as well as the true stress-strain curve, are shown in Figure 5-18.

Table 5-3 Physical and Mechanical Properties of the SPS02 Specimen in (Zheng, 2014)

Physical properties		
Pipe Outer Diameter_ D (mm)	Pipe Wall Thickness_ t (mm)	Pipe Length_ L (mm)
141.3	6.55	1500
Mechanical properties (based on API Grade B)		
Elastic Modulus_ E (MPa)	Yield Strength_ fy (MPa)	Ultimate Strength_ fu (MPa)
202635	341.98	455

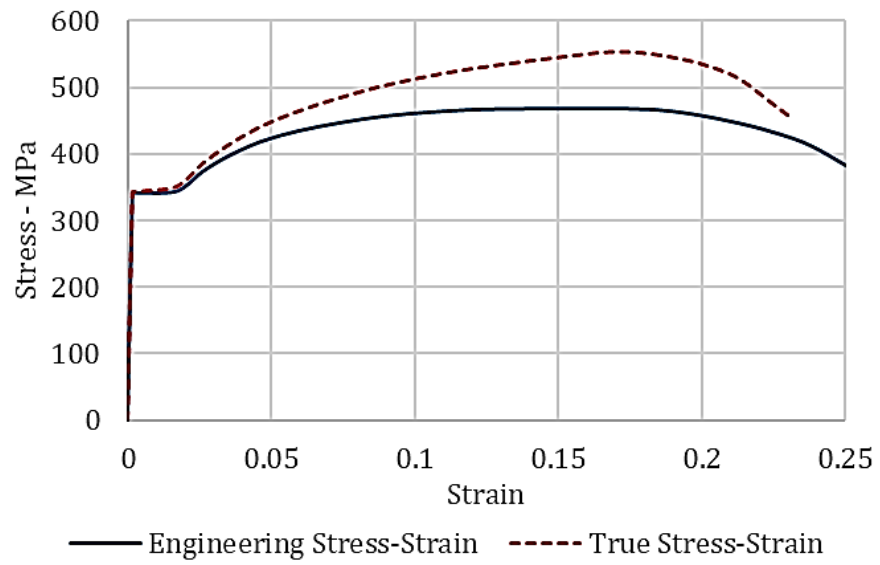


Figure 5-18 Engineering and True Stress-Strain Curve from (Zheng, 2014)

Figure 5-19 shows that the FE results of the present study are in excellent agreement with those obtained by Zheng (2014). However, both FE results overestimate the test data; the discrepancy may be due to the idealization of the boundary conditions in the numerical models.

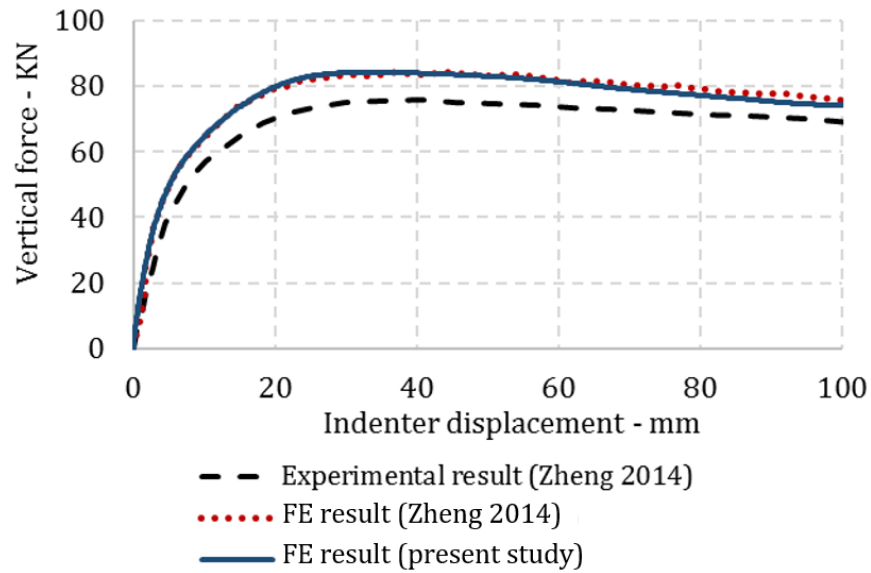


Figure 5-19 Vertical Load-Displacement Result: Experimental Result Versus Numerical Prediction from (Davaripour et al., 2020a)

5.3.2.1.2 Impact Test

Zheng (2014) performed a series of dropped object tests on a pipe with outer diameter and thickness equal to 141.3, and 6.55 mm, respectively. The specimen defined as I-SPS02 in (Zheng, 2014)) is used for benchmarking the hybrid model. The physical and mechanical properties of the specimen are presented in Table 5-3. Also, the mass of the indenter (steel blocks and indenter altogether) is set to 1350 kg with the initial velocity equal to 2.99 m/sec.

As shown in Figure 5-20, the numerical results of the present study compare well with (Zheng, 2014). However, both of the FE outcomes lead to lower results compared with

the test data. A sensitivity case is also examined with the indenter's mass set to 1400 kg; as reported in (Zheng, 2014), the indenter's mass could reach 1400 kg. Figure 5-20 shows that the results of the sensitivity case lead to a better prediction of the experimental result.

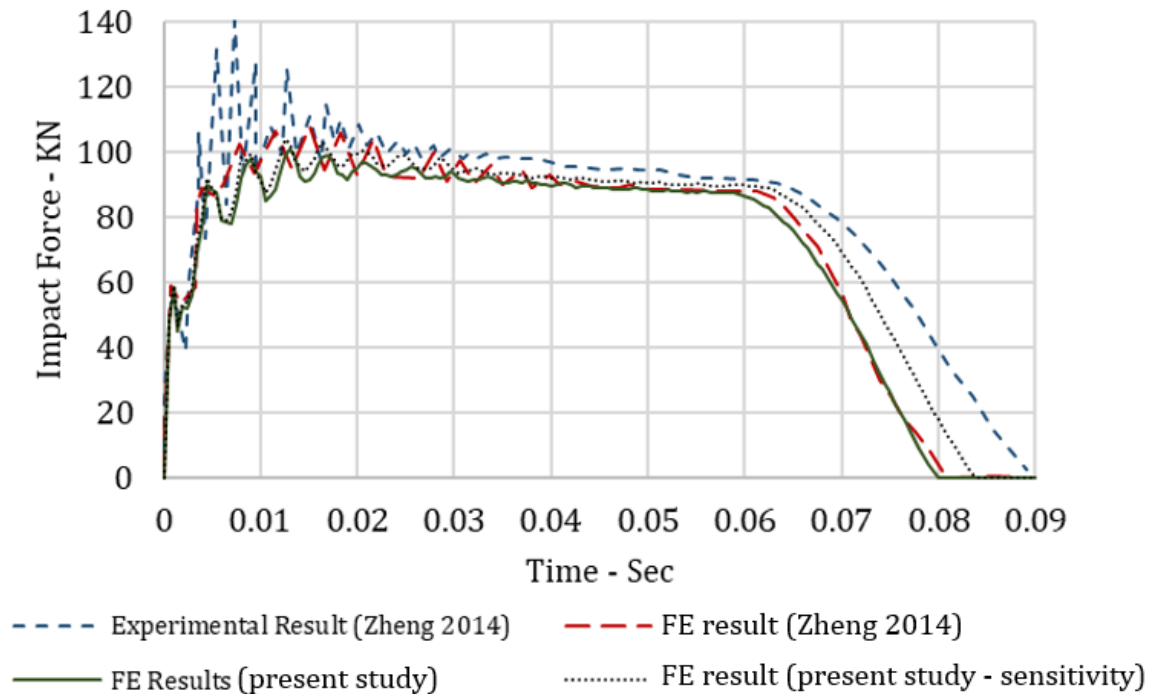


Figure 5-20 The Vertical Load Resisted by the Specimen Against the Impact Versus Time; Numerical Versus Experimental Results (Davari pour et al., 2020a)

Based on the parametric studies, and the notes presented in (Zheng, 2014), the following conditions are employed for the numerical simulation; a) to prevent the pipe from jumping at the time of impact, two omega clamps are used to cover the pipe at the ends; b) the rotation center of the supports is set to the bottom center; c) 5 mm penetration of omega clamps into the pipe ends is assumed to consider the pressure applied by the omega

against the specimen; d) Only 62.5% of the support length is used to interact with the pipe's ends; e) interaction properties with no-separation-allowed are used between the pipe and the supports; f) the steel blocks, as well as the indenter, are all modelled at full size. A surface to surface contact is used between the steel blocks.

5.3.2.2 Verification Using Present Study Physical Test

The hybrid model is validated against the experimental data presented in Section -. The boundary conditions for the specimen include the saddle-shaped support, which restrains the global deformation of the pipe, and the mounts at both ends of the specimen, which restrain the axial deformation of the pipe.

Using the same test apparatus, Quinton (2015) reported an elastic deformation in the apparatus during the test. The author conducted sensitivity analyses and stated that the elastic stiffness of the test apparatus could be set within the range of $1e7$ to $2.5e7$ N/mm. Accordingly, for the interaction between the pipe and the saddle-shaped support, surface-to-surface contact with elastic pressure-overclosure behaviour is defined for the normal contact behaviour; the spring stiffness is set to $0.5e7$ N/mm according to sensitivity analyses, which is slightly less than the one reported in (Quinton, 2015), as more bolted connections are used in the test setup of the present work. Also, the interaction between the indenter and the specimen is assumed frictionless due to using the rolling indenter, as well as the lubrication between the indenter and the specimen.

Figure 5-21 shows a separate numerical simulation which is conducted to obtain the stiffness of the mounts against the load path applied during the test, where a) reduced integration solid elements (C3D8R) are used to model the mounts; b) at the location of key stock only the x-axis is restrained, and at the location of bolts, mesh nodes are restrained in all degrees of freedom (Figure 5-21-a); c) the tied points shown in Figure 5-21-b are constrained to move 20 mm in the opposite direction of the x-axis.

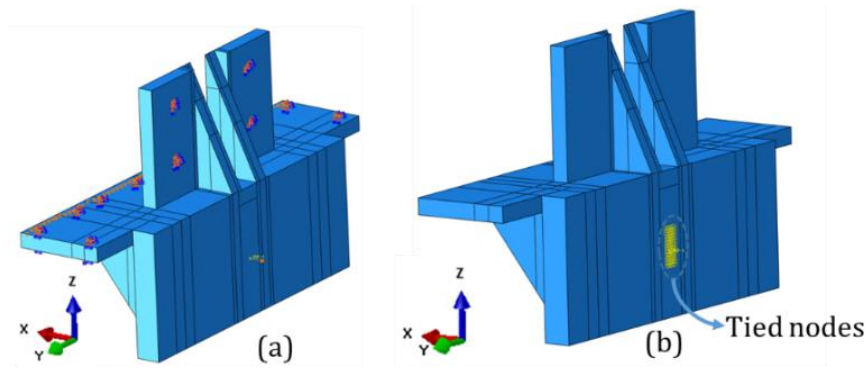


Figure 5-21 Numerical Simulation of the Mount

Figure 5-22 shows the stiffness of the mounts, assuming that the connection between the mounts and the carriage is rigid. Axial connectors at both ends of the pipe are used to represent the stiffness provided by the mounts (Figure 5-23). Furthermore, except for the 940 mm deformable length of the specimen in the middle, the rest of the specimen is rigidly constrained; the end flanges, as well as hinges (Figure 5-4), are considered relatively rigid, compared to the middle cylindrical part of the specimen.

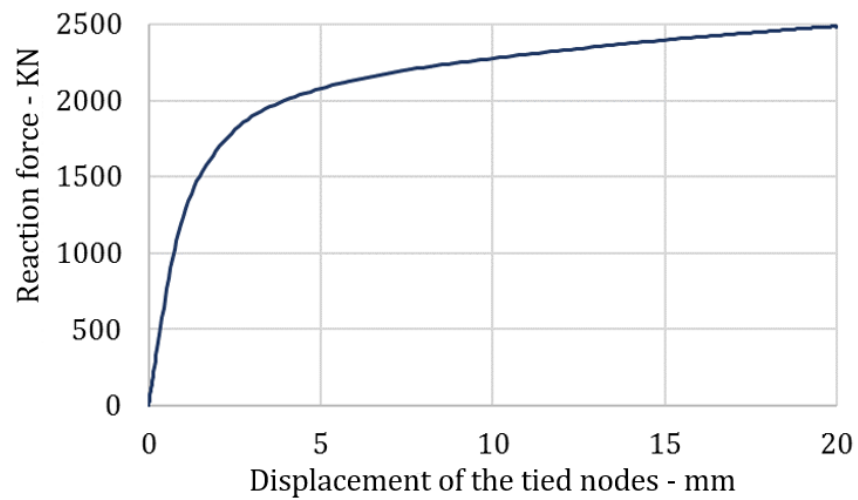


Figure 5-22 Force-Displacement Curve of the Mount Being Pulled at the Center of the Tied Nodes



Figure 5-23 Axial Connector Used to Represent the Stiffness Provided by the Mounts

Figure 5-24 shows that there is generally a good agreement between the physical and numerical results. Accordingly, during phase-1 (150 kN quasi-static perpendicular load), the numerical results match the experimental data. During phase 2, the numerical result

slightly underestimates the experimental data particularly in the second half; this discrepancy could be due to the idealization of the boundary conditions in the numerical model, as the carriage and other parts of the test apparatus are not included in the numerical model.

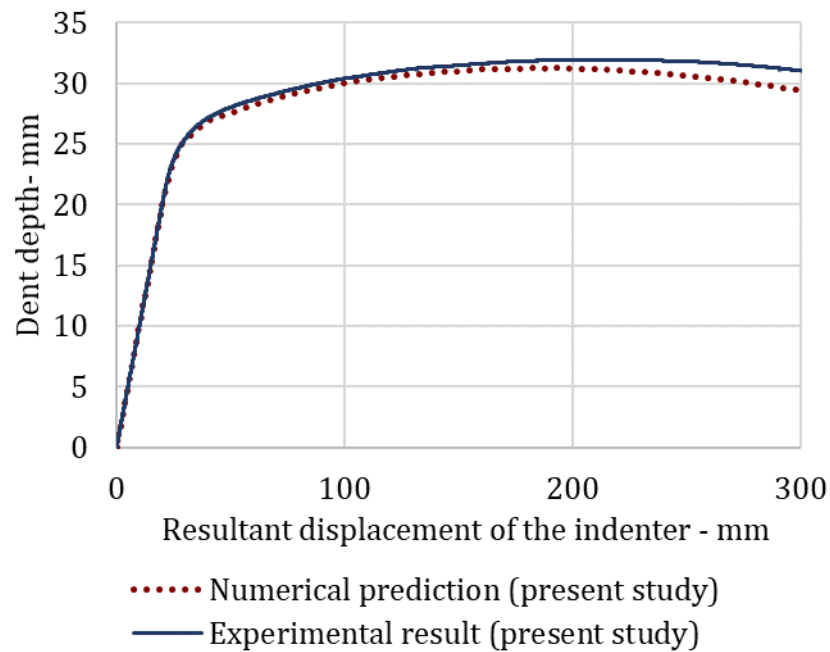


Figure 5-24 The Vertical Displacement of the Indenter (or Dent-Size Imposed on the Specimen) Versus Resultant Displacement of the Indenter; Numerical Versus Experimental Result

The numerical prediction is also compared to the scanned view of the deformed specimen. Accordingly, as shown in Figure 5-25, there is generally an excellent agreement between the finite element result and the physical outcome.

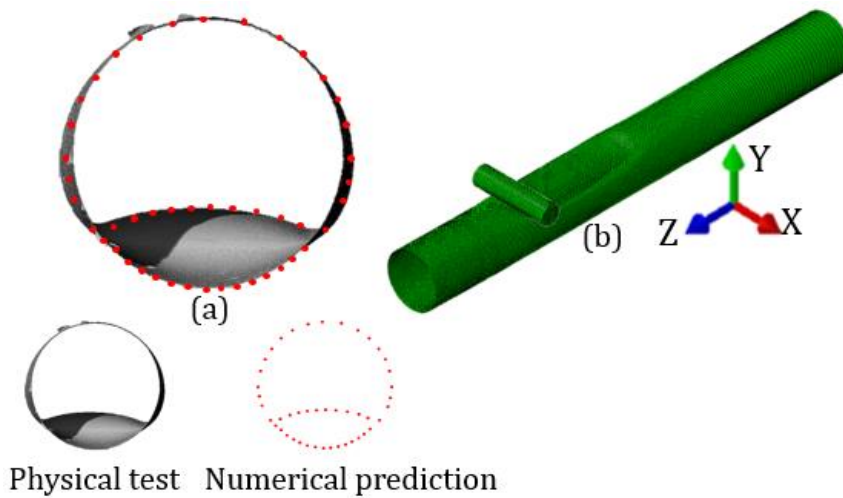


Figure 5-25 A Comparison Between the Scanned View of the Deformed Specimen and the Numerical Prediction (a), an Isotropic View of the Numerical Model (b)

5.3.2.3 Mesh Convergence Analysis

A mesh convergence analysis was performed for the shell and beam elements; for shell elements, four element edge lengths were used, including 5.0, 3.75, 2.5, 1.75 mm; for beam elements, three edge lengths were used, including 250, 125, 62.5 mm. As such, the convergence was achieved for shell element with edge length equal to 2.5 mm (Figure 5-26), and beam element with edge length equal to 125 mm (Figure 5-27).

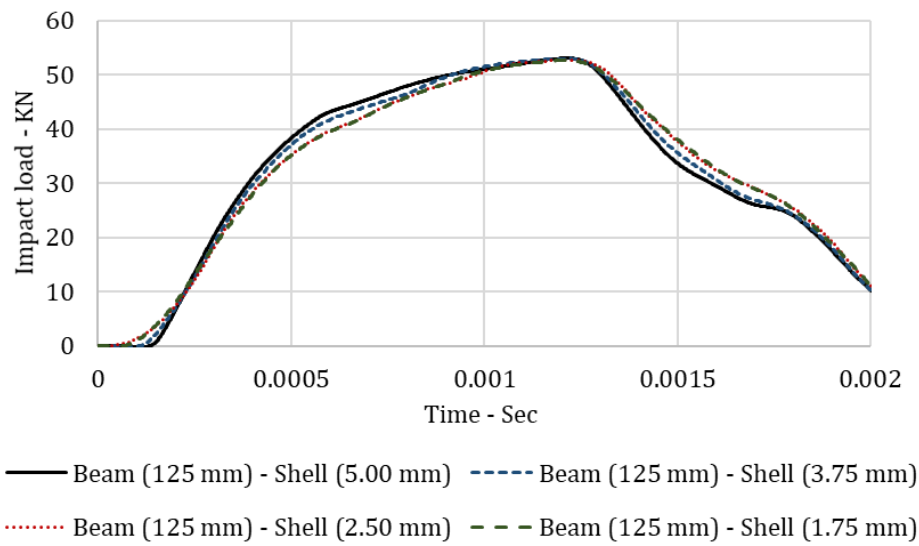


Figure 5-26 Mesh Convergence Analysis for the Hybrid Model: Shell Elements (Davaripour et al., 2020a)

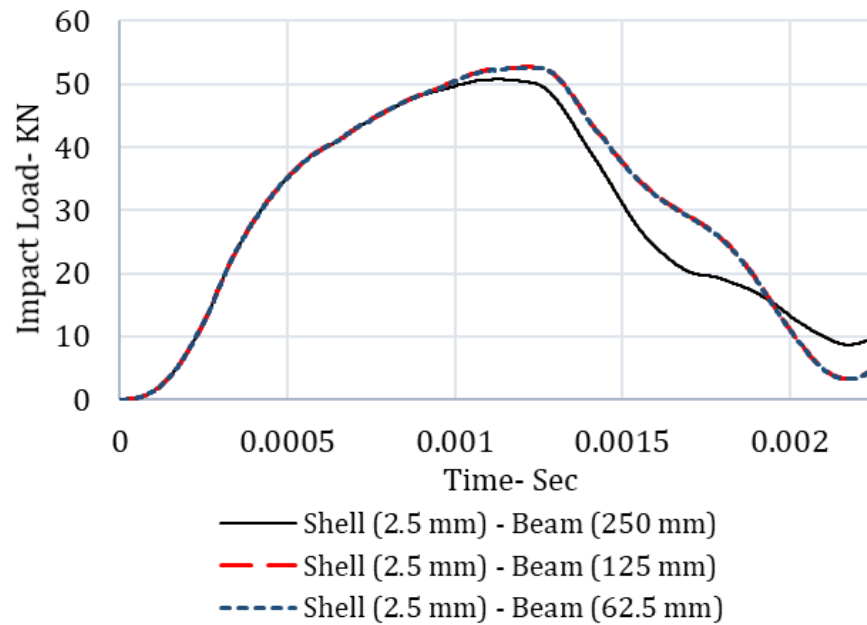


Figure 5-27 Mesh Convergence Analysis for the Hybrid Model: Beam Elements (Davaripour et al., 2020a)

5.3.3 Results and Discussion

Figure 5-28 shows the max dent depth for a 5-inch diameter pipe when subjected to a trawl impact of case-1 (with 30 deg angle relative to the pipe perpendicular) versus case-2 (with only the normal component of the trawl impact of case-1). Figure 5-28 shows that while both cases have the same normal initial velocity, case-1 results in up to 20% more dent depth. This result is aligned with the experimental outcomes of this the present work, where the damage progression along the pipe decreases the pipe's structural resistance. Similarly, due to the progression of damage induced by the tangential component of the non-perpendicular impact in case-1, the resulting dent depth on the specimen is around 20% higher compared to case-2, where the tangential component of the diagonal impact is disregarded.

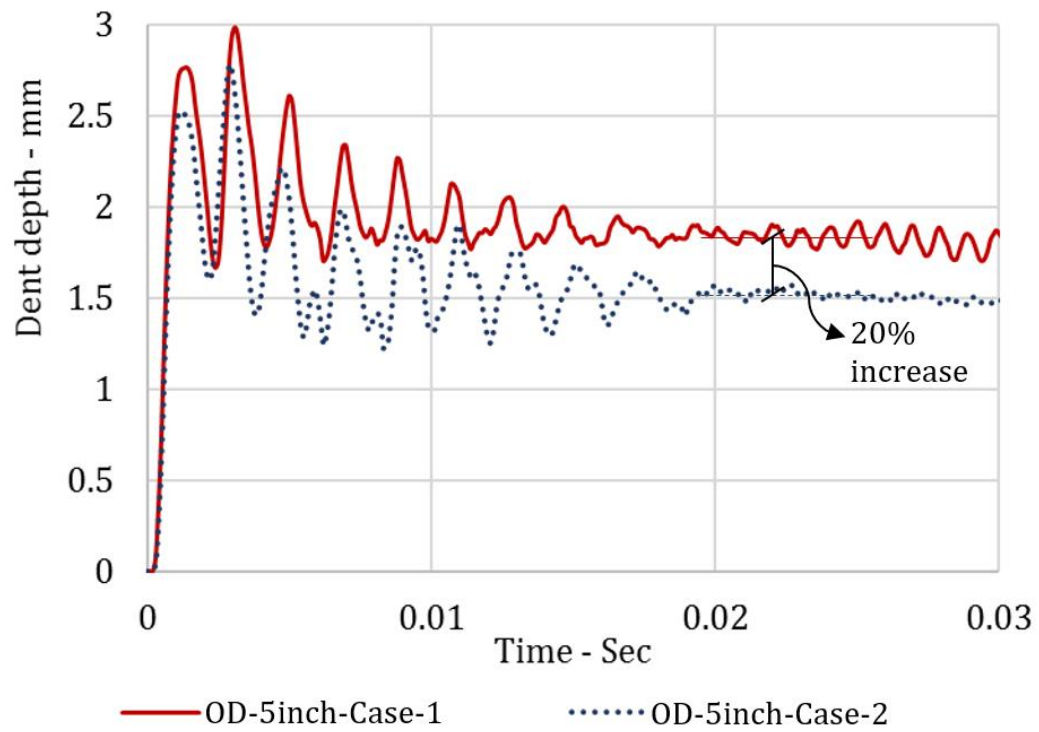


Figure 5-28 Dent Depth in a 5-inch Diameter Pipe for Case-1 and Case-2

5.3.3.1 Sensitivity Analyses

Similar to a 5-inch diameter pipe, for a 14-inch diameter pipe with a wall thickness equal to 16 mm, the trawling impact of case-1 leads to around 20% more dent depth in the pipe versus the impact of case-2 (Figure 5-29).

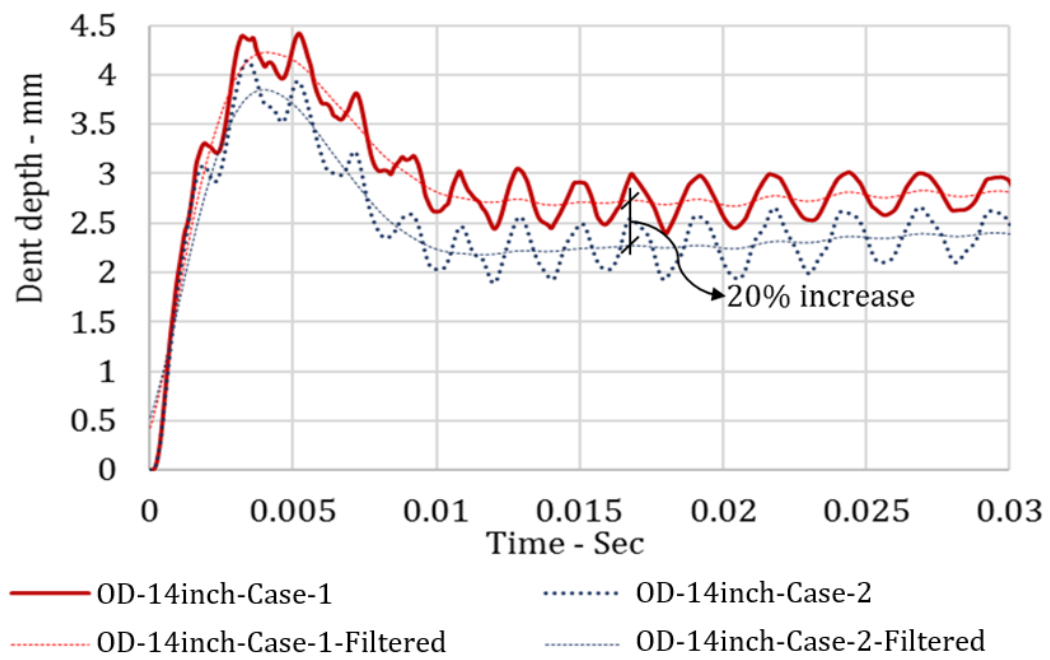


Figure 5-29 Dent Depth in a 14-inch Diameter Pipe for Case-1 and Case-2

5.4 Conclusions

An experimental investigation was performed under the quasi-static condition on a 5-inch diameter pipe to investigate the effect of damage progression on the pipe's structural resistance. The loading condition during the test involved two separate phases, including phase 1, where the specimen was indented by a 150 KN perpendicular load; phase 2, where the indenter started to translate along the pipe, while the applied perpendicular load remained essentially constant at 150 KN.

The experimental results showed that due to the damage progression along the pipe during phase-2, under almost the same applied perpendicular load, the resulting dent size on the pipe increased up to 52%; at the beginning of phase 2 the applied load dropped by 4% which is an unavoidable error; without this error, the dent depth could have increased even more than 52%. It is concluded that the damage progression along the pipe reduces the structural resistance of a pipe. This finding should be considered in the sensitivity studies of subsea pipelines against accidental loads which could induce plastic damage with the possibility of progression of damage along the pipe (e.g., a subsea pipeline under a diagonal trawl impact)

The numerical studies are also conducted to investigate the structural resistance of a pipe subject to a diagonal trawl impact. The main objective was to examine the effect of the tangential component of the diagonal impact on the resulting pipe's dent size.

Accordingly, two cases were examined case-1) where the pipe is subject to a non-perpendicular trawl impact with 30 degrees angle and the velocity of 2.6 m/sec, and case-2) where the pipe is subject to only the normal component of the diagonal impact with the velocity equal to 2.25 m/sec. The results of this study showed that the imposed dent depth on a pipe under case-1 is around 20% higher than the one under case-2. This finding is in agreement with the experimental results of this work, and shows the progression of damage, induced by the tangential component of the non-perpendicular impact in case-1, decreases the structural resistance of the pipe, and leads to larger resulting dent size on the pipe; compared to case-2 where the tangential component of the impact is disregarded.

In conclusion, to assess a scenario where a subsea pipeline is subject to a diagonal trawl impact, the BSM model should be improved to account for the tangential component of the impact as well as the progression of damage along the pipe. In this regard, the hybrid shell-beam model, which is proposed in (Davaripour et al., 2020a) and presented in this paper, is a suitable and numerically efficient alternative.

Future Work

This paper numerically examined and showed the damage progression effect on a subsea pipeline under a diagonal trawl impact for 5 and 14-inch diameter pipes. To further investigate this topic, more sensitivity studies should be performed on, i.e., pipe size, pipe wall-thickness, pipe-soil interaction, etc.

This work only examined the effect of the damage progression on a subsea pipeline subject to a diagonal trawl impact. However, there are several other applications of the damage progression effect on subsea pipelines, which should be investigated, i.e., a subsea pipeline under a pull-over load that scrapes along the pipe.

Acknowledgment

This research became possible through the funds provided by the Natural Sciences and Engineering Research Council's (NSERC) Discovery Grant program, as well as the Mitacs Accelerate Program. The authors sincerely appreciate the valuable comments provided by Richard Persaud from Genesis.

Reference

- Bai, Y., Bai, Q., 2005. Subsea Pipelines and Risers. Mater. Mech. 1–700.
<https://doi.org/10.1016/B978-008044566-3.50023-3>
- Davaripour, F., Pike, K., Quinton, B.W.T., Persaud, R., 2020a. An Assessment on the Overtrawlability of Small Pipe Sizes Using a Hybrid Shell- Beam Model : The Initial Trawl Impact Phase (Revision Requested). Appl. Ocean Res.
- Davaripour, F., Quinton, B., Pike, K., 2020b. A Numerical Investigation on a Pipe Subject to a Non- Perpendicular Trawl Impact Using a Hybrid Shell-Beam Model, in: Offshore Pipeline Conference (OPT 2020). Amsterdam, pp. 1–12.
- Davaripour, F., Quinton, B.W.T., 2018. An Investigation of the Load Carrying Capacity of Pipelines Under Accidental and Longitudinal Moving (Sliding) Loads, in: International Pipeline Conference (IPC). pp. 1–7.
- DNV-RP-F105, 2006. Det Norske Veritas - Free spanning pipelines 138.
- DNV-RP-F111, 2014. Det Norske Veritas - Interference Between Trawl Gear and Pipelines.
- Ellinas, C.P., Walker, A.C., 1983. Damage on offshore tubular bracing members, IABSE reports = Rapports AIPC = IVBH Berichte.
<https://doi.org/http://doi.org/10.5169/seals-32425>
- Fryba, L., 1999. Vibration of solids and structures under moving loads, Telford, London. Springer.

- Jones, N., Birch, R.S., 1996. Influence of internal pressure on the impact behavior of steel pipelines. *J. Press. Vessel Technol. Trans. ASME* 118, 464–471. <https://doi.org/10.1115/1.2842215>
- Ng, C.S., Shen, W.Q., 2006. Effect of lateral impact loads on failure of pressurized pipelines supported by foundation. *Proc. Inst. Mech. Eng. Part E J. Process Mech. Eng.* 220, 193–206. <https://doi.org/10.1243/0954408JPME97>
- Parkes, E.W., 1958. How to cross an unsafe bridge. *A Divers. Dyn. Plast. Eng.* 186, 606–608.
- Quinton, B., 2015. Experimental and numerical investigation of moving loads on hull structures. PhD thesis, Memorial University of Newfoundland.
- Quinton, B., 2008. Progressive damage to a Ship's structure due to ice loading. Master thesis, Memorial University of Newfoundland. <https://doi.org/10.13140/RG.2.1.1395.6562>
- Shen, W.Q., Jones, N., 1991. A comment on the low speed impact of a clamped beam by a heavy striker. *J. Struct. Mech.* 19, 527–549.
- Symonds, P.S., Neal, B.G., 1960. Traveling loads on rigid-plastic beams. *J. Eng. Mech. Div.* 86, 79–90.
- Thomas, S.G., Reid, S.R., Johnson, W., 1976. Large deformations of thin-walled circular tubes under transverse loading—I: an experimental survey of the bending of simply supported tubes under a central load. *Int. J. Mech. Sci.* 18, 325–333.

- Toridis, T.G., Wen, R.K., 1966. Inelastic response of beams to moving loads. J. Eng. Mech. Div. 92, 43–62.
- Wichtmann, T., Triantafyllidis, T., 2009. On the correlation of “static” and “dynamic” stiffness moduli of non-cohesive soils. Bautechnik 86, 28–39.
<https://doi.org/10.1002/bate.200910039>
- Zheng, J., 2014. Overtrawlability and Mechanical Damage of Pipe-in- Piped, PhD thesis. NATIONAL UNIVERSITY OF SINGAPORE. <https://doi.org/10.1115/1.4024877>
- Zheng, J., Palmer, A., Lipski, W., Brunning, P., 2012. Impact Damage on Pipe-in-Pipe Systems, in: International Offshore and Polar Engineering Conference. Rhodes, Greece, pp. 152–157.

6 CHAPTER 6

EFFECT OF DAMAGE PROGRESSION ON THE PLASTIC CAPACITY OF A SUBSEA PIPELINE

Abstract

The investigation of buckle propagation in subsea pipelines has been the subject of several works in the past few decades. Accordingly, it was shown that the external pressure required to develop the initial plastic damage on the pipe is considerably more than the pressure required to propagate the initiated local buckle along the pipe. In this respect, a relevant phenomenon could be framed for a pipe that is subject to a substantial lateral interference load; where the load imposes plastic damage on the pipe and induces the damage along the pipe. As such, the present work assesses the pipe's load-carrying capacity during the progression of plastic damage, using a novel test apparatus. In addition, in order to identify and investigate an application of damage progression on subsea pipelines, a numerical study is conducted on a pipe subject to repeated indentations at adjacent locations. This case represents an idealization of a subsea pipeline subject to subsequent fishing gear impacts. The physical tests show that the load-carrying capacity of the pipe could drop significantly (i.e., 33.5% as reported in test 1) due to the damage progression effect. Furthermore, the finite element findings show that the dent depth imposed on the present study pipe increases by 37.2% due to this effect. In conclusion, the damage progression effect should be considered in the assessment of subsea pipelines, where applicable.

Keywords: Subsea pipeline, Damage progression, Buckle propagation, Trawl interference, DNV-RP-F111

6.1 Introduction

The propagation of local buckle on a subsea pipeline has been the subject of several studies in the past few decades, i.e., (Hahn et al., 1993; Kyriakides, 1994; Liang et al., 2019); where The buckle propagation refers to the longitudinal propagation of the local buckle (plastic damage) along the subsea pipeline due to the external pressure. In this regard, it was shown that the pressure required to buckle a pipeline is more than the pressure needed to propagate the buckle, i.e., (Chater and Hutchinson, 1984). Therefore, pipelines have more structural resistance against the development of the initial plastic damage compared to the propagation of the initiated damage along the pipe. This provides a framework for a relevant phenomenon where the pipe is subject to a lateral load by a third party (i.e., bottom fishing gear), which applies plastic damage to the pipe and translates and induces the imposed damage along the pipe. The goal of the present thesis is to address this phenomenon in SWP and PiP systems.

According to recent studies on a pipe under a lateral indentation (i.e., (Davaripour et al., 2020b; Davaripour and Quinton, 2018)), the plastic capacity of a pipe could decrease significantly when the initiated plastic damage on the pipe progresses along the pipe. In other words, the lateral load required to develop the initial plastic damage on a pipe could be significantly more than the (sliding) load required to translate and induce the plastic damage, with the same size, along the pipe. The plastic capacity of a pipe refers to the load-carrying capacity (or structural resistance) of the pipe, where the load imposes

plastic damage to the pipe. This capacity is measured in the present work according to the dent size imposed on the pipe (in the load-controlled condition), or the perpendicular load withstood by the pipe (in the displacement-controlled condition). Accordingly, novel physical apparatus is employed in the present study to validate and further investigate the damage progression along a pipeline, which is imposed by a non-rupture type interference load (trawl board impact in this work); the trawl impact is the first phase during trawl gear interference with a subsea pipeline (prior to pullover phase) and lasts for some hundredth of a second (DNV-RP-F111, 2014); the trawl board is used in other trawl types to keep the net open during the trawling (DNV-RP-F111, 2014).

6.1.1 Literature Review

The topic of a pipe subject to a perpendicular impact has been investigated by several studies in the past decades. Ellinas and Walker (1983) developed a semi-empirical model by employing the test results of Thomas et al. (1976). The authors assumed that the pipe response during the indentation could be idealized into the separate phases of purely local deformation and the global deformation with some additional local response. However, from the very beginning of the indentation, the pipe response involves the combination of both local and global deformation, where the local deformation increases with a higher growth rate at the beginning of the indentation. Then, due to the change in the cross-section of the pipe, the bending stiffness decreases, which leads to more global rather than local deformation (Zheng et al., 2012). Furthermore, Soreide and Amdahl (1982)

studied the clamped pipe without axial restraint, subject to transverse indentation under quasi-static and impact conditions. This boundary condition arrangement considers both local and global deformation of the pipe, which is a suitable idealization for a subsea pipeline. Alexander (2007) examined several impact events on a 12-inch pipe and presented a classification of major damages in a pipe. However, the reported velocity of impact in his work (~ 13 m/sec) is significantly greater than the one in common impact events imposed on the pipeline system from the trawling activity (~ 2.6 m/sec).

Jones and Birch (1996) performed 54 impact tests on a pipe with a fully clamped boundary condition. Using different ranges of impact energy and internal pressure, the authors presented different failure modes of a pipe subject to a wedge-shaped indenter. Ng and Shen (2006) incorporated the foundation support in the test setup and concluded that the failure threshold of a pipe could change when considering the circumferential stress developed due to the pipe foundation interaction. However, the trawl impact occurs along the seabed, and the pipe-soil interaction is insignificant.

In addition to perpendicular indentation, there are interference events where the imposed damage could progress along the pipe, such as a subsea pipeline subject to a non-perpendicular trawl impact (Davaripour et al., 2020b) or under repeated perpendicular trawl impacts at adjacent locations; the latter case is within the scope of the present study. In these scenarios, the structural response of the pipe is path-dependent; where path-

dependency refers to the effects of the plastic deformation imposed on the pipe at the previous time increment on the current response of the pipe. In this regard, several studies have been conducted on the path-dependent behaviour of a structure subject to a moving load. Parkes (1958) presented a solution for the plastic response of a massless rigid plastic beam under a traveling mass. Symonds and Neal (1960) extended the study of (Parkes, 1958) using the mass-included rigid plastic beam. Toridis and Wen (1966) did an analytical investigation on the dynamic response of an elasto-plastic beam under a moving load. They proposed a solution for a discrete beam with massless rigid panels connected by joints with a point mass. Frýba (1999) reviewed and presented analytical solutions for multiple examples of simple moving load scenarios. The author provided an analytical solution for a rigid plastic beam with a stationary hinge in the middle subject to a concentrated load translating along the beam.

Quinton (2015, 2008) investigated the collision of a hull structure with sliding ice loads and showed a reduction in the structural resistance of the plate when the non-rupture type load slides along the plate versus when it is only perpendicular to the plate. The investigation of this reduction in cylindrical structures is the main focus of the present study and termed as the damage progression effect throughout this paper.

Davaripour and Quinton (2018) numerically examined the damage progression effect in pipes. They showed that for a pipe subject to a moving indentation, the damage

progression effect only occurs if the load applies plastic damage to the pipe. They concluded that the lesser resistance of the pipe on the trailing side of the sliding load compared to the leading side is the main source of the damage progression effect (the trailing side is the part of the pipe behind the sliding load, and the leading side is the part ahead of the sliding load). The authors showed that the damage progression effect grows when the extent of plastic damage, which is translated along the pipe, increases. Davaripour et al. (2020b) used finite element analyses to examine an application of the damage progression effect for subsea pipelines, where the pipe is subject to a diagonal trawl impact. In this scenario, the tangential component of the trawl impact pushes the resulting plastic damage along the pipe. The authors showed that due to the damage progression effect, the resulting dent depth on a 5 inches pipe under a diagonal trawl impact with 30 degrees angle is up to 20% higher compared to the case where only the normal component of the trawl impact was applied to the pipe; the tangential component of diagonal trawl impacts are commonly disregarded in overtrawlability assessments of pipelines (Davaripour et al., 2020b).

DNV-RP-F111 (2014) states that the subsequent trawl pullover load and the resulting accumulation of plastic strain should be considered in the overtrawlability assessment of pipelines. The number of subsequent interactions is dependent on the trawl frequency in the field. However, if no specific data is available, DNV-RP-F111 (2014) recommends considering the effect of four subsequent pullover loads at the same location. Likewise,

the subsequent initial trawl impact should be examined where applicable. Also, parametric studies of the scenario where a pipe is subject to repeated trawl impacts should be assessed. In this regard, if the repeated impacts occur at neighboring locations on a pipe, it can lead to the progression of damage. As reported by Davaripour and Quinton (2018), due to the damage progression effect, the structural resistance of a pipe could drop significantly as the resulting plastic damage travels along the pipe. As such, in the present study, the case of a pipe subject to repeated indentations at adjacent locations is numerically examined, which is an application of the damage progression effect on subsea pipelines.

Shen and Jones (1991) proposed an alternative quasi-static approach to replicate the dynamic effect of a rigid perfectly-plastic clamped beam struck transversely by an indenter. The authors stated that where the indenter is heavy and moves at a relatively low speed, the predicted energy absorbed by the structure using the quasi-static analysis is similar to the one in the real problem. Furthermore, Zheng (2014) did a series of experimental and numerical investigations on pipes subject to transverse indentations and concluded that quasi-static conditions could be employed for trawling impact problems. As such, the quasi-static experimental and numerical works presented in the present paper are representatives of actual trawl gear interference with subsea pipelines.

The topic of the damage progression effect in subsea pipelines is a novel topic. In this regard, Davaripour et al. (2020c) provided a physical test under the quasi-static and load-controlled condition. The present work extends the physical findings of Davaripour et al. (2020c) by presenting high-quality data regarding additional three physical tests. Furthermore, a numerical model is developed and verified against one of the physical tests, which is then employed to examine the pipe's response under repeated quasi-static indentations at adjacent locations; these analyses represent an idealization of a subsea pipeline subject to repeated trawl impacts at adjoining locations.

6.1.2 Notes on the Research Scope

The main objective of the present study is to provide evidence regarding the effect of damage progression on the plastic capacity of a pipeline. Furthermore, the present study introduces and investigates a novel application of the damage progression effect in the event of trawl gear interference with subsea pipelines. In this regard, while the recommendations of DNV-RP-F111 were incorporated in the methodologies of the present work, the test setup, as well as the numerical model, do not fully represent a scenario of a trawl interference event with a subsea pipeline. However, the following points justify the validity of the approach employed in the present work for both physical test setup and numerical model:

- The dynamic effect of a trawl impact scenario could be replicated by an equivalent quasi-static analysis, as reported in Shen and Jones (1991) and then examined by

Zheng et al. (2013) for the case of a trawl interference with a pipeline. As such, the physical tests, as well as numerical studies, are conducted under the quasi-static condition.

- The direction of the trawl impact is parallel to the seabed. Therefore, the pipe-soil interaction is negligible during the trawl interference event (Zheng et al., 2012). As such, the pipe-soil interaction is not incorporated in the physical test as well as numerical studies.
- The initial phase of the trawl impact (which is the focus of the present scope) occurs in some hundredths of a second (DNV-RP-F111, 2014), and hence the global deformation of the pipe is negligible and could be disregarded. Therefore, in three out of four physical tests as well as the numerical models, the lateral deformation of the pipe is restrained.

Furthermore, the physical tests in the present study employ a two-phase loading condition to investigate the pipe's response, where in phase 1, the pipe is subject to a perpendicular indentation, and in phase 2, the resulting damage in phase 1 translates and induces along the pipe. In this regard, the first phase partially represents the fishing gear impact on a subsea pipeline (considering the above-mentioned points). However, the second phase employed (only) to highlight the effect of damage progression on the load-carrying capacity of the pipe, and may not represent any particular scenario in the pipeline industry.

6.2 Experimental Investigation

As there are no previous experiments (at laboratory scale, or otherwise) on the subject of the damage progression effect on cylindrical structures, a novel experimental apparatus was used to explore this effect.

6.2.1 Methodology

6.2.1.1 Test Apparatus

Figure 6-1 shows an overall view of the test apparatus that was employed to perform the laboratory tests. The apparatus was originally devised by Quinton (2015) to examine the structural behaviour of plates and stiffened plates subject to sliding loads; the apparatus was modified for the present study to investigate the behaviour of hollow cylindrical structures subject to sliding rigid indentations.

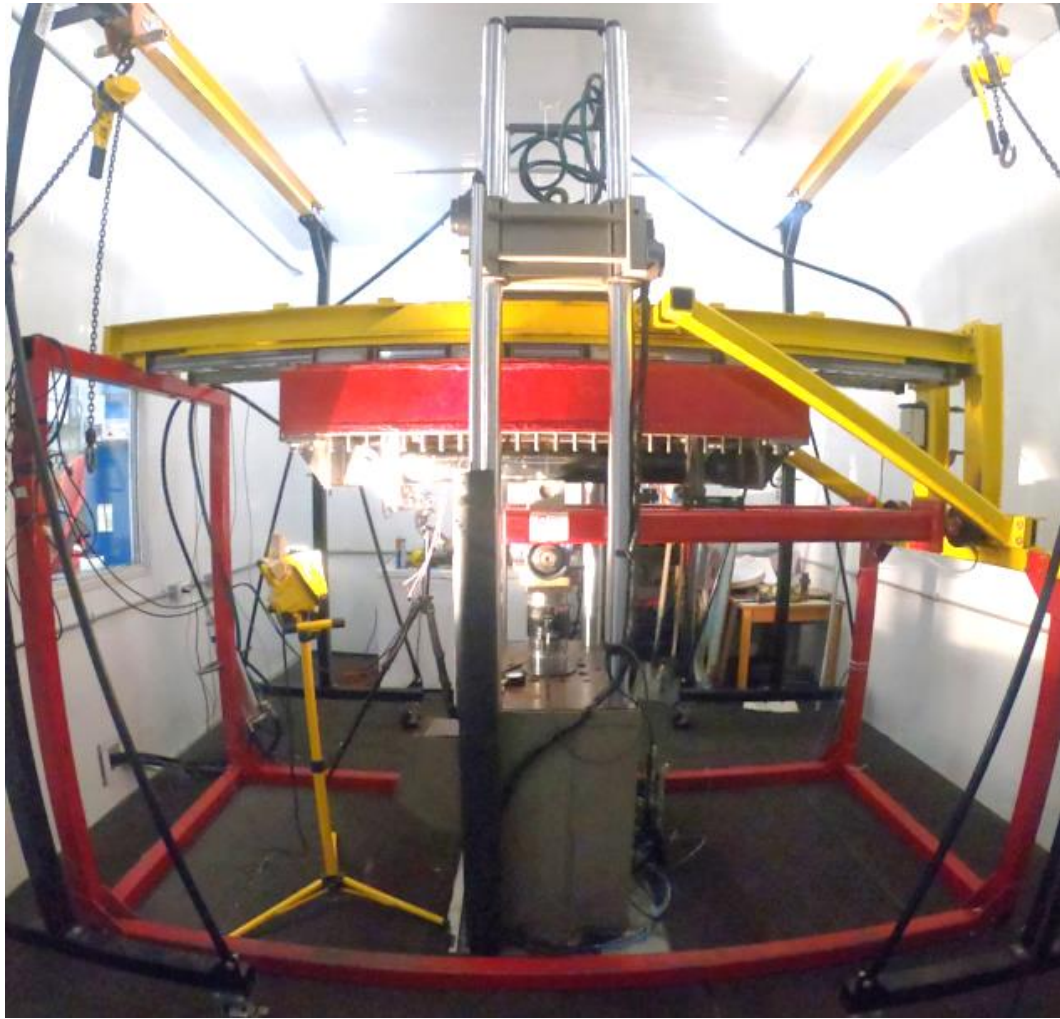


Figure 6-1 An Overall View of the Test Apparatus

The vertical load path in the test apparatus (Figure 6-2) involves the MTS test frame, which provides the maximum vertical force of 500 kN via the hydraulic ram. The MTS test frame is a self-reacting frame that could apply a precise load to conduct a uniaxial material test. The vertical ram pushes the cylindrical indenter against the test specimen, which is bolted to the carriage. The load path will end with the MTS test frame's crossheads.

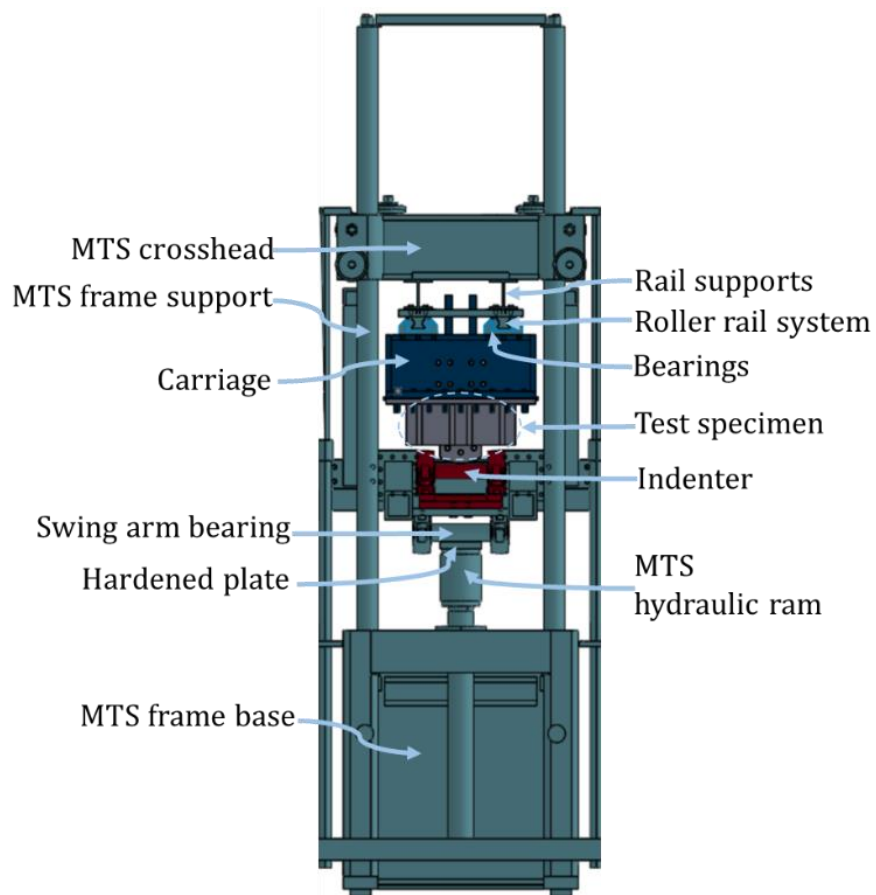


Figure 6-2 Components of the Test Apparatus in the Vertical Load Path

The horizontal load path refers to the direction along the long edge of the carriage, which is shown in Figure 6-3. The load path starts with the horizontally oriented hydraulic ram, which provides the maximum load of 225 KN. The ram is connected to a base plate from the left side and to the carriage from the right side and pushes the carriage to translate along the rail. As the horizontal load starts, from the contact between the indenter and the pipe, the horizontal load is transferred from the carriage to the pipe and the indenter. The load is then transferred to the horizontal load cell via the swing-arm.

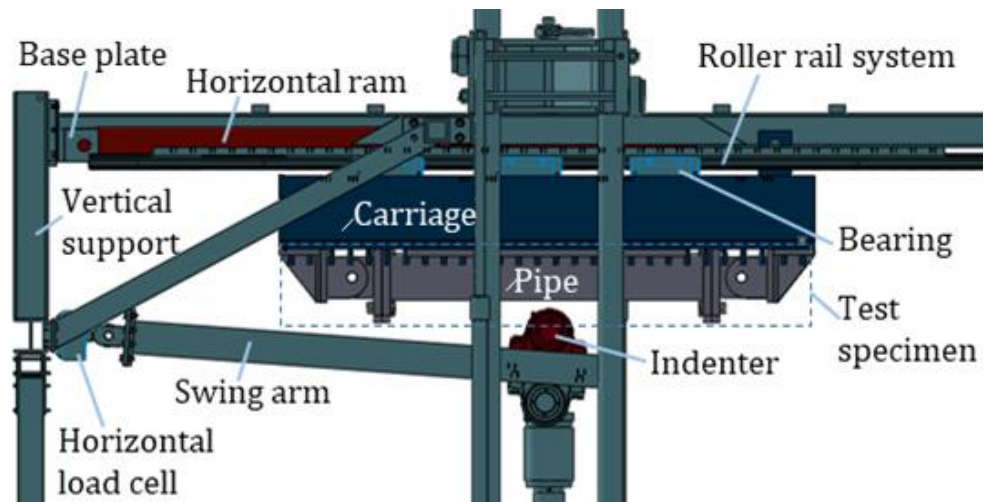


Figure 6-3 Components of the Test Apparatus Along the Horizontal Load Path

6.2.1.2 Test Setup

The modifications to the test apparatus were designed to provide a test setup incorporating the recommendations of DNV-RP-F11 (2014). Figure 6-4 shows an overall view of the test setup bolted to the carriage, including isotropic view (a), X-view (b), and Y-view (c). The test setup comprises three main components, including the cylindrical specimen, the saddle-shaped support, and the mounts.

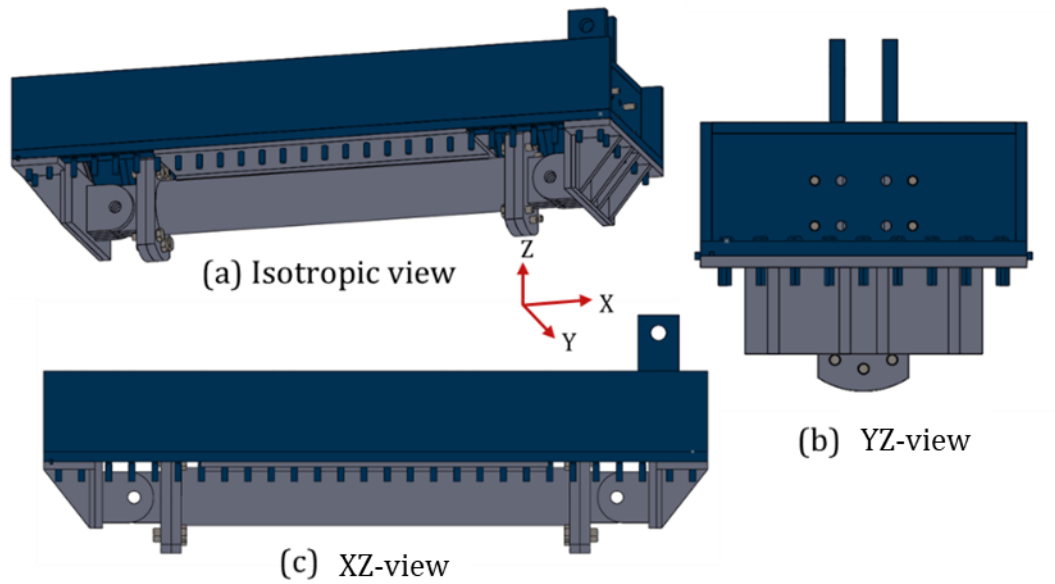


Figure 6-4 An Overall View of the Test Setup: Isotropic View (a), YZ-View (b), and XZ-View (c)

The cylindrical test specimen (i.e., pipe) has an outer diameter of 5-inch (Schedule 40). The mechanical properties of the pipe were obtained from standard tensile tests (ASTME8/E8M-13, 2013). Figure 6-5 shows the stress-strain curve averaged from the tensile tests, and Table 6-1 summarizes the physical and mechanical properties of the pipe.

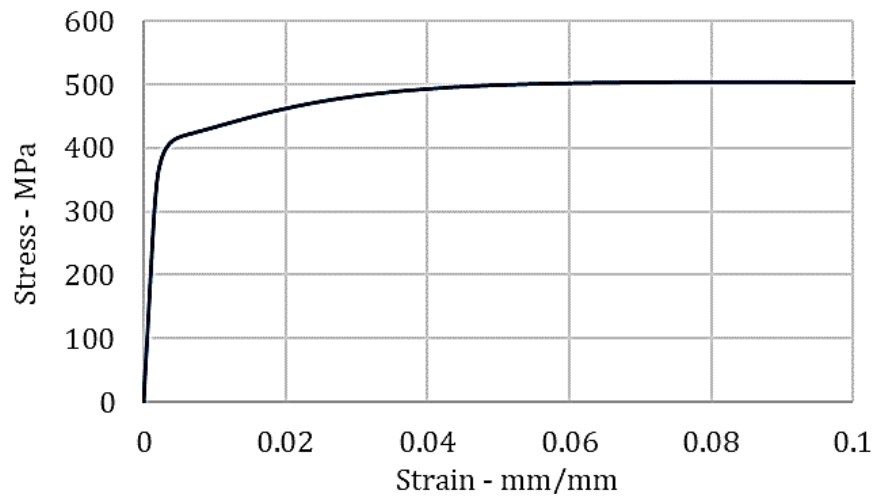


Figure 6-5 Engineering Stress-Strain Curve for the Cylindrical Specimen (Davaripour et al., 2020a)

Table 6-1 Physical and Mechanical Properties of The Cylindrical Specimen

Physical properties		
Outer Diameter_ D (mm)	Pipe Wall Thickness_ t (mm)	Pipe Length_ L (mm)
140.97	6.15	1200
Mechanical properties		
Elastic Modulus_ E (MPa)	Yield Strength_ fy (MPa)	Ultimate Strength_ fu (MPa)
201404	412.2	503.6

The total length of the specimen between the pins is 1200 mm, and the deformable part between the end flanges is 965.2 mm long (Figure 6-6). The end flanges, as well as hinges, are considered relatively rigid in comparison to the cylindrical part in the middle.

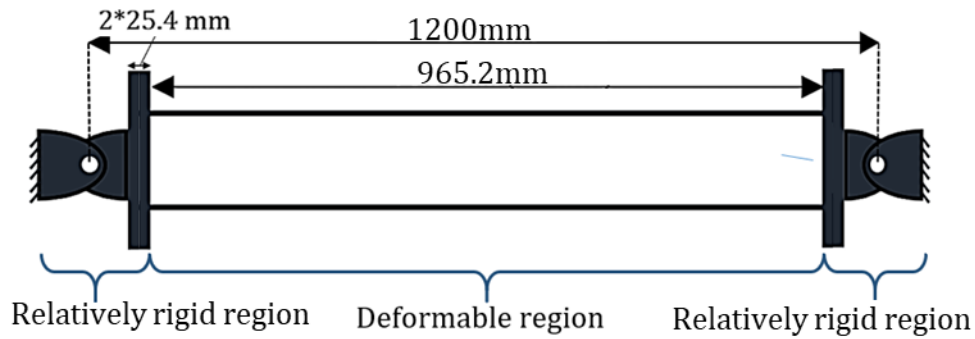


Figure 6-6 Deformable and Non-Deformable Parts of the Cylindrical Specimen (Davari pour et al., 2020a)

The saddle-shaped support is shown in Figure 6-7. It is designed to restrain the global deformation of the specimen. It comprises an 863.6 mm (34-inch) long plate with a width equal to that of the support carriage, and 25.4 mm (1-inch) thickness. The plate is cut in the center to 70.65 mm radius (matching the pipe radius); the final curved shape in the center of the plate provides 60 degrees circumferential area for the interaction with the specimen, as recommended by DNV-RP-F11 (2014). The saddle-shaped support is connected to the carriage via bolts along the two long edges of the plate, as well as the I-beam welded to the plate, and rests against the inside top of the carriage (Figure 6-8).

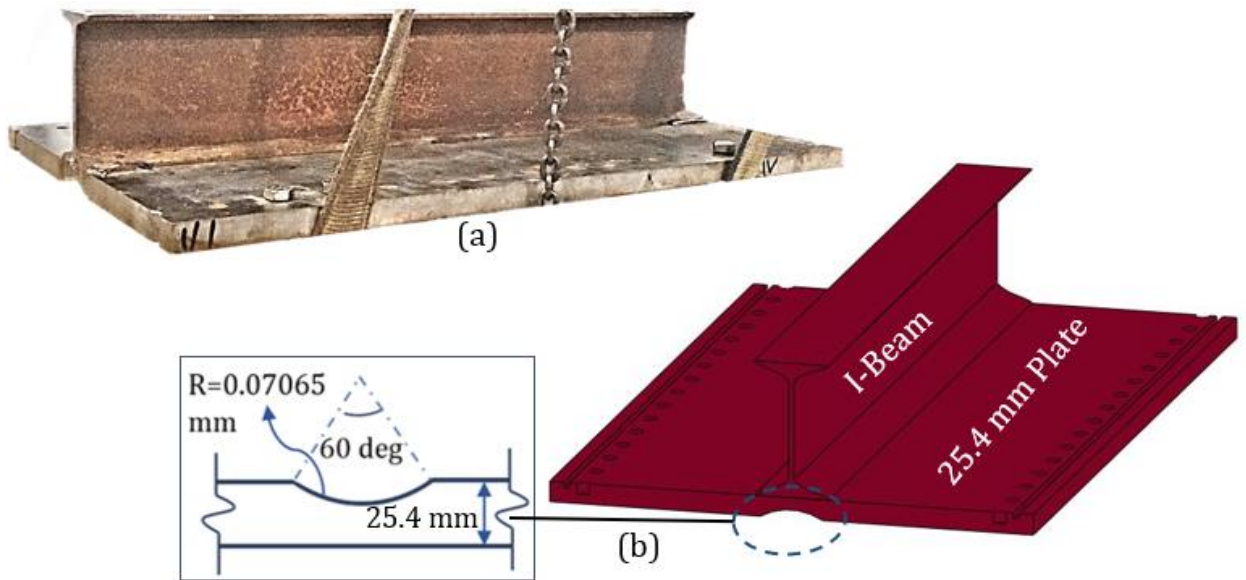


Figure 6-7 Saddle-shaped Support (a), and the 1 inch Plate (b) (Partly Edited from Davaripour et al. (2020c))

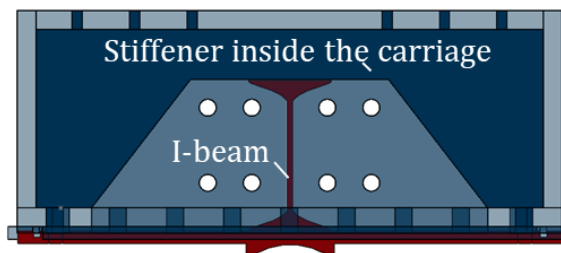


Figure 6-8 The Connection Between the I-Beam with a Stiffener Inside the Carriage (Edited from Davaripour et al. (2020c))

Figure 6-9 shows the mounts, which are devised to connect the ends of the specimen to the carriage via the key stock, and bolts. The mounts are made of high strength steel (ASTM 514) with a yield strength of 779 MPa and ultimate strength of 827 MPa, as reported in the mill material certification.

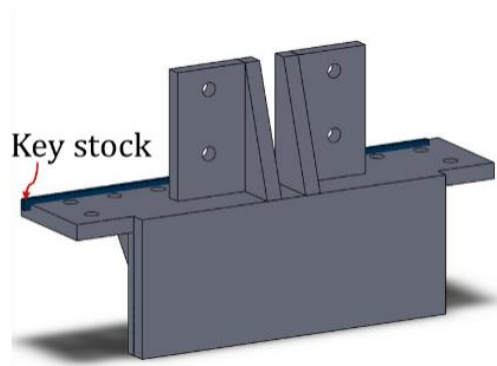


Figure 6-9 Schematic View of the Mount (Partly Edited from Davaripour et al. (2020c))

6.2.1.3 Indenter

The indenter is a solid shaft made of medium tensile strength steel (C1035) with a radius of 25 mm, representing a trawl door according to DNV-RP-F11 (2014). The leading edge of the indenter is used for the tests with the length of 203 mm for the frictionless indenter (Figure 6-10-a), and the length of 187 mm for the friction-included indenter (Figure 6-10-b). For the frictionless type, the sliding friction between the indenter and the specimen is eliminated using a rolling indenter mounted on two pillow block bearings, as well as using lubrication at the region of contact.

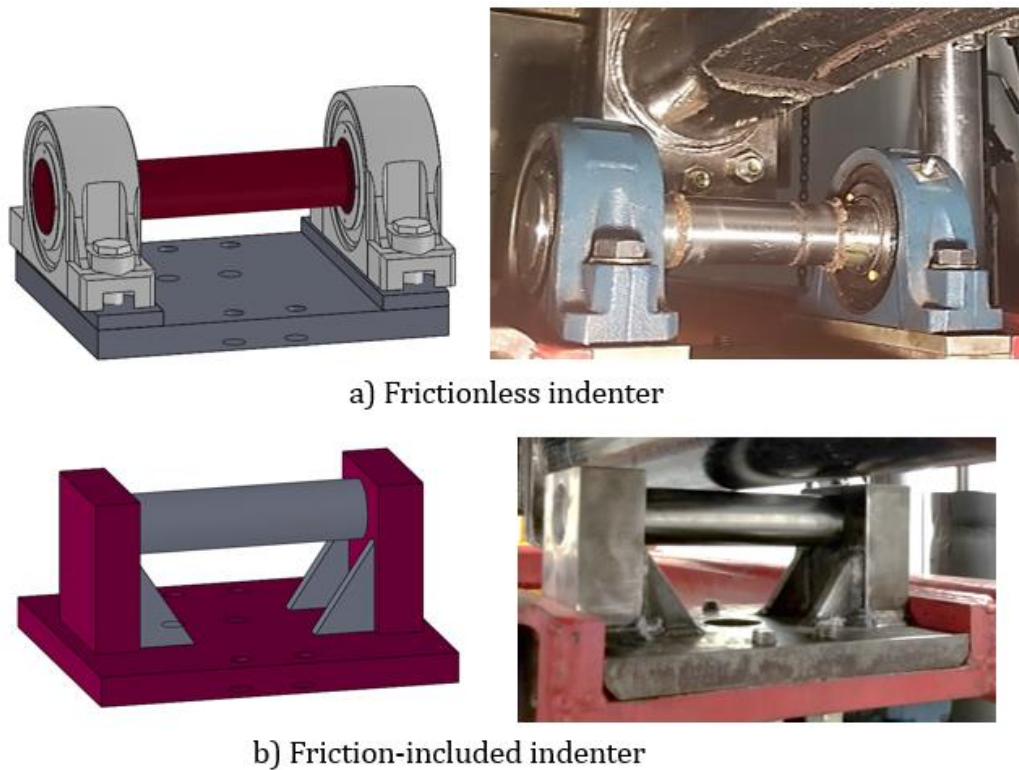


Figure 6-10 Solid Tube-Shaped Indenters: Frictionless Indenter (a), and Friction-Included Indenter (b) (Partly Edited from Davaripour et al. (2020c))

6.2.1.4 Boundary Conditions

Two boundary conditions (BC) were examined during the tests (Figure 6-11), including BC-1, where the global deformation of the pipe is restricted using the saddle-shaped Support, and BC-2, where the global and local deformation of the pipe is allowed (i.e., the saddle-shaped support is removed from the test setup).

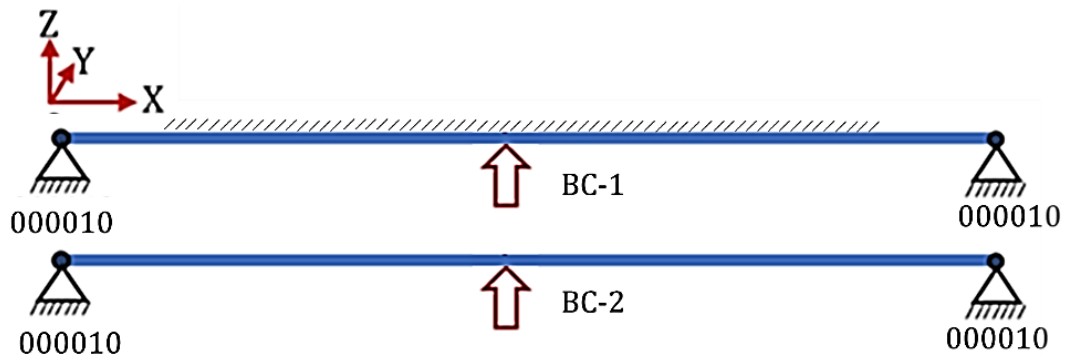


Figure 6-11 Boundary Conditions Employed in the Laboratory Tests

6.2.1.5 Instrumentation

The MTS test frame data acquisition system as well as laser scanning technologies, and imaging technologies were employed during the test to record (a) the vertical and horizontal force applied by the indenter to the specimen; (b) the vertical displacement of the indenter; (c) the horizontal displacement of the indenter relative to the specimen; (d) the side view of the cylindrical specimen during the indentation; (e) the spatial position of the deformed specimen after the test.

6.2.1.6 Test Procedure

All tests are performed under the quasi-static condition and contain two phases:

1. Phase 1 Figure 6-12-a), where the horizontal hydraulic ram is held steady and the vertical hydraulic ram pushes the indenter against the specimen. Accordingly, in the load-controlled test, the vertical ram applies 150 kN to the specimen through the indenter with a rate equal to 3 kN/sec. Also, in the displacement-controlled test, the

vertical hydraulic ram moves the indenter by 35 or 75 mm against the specimen with a rate equal to 1.0 mm/sec.

2. Phase 2 (Figure 6-12-b), where the horizontal hydraulic ram starts to push the carriage along the rail, for 300 mm, in a displacement-controlled condition (1 mm/sec). Accordingly, where phase 1 is in the displacement-controlled condition, the vertical position of the hydraulic ram remains steady. Also, where phase 1 is in the load-controlled condition, the 150 kN vertical load applied by the hydraulic ram remains steady.

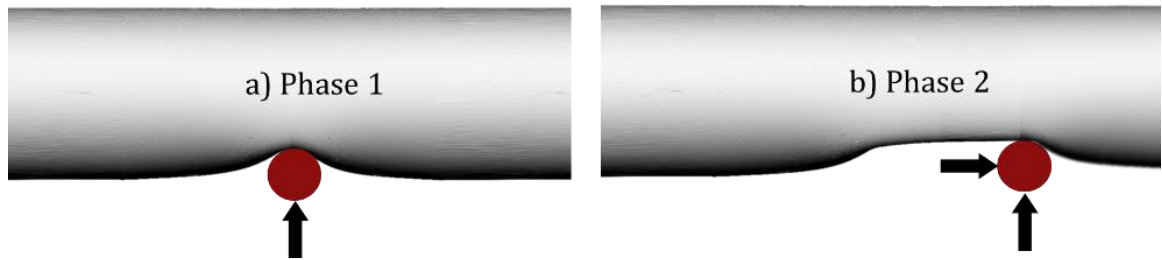


Figure 6-12 Loading Condition Including Phase 1 and 2 (Edited from Davaripour et al. (2020c))

Figure 6-13 shows the deformed cylindrical specimen prior to the indentation (a), at the end of phase 1 (b), and at the end of phase 2 (c).

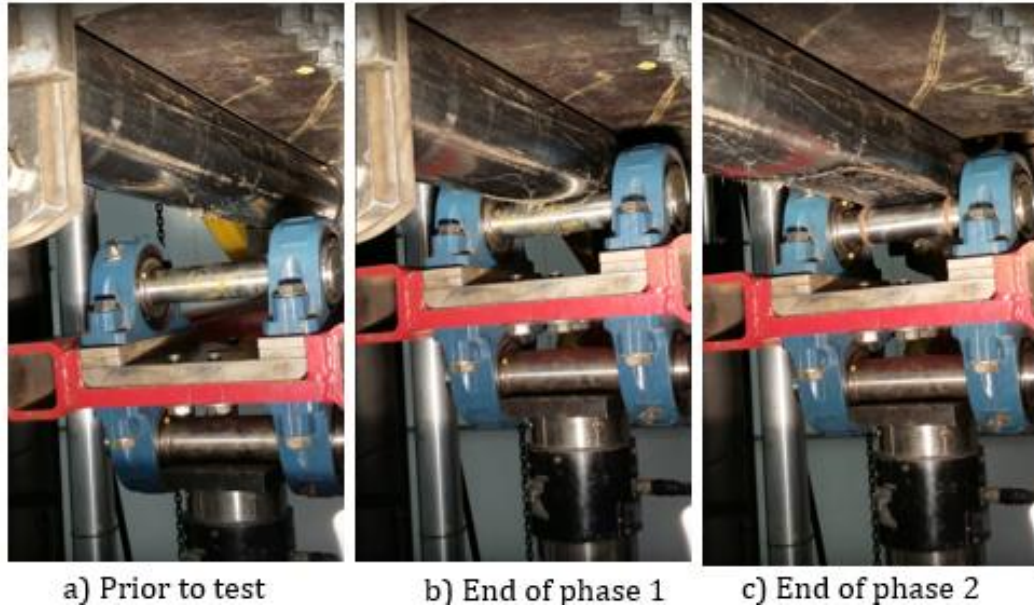


Figure 6-13 Test Procedure: 1) Before the Indentation, b) End of Phase 1, c) End of Phase 2
(Edited from Davaripour et al. (2020c))

6.2.1.7 Test Matrix

As presented in Table 6-2, four laboratory tests are conducted to investigate the damage progression effect in a pipeline. The vertical indentation/load values in Table 6-2 refer to the displacement of the indenter and the load applied by the indenter during phase 1, respectively.

Table 6-2 Test Matrix

Test no	Boundary condition (BC)	Indenter type	Vertical indentation - mm	Vertical load - KN	Analysis type	
					Phase 1	Phase 2
1	BC-1	FI	35	NA	DC	DC
2	BC-1	FL	35	NA	DC	DC
3	BC-1	FL	NA	150	LC	DC

4	BC-2	FL	75	NA	DC	DC
BC-1	The boundary condition type 1 (Figure 6-11)					
BC-2	The boundary condition type 2 (Figure 6-11)					
FL	Frictionless indenter (Figure 6-10-a)					
FI	Friction-included indenter (Figure 6-10-b)					
NA	Not applicable					
DC	Displacement-controlled					
LC	Load-controlled					

6.2.2 Result and Discussion

In this section, the data recorded during the physical tests are provided. In this regard, it is worth noting that the results of the first phase of Test 1 were partially provided in an article by the authors (Davaripour et al., 2020a). Furthermore, the results of Test 3 were partially presented in another article by the authors (Davaripour et al., 2020c). However, the majority of the physical test results are provided herein.

6.2.2.1 Test 1 and 2

6.2.2.1.1 Test 1 (BC-1, FI, DC-DC)

Test 1 was performed to investigate the effect of friction on the damage progression effect. Figure 6-14 shows the deformed shape of the specimen after the test. Also, Figure 6-15 shows the vertical displacement of the indenter (or resulting dent depth on the specimen) versus time, as well as the vertical load resisted by the specimen against the imposed indentation versus time. As shown in the figure, during phase 1, the vertical indentation increases and reaches to 35 mm. Consequently, the vertical load resisted by

the specimen against the imposed indentation increases and reaches to 221 KN. During phase 2, while the vertical position of the indenter (i.e., the dent depth imposed on the specimen) remains constant, the vertical resistance in the pipe decreases up to 33.5%. The significant drop occurs upon the initiation of phase 2 and promptly reaches the steady-state condition at 146.5 KN. Then close to the end of phase 2, the vertical resistance of the specimen slightly increases as the indenter approaches the end boundary condition.



Figure 6-14 A View of the Deformed Shape of the Specimen in Test 1

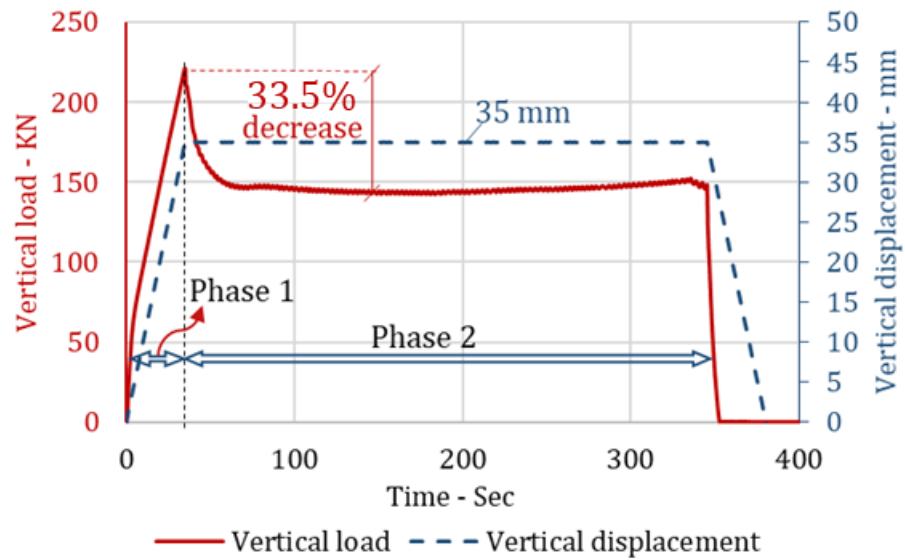


Figure 6-15 Results of Test 1: Vertical Load Resisted by the Specimen Against the Applied Indentation Versus Time (Left); Vertical Displacement of the Indenter (or the Resulting Dent Depth on the Specimen) Versus Time (Right)

Figure 6-16 shows the horizontal load resisted by the specimen, as well as the resultant load during the test. The horizontal direction refers to the direction along the carriage's motion path.

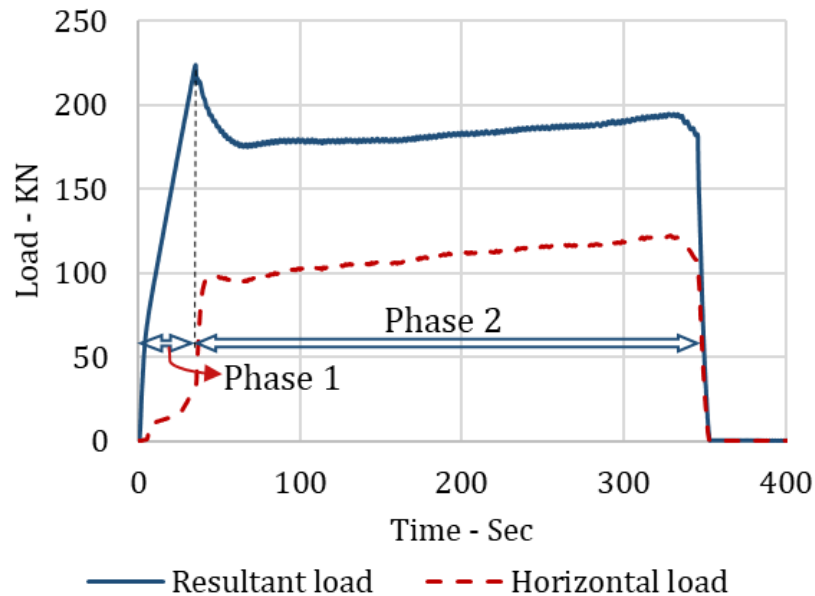


Figure 6-16 Results of Test 1: the Horizontal Load as Well as the Resultant Load Imposed to the Specimen Versus Time

6.2.2.1.2 Test 2 (BC-1, FL, DC-DC)

Test 2 was conducted using the frictionless indenter to provide test data to be compared against the results obtained from test 1; this comparison is employed to assess the effect of friction on the damage progression effect in pipelines. Figure 6-17 shows the deformed shape of the cylindrical specimen, where (a) Figure 6-17-a shows the initiation and direction of the moving load during phase 2; (b) Figure 6-17-b shows the test setup, after the experiment is conducted; (c) Figure 6-17-c shows the laser-scanned isotropic view of a section-cut of the deformed specimen; (d) Figure 6-17-d shows the y-z elevation view of the laser-scanned pipe. The indentation was applied uniformly during phase 2. However, the dent depth is not fully consistent along the pipe, which is due to the path-

dependent behaviour of the pipe during phase 2. In other words, the plastic deformation in any location of the pipe was affected by the indentation imposed on the pipe at adjacent locations in next time increments; (e) Figure 6-17-e shows the x-z view of a section cut of the scanned pipe.

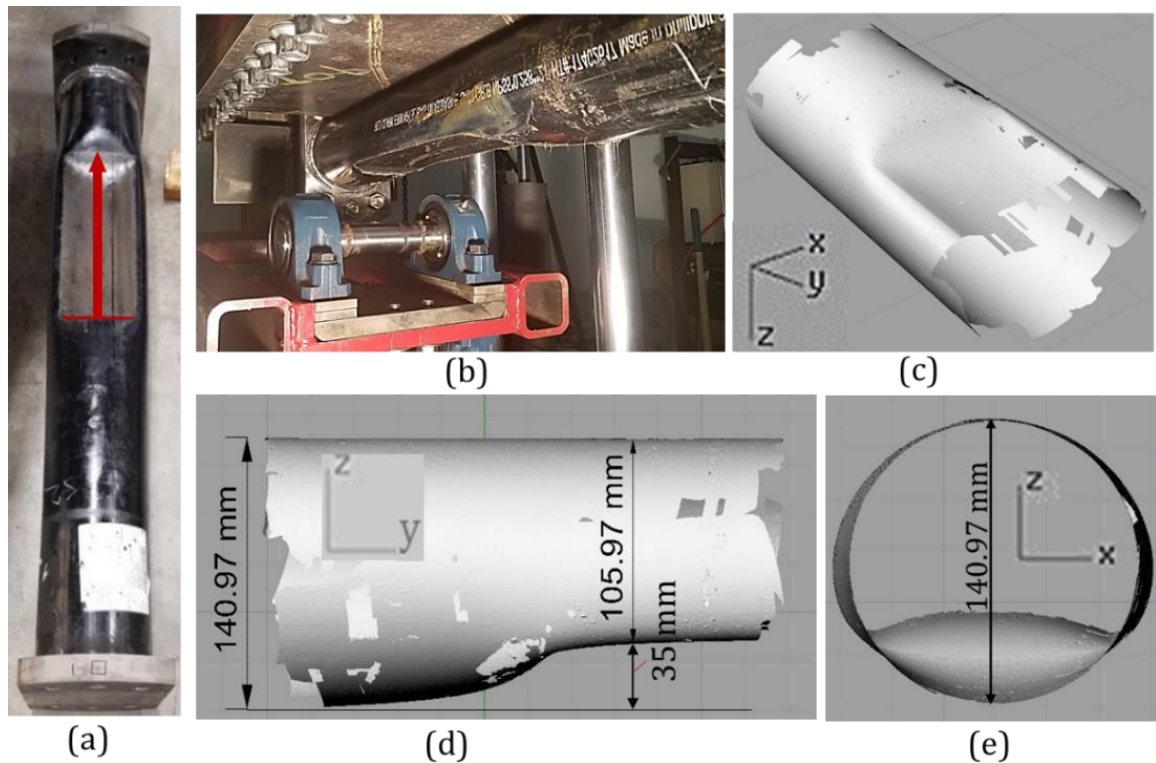


Figure 6-17 Test 2: Deformed Shape of the Cylindrical Specimen After Test 2; Views of the Laboratory Test (a and b); Scanned Views of a Section Cut of the Deformed Specimen (c, d, and e)

Figure 6-18 shows the vertical displacement of the indenter (or resulting dent depth on the specimen) versus time, as well as the vertical load resisted by the specimen against the imposed indentation versus time. As shown in the figure, during phase 1, the vertical

indentation increases and reaches 35 mm. Consequently, the vertical load resisted by the specimen against the imposed indentation increases and reaches 215 kN. During phase 2, while the vertical position of the indenter remains constant, the vertical resistance in the pipe decreases up to 32%; this significant drop occurs upon the initiation of phase 2 and promptly reaches the steady-state condition at 146 kN; then close to the end of phase 2, the vertical resistance of the specimen slightly increases as the indenter approaches the end boundary condition. Also, Figure 6-19 shows the horizontal load as well as the resultant load resisted by the specimen during the test.

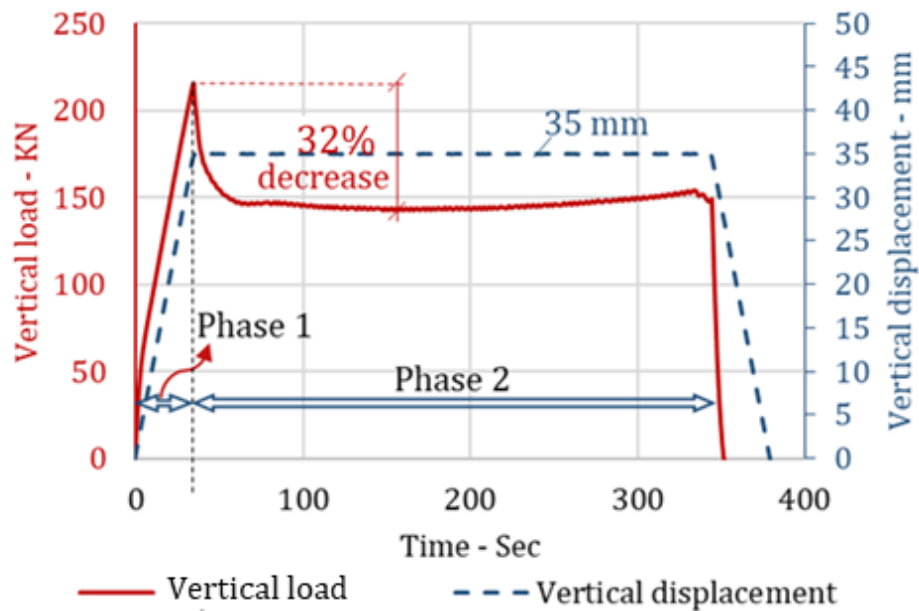


Figure 6-18 Results of Test 2: Vertical Load Resisted by the Specimen Against the Applied Indentation Versus Time (Left); Vertical Displacement of the Indenter Versus Time (Right)

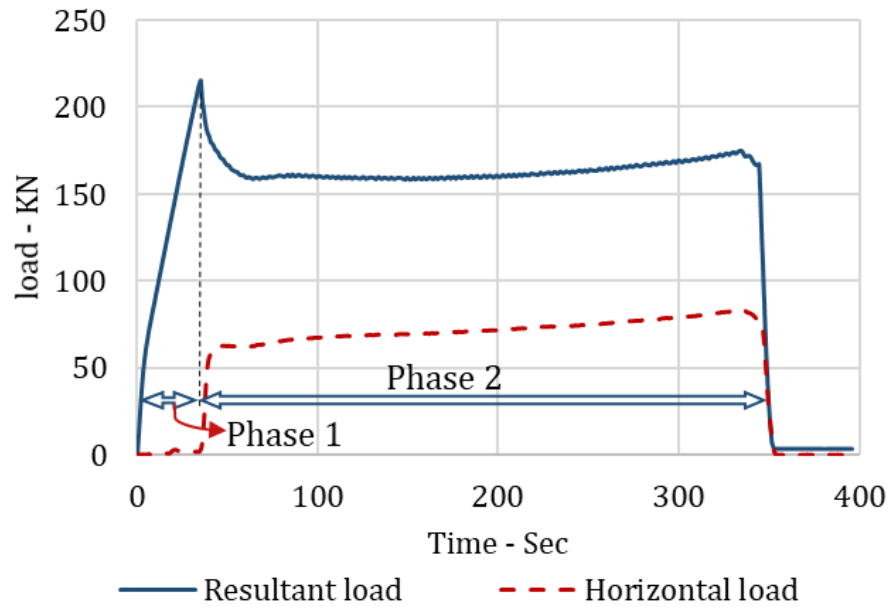


Figure 6-19 Results of Test 2: Resultant and Horizontal Load Imposed to the Specimen Versus Time

6.2.2.1.3 Comparison (Test 1 and 2)

Figure 6-20 shows that the vertical load resisted by the specimen in Test 2 is nearly identical to the one in Test 1, demonstrating that, at least for experimental conditions of the present study, the effect of sliding friction on pipe's vertical structural resistance is insignificant. In other words, the damage progression effect is not dependent on the sliding friction considering the present test condition. However, the horizontal load resisted by the specimen in test 2 is significantly lower than the one in test 1 (Figure 6-20), which is due to the effect of sliding friction between the specimen and the FI indenter in test 1. As such, as shown in Figure 6-21, the resultant load resisted during test 2 is significantly less than the one in test 1.

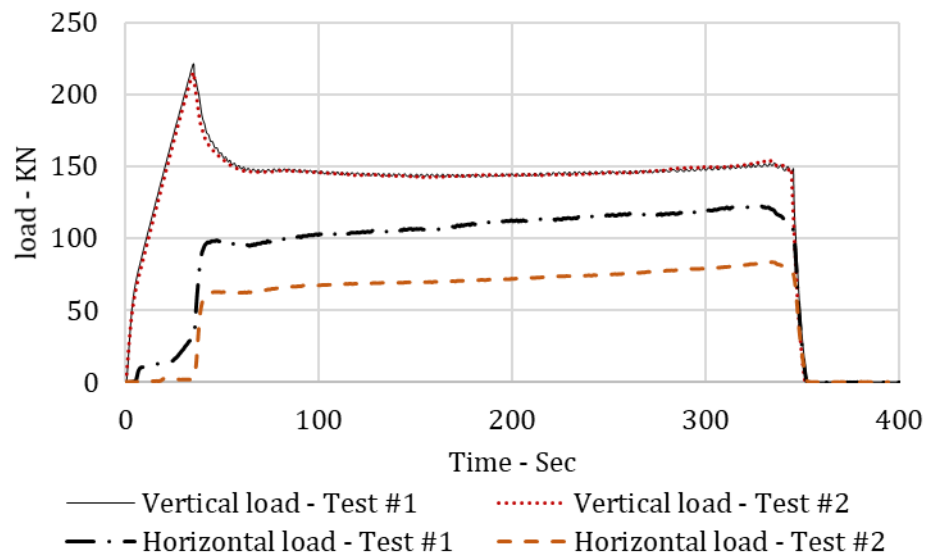


Figure 6-20 Results of Test 1 and 2: Vertical Load as well as Horizontal Load Resisted by the Specimen Against the Applied Indentation Versus Time

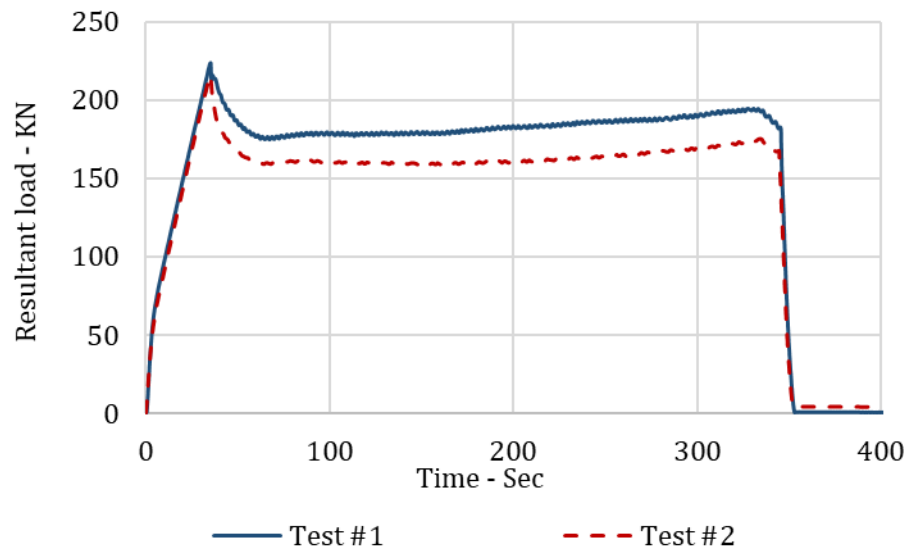


Figure 6-21 Results of Test 1 and 2: Resultant Load Resisted by the Specimen Against the Applied Indentation Versus Time

The test setup in test 1 versus test 2 is the same, except in test 1, the friction-included indenter was employed, while in test 2, the frictionless indenter was used. As such, the higher horizontal load in test 1 versus test 2 (Figure 6-20) is due to the sliding friction between the indenter and the specimen in test 1. In this regard, the friction coefficient between the friction-included indenter and the specimen could be derived from the difference between the horizontal load in test 1 and 2 over the vertical load in test 1. Figure 6-22 shows the load difference, the vertical load in test 1, and the variation of the friction coefficient between the indenter and specimen during test 1. The average friction coefficient where the curve reaches steady-state condition is equal to 0.26~0.3.

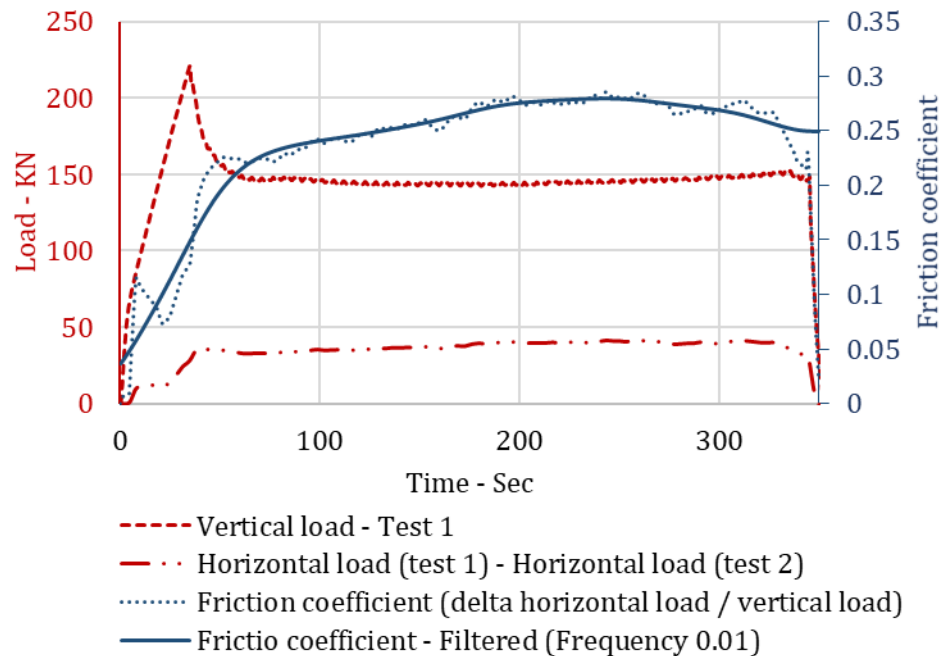


Figure 6-22 Vertical Load (Test 1) and Horizontal Load (Test 1&2) versus Time (Left); Friction Coefficient Versus Time During Test 1 (Right)

6.2.2.2 Test 3 (BC-1, FL, LC-DC)

Test 3 was performed to investigate the damage progression effect in cylindrical specimens under the load-controlled condition. Figure 6-23 shows the vertical load applied by the indenter against the specimen versus time, as well as the vertical displacement of the indenter (or the resulting dent depth imposed on the specimen) versus time. As shown in the figure, during phase 1, the applied load increases to 150 KN. Consequently, the dent depth imposed on the specimen increases to 20.7 mm. During phase 2, while the vertical load almost remains constant, the imposed dent depth on the specimen increases up to 52% and reaches 32 mm. This demonstrates the need to consider the damage progression effect for the assessment of impact scenarios on subsea pipelines, where denting limit states and its associated design criteria may be governing.

Also, Figure 6-23 shows that during phase 2, while the MTS control software held the 150 kN force (as measured by the vertical ram's load cell), the actual vertical load drops slightly (4%) due to the generated moment along the swing arm, as discussed in Appendix. This is an unavoidable experimental error, as the MTS software control is based only on the vertical ram force, and there is no way to compensate for the difference resulting from the swingarm moment. This implies that if the imposed vertical load was remained perfectly constant at 150 KN (instead of slightly decreasing), then the increase in the imposed dent depth could be even larger than 52%. Also, Figure 6-24 shows the horizontal load resisted by the specimen during the test.

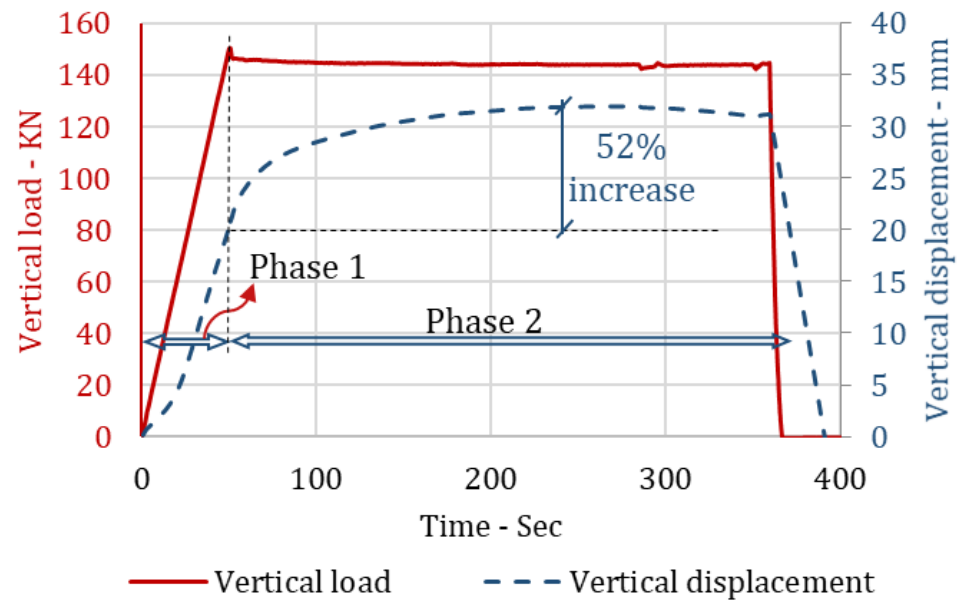


Figure 6-23 Results of Test 3: Vertical Load Applied by the Indenter Against the Specimen Versus Time (Left); Vertical Displacement of the Indenter Versus Time (Right) (Davaripour et al., 2020c)

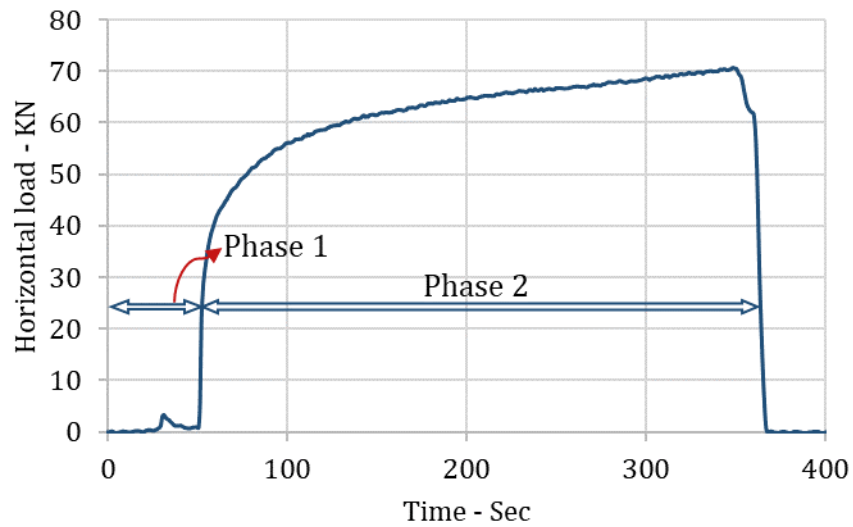


Figure 6-24 Results of Test 3: Horizontal Load Imposed to the Specimen Versus Time

6.2.2.3 Test 4 (BC-2, FL, DC-DC)

Test 4 was performed to assess the potential mitigating effects of bending response in cylindrical specimens on the damage progression effect. Figure 6-25 shows the deformed shape of the cylindrical specimen. As shown in the figure, the saddle-shaped support is removed, and the specimen has both local and global deformation.

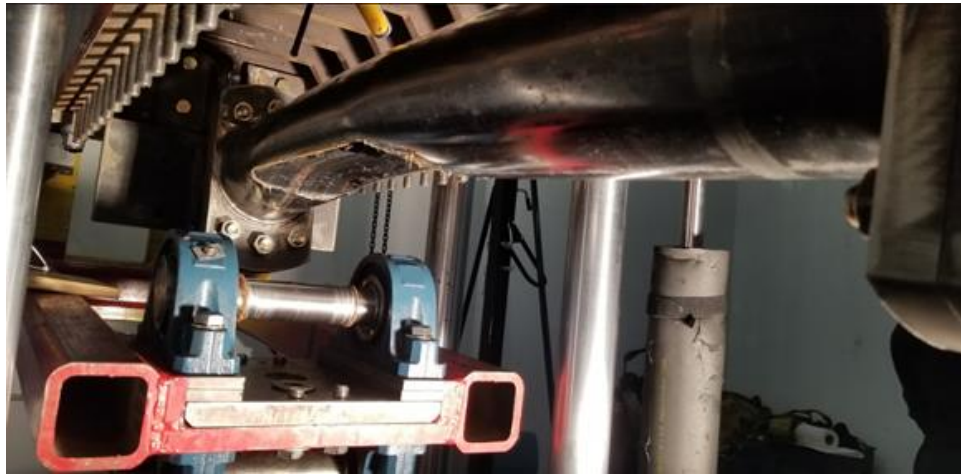


Figure 6-25 Deformed Shape of the Specimen After Test 4

Figure 6-26 shows the scanned views of the deformed cylindrical specimen, where (a) Figure 6-26-a shows an isotropic view of the specimen; (b) Figure 6-26-b shows the x-z view of a specimen; (c) Figure 6-26-c shows the y-z elevation view of the pipe with the dimensions of two regions highlighted including where the pipe is (1) intact by the indentation after the test; (2) the dent size on the specimen reaches the steady-state condition.

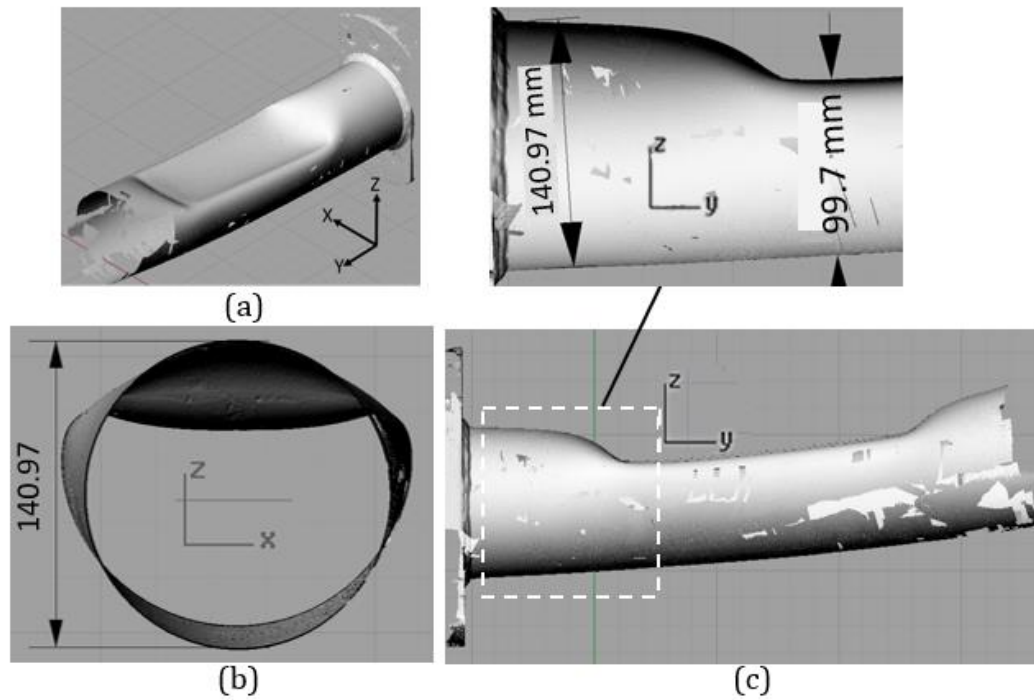


Figure 6-26 Scanned Views of a Section-Cut of the Deformed Specimen in Test 4

Figure 6-27 shows the vertical load resisted by the specimen versus time, as well as the vertical displacement of the indenter versus time. As shown in the figure, during phase 1, the displacement of the indenter increases to 75 mm. Consequently, the load withstood by the pipe increases to 157 kN. During phase 2, while the vertical position of the indenter remains constant, the structural resistance of the pipe decreases up to 12%; the maximum drop occurs upon the initiation of phase 2 and promptly reaches the steady-state condition at 138 kN; then, the pipe response increases as the indenter approaches the end boundary condition. Also, Figure 6-28 shows the horizontal load as well as the resultant load resisted by the specimen during the test.

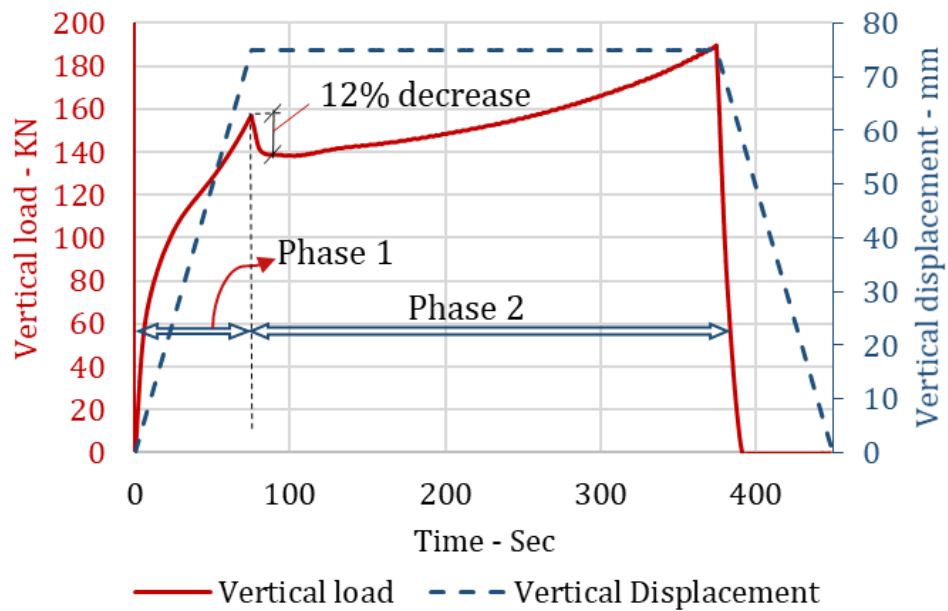


Figure 6-27 Results of Test 4: the Vertical Load Resisted by Specimen Versus Time (Left); Vertical Displacement of the Indenter Versus Time (Right)

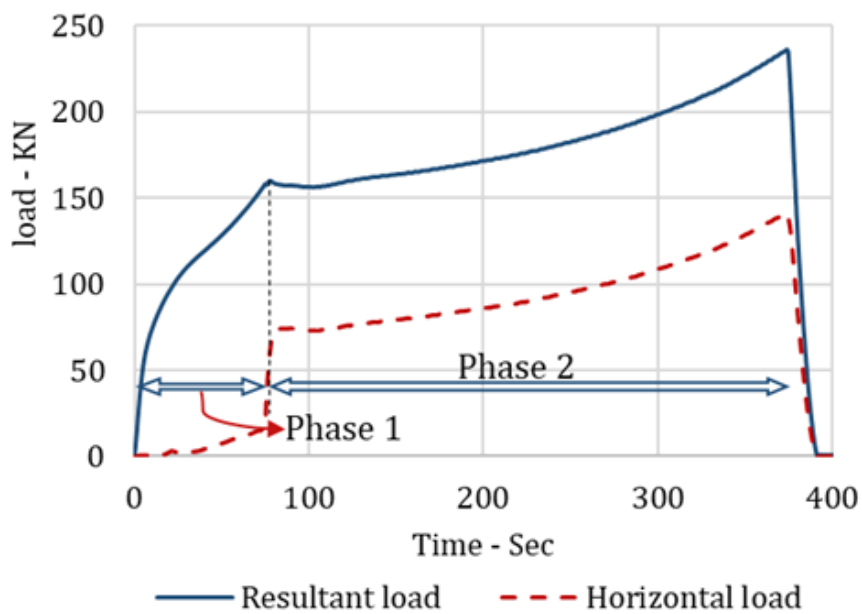


Figure 6-28 Results of Test 4: Resultant Load as well as the Horizontal Load Applied to the Specimen Versus Time

Figure 6-29 shows the vertical displacement of the specimen in the middle at the top and bottom points of the cross-section, during the 75 mm indentation (phase 1 of loading); Figure 6-29 also shows the difference between these curves, which is the resulting dent depth imposed on the pipe at the region of indentation.

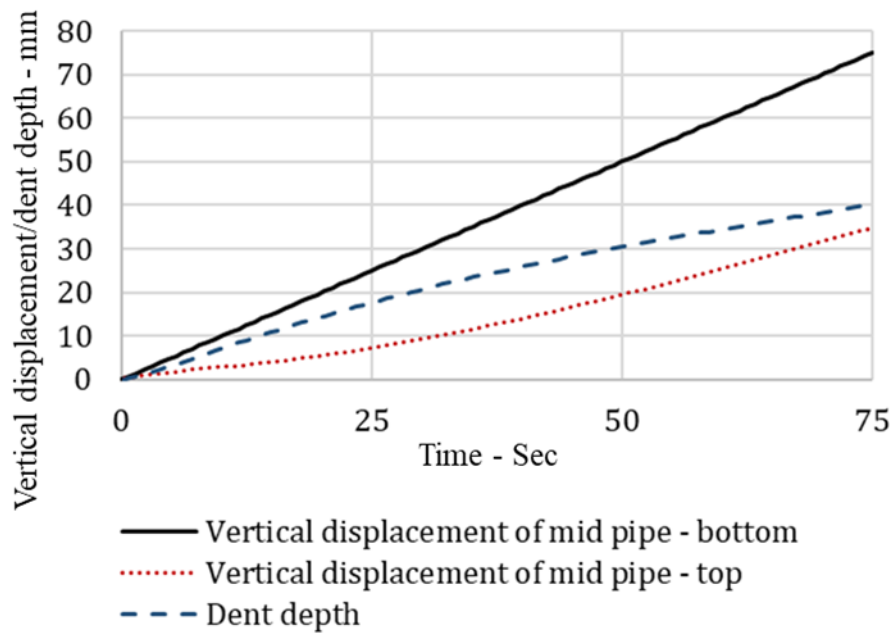


Figure 6-29 Vertical Displacements of the Top and Bottom Points of the Mid-Pipe as well as the Resulting Dent Depth Imposed on the Specimen during Phase 1 of the Loading

6.2.2.3.1 Comparison (Test 2 and 4)

According to the results obtained in Test 2 and 4, the damage progression effect in test 4 (12%) is significantly less than the effect observed in Test 2 (32%); the size of the dent imposed on the pipes is relatively similar in Test 2 and 4 (35 mm in Test 2 and 40.6 mm in Test 4). As such, the bending response of the pipe has mitigating effects on the damage

progression effect on subsea pipelines. Figure 6-30 shows the vertical load resisted by the specimen in test 4 versus test 2.

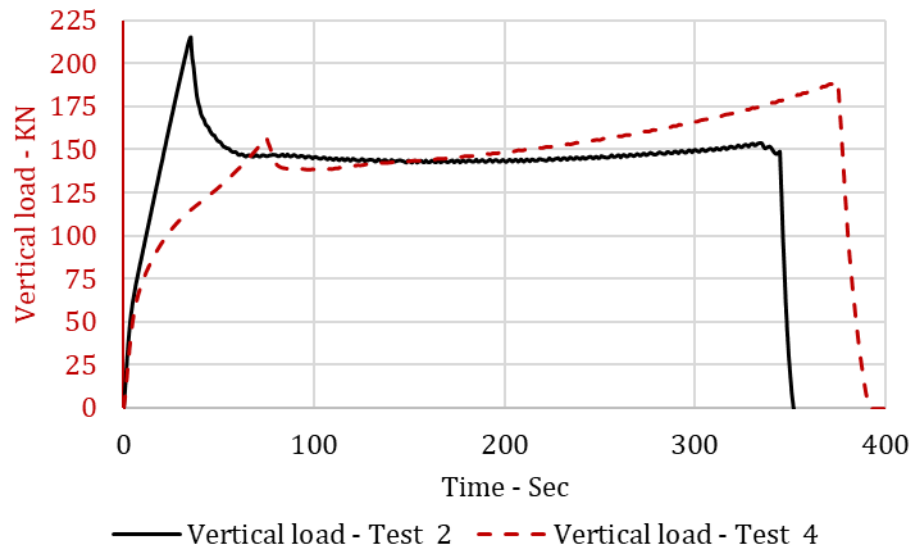


Figure 6-30 Results of Test 2 and 4: the Vertical Load Resisted by Specimen Versus Time

6.3 Numerical Investigations

A numerical investigation is conducted, using Abaqus Explicit, to examine a scenario of a subsea pipeline subject to subsequent trawl impacts. The finite element method is employed to show the damage progression effect when a pipe is indented by repeated trawl impacts at neighbouring locations; the subsequent indentation of a pipe at adjoining locations leads to the progression of plastic damage along the pipe. This novel scenario examines the statement of DNV-RP-F11 (2014) that “repeated impacts at same locations need to be considered, reflecting the trawling frequency”. The idealized numerical model is built according to DNV-RP-F11 (2014) and validated against the results of Test 3. Furthermore, in order to computationally enhance the numerical analyses, the semi-automatic mass scaling in Abaqus is implemented in the numerical model using scale factor of 1000.

6.3.1 Element Type

The specimen is modelled with reduced integration shell elements (S4R) with aspect ratio equal to 1, and edge length equal to 3 mm. The cylindrical indenter and the saddle-shaped support are modelled with rigidly constrained solid elements.

6.3.2 Load Path

Test 3 is performed in two phases including (a) phase 1, where the indenter imposes 150 KN load via the cylindrical indenter against the specimen in the load-controlled condition; (B) phase 2, where the 150 KN imposed load remains nearly constant (4% reduction), and the indenter translates along the pipe for 300 mm. Figure 6-31 shows the load path during phase 1 and 2.

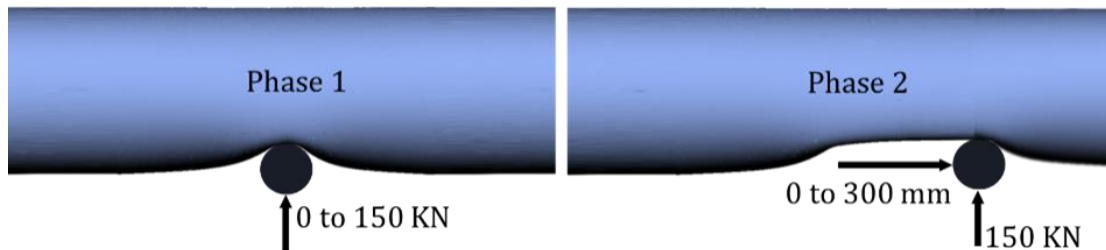


Figure 6-31 Load Path During Phase 1 and 2 in Test 3 (Edited from Davaripour et al. (2020c))

6.3.3 Boundary Conditions

The boundary conditions implemented in the test setup include the 1-inch saddle shape support, which restrains the global deformation of the specimen, and the mounts at both ends, which restrain the axial deformation of the specimen. These boundary conditions are schematically shown in Figure 6-32. Furthermore, considering the groove welding between the two end edges of the specimen and the flange plates (Figure 6-6), the length of the specimen's deformable region in Figure 6-6 is set to 940 mm, and the rest of the specimen's length is rigidly constrained.

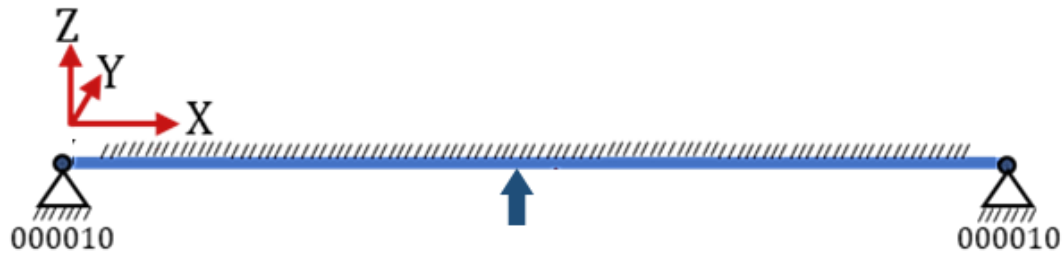


Figure 6-32 Boundary Conditions Employed in Test 3

Quinton (2015) used a similar test apparatus and reported a vertical elastic deformation in the apparatus during the applied indentation. The author performed sensitivity studies and concluded that the elastic stiffness is within the range of $1e7$ to $2.5e7$ N/mm. In the present study, for the interaction between the saddle-shaped support and the specimen, the elastic pressure-overclosure behaviour is employed with the spring stiffness set to $0.5e7$ N/mm, based on sensitivity analyses. This value is slightly less than the values reported by Quinton (2015), due to the modifications which are applied to the test apparatus in the present work. Furthermore, additional finite element analyses are conducted to obtain the stiffness of the mounts (Figure 6-33), where for the boundary conditions: (a) at the location of the key stock, the nodes are restrained along the x-axis, and (b) at the location of the bolts, nodes are restrained in all degrees of freedom. Furthermore, the tied nodes are rigidly constrained and pulled by 20 mm in the opposite direction of the x-axis. The mount is modelled using the reduced-integration solid elements (C3D8R) with the deformed shape presented in Figure 6-33-b.

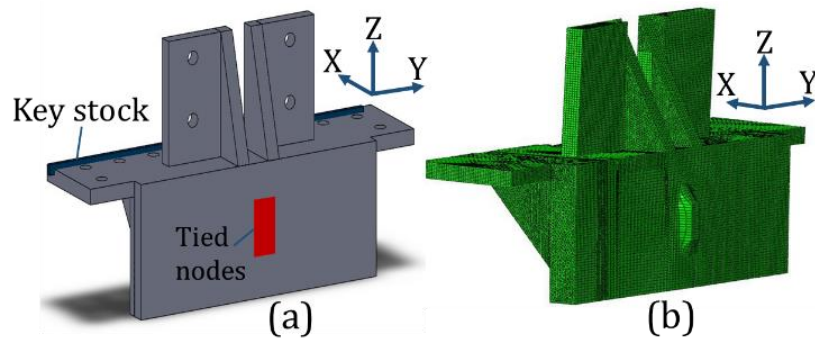


Figure 6-33 Numerical Simulation of the Mount (Partly Edited from Davaripour et al. (2020c))

Figure 6-34 shows the load-displacement curve from which the stiffness of the mounts could be obtained. In this regard, axial connectors (as presented in Abaqus Documentation (2019)) at both ends of the pipe are used to represent the stiffness provided by the mounts (Figure 6-35).

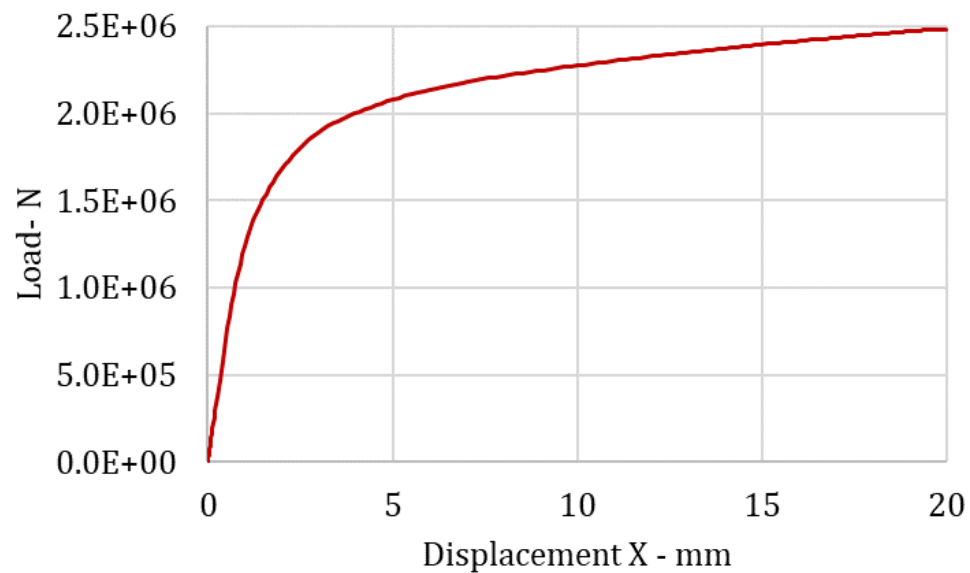


Figure 6-34 Load-Displacement Curve of the Mount (Edited from Davaripour et al. (2020c))

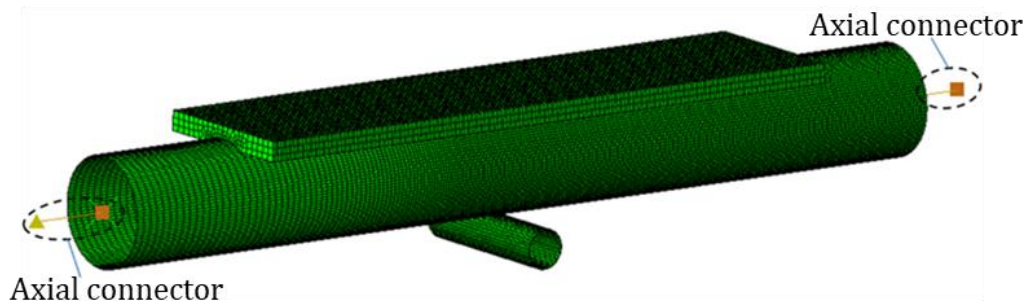


Figure 6-35 Axial Connectors employed to Represent the Stiffness Provided by the Mounts
(Edited from Davaripour et al. (2020c))

6.3.4 Interaction Properties

The numerical model comprises two interactions, including the contact between the indenter and the specimen and the contact between the specimen and the saddle-shaped support (Figure 6-35). For the first contact definition, the sliding friction coefficient is assumed 0 due to using the frictionless indenter. For the latter one interaction, according to the test setup, there is nearly no relative displacement between the specimen and the support. In this regard, sensitivity studies are performed using finite element analyses (Section 6.3.6.1), which shows that the sliding friction coefficient between the specimen and the saddle-shaped support does not affect the Pipe's response. As such, a reasonable friction coefficient of 0.3 is employed for analyses in the present study.

6.3.5 Mesh Convergence Analysis

Mesh convergence analyses are conducted to determine the shell element size in the specimen. Figure 6-36 shows the result of the analyses for three mesh sizes, including 3,

5, and 6 mm. As shown in the figure, the results of all three cases are very similar, particularly for the maximum vertical displacement of the indenter. The mesh size equal to 3 mm is used for the analyses.

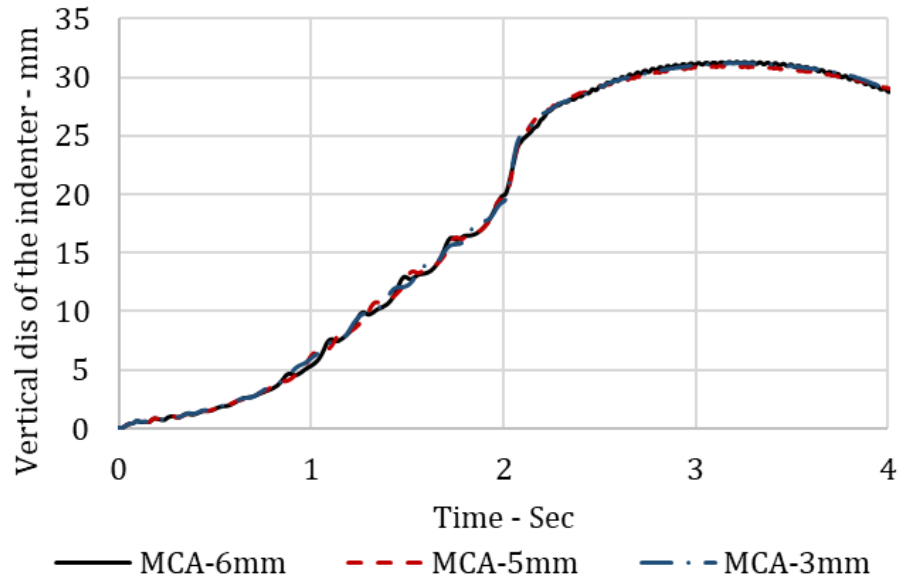


Figure 6-36 Mesh Convergence Analyses Including Three Mesh Sizes: 3, 5, and 6 mm

6.3.6 Results

Figure 6-37 shows a good agreement between the numerical outcome and the physical data; during phase 1, the numerical result is perfectly aligned with the test data; during phase 2, the numerical prediction slightly underestimates the physical data in the second half of the phase; this discrepancy could be sourced in the simplification and idealization of the boundary conditions in the numerical model.

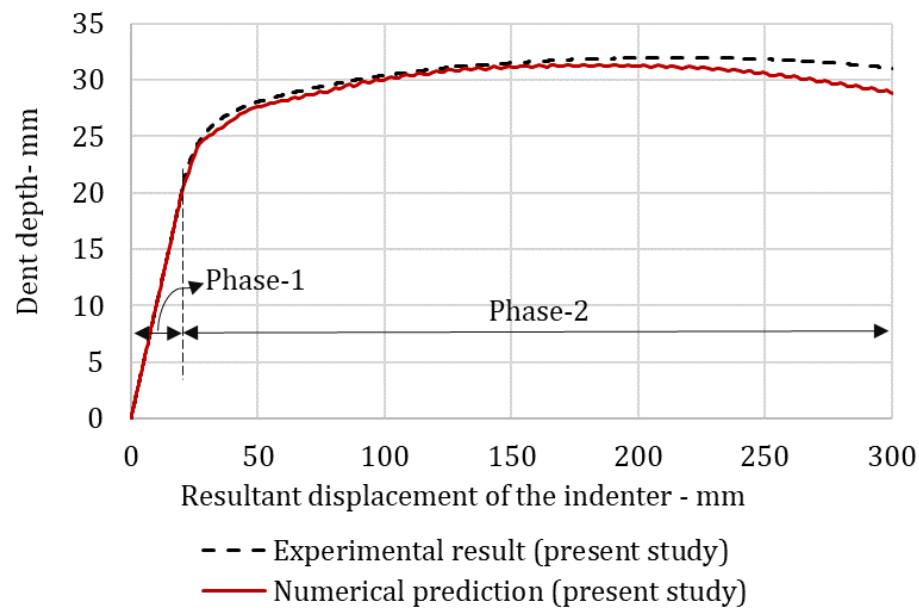


Figure 6-37 The Vertical Displacement of the Indenter (or Imposed Dent Depth on the Specimen) Versus Resultant Displacement of the Indenter; Numerical Versus Experimental Result (Edited from Davaripour et al. (2020c))

6.3.6.1 Sensitivity Study

A sensitivity study is conducted using finite element analysis to examine the effect of the friction coefficient between the specimen and the saddle-shaped support on the pipe's response. Accordingly, Figure 6-38 presents the dent depth of the specimen under varied friction coefficients 0.0, 0.3, and 0.5, and shows the dent depth of the specimen is not affected by the value of the friction coefficient.

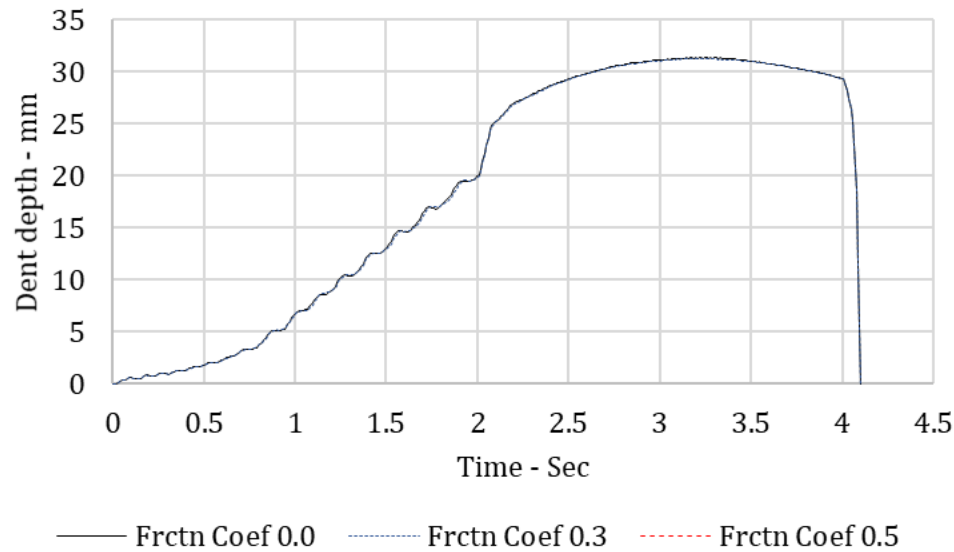


Figure 6-38 Sensitivity Studies: Friction Coefficient (Specimen Against the Saddle-shaped Support): 0.0, 0.3, 0.5

6.3.7 Repeated Trawl Impacts

DNV-RP-F111 (2014) states that “repeated impacts at same locations need to be considered, reflecting the trawling frequency”. However, if the subsequent impacts are imposed at neighbouring locations on the pipe, it could lead to the damage progression along the pipe. In other words, if a pipe is indented at locations that are sufficiently close to each other, the resulting plastic damage on the pipe translates longitudinally, as if the load is sliding along the pipe. In this regard, a novel scenario is introduced and studied where a cylindrical specimen is subject to several identical quasi-static perpendicular indentations at adjoining locations. In total, 11 adjacent indentations (15 mm away from each other) are applied to the pipe, using the verified numerical model introduced in

Section 6.3. Figure 6-39 shows schematic views for 3 out of 11 indentations along the specimen; each indentation imposes a 150 kN on the pipe, in the load-controlled condition.

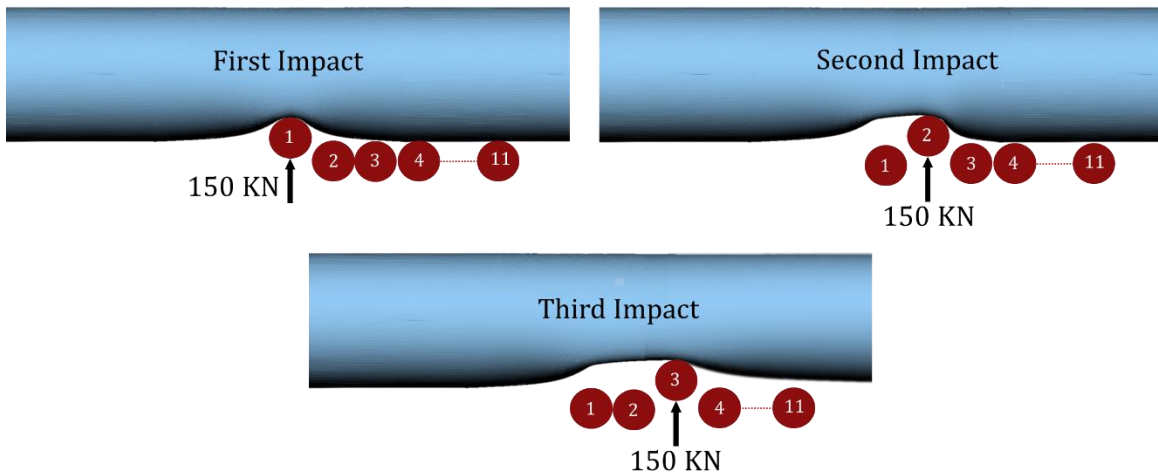


Figure 6-39 Schematic Views of the Deformed Pipe under Repeated Indentations at Adjacent Locations

Figure 6-40 shows the deformed shape of the specimen after 11 adjacent indentations. As shown in the figure, after each indentation, the imposed damage on the specimen progresses longitudinally; the length of the dent reaches 150 mm after the final indentation. Furthermore, by the progression of the imposed damage, the dent depth increases until it reaches a steady-state value.

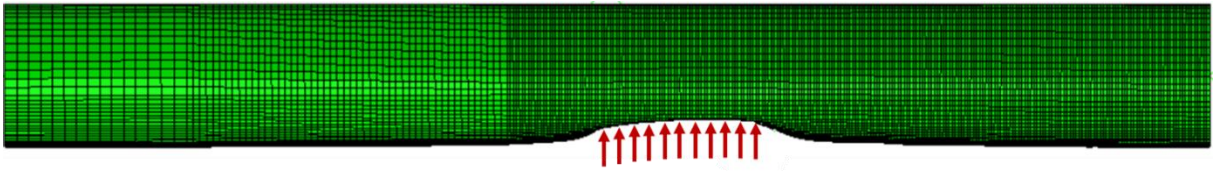


Figure 6-40 The Deformed Shape of the Specimen After 11 Indentations

Figure 6-41 shows the maximum vertical displacement of the indenter along the pipe after each indentation; each data marker represents one indentation. The results of Test 3 are also provided for comparison. As shown in Figure 6-41, the damage size in the specimen increases from 21 mm to 29 mm (38.2% increase) until it reaches a steady-state condition. Furthermore, comparing the numerical results against the physical data of Test 3 (Figure 6-41) shows a good overall agreement. However, the specimen under the repeated indentations leads to less damage progression effect.

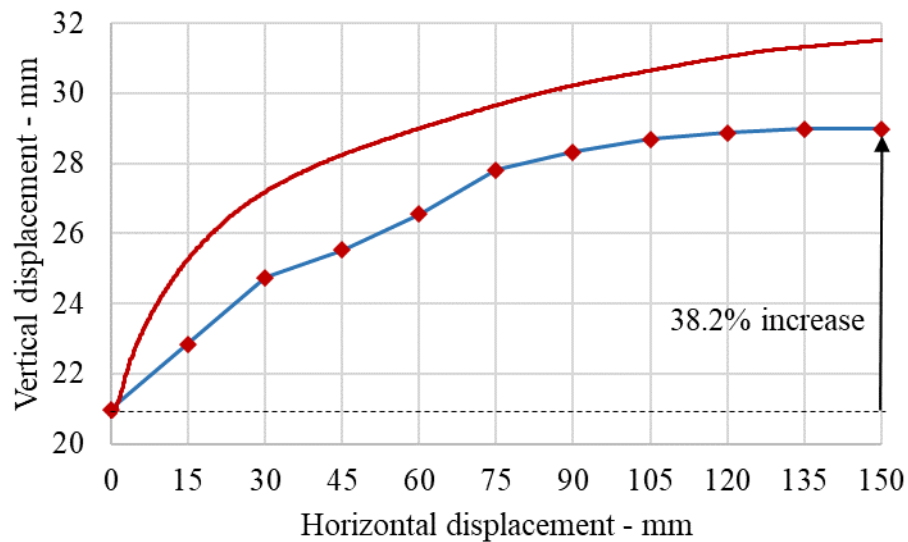


Figure 6-41 Numerical Results Versus Physical Data of Test 3: Vertical Displacement Versus Horizontal Position of the Indenter Relative the Pipe Middle Length

In the present numerical investigation, repeated trawl impact on a subsea pipeline is examined under the quasi-static load controlled condition; as accordingly to (Shen and Jones (1991) and Zheng (2014) dynamic effect of the trawl interference event could be replicated using quasi-static analyses. As a result of this numerical study, it is shown that the load-carrying capacity of a pipe decreases as the plastic damage progresses longitudinally under repeated identical quasi-static indentations at adjacent locations. These results show that considering the subsequent trawl impact at adjoining locations on a pipe could lead to more dent depth compared to a case where the pipe is subject to repeated trawl impacts at the same location, as recommended by DNV-RP-F111 (2014); subsequent identical quasi-static indentations at the same location on a pipe does not change the resulting dent depth imposed after the first indentation. This is a clear application of the damage progression effect in the offshore pipeline industry.

6.3.7.1 Equivalent Stress Contour

Figure 6-42 shows the side views of the pipe subject to repeated indentations and demonstrates the plastic stress contour in the range of yield stress to ultimate stress (Table 6-1). Accordingly, for the pipe under the first indentation, there is the symmetrical distribution of stress contour. However, for the pipe under the third indentation (30 mm away from the first one), the trailing side of the pipe does not have a significant contribution compared to the leading side, where the trailing side is a portion of pipe behind the indenter, and the leading side is the portion of the pipe ahead of the indenter.

The progression of damage along the pipe involves high (geometric, material, and BC) nonlinearities. In this respect, the following assumptions are made to understand the source of this considerable change in the pipe's stress contour under the first versus the third indentation:

- The pipe's stiffness against the lateral indentation involves longitudinal bending and stretching stiffness as well as circumferential bending and membrane stiffness. According to findings of the work conducted by Hahn et al. (1993), which employed the analytical method to investigate local buckle and buckle propagation in the subsea pipeline under external pressure, the first stiffness is negligible compared to the latter one. In this regard, considering the similar cross-sectional deformation of a pipe subject to external pressure and lateral indentation, it could be assumed that the pipe's response during the lateral indentation is also controlled by the circumferential bending and membrane stiffness. As such, pipe's plastic capacity under repeated adjacent indentations could be simplified and investigated by the load-carrying capacity of a ring subject to a lateral indentation.
- Hahn et al. (1993) developed an analytical equation to predict the external pressure required to develop radial displacement on a ring for both before and after the buckling. The authors showed that for thin-walled pipes (for example, the pipe of the present study with $D/t > 20$) if $P = P_e$ (Equation 6-1), the ring experiences elastic buckling and becomes unstable under bending actions. In this regard, the ring action under the lateral indentation is examined using the modified version of the numerical

model presented in Figure 6-43; where the pipe's length decreased to 1 cm. Figure 6-43 shows the plastic equivalent stress contour on the ring after 35 mm indentation. Also, Figure 6-44 shows the load-displacement curve during the indentation, which demonstrates that by the formation of plastic hinges on the ring, it no longer withstands any additional lateral load. This finding is in agreement with the results of Hahn et al. (1993) regarding the post-buckling behaviour of a ring under external pressure. However, according to the findings of Hahn et al. (1993), after the elastic buckling of the ring, even by a reduction of the external pressure, the ring could be crushed. However, the load-carrying capacity of the ring after the formation of plastic hinges remains constant.

$$P_e = 2E_1 \left(\frac{t}{D} \right)^3 \quad \text{Equation 6-1}$$

Where, E_1 is the elastic modulus for the pipe; D and t are the outer diameter and nominal thickness of the ring, respectively.

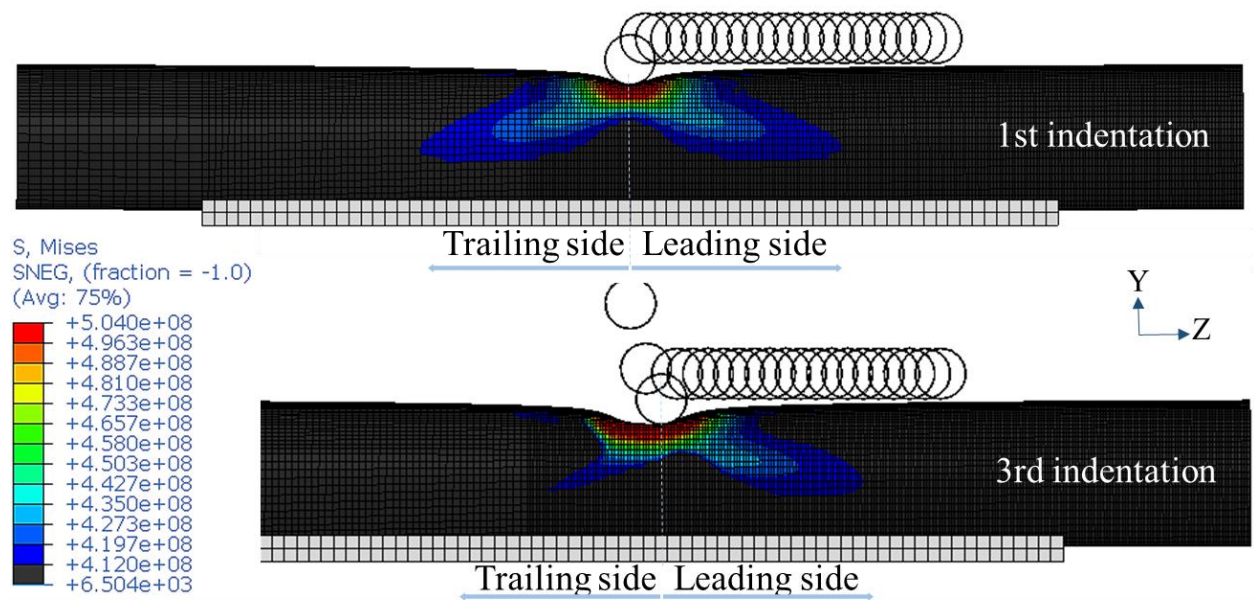


Figure 6-42 Plastic Equivalent Stress Contour Under Indentation Number 1 and 3

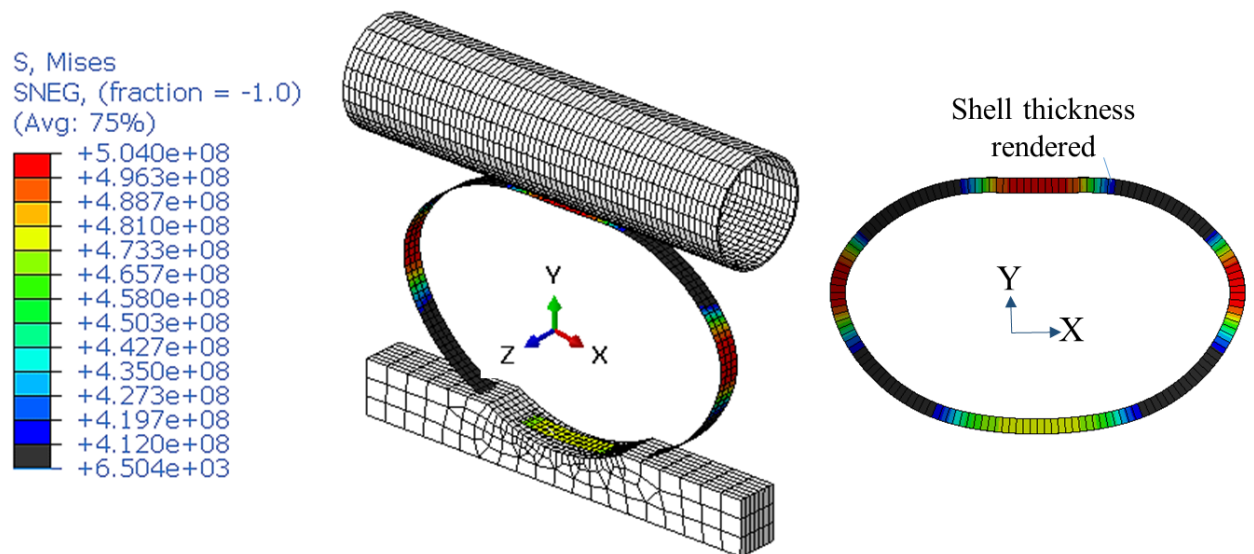


Figure 6-43 Plastic Equivalent Stress Contour of a Ring under a Lateral Indentation

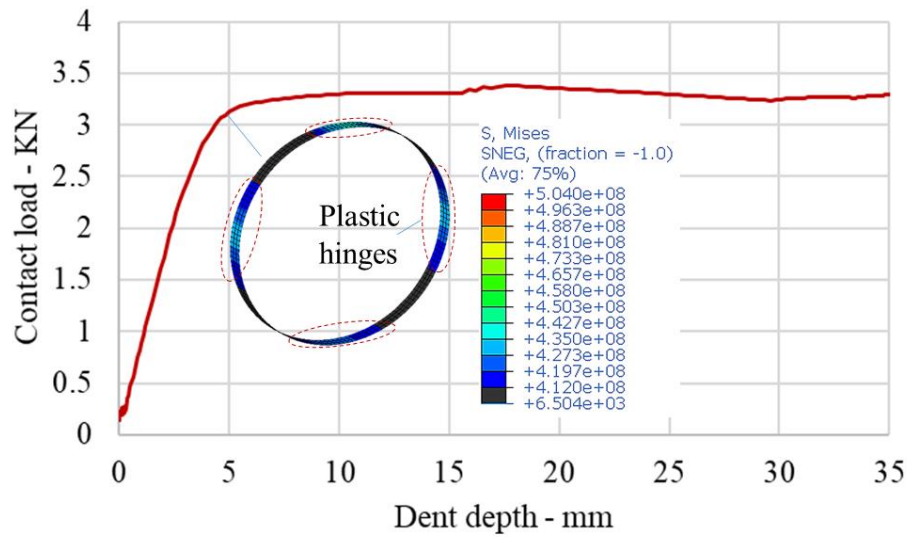


Figure 6-44 Load-Displacement Curve of a Ring under the Lateral Indentation

According to the above points, after the initial plastic damage on the pipe, for the following indentations (i.e., third indentation), the trailing side of the pipe has already buckled. According to the above findings regarding the post-buckling behaviour of a ring under a lateral indentation, the distribution of stress along the trailing side of the pipe is not (fully) possible, as the pipe in the buckled regions is unable to pass more than 3 KN per 1 cm length (Figure 6-44). As such, the buckled region on the trailing side of the pipe acts like a weak link. Therefore, the structural contribution of the pipe on the leading side is significantly more than the trailing side, which could be observed via the change in the plastic stress contour on the pipe under the first versus third indentation (Figure 6-42).

6.3.8 Overtrawlability Assessment

DNV-RP-F111 (2014), which is the present guideline for the overtrawlability assessment of subsea pipelines, recommends two approaches to analyze the trawl impact load during the interference event with a subsea pipeline, including the analytical approach and numerical method. These methods are employed to find the range of impact loads which could impose on the pipe of the present study (Table 6-1), using the input data provided in appendix B of DNV-RP-F111 (2014) (Table 6-3). The main motivation of these analyses is to justify and validate the equivalent quasi-static loads that were employed in the physical tests and numerical studies of the present work (i.e., 225 KN in test 1&2, 150 KN in test 3, and 167 KN in test 4). The following parameters are not incorporated in the analyses, including non-structural weight, metocean forces, buoyancy force, hydrostatic pressure, internal pressure, strain rate effect, and thermal expansion force.

Table 6-3 The Input Parameters for the Pipe, Trawl Board, and Soil

Pipeline	Value	Units	Trawl board	Value	Units
Outside diameter	140.97	mm	Trawl board steel mass	4000	kg
Nominal thickness	6.15	mm	Added mass	8560	kg
Elastic Modulus	201404	MPa	Tow velocity of a trawler	2.6	m/s
Yield Strength	412.2	MPa	In-plane board stiffness	500E6	N/m
Ultimate Strength	503.6	MPa	Out-of-plane (bending) board stiffness	10E6	N/m

Reduction factor based on pipe size and soil type	0.1		Half the trawl board height	1.75	m
Material strength factor	1		Soil	Value	Units
Span height	0	m	Friction coefficient for the lateral/axial direction	0.6	
Reduction factor for impact energy associated with steel mass	0.5				
Coefficient of the effect of span height on impact velocity	0.85				

6.3.8.1 Analytical Approach

The analytical approach is employed to find the upper bound of the trawl load range, which could be experienced by the pipeline of the present study. The analytical method is conservative as the equation based on the assumption that the kinetic energy applied during the first phase of the trawl impact is locally absorbed by the bare pipe (DNV-RP-F111, 2014). In this regard, the impact load experienced by the pipe shell (F_{sh}) is derived from Equation 6-2 (DNV-RP-F111, 2014):

$$F_{sh} = m_p \cdot \alpha \cdot [(E_{loc} / m_p \cdot D) * (\beta + 1) / \alpha]^{\beta / (\beta + 1)} \quad \text{Equation 6-2}$$

$$E_{loc} = \max \left(\frac{E_s}{E_a} \right) \quad \text{Equation 6-3}$$

$$m_p = 1/4 \cdot f_y \cdot t^2 \quad \text{Equation 6-4}$$

$$\alpha = 37 \cdot [\ln(D/t) - 1/2] \quad \text{Equation 6-5}$$

$$\beta = 0.125 \cdot [\ln(D/t) + 1] \quad \text{Equation 6-6}$$

Where m_p is the plastic moment capacity for a pipe (Equation 6-4); α and β are factors calculated based on Equation 6-5 and Equation 6-6; E_{loc} is the kinetic energy; E_s and E_a are the impact energies associated with the steel mass of the trawl board and the hydrodynamic added mass, respectively.

Using the analytical approach for the pipeline with the properties presented in Table 6-3, the maximum impact force experienced by pipe shell is equal to 295.1 KN.

6.3.8.2 Numerical Approach

The finite element method is also employed to find the lower bound of the trawl impact range, which could be experienced by the present study pipeline. The numerical approach, recommended in DNV-RP-F111 (2014), is based on the beam and spring-mass (BSM) model, which is shown schematically in Figure 6-45, where pipe-soil interaction is represented via discrete springs (K_{ps}) attached to beam elements; the global stiffness of the pipe is modelled with beam elements (K_{pb}); the local shell stiffness of the pipe is modeled with a spring (K_s) with the stiffness derived from the load-displacement curve given by Equation 6-7; the in-plane stiffness (K_t) and out-of-plane stiffness (K_a) of the

trawl board are modeled with two elastic springs; and point masses are used to represent the pipe mass (M_p), the indenter mass (M_t), and the added mass (M_a).

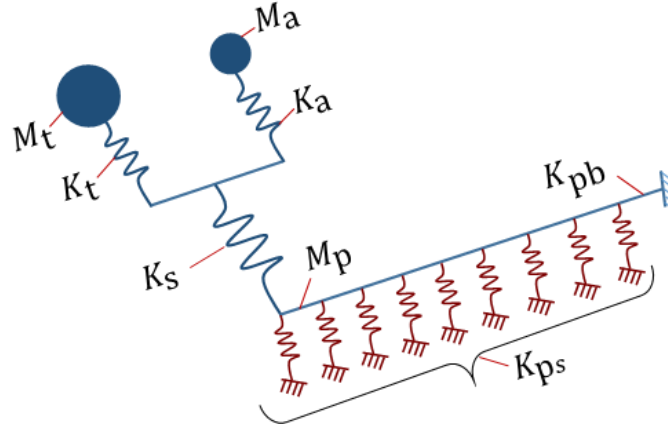


Figure 6-45 Schematic View of the BSM Model (Edited from Davaripour et al. (2020a))

$$f = m_p \cdot \alpha \cdot (H_t/D)^\beta \quad \text{Equation 6-7}$$

Where f is the impact force applied to the pipe shell; H_t is the total (permanent and elastic) dent depth; m_p is the moment capacity of the pipeline (Equation 6-4); α and β are a function of the pipeline's geometrical and mechanical properties (Equation 6-5 and Equation 6-6); t is the nominal thickness; D is the outer diameter of a pipeline; and f_y is the yield strength (DNV-RP-F111, 2014).

The load path in the BSM model involves (a) an initial velocity is applied to m_t and m_a ; (b) then, the resulting kinetic energy is transferred via K_t and K_a and absorbed by the

local deformation of the pipe (K_s), pipe's global deformation (K_{pb}), and pipe-soil interaction (K_{ps}).

In order to validate the accuracy of the BSM model, the data presented in Appendix B of DNV-RP-F111 (2014) is employed. Figure 6-46 shows an excellent agreement between the numerical result of the present study and data provided by DNV-RP-F111 (2014). Also, Figure 6-47 shows the impact load imposed on the present study pipe during a typical trawl interference event. Accordingly, the maximum trawl impact load is 47 KN, which is significantly lower than the conservative prediction obtained from the analytical approach, which is equal to 295.1 KN. Therefore, the range of the trawl load that the pipe of the present study could be experienced is in the range of 47 to 295.1 KN. Therefore, the load magnitudes applied to the specimen in the present study physical tests (i.e., 225 KN in test 1&2, 150 KN in test 3, and 167 KN in test 4) are within the reasonable range.

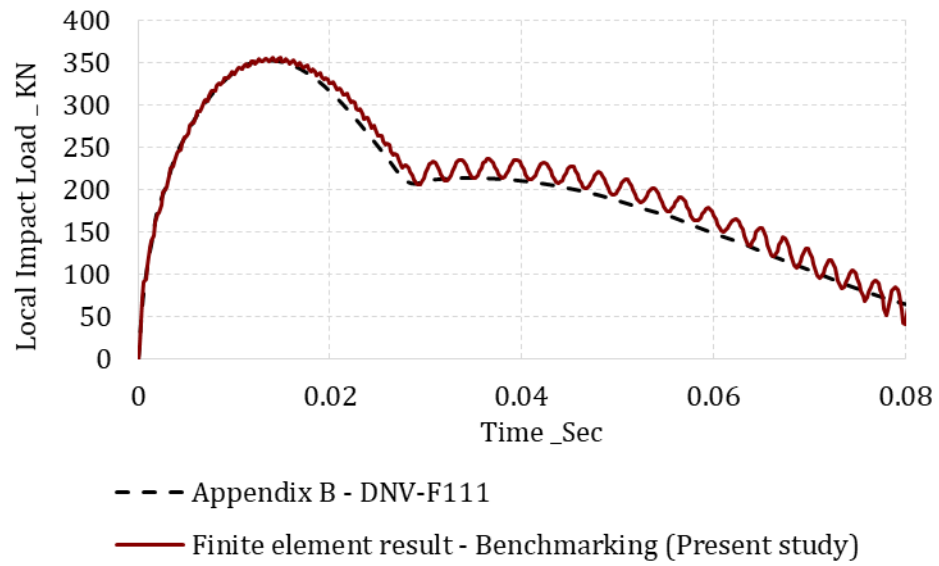


Figure 6-46 Benchmarking the BSM Model (Davaripour et al., 2020a)

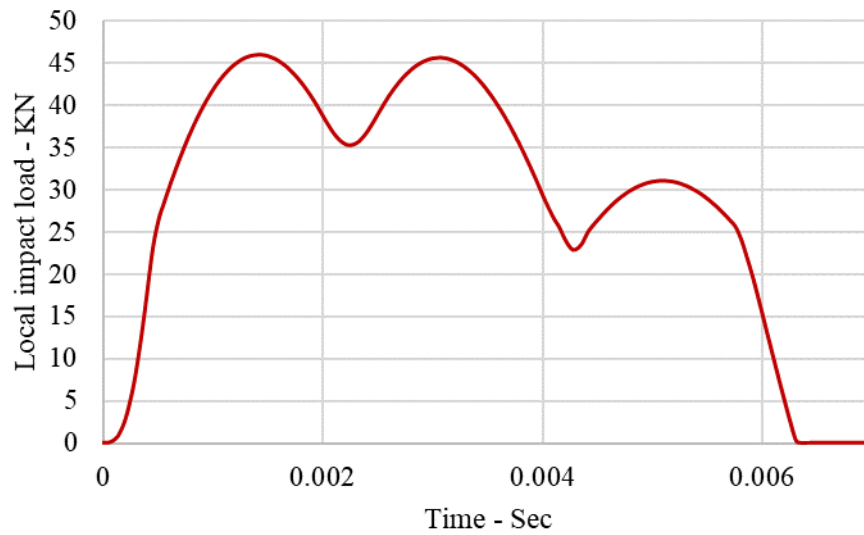


Figure 6-47 Maximum Trawl Load Imposed on the Pipeline of the Present Study – Finite Element Result using the BSM Model

6.4 Conclusions

A series of experimental investigations were performed on a 5-inch pipe (schedule 40) subject to a two-phase lateral indentation to investigate the effect of damage progression on the plastic capacity of a pipe; where during phase 1, initial plastic damage was developed perpendicularly by a cylindrical indenter, and in phase 2, the indenter induced and translated the resulting damage (developed in phase 1) along the pipe. Accordingly, four tests were performed under the quasi-static condition, and the pipe's structural response was assessed with respect to three variables, including the friction between the pipe and indenter, the boundary condition, and the loading condition. The results showed that:

- Due to the progression of plastic damage along the pipe during phase 2 of loading, the pipe's load-carrying capacity drops significantly (33.5% in Test 1). These results provide evidence regarding the damage progression effect in pipes.
- The friction between the indenter and the pipe does not change the damage progression effect; at least for the experimental conditions of the present study.
- By translating a (nearly) constant vertical load along the pipe, the resulting dent depth increases by 52%.
- The drop in the pipe's load-carrying capacity is significantly larger where the pipe response is within the pure local deformation versus the combination of local and global deformation.

Numerical simulations were performed to replicate the result of Test 3. The finite element results showed excellent agreement with the physical test result. The verified finite element model was then used to examine a pipe subject to several adjacent perpendicular indentations applied under the quasi-static condition; this scenario represents an idealization of a subsea pipeline subject to repeated trawl impacts. The results showed that by the progression of damage along the pipe, under the same imposed perpendicular loads, the size of dent depth increases by 38.2%. This result is aligned with the findings of the physical tests that the progression of damage along a pipe decreases the load-carrying capacity of the pipe. These findings also show that the effect of damage progression should be considered in controlling the denting limit state for the pipe design against accidental interference loads.

Furthermore, the von-Mises stress contour obtained from the numerical analyses was presented, which showed that the source of the damage progression effect is due to the less structural contribution of the trailing side of the pipe compared to the leading side. It was also discussed that this behaviour is associated with the post-buckling behaviour of the pipe under lateral indentation. Accordingly, the trailing side of the pipe during the subsequent indentations acts as a weak link, which causes the lesser distribution of stresses along the trailing side of the pipe compared to the leading side.

Future Work

Among other things, this paper examined a particular load path on a pipe, where the pipe is subject to repeated indentations at adjacent locations. Varied random load patterns should also be examined to provide further insight regarding the damage progression effect on a pipe under repeated indentations. In addition, the analyses were conducted under the quasi-static condition. Similar studies should also be performed for a pipe under dynamic repeated impacts at adjacent locations. Furthermore, the contribution of the internal pressure, thermal expansion, and dent spring-back on the damage progression effect in pipelines should be considered in the future sensitivity studies.

DNV-RP-F111 (2014) states that both local and global failure probabilities should be considered for assessing the overtrawlability of pipelines against the subsequent pullover loads. As such, the scope of the present study should be employed for investigating the pipe response under repeated pull over trawl loads at adjacent locations on the pipeline.

Acknowledgment

This research became possible through the funds provided by the Natural Sciences and Engineering Research Council's (NSERC) Discovery Grant program, as well as the Mitacs Accelerate Program. The authors sincerely appreciate the valuable comments provided by Richard Persaud from Genesis, and Dr. Stephen Bruneau from the Memorial

University of Newfoundland. Also, the help of Dr. Ahmed Elruby and Mr. Sthéfano Lande Andrade during the physical tests is mostly appreciated.

Reference

Abaqus Documentation, 2019. Analysis User's Manual.

Alexander, C., 2007. ASSESSING THE EFFECTS OF IMPACT FORCES ON SUBSEA FLOWLINES AND PIPELINES, in: The 26th International Conference on Offshore Mechanics and Arctic Engineering. San Diego, California USA.

ASTME8/E8M-13, 2013. Standard Test Methods for Tension Testing of Metallic Materials. <https://doi.org/10.1520/E0008>

Chater, E., Hutchinson, J.W., 1984. on the Propagation of Bulges and Buckles. Am. Soc. Mech. Eng. Press. Vessel. Pip. Div. PVP 84, 123–136.

Davaripour, F., Pike, K., Quinton, B.W.T., Persaud, R., 2020a. An Assessment on the Overtrawlability of Small Pipe Sizes Using a Hybrid Shell- Beam Model : The Initial Trawl Impact Phase (Revision Requested). Appl. Ocean Res.

Davaripour, F., Quinton, B., Pike, K., 2020b. A Numerical Investigation on a Pipe Subject to a Non- Perpendicular Trawl Impact Using a Hybrid Shell-Beam Model, in: Offshore Pipeline Conference (OPT 2020). Amsterdam, pp. 1–12.

Davaripour, F., Quinton, B., Pike, K., 2020c. An Assessment on a Subsea Pipeline Subject to a Diagonal Trawl Impact (Under Review). Appl. Ocean Res.

Davaripour, F., Quinton, B.W.T., 2018. An Investigation of the Load Carrying Capacity of Pipelines Under Accidental and Longitudinal Moving (Sliding) Loads, in: International Pipeline Conference (IPC). pp. 1–7.

- DNV-RP-F111, 2014. Det Norske Veritas - Interference Between Trawl Gear and Pipelines.
- Ellinas, C.P., Walker, A.C., 1983. Damage on offshore tubular bracing members, IABSE reports = Rapports AIPC = IVBH Berichte.
<https://doi.org/http://doi.org/10.5169/seals-32425>
- Frýba, L., 1999. Vibration of solids and structures under moving loads, Telford, London. Springer.
- Hahn, G.D., She, M., Carney, J.F., 1993. Buckle Propagation in submarine Pipelines 45, 177–215.
- Jones, N., Birch, R.S., 1996. Influence of internal pressure on the impact behavior of steel pipelines. J. Press. Vessel Technol. Trans. ASME 118, 464–471.
<https://doi.org/10.1115/1.2842215>
- Kyriakides, S., 1994. Propagating instabilities in structures. Adv. Appl. Mech. 30.
- Liang, H., Zhou, J., Lin, J., Jin, F., Xia, F., Xue, J., Xu, J., 2019. Buckle Propagation in Steel Pipes of Ultra-high Strength: Experiments, Theories and Numerical Simulations. Acta Mech. Solida Sin. 1–18.
- Ng, C.S., Shen, W.Q., 2006. Effect of lateral impact loads on failure of pressurized pipelines supported by foundation. Proc. Inst. Mech. Eng. Part E J. Process Mech. Eng. 220, 193–206. <https://doi.org/10.1243/0954408JPME97>
- Parkes, E.W., 1958. How to cross an unsafe bridge. A Divers. Dyn. Plast. Eng. 186, 606–608.

- Quinton, B., 2015. Experimental and numerical investigation of moving loads on hull structures. PhD thesis, Memorial University of Newfoundland.
- Quinton, B., 2008. Progressive damage to a Ship's structure due to ice loading. Master thesis, Memorial University of Newfoundland.
<https://doi.org/10.13140/RG.2.1.1395.6562>
- Shen, W.Q., Jones, N., 1991. A comment on the low speed impact of a clamped beam by a heavy striker. *J. Struct. Mech.* 19, 527–549.
- Soreide, T.H., Moan, T., Amdahl, J., Taby, J., 1982. Analysis of Ship/Platform Impacts. *Behav. Off-Shore Struct.* 2, 257–278.
- Symonds, P.S., Neal, B.G., 1960. Traveling loads on rigid-plastic beams. *J. Eng. Mech. Div.* 86, 79–90.
- Thomas, S.G., Reid, S.R., Johnson, W., 1976. Large deformations of thin-walled circular tubes under transverse loading—I: an experimental survey of the bending of simply supported tubes under a central load. *Int. J. Mech. Sci.* 18, 325–333.
- Toridis, T.G., Wen, R.K., 1966. Inelastic response of beams to moving loads. *J. Eng. Mech. Div.* 92, 43–62.
- Zheng, J., 2014. Overtrawlability and Mechanical Damage of Pipe-in-Pipe, PhD thesis. NATIONAL UNIVERSITY OF SINGAPORE.
- Zheng, J., Palmer, A., Lipski, W., Brunning, P., 2012. Impact Damage on Pipe-in-Pipe Systems, in: *International Offshore and Polar Engineering Conference*. Rhodes, Greece, pp. 152–157.

7 CHAPTER 7

AN ASSESSMENT ON THE PLASTIC CAPACITY OF PIPE IN PIPE SYSTEMS UNDER DAMAGE PROGRESSION EFFECT

Abstract

In recent years, pipe in pipe (PiP) systems have been employed in an increasing number of subsea projects due to the benefits associated with thermal insulation. In this regard, the propagation of local buckle along a subsea PiP system under external pressure has been studied in the past couple of decades. Accordingly, it was shown that the external pressure required to develop the initial local buckle on the PiP system is significantly higher than the pressure required to propagate the buckle along the system. In this respect, it is reasonable to investigate a novel scenario where the plastic damage progresses along the pipe under a lateral interference load (i.e., diagonal fishing gear impact). In this regard, recent studies on single-walled pipes (SWP) showed the progression of plastic damage along the pipeline under a lateral interference load could significantly lower the load-carrying capacity of the pipe. Accordingly, a novel physical test is performed in the present study to assess the structural behaviour of a PiP specimen under a two-phase loading condition, where in phase 1, the PiP solution is subject to 75 mm perpendicular indentation, and in phase 2, the resulting plastic damage on the PiP solution is translated and induced longitudinally along the pipe. Furthermore, using finite element analyses, the effect of axial load on the plastic capacity of the PiP specimen against a lateral indentation is investigated. The test results show that upon the initiation of damage

progression in phase 2, the load-carrying capacity of the PiP specimen against the lateral indentation declines by 10%. Also, the numerical results show that the plastic capacity of a PiP specimen against a lateral indentation drops significantly when the inner pipe is subject to axial compression. In conclusion, the present study shows that the load-carrying capacity of PiP systems against lateral indentation could decline significantly due to the progression of plastic damage as well as the combined loading condition.

Keywords: Subsea pipeline, Pipe in pipe, Damage progression, Trawl impact, Path-dependent behaviour, DNV-RP-F111

7.1 Introduction

In recent years, pipe in pipe (PiP) systems have been employed in an increasing number of subsea projects due to the benefits associated with thermal insulation in the PiP systems. However, the assessment of PiP solutions has traditionally been performed in the same manner as for single-walled pipes (SWP). This approach leads to conservatism as the carrier pipe is not resisting the internal pressure and not carrying the hydrocarbons. Therefore, there is less risk associated with the damage of the carrier pipe in PiP systems versus SWPs (J. Zheng et al., 2014).

The propagation of local buckle along a subsea PiP system under external pressure has been studied in the past couple of decades. Accordingly, it was shown that the external pressure required to develop the initial local buckle on the PiP system is significantly higher than the pressure required to propagate the buckle along the system. In this respect, it is reasonable to investigate a novel scenario where the plastic damage progresses along the PiP under a substantial lateral interference load (i.e., diagonal fishing gear impact). In this regard, recent studies on SWPs, i.e., (Davaripour et al., 2020d; Davaripour and Quinton, 2018), showed the progression of plastic damage along the SWPs could significantly lower the plastic capacity of the pipe; the plastic capacity of the pipe refers to the load-carrying capacity (or structural resistance mobilized) against the lateral plastic indentation in the direction normal to the undeformed shape of the pipe. However, there is no prior work on the subject of damage progression effect on PiP systems. As such, the

present study investigates the damage progression effect on a PiP product where the PiP solution is subject to a substantial lateral interference load (trawl impact load in this study). Trawl gear impact with the PiP solution is the first phase during trawl gear interference with a pipeline and lasts for a few hundredths of a second (DNV-RP-F111, 2014). The second major phase is the pull-over phase, where the pipe is pulled by the trawl gear, and the pipe's response is mainly within the global (bending) deformation (DNV-RP-F111, 2014).

7.1.1 Literature Review

The common engineering practice to assess a pipeline against an impact event is to examine a case where the pipe is subject to a knife-edge indenter, with its front radius in the range of 10 to 25 mm, which imposes a perpendicular load on the pipe (i.e., as recommended in DNV-RP-F111 (2014)). In this regard, the structural behaviour of a pipe under a perpendicular indentation by a knife-edge indenter has been the subject of several studies. Shen and Jones (1991) showed that the dynamic effect of an impact event could be replicated using quasi-static analyses if the indenter is heavy and moves at relatively slow speed. This conclusion is examined by Zheng et al. (2013) for trawl gear interference with a subsea pipeline, where the authors showed that a pipe response under impact and quasi-static analyses are within the same range.

Wierzbicki and Suh (1988) proposed an analytical model assuming the impact load is absorbed by a pure crumpling (local) behaviour of the pipe. Ellinas and Walker (1983) presented a semi-empirical model partially based on the experimental data reported in (Thomas et al., 1976). The authors assumed that the pipe structural response could be decoupled into two phases: phase-1) the local deformation; and subsequently phase-2) global deformation. However, Zheng et al. (2012) conducted experimental and numerical investigations and concluded that from the very beginning of the impact, the pipe has both local and global modes of deformation. The local deformation grows faster than the global deformation at the beginning of the impact; then, the global deformation increases as the cross-sectional deformation lowers the bending stiffness of the pipe (Zheng et al., 2012).

Thomas (1976) conducted a series of quasi-static tests on a simply supported pipe, which was transversely indented by a knife-edge indenter. Due to the very short span of the pipe, the structural response was mainly within the crumpling mode of deformation. Soreide and Amdahl (1982) did physical tests and investigated the structural response of a tube under the fully clamped boundary condition (BC). The authors did physical tests under both quasi-static and impact conditions, with the indentation rate set to 0.15 and 54 mm/sec, respectively. Alexander (2007) presented the results of an experimental and numerical investigation with an attempt to provide a general insight regarding the major defect classifications in a subsea pipeline as well as methodologies to examine these

defects. The author studied several dropped object events on a 12 inch pipe including one with the indenter mass equal to 10900 kg falling from 9.1 m height which leads to an impact velocity much greater than common trawling impact events.

On the contrary to the common industry practice where the impact load is perpendicular to the pipe, recent studies showed that the scenarios where the loading condition translates and induces the plastic damage longitudinally along the pipe could cause more damage to the pipe. In this regard, Quinton (2015, 2008) investigated the progression of damage in a ship hull structure against a moving ice load, using numerical and experimental methods. The author showed that the plastic capacity of the plate drops when imposed damage on the plate develops and translates. Davaripour and Quinton (2018) performed numerical investigations and studied a similar concept on a cylindrical structure and obtained comparable results. However, the authors did not present any application of this phenomenon in the subsea pipeline industry.

Davaripour et al. (2020b) investigated the progression of damage in a subsea pipeline against a diagonal trawl impact, using a hybrid shell-beam model, which is an improved version of the model recommended in DNV-RP-F111 (2014). The authors examined two cases of a pipe 1) under a diagonal trawl impact, and 2) under only the normal component of the diagonal trawl impact. The results showed that the first case leads to 20 percent more dent size on the pipe. This discrepancy is discussed to be due to the tangential

component of the trawling impact, which translates and induces the imposed damage on the pipe in a direction along the pipe. Davaripour et al. (2020d) conducted a series of physical tests as well as numerical investigation and examined the accumulation of local plastic damage on a pipe under subsequent trawl impacts. The authors showed that the progression of damage along the pipe under repeated trawl impacts at adjacent locations on the pipe leads to a drop in the pipe's plastic capacity. The authors concluded that the assessment of a subsea pipeline under subsequent trawl impact at the same spot, which is the case recommended by DNV-RP-F111 (2014), is not the most severe scenario, and the case of repeated impact at adjoining locations on the pipe should be assessed, where applicable.

The recent works on the damage progression effect were a part of a research project which focused on SWPs. The present paper expands previous works by investigating the damage progression effect in PiP systems. The PiP systems have been employed in an increasing number of subsea projects due to the benefits associated with thermal insulation (Zheng et al., 2013). In this regard, the assessment of PiP solutions has traditionally been performed the same as SWPs (i.e., for overtrawlability assessment of subsea pipelines as recommended in DNV-RP-F111 (2014). This leads to conservatism as the carrier pipe is not resisting the internal pressure and not containing the hydrocarbons. Hence, there is less risk associated with the damage of the carrier pipe in PiP systems versus SWPs (J. Zheng et al., 2014). In this regard, Sriskandarajah et al.

(1999) provided an overall view of the interaction between trawl gear and PiP systems. The authors stated that the higher mass of the PiP versus SWP system leads to it absorbing more kinetic energy and, consequently, more dent size during the trawl impact. However, the carrier pipe could bear more dent depth as it does not contain hydrocarbon. As such, the employment of the SWP's conventional design method for the PiP systems leads to an over-conservative solution.

Zheng et al. (2014; 2013, 2012) performed numerical investigations, as well as a series of physical tests on PiP specimens subject to quasi-static and dynamic transverse indentation to provide further insight regarding the structural resistance of the PiP systems against lateral indentations by a knife-edge indenter. The authors showed that the PiP specimen provides a significant additional plastic capacity compared to the case of an SWP pipe. Zheng et al. (2014) examined the effect of internal and external pressure on the denting process in a pipeline and concluded that buckle propagation occurs more likely in SWPs versus PiPs. Wang et al. (2014) investigated the response of a PiP system subject to a dropped object impact, where the space between the inner pipe and the carrier pipe was filled with ultralight cement composite. The authors concluded that the presence of the composite enhances the PiP resistance against the development of the local damage. Additionally, the inner pipe contributes to the confinement of the composite material and improves the PiP response.

In the present study, a novel test apparatus is employed to investigate the load-carrying capacity of a PiP specimen under two-phase loading: phase-1) the pipe is subject to a perpendicular indentation, and phase 2) the resulting indentation in phase 1 is held constant and the indenter translates and induces the resulting plastic damage longitudinally along the pipe. Also, numerical studies are conducted that reproduce the physical test and provide further understanding regarding the PiP behaviour under the combined loading.

7.1.2 Notes on the Research Scope

The present work aims to provide evidence regarding the effect of damage progression on the plastic capacity of a PiP system, where the PiP solution is subject to a substantial lateral interference load. Furthermore, to highlight the applicability of the damage progression effect in the pipeline industry, the present study test setup is partly designed according to the recommendations presented by DNV-RP-F111 (2014). However, the present study physical test and numerical simulation do not fully represent a trawl gear interference event. Nevertheless, the following points could validate and justify the methodologies employed in the present work:

- The physical test and numerical study in the present work are conducted under the quasi-static condition. In this respect, Shen and Jones (1991) showed that using the quasi-static condition could reproduce the dynamic effects in a pipeline during an impact event, provided that the indenter is heavy and moves at relatively slow

speed. Also, Zheng et al. (2013) conducted physical tests under quasi-static and dropped object conditions and showed that for the assessment of subsea pipelines subject to trawl impact, the pipe's response under both loading conditions is in the same range. As such, the dynamic effect of the trawl impact on the pipe's response is insignificant.

- The physical test and numerical study of the present work do not incorporate the pipe-soil interaction in the test setup. In this respect, the trawl impact occurs in some hundredths of a second where the pipe's response is mainly local (DNV-RP-F111, 2014). Additionally, the direction of the trawl impact is parallel to the seabed. As such, for a scenario of a pipe laid on the seabed, the pipe-soil interaction during the impact is negligible.

Furthermore, the loading condition employed in the physical test involves two phases, including phase 1, where the pipe is subject to a perpendicular indentation and phase 2, where the resulting plastic damage in phase 1 translates and induces along the pipe in the displacement-controlled condition. In this regard, while the first phase could represent an event of a fishing gear interference with a subsea pipeline (with respect to the above-mentioned points), the second phase is employed to investigate the effect of damage progression on the load-carrying capacity of the pipe. Therefore, the second phase may not represent the trawl impact event.

7.2 Physical Test

As there is no prior work on the subject of damage progression effect on a PiP system when the PiP solution is subject to a substantial lateral load, the present study employs a novel test setup and conducts a lab-scale physical test to investigate this effect on the plastic capacity of a PiP specimen.

7.2.1 Methodology

7.2.1.1 Test Apparatus

The test apparatus (Figure 7-1) was firstly devised by Quinton (2015) to investigate the damage progression effect in plates under sliding loads. For the present study, the test apparatus was modified to perform physical tests on cylindrical specimens.



Figure 7-1 An Overall View of the Test Apparatus

Figure 7-2 shows the components of the test apparatus, which provide two separate loading mechanisms: 1) the vertical load path along the Y-axis, where the MTS hydraulic ram pushes the indenter against the specimen, and 2) the horizontal load path along the X-axis, where the horizontal hydraulic ram, which is connected to the base plate at one end and to the carriage at another end, translates the carriage along the rail. The lateral motion of the carriage translates and induces the plastic damage imposed on the specimen

by the MTS hydraulic ram, along the X-axis. The horizontal force is then transmitted via the swing-arm to the horizontal load cell.

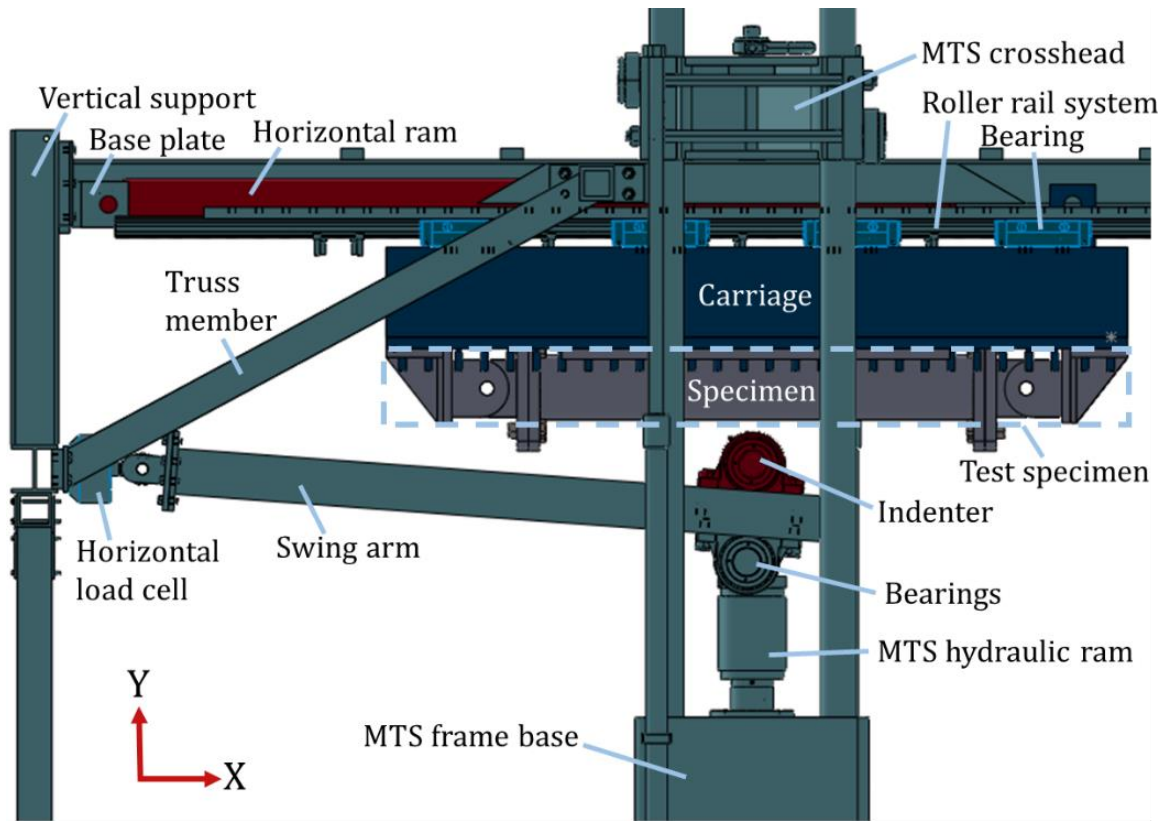


Figure 7-2 Components of the Test Apparatus (Partly Edited from Davaripour et al. (2020c))

7.2.1.2 Test Setup

Figure 7-3 shows an overall view of the test setup bolted to the carriage, including isotropic view (a), YZ-view (b), and XZ-view (c). The test setup comprises the PiP specimen and the mounts.

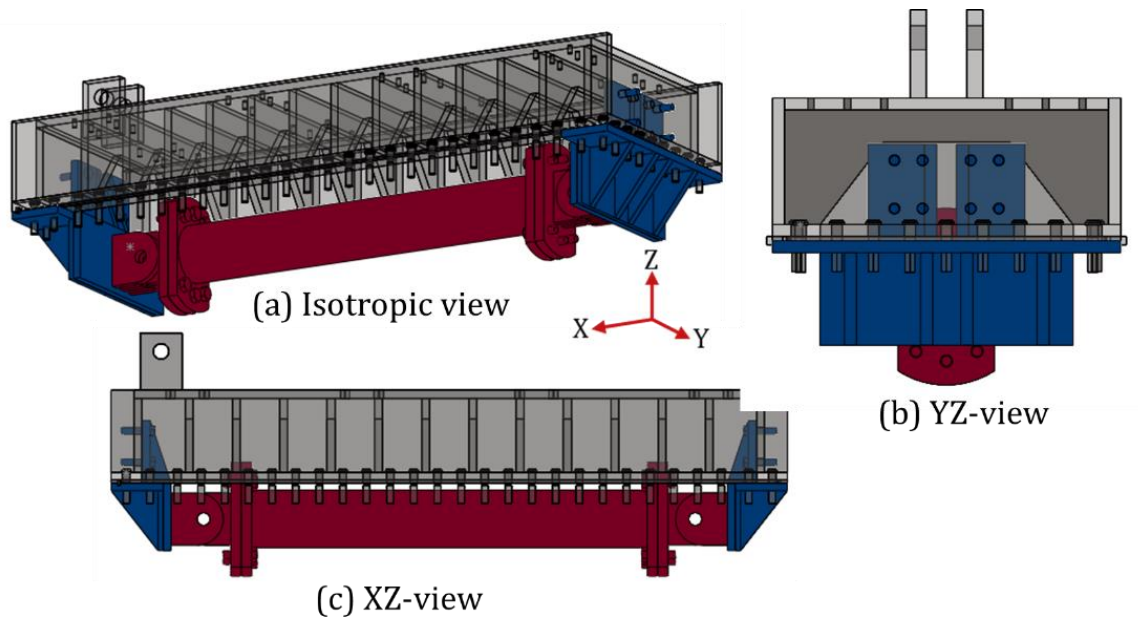


Figure 7-3 An Overall View of the Test Setup Bolted to the Carriage: Isotropic View (a), YZ-View (b), and XZ-View (c) (Partly Edited from Davaripour et al. (2020c))

7.2.1.2.1 PiP Specimen

For the PiP specimen, the carrier pipe has a diameter of 5 inches (schedule 40). Its mechanical properties were obtained from standard tensile tests. Figure 7-4 shows the engineering stress-strain curve averaged from the coupon tests, as well as the true stress-strain curve. Table 7-1 summarizes the physical and mechanical properties of the carrier pipe. The inner pipe has the outer diameter equal to 3 inches (schedule 40) with the mechanical properties obtained from the mill test certificate and presented in Table 7-1.

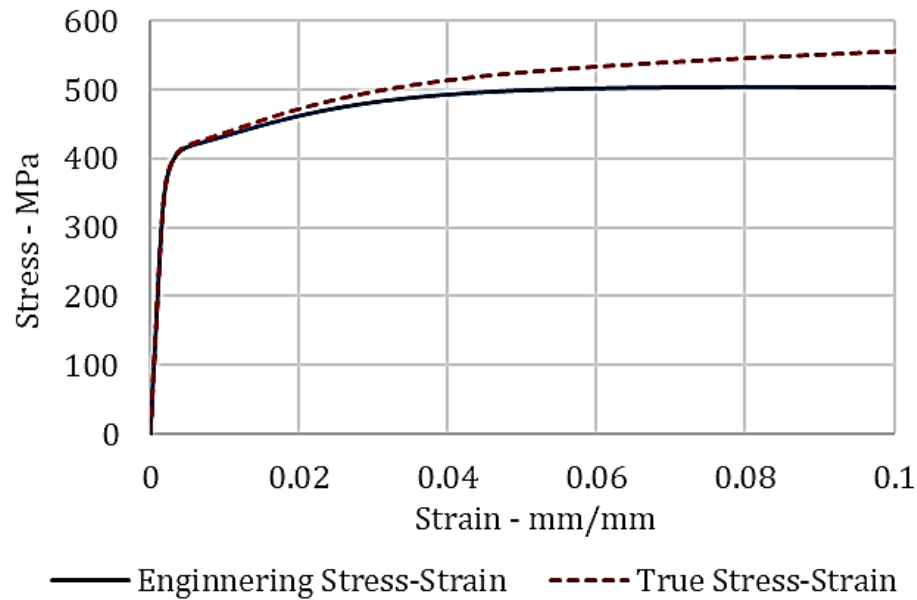


Figure 7-4 Engineering and True Stress-Strain Curves for the Carrier Pipe (Partly Edited from Davaripour et al. (2020c))

Table 7-1 Physical and Mechanical Properties of The Cylindrical Specimen

Carrier pipe			Inner pipe		
Physical properties			Physical properties		
D (mm)	t (mm)	L (mm)	D (mm)	t (mm)	L (mm)
140.97	6.1468	1200	88.9	5.49	927.1
Mechanical properties			Mechanical properties		
E (MPa)	f_y (MPa)	f_u (MPa)	f_y (MPa)	f_u (MPa)	
201404	412.26	503.56	330.91	454.9	

The PiP specimen is shown in Figure 7-5, with a total length of 1200 mm between the pins. It involves a 5-inch diameter carrier pipe, flange connections, sets of pin hinges, a 3-inch diameter inner pipe, bell-shaped end connections (also referred as end connection), and ball supports. Also, Figure 7-6 shows the assembly of the inner pipe mounted by the ball supports.

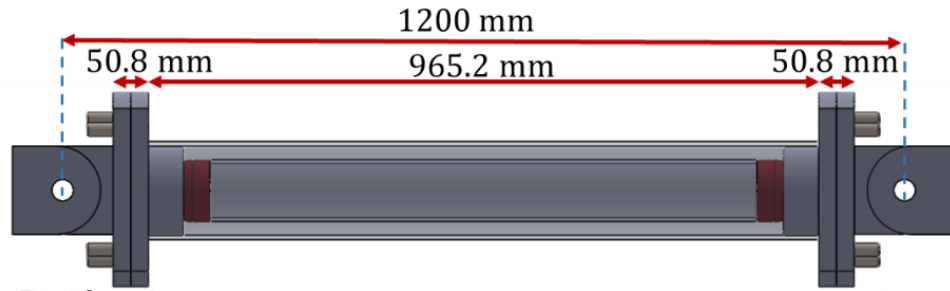


Figure 7-5 A Schematic View of the PiP Specimen Components

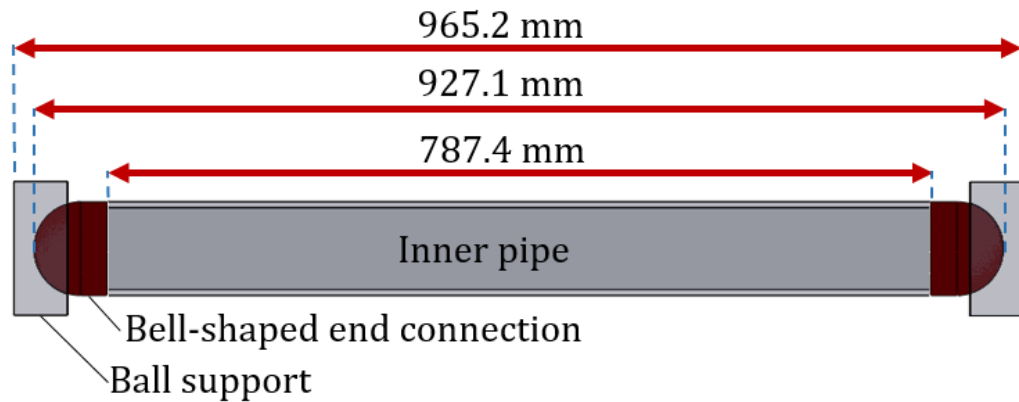


Figure 7-6 A Schematic View of the Inner Pipe Assembly Including the Inner Pipe and Bell-Shaped End Connections Which is Mounted by the Ball Supports

Figure 7-7 presents the end connections as well as the ball supports, which are employed to centralize the inner pipe inside the carrier pipe. The ball support is made of a 2-inch plate that is machined in the center and provides the end BC for the inner pipe. Also, the bell-shaped end connections are solid shafts that are machined at one end. Using these two components, the inner pipe could rotate freely at both ends in three dimensions, and

the rigid body motion of the inner pipe with respect to the carrier pipe is restricted. Figure 7-8 presents the detailed dimensions of the end connections as well as the ball supports.



Figure 7-7 Bell-Shaped End Connections and Ball Supports Used to Centralize the Inner Pipe Inside the Carrier Pipe

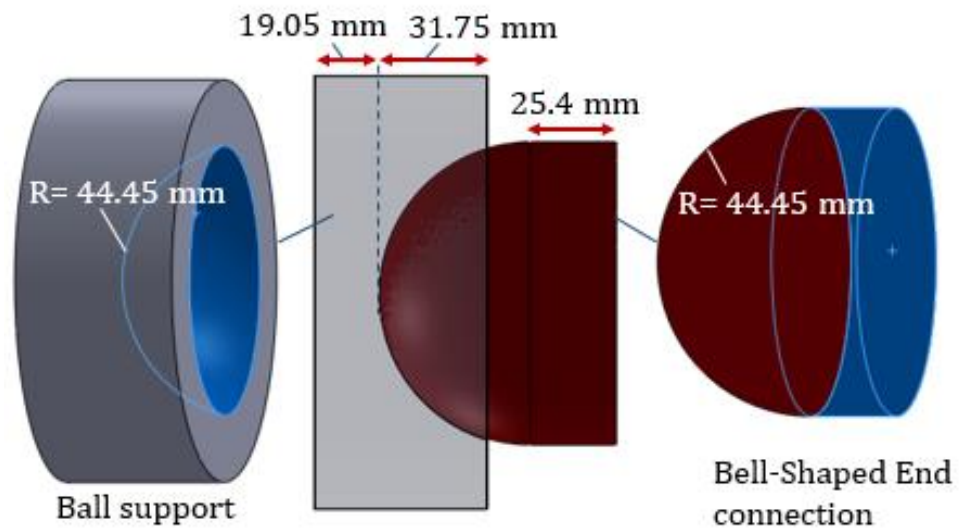


Figure 7-8 Ball Support (Left), Assembly (Middle), and Bell-Shaped End Connection (Right)

The assembly procedure for the PiP specimen is 1) the ball supports are welded to the flange connections, 2) the carrier pipe is welded to a flange connection from one end, 3) the assembly of the inner pipe and two bell-shaped end connections are passed through the carrier pipe, 4) the other end of the carrier pipe is welded to another flange connection.

7.2.1.2.2 Mounts

The PiP specimen is supported at both ends via the mounts. The load transmission from the specimen to the carriage is conducted via the mounts, using the key stock and the bolts (Figure 7-9). The mounts are made of high strength steel (ASTM 514) with the yield strength of 779 MPa and the ultimate strength of 827 MPa, as reported in the mill certificate.

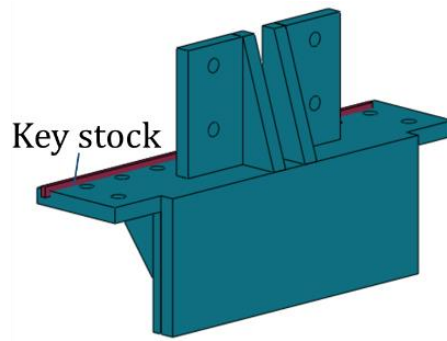


Figure 7-9 A Schematic View of the Mount (Partly Edited from Davaripour et al. (2020c))

7.2.1.3 Indenter

The indenter is a solid cylinder with a diameter of 50 mm, which is made of medium tensile strength steel (C1035) and mounted by the pillow block bearings (Figure 7-10); the indenter could represent the edge of the trawl door or clump weight according to DNV-RP-F111 (2014). The length of the indenter between the bearings is 187 mm, which is lubricated with heavy grease. This lubrication and spinning freedom of the indenter are employed to nearly eliminate the sliding friction at the region of contact between the specimen and the indenter.

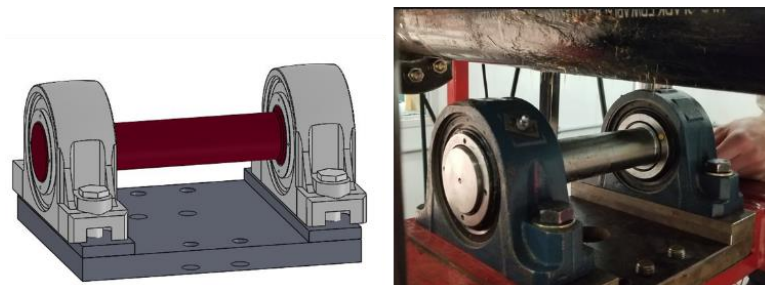


Figure 7-10 The Solid Cylindrical Indenter (Davaripour et al., 2020c)

7.2.1.4 Boundary Condition (BC)

The BC, which is used for the PiP specimen, is schematically shown in Figure 7-11. Using this BC, both global and local stiffnesses of the PiP specimen are incorporated in the overall PiP system's resistance to indentation. The carrier pipe is restrained in all degrees of freedom at both ends, excepting rotation around the Y-axis. Also, the BC, which is employed for the inner pipe is simply supported BC except that the deformation of the inner pipe against axial expansion is restrained. This BC for the inner pipe prevents the rigid body motion of the inner pipe inside the carrier pipe during phase 2 of loading, where the indenter translates and induces the plastic damage longitudinally along the PiP specimen.



Figure 7-11 Boundary Conditions Employed for Carrier and Inner Pipes

7.2.1.5 Instrumentation

By the employment of visual data, load cells, and sensors, the following variables were recorded: the vertical load applied to the specimen (Table 7-2-a), the horizontal load imposed to the specimen (Table 7-2-b), the vertical displacement of the indenter (Table

7-2-c) and horizontal displacement of the carriage (Table 7-2-d), the vertical displacement of the top of the carrier pipe (Table 7-2-e), side view of the specimen (Table 7-2-f), and spatial points of the deformed specimen (Table 7-2-g).

Table 7-2 Test Variables and Corresponding Instruments

Variable	Instrument	Description
a	MTS load cell- Model: 661.21E-01	MTS internal data acquisition system
b	Tovey load cell 1 and 2 – Model: SW20-50K	Donut load cells connected to the swing-arm (Figure 7-2)
c	MTS linear variable differential transducer (LVDT)	MTS internal data acquisition system
d	Horizontal Linear Position Transducer (yo-yo pot)	Records the relative displacement between the test frame and the carriage
e	Laser	Placed inside the carriage and pointed to the top of the specimen
f	GoPro Hero-07 camera	Placed outside the carriage
g	Laser scanning technologies (Faro Platinum Arm with the Faro Laser Line Probe 3 (LLP3) attachment)	Records the permanent deformation in the specimen after the test

7.2.1.6 Load Condition

The physical test was conducted in two phases and under quasi-static and displacement-controlled conditions. In phase 1, the vertical hydraulic ram pushes the indenter against the PiP specimen until an indentation of 75 mm is achieved (Figure 7-12-a). This phase is followed by phase 2, where the horizontal hydraulic ram pushes the carriage for 300 mm along the rail, while the vertical position of the indenter is maintained. In other words,

the indenter induces the plastic damage imposed during phase 1, longitudinally along the PiP specimen (Figure 7-12-b). Figure 7-13 shows the deformed carrier pipe prior to the test (a), at the end of phase 1 (b), and at the end of phase 2 (c).

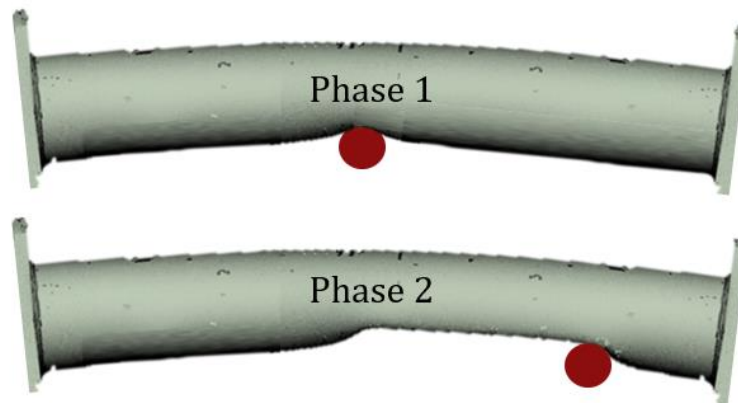


Figure 7-12 Loading Condition Including Phase 1 and 2

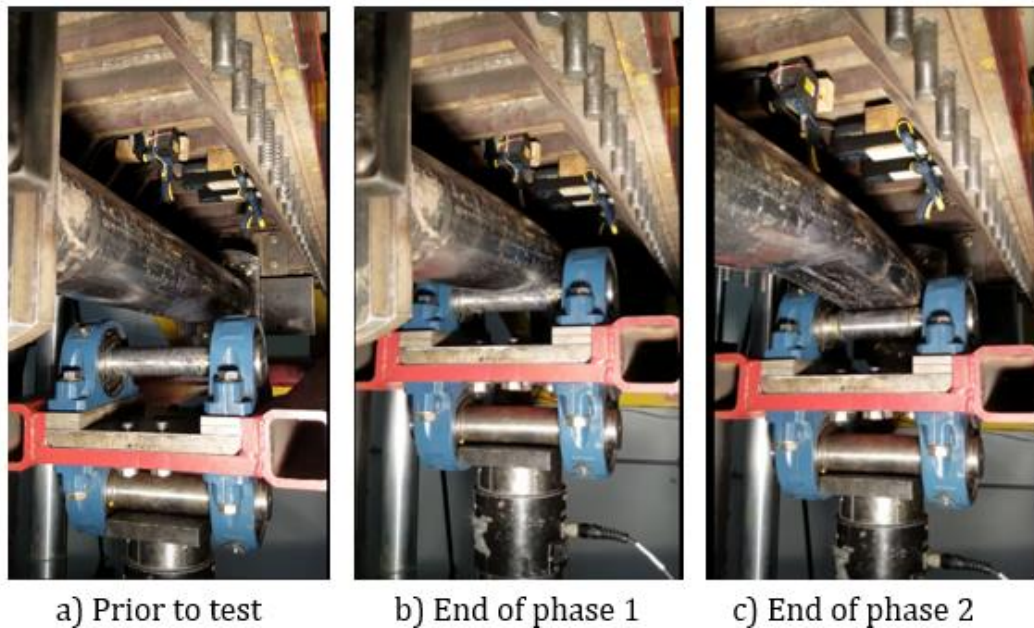


Figure 7-13 Test Procedure: 1) Before the Indentation, b) End of Phase 1, c) End of Phase 2

7.2.2 Results

This section presents the data that was recorded during the physical test on the PiP specimen. Additionally, the results of another test (originally reported in (Davaripour et al., 2020d)) with the same specifications but on only a single-walled carrier pipe specimen are also presented for comparison and understanding regarding the contribution of the inner pipe to the overall PiP system's load-carrying capacity. Furthermore, Zheng et al. (2013) performed physical tests on SWP and PiP specimens under perpendicular 100 mm indentation. The physical and mechanical properties of the test specimen in (Zheng et al., 2013) are similar to those employed in the present study. However, Zheng et al. (2013) used a simply supported BC with 1.5 m pipe length, and the present work employed 1.2 m specimen using the BC shown in Figure 7-11. The results of the present paper are compared against the findings of Zheng et al. (2013) to provide a further understanding of the mechanical behaviour of PiP systems.

7.2.2.1 Pipe in Pipe (PiP) Physical Test

Figure 7-14 shows the deformed view of the PiP specimen, after the physical test was conducted. Furthermore, Figure 7-15 and Figure 7-16 show the scanned views of the deformed carrier pipe and the inner pipe. These figures show full incorporation of the inner pipe during the response to indentation and provide valuable data used to validate numerical studies of the PiP specimen. The short bar that connects the inner pipe to the

carrier pipe in Figure 7-15-b is welded after the test only for the purpose of maintaining the position of the inner pipe inside the carrier pipe during the laser scanning.



Figure 7-14 A View of the Deformed Shape of the PiP Specimen After the Test

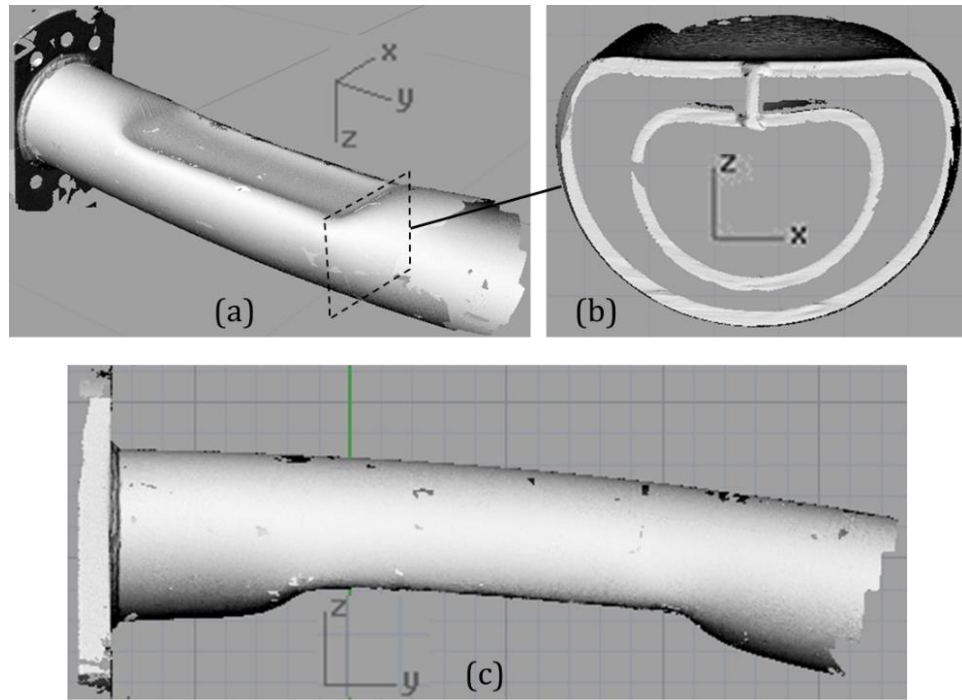


Figure 7-15 Scanned Views of the Deformed PiP Specimen Including the Isotropic View (a), View of the Cross-Section Where Phase 1 ends (b), and Elevation View (c)

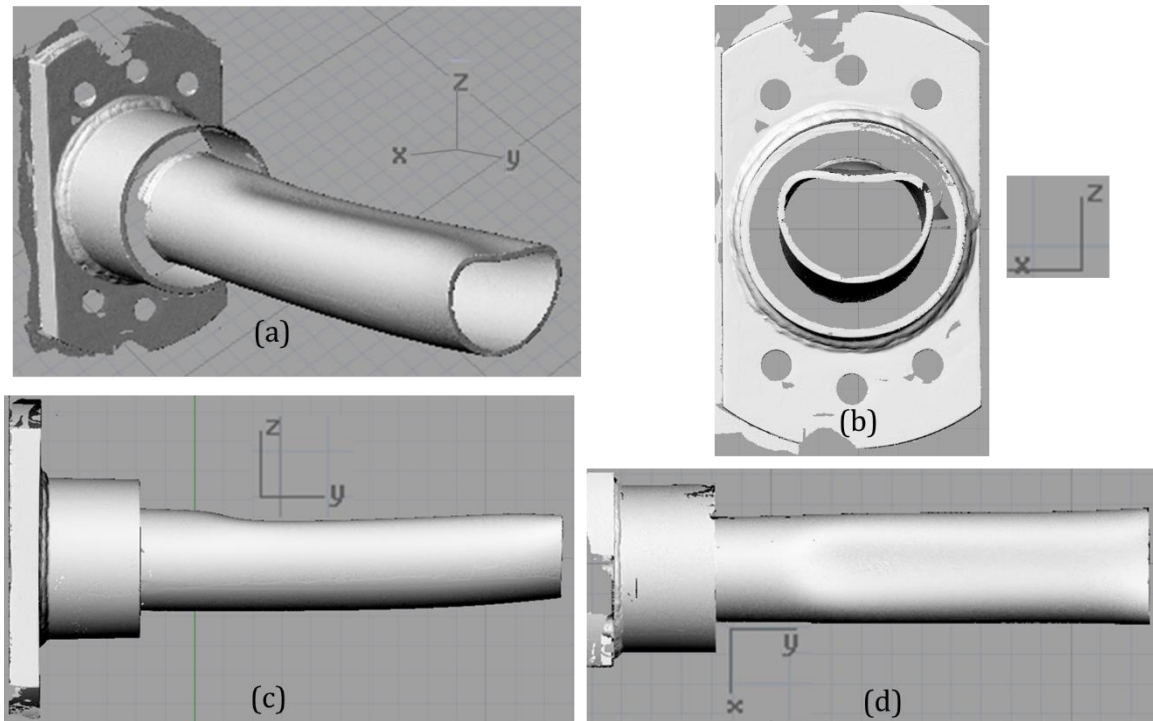


Figure 7-16 Scanned Views of the Deformed Inner Pipe Including Isotropic View (a), a View of the Cross-Section (b), Elevation View (c), View from the Top (d)

Figure 7-17 shows the vertical load resisted by the PiP specimen versus vertical displacement of the indenter during phase 1 of loading, where 75 mm perpendicular indentation was imposed on the specimen. In this regard, in the first portion of the curve (part-a), the vertical load increases to 120 KN with a gradual decreasing slope. Then, at the beginning of part-b, there is a jump in the response of the PiP specimen. This sudden jump in the vertical load shows that by the initiation of the second portion of the curve (part-b), the inner pipe comes into contact with the carrier pipe. Along part-b of the load-displacement curve, the slope of the curve involves three phases, including 1) relatively constant slope, 2) declining slope with a sharp rate, and 3) increasing slope. In this regard,

the sudden decline of curve stiffness shortly after the start of part-b suggests that the inner pipe was subject to a combined load (i.e., axial compression combined with lateral indentation), which affected its structural capacity; the axial compression could considerably decrease the resistance of a pipe against a lateral indentation, as reported in (SUH, 1987). This is further corroborated in the numerical model presented in Section 7.3.

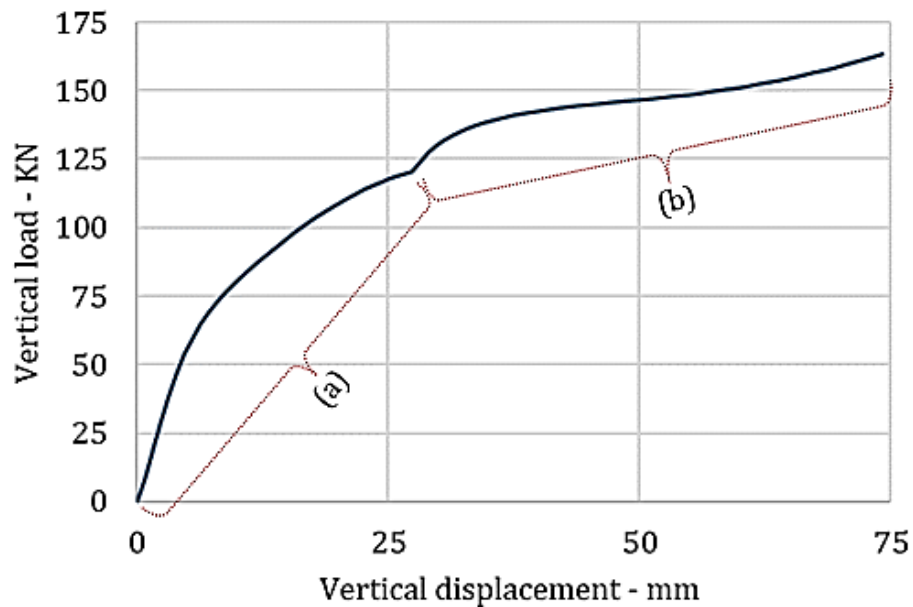


Figure 7-17 Load Displacement Curve During the First Phase of Physical Test on the PiP Specimen

Figure 7-18 shows 1) the vertical displacement of the indenter versus time, and 2) the vertical load resisted by the specimen against the imposed indentation versus time. As shown in the figure, during phase 1, the vertical indentation increases and reaches 75 mm. Consequently, the vertical load resisted by the specimen increases and reaches 160 KN.

During phase 2, while the vertical position of the indenter remains constant, the vertical resistance in the PiP specimen decreases up to 10%; this significant drop occurs upon the initiation of phase 2 and promptly reaches 148 KN; then the vertical resistance of the specimen increases in the proximity of the end BC. Also, Figure 7-19 shows the horizontal load as well as the resultant load resisted by the specimen during the test. Furthermore, Figure 7-20 shows the vertical displacement of the middle section of the PiP specimen at the top and bottom points during phase 1. The dent depth on the PiP specimen, induced during phase 1, is derived by subtracting the displacement of the indenter from the displacement of the top middle section of the specimen. The displacement of the top point of the carrier pipe in the middle is recorded using a laser displacement sensor, which was installed inside the carriage.

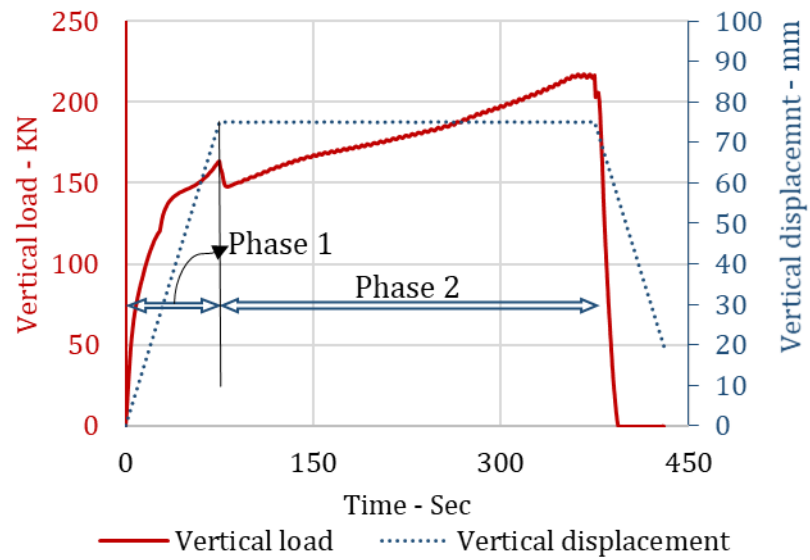


Figure 7-18 Vertical Load Resisted by PiP Specimen Versus Time (Left); Vertical Displacement of the Indenter Versus Time (Right)

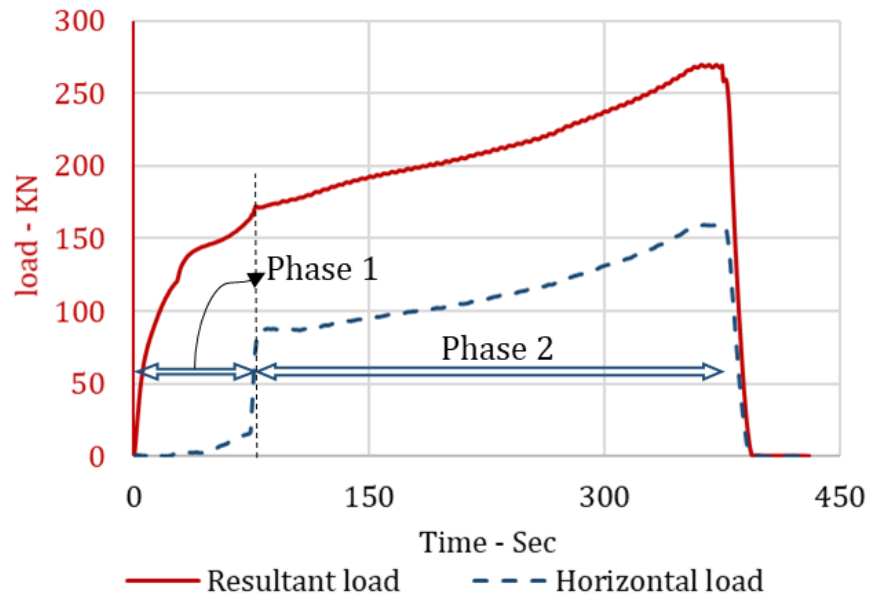


Figure 7-19 Resultant Load as well as Horizontal Load Imposed to the PiP Specimen

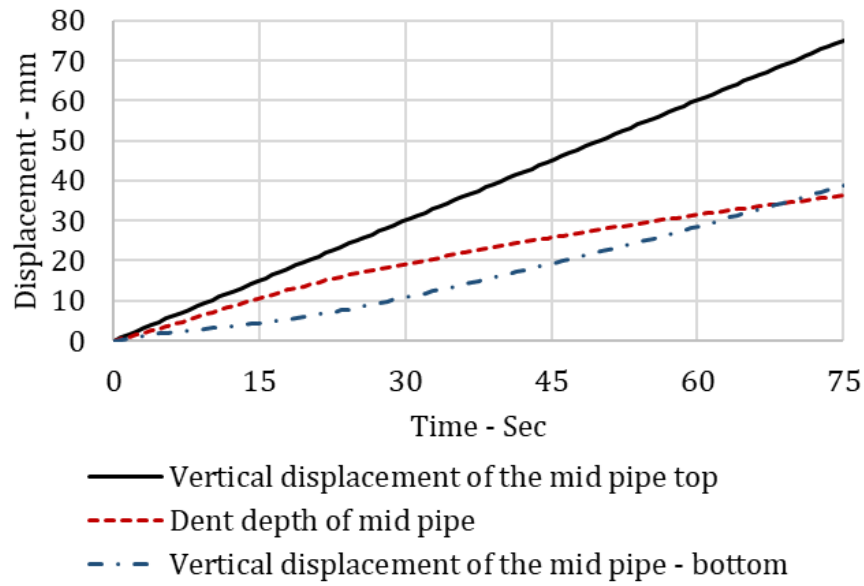


Figure 7-20 Vertical Displacement of the PiP Specimen in the Middle at the Top and Bottom Points as Well as the Induced Dent Depth on the Specimen

7.2.2.2 Discussion

Zheng et al. (2013) conducted physical tests on SWP and PiP specimens under 100 mm perpendicular indentation. The specimens employed in Zheng et al. (2013) have similar mechanical and physical properties with those used in the present study. However, Zheng et al. (2013) employed a simply supported BC for the specimens, whereas the present study used the BC presented in Section 7.2.1.4. In addition, the length of the specimen in Zheng et al. (2013) is 1.5 m, while in the present work, the length of the specimen is 1.2 m. Figure 7-21 shows that the load-displacement curves reported in Zheng et al. (2013) for both SWP and PiP specimens are in a great agreement up to point-a. Then, there is a

jump in the structural response of the PiP specimen, and the resulting additional vertical load compared to the SWP specimen remains almost constant up to the end of the test.

Furthermore, a physical test on an SWP pipe was conducted by Davaripour et al. (2020d). The experiment was performed by employing the same test apparatus used in the present work. Also, the cylindrical specimen in Davaripour et al. (2020d) had the exact same properties as of the carrier pipe in the present study. Figure 7-21 shows the load-displacement curve for the PiP specimen of the present study, as well as the SWP specimen reported in Davaripour et al. (2020d), during phase 1 of loading. Considering that the jump in PiP response at point-b is where the inner pipe comes into contact with the carrier pipe, the discrepancy between the two curves before point-b shows that the carrier pipe in the PiP specimen has higher structural capacity compared to the SWP specimen. This additional capacity could be due to the residual (tensile) stress imposed at two ends of the carrier pipe during the assembly procedure, as presented in Section 7.2.1.2.1. Then at point-c, the contribution of the inner pipe declines significantly, which could be due to the compressive force at both ends of the inner pipe, which was induced during the assembly procedure.

With respect to the test results reported in Zheng et al. (2013), the response of the SWP and PiP specimens are alike before point a. Also, the additional strength in PiP versus SWP specimen is nearly consistent after point a until the end of the test. However, the

comparison between the response of the PiP specimen in the present work with the SWP specimen reported in Davaripour et al. (2020d) shows that before point b, the vertical load resisted by the PiP specimen is higher than the one resisted by the SWP specimen. Moreover, the additional strength provided by the incorporation of the inner pipe declines promptly after point c. This different behaviour of the PiP specimen in the present study suggests that both carrier and inner pipes were under residual stress, which was induced during the assembly time. This suspicion is investigated using finite element analyses in Section 7.3.

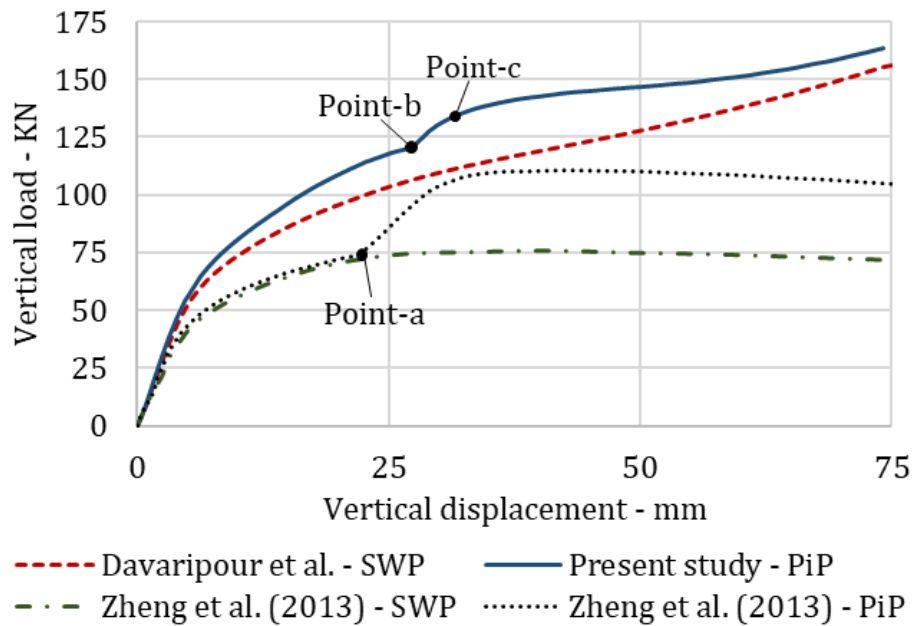


Figure 7-21 Vertical Load Versus Vertical Displacement of the SWP and PiP Specimens in the Present Study, and Previous Works by Davaripour et al. (2020d) and Zheng et al. (2013)

Figure 7-22 shows the vertical load versus resultant displacement curves obtained from the PiP specimen in the present study as well as the SWP specimen reported in Davaripour et al. (2020d). During phase 2, the vertical load resisted by the PiP specimen provides a relatively consistent additional structural strength, compared to the SWP curve, which is due to the incorporation of the inner pipe in the structural response of the PiP specimen.

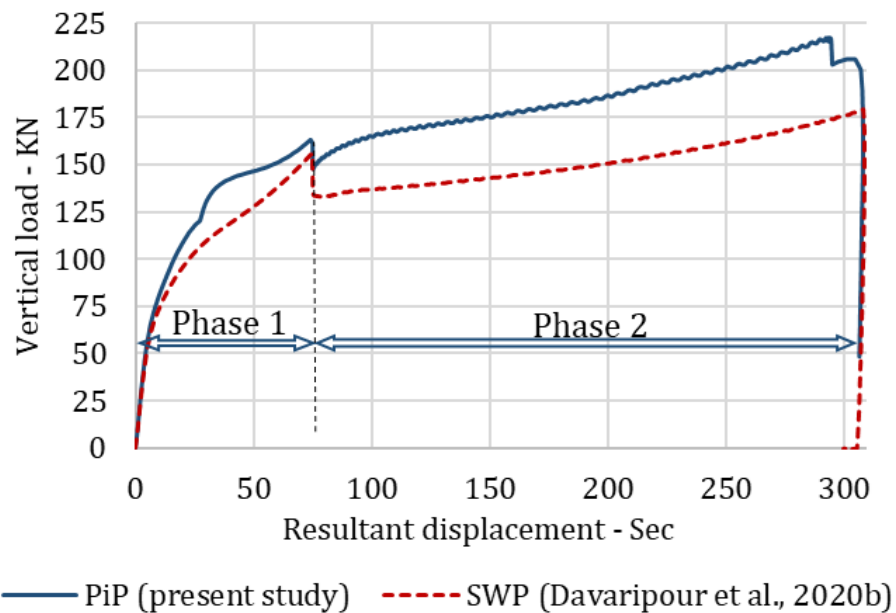


Figure 7-22 Vertical Load Imposed to the PiP (Present Study) and SWP (Davaripour et al., 2020d) specimens Versus the Resultant Displacement of the Indenter

7.2.3 Summary

A novel physical test was conducted on a PiP specimen subject to an interference load applied by a cylindrical indenter. The load path during the test includes a) phase 1, where

the specimen is subject to a 75 mm imposed perpendicular indentation, b) phase-2, where the indenter induces the imposed plastic damage along the pipe for 300 mm, while the vertical position of the indenter is maintained.

The load-displacement curve resulting from the physical test showed that by the initiation of phase 2, due to the progression of the plastic damage along the pipe, the structural resistance of the PiP system drops by 10%, which provides evidence of the damage progression effect in PiP solutions. Also, comparing the load-displacement curves obtained in the present study with those from the previous physical works suggest that there was residual stress in the carrier and inner pipes, which was induced during the assembly procedure. The presence of the residual stress affected the load-carrying capacity of the PiP specimen in the first phase of loading.

7.3 Finite Element Analysis

A numerical investigation is conducted to enhance the understanding of the mechanical behaviour of the PiP specimen in the present study. The finite element model is developed and validated against the test data using commercially available software LS-Dyna. The quasi-static analyses are conducted using an explicit time integration method. In order to maintain the quasi-static condition, the ratio of kinetic energy to internal energy is controlled to remain under 5%. Also, to lower the computational cost for the analyses, using the time-step card in LS-Dyna, mass scaling is implemented in the numerical model. Accordingly, the time step size for mass scaled solutions was increased to $1\text{e-}6$ sec. Without mass scaling, the maximum stable time step for these simulations would be $6\text{e-}7$ sec. The elastoplastic material model is employed for carrier and inner pipes using the inputs in Table 7-1. For the carrier pipe, the true stress-strain curve presented in Figure 7-4 is implemented in the numerical model. Also, for the inner pipe, the stress-strain curve was developed using the Ramberg-Osgood equation and the mechanical properties presented in Table 7-1.

7.3.1 Element Type

Figure 7-23 shows the isotropic view of the numerical model (Figure 7-23-a), longitudinal cutaway section of the numerical model (Figure 7-23-b), and the BC of the inner pipe including the end connection and the ball support (Figure 7-23-c). Both carrier and inner

pipes in the PiP specimen are modelled with the Belytschko-Tsay reduced integration shell elements with aspect ratio equal to 1, and edge length equal to 3 mm. The indenter is modelled with a tube-shaped object with rigid material properties and solid elements. The end connection is modelled with a hollow sphere with shell elements (Figure 7.23), which is rigidly constrained to the end edge of the inner pipe. The ball support is modelled with the solid elements, and is rigidly constrained to the end edge of the carrier pipe.

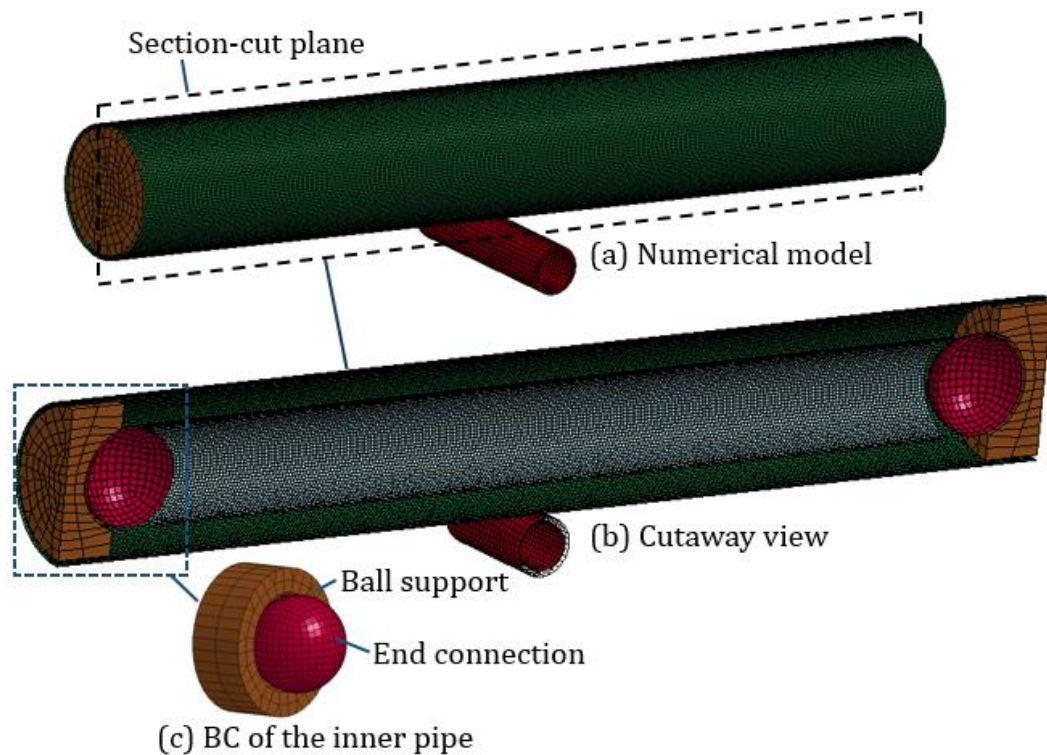


Figure 7-23 An Isotropic View of the Numerical Model (a), Cut-away View of The Model (b), and a View of the End Connection and Ball Support (c)

7.3.2 Boundary Condition (BC)

The BCs employed during the test are schematically shown in Figure 7-24. The two ends of the PiP specimen are restrained in all degrees of freedom except rotation around the y-axis. As shown in Figure 7-24, the end restraints are provided using mounts that connect the PiP specimen to the carriage.



Figure 7-24 Boundary Conditions Employed for the PiP Specimen

In order to simplify the numerical model, only the PiP specimen and the indenter are modelled. The end BCs are simplified with two springs representing vertical and axial stiffness provided by the end mounts. Also, the flange connections and pins which link the PiP specimen to the mounts, as shown in Figure 7-25, are not modelled. The end edges of the carrier pipe and the end surface of the ball support are constrained, in all degrees of freedom, to point-a (Figure 7-25), using nodal rigid body constraint in LS-Dyna (LS-Dyna Documentation, 2018).

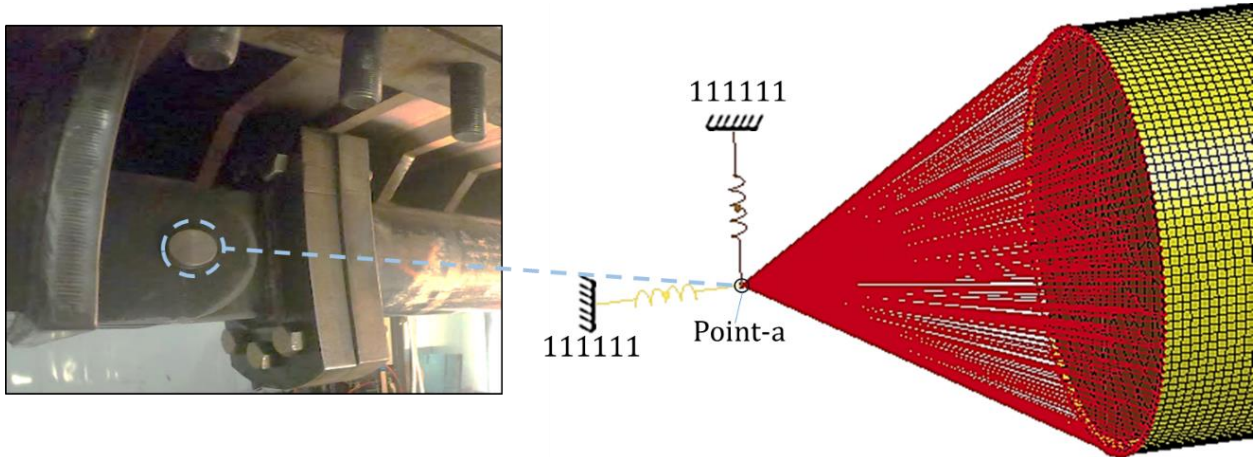


Figure 7-25 Simplified Representation of End Mounts in the Finite Element Model

Regarding the stiffness of the springs shown in Figure 7-25, Quinton (2015) used the same test apparatus employed in the present study and reported a vertical elastic deformation in the apparatus during the applied indentation. In this regard, the present work conducted sensitivity studies and concluded that the axial and vertical stiffness of the springs are $0.5e7$ and $0.14e7$ N/mm, respectively. Furthermore, as an additional consideration in the numerical model, the carrier pipe at two ends along the width of the ball supports are rigidly constrained due to the minimal distance between the carrier pipe and the ball supports.

7.3.3 Load Path

As presented in Section 7.2.1.6, the loading condition included a) phase 1, where the solid indenter moves vertically (perpendicular to the PiP specimen) for 75 mm, and b) phase

2, where the vertical position of the indenter remains constant, but the indenter translates longitudinally for 300 mm and induces the plastic damage along the specimen.

7.3.4 Interaction Properties

The interactions in the numerical model comprise contact between a) the indenter and the carrier pipe; b) the carrier pipe and the inner pipe; c) end connections and the ball supports. Automatic surface to surface type contact is employed for all the interactions with the friction coefficient equal to 0. Interaction type-a involves insignificant friction due to using rolling indenter as well as lubrication at the region of contact. Also, the sensitivity studies presented in Section 7.3.6 show the effect of friction coefficient on interaction type-b and c is negligible.

7.3.5 Mesh Convergence Analysis

Mesh convergence analyses are conducted for both carrier and inner pipes to determine the shell element size in the specimen. Figure 7-26 shows the result of the analyses performed for two mesh sizes with an aspect ratio equal to 1, including 3 and 5 mm. As shown in the figure, the results of both cases are very similar. As such, the mesh size equal to 3 mm is used for the analyses.

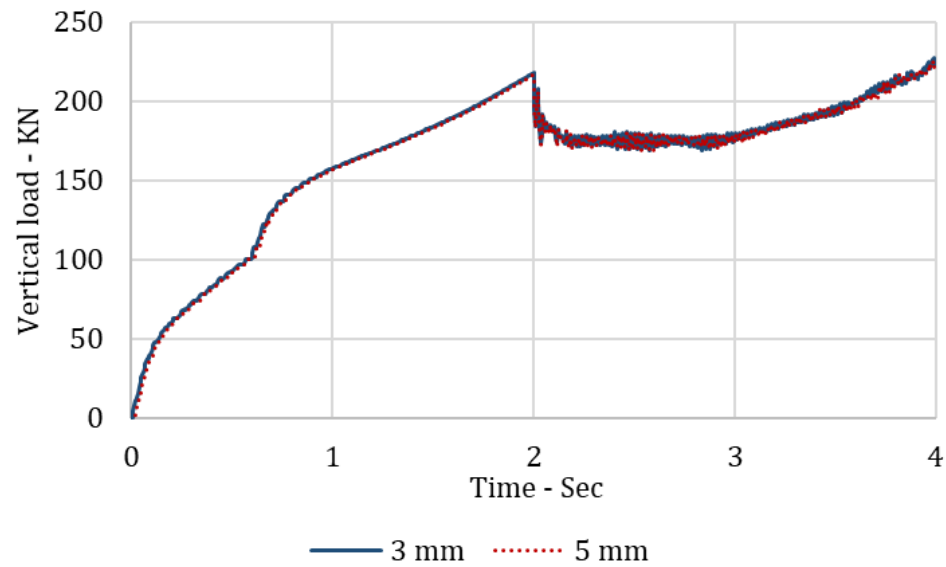


Figure 7-26 Mesh Convergence Analyses Including Two Mesh Sizes for the Carrier and Inner Pipes: 3, 5, mm

7.3.6 Sensitivity Case

A sensitivity study is performed for friction coefficient in the region where the carrier pipe and inner pipe comes into contact (interaction type-b) and where the end connection slides inside the ball supports (interaction type-c). Accordingly, the friction coefficient of 0.3 is used for the sensitivity case and compared against the base case with no friction. Figure 7-27 shows that the effect of friction in interaction type-b and c on the load-displacement curve is negligible. Accordingly, the base case with no friction is used for the analyses of the present study.

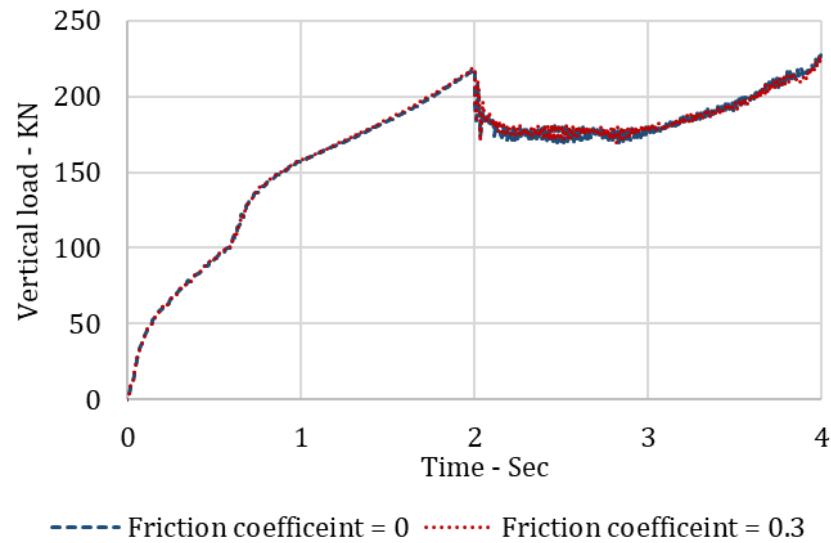


Figure 7-27 Sensitivity Study on the Effect of Friction Coefficient in the Contact Regions Type-b and c

7.3.7 Results

Figure 7-28 shows the load-displacement curves obtained from the physical test and finite element analysis. As presented in Section 7.2.2.2, comparing the results of the PiP test in the present study against the previous physical studies reported in Davaripour et al. (2020d) and Zheng et al. (2013) shows that 1) before point b, the response obtained from the PiP specimen is higher than expected; 2) after point c, the structural response of the PiP specimen is lower than expected. The main suspect for the source of these discrepancies is the residual stresses in the carrier and inner pipes, induced during the assembly procedure.

As presented in Section 7.2.1.2.1, for the assembly of the PiP specimen, while the inner pipe was mounted inside the carrier pipe by the ball supports, the carrier pipe was welded to the flange connection. As no clearance was considered between the inner pipe and the ball supports, welding contraction of the carrier pipe was resisted by the inner pipe. As such, the carrier pipe goes under tension, and the inner pipe goes under compression. Accordingly, before point b, where the indentation is only resisted by the carrier pipe, the numerical prediction underestimates the test result. This could be due to the fabrication induced tension in the carrier pipe, which increases the pipe's structural capacity; as reported in, i.e., (Ruggieri and Ferrari, 2004), the tensile axial force could increase the pipe's load-carrying capacity against the lateral indentation. Furthermore, after point b, where the indentation is resisted by both carrier and inner pipes, the numerical result overestimates the test data. This could be due to the fabrication induced compression in the inner pipe. This axial compression could significantly decrease the pipe's resistance against the lateral indentation, as reported in SUH (1987) and Wierzbicki and Suh (1988).

With regards to the numerical prediction in Figure 7-28, there is a significant drop in the pipe's structural response by the initiation of phase-2 (18.5%), which provides evidence of the damage progression effect in a PiP specimen. The damage progression effect obtained from the finite element analysis is approximately twice that which was recorded during the physical test (Section 7.2.2.1). Furthermore, in contrast to phase 1, there is

excellent agreement between the test result and numerical prediction during the second phase of the test.

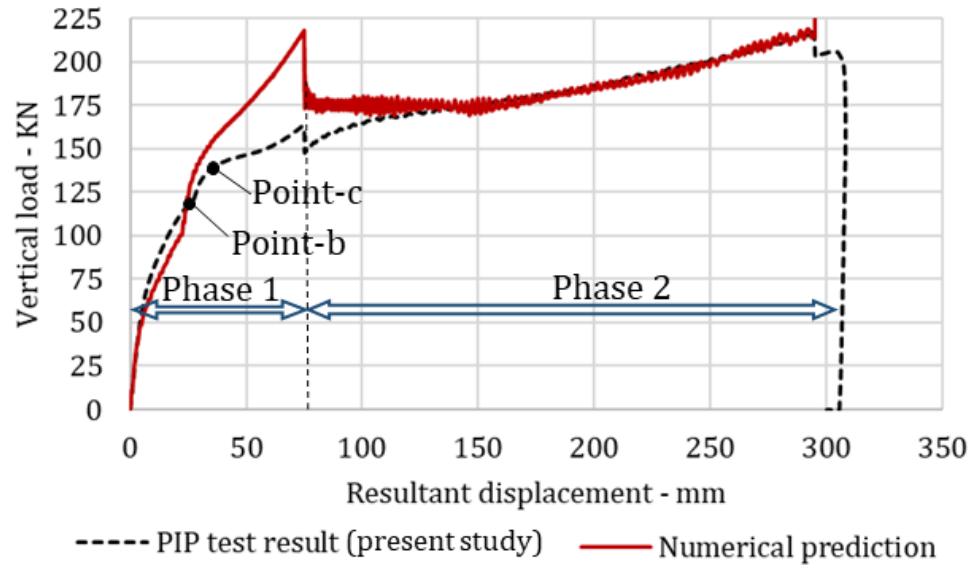


Figure 7-28 Vertical Load Imposed to the PiP Specimen: Test Data Versus Numerical Prediction

In order to confirm the above-mentioned suspicions about the effects of the fabrication induced tension and compression in the outer and inner pipes, respectively, axial forces were imposed on each end of a) the inner pipe to compress the pipe, and b) the carrier pipe to extend the pipe. Since the inner and carrier pipes share common end conditions, their associated compressive and tensile forces must be equal and opposite. The axial imposed load was varied (0, 100, 200 KN), and the PiP response during the first phase of the loading was assessed. Accordingly, as shown in Figure 7-29, by increasing the axial load, the numerical prediction approaches the test data, which provides evidence regarding the presence of residual stress in the PiP specimen before the test. In this regard,

by further increasing the axial load (i.e., 300 KN), the numerical prediction could reach a better agreement with the test data. However, as the axial load is imposed in the load-controlled condition, the inner pipe may become unstable before the completion of the analysis. To address this issue, a more accurate representation of the residual stress in the PiP specimen is required, which is not within the scope of the present work.

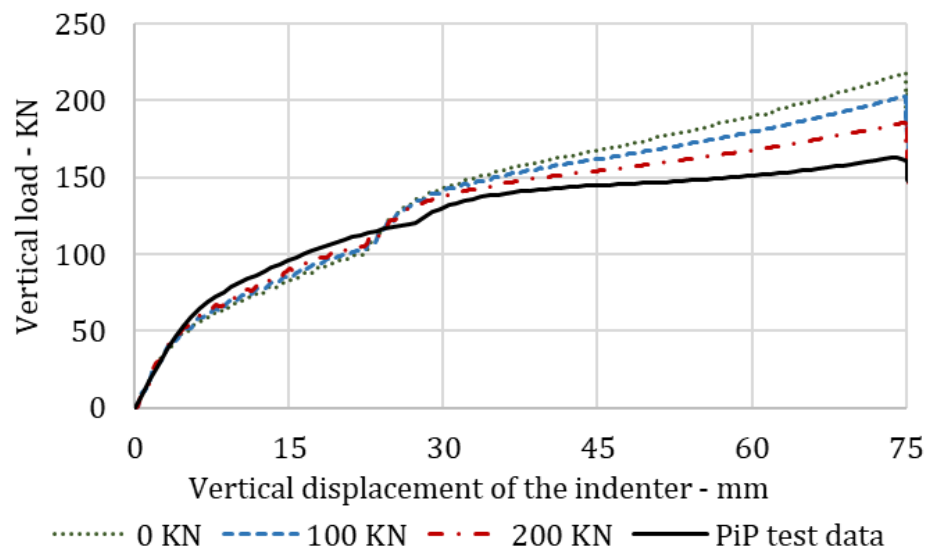


Figure 7-29 Vertical Load Imposed on the PiP Specimen Versus Vertical Displacement of the Indenter: Test Data Versus Numerical Prediction (Under 1, 100, and 200 KN Axial Load)

7.4 Summary and Conclusions

A novel experimental investigation was performed to assess the damage progression effect in PiP systems. Accordingly, a PiP specimen was examined under the two-phase loading condition where a) in phase 1, the specimen was subject to 75 mm perpendicular

indentation, and b) in phase 2, the vertical position of the indenter was maintained; however, the indenter translated longitudinally and induced the plastic damage along the specimen. The test data shows that during phase 1, the vertical resistance of the specimen shows a sudden jump when the inner and carrier pipes come into contact. However, shortly after the involvement of the inner pipe, the slope of the load-displacement curve declines noticeably. The comparison of these results in the present work with those in the previous physical studies suggests that the structural behaviour of the PiP specimen was affected due to the presence of residual stress in the carrier and inner pipes, induced during the assembly procedure.

A simplified numerical model of the physical test was examined using the finite element method. It was shown that implementing the residual stress on the PiP specimen in the form of an axial force leads to a better numerical prediction; an axial tensile and compressive force was imposed on both ends of the carrier and inner pipes, respectively. Accordingly, the results showed that by increasing the axial force at both ends of the PiP specimen, the finite element results approach the test data, which provides evidence regarding the interference of the residual stress on the PiP structural behaviour. Furthermore, the numerical results showed that the PiP load-carrying capacity could lower significantly where the inner pipe is subject to a compressive force. In other words, the compressive force which is induced in a PiP system (due to, i.e., thermal expansion

or internal pressure) could decrease the structural capacity of the PiP system under an interference load (i.e., trawl gear impact).

The results obtained from the lab-scale physical test showed a significant drop (10%) in the load-carrying capacity of the PiP specimen by the initiation of phase 2 of loading. These findings are aligned with the previous works on the subject of damage progression effect in SWPs, i.e., (Davaripour et al., 2020b, 2020d). In conclusion, the damage progression effect should be considered in the assessment of failure limit states in PiP systems, where the PiP is subject to a substantial lateral load (i.e., trawl gear impact). In other words, if the damage progression effect is not considered in the pipeline assessment against lateral interference loads, it could lead to a significant underestimation of the resulting damage, predicted during the overtrawlability analyses.

Future Work

The test data on a PiP specimen during the 75 mm perpendicular indentation showed only a small additional strength compared to the exact same test but on the carrier pipe. Using finite element analyses, it was shown that the structural behaviour of the PiP specimen was affected by the residual stress induced during the assembly procedure. Therefore, a further experimental study is required to examine the structural response of the PiP specimen by improving the test setup to avoid residual stress.

The numerical results of the present study showed that where the inner pipe is subject to a compressive force, the overall capacity of the PiP system could decline significantly. Accordingly, lab-scale tests on a PiP specimen subject to a varied range of axial forces accompanied by interference loads, are required to further investigate the effect of combined loading on the PiP mechanical behaviour.

Acknowledgment

This research became possible through the funds provided by the Natural Sciences and Engineering Research Council's (NSERC) Discovery Grant program, as well as the Mitacs Accelerate Program.

Reference

- Alexander, C., 2007. ASSESSING THE EFFECTS OF IMPACT FORCES ON SUBSEA FLOWLINES AND PIPELINES, in: The 26th International Conference on Offshore Mechanics and Arctic Engineering. San Diego, California USA.
- Davaripour, F., Quinton, B., Pike, K., 2020b. A Numerical Investigation on a Pipe Subject to a Non- Perpendicular Trawl Impact Using a Hybrid Shell-Beam Model, in: Offshore Pipeline Conference (OPT 2020). Amsterdam, pp. 1–12.
- Davaripour, F., Quinton, B., Pike, K., 2020c. An Assessment on a Subsea Pipeline Subject to a Diagonal Trawl Impact (Under Review). Appl. Ocean Res.
- Davaripour, F., Quinton, B.W.T., 2018. An Investigation of the Load Carrying Capacity of Pipelines Under Accidental and Longitudinal Moving (Sliding) Loads, in: International Pipeline Conference (IPC). pp. 1–7.
- Davaripour, F., Quinton, B.W.T., C, K.P., 2020d. Effect of Damage Progression on the Plastic Capacity of a Subsea Pipeline (Under Review). Ocean Eng.
- DNV-RP-F111, 2014. Det Norske Veritas - Interference Between Trawl Gear and Pipelines.
- Ellinas, C.P., Walker, A.C., 1983. Damage on offshore tubular bracing members, IABSE reports = Rapports AIPC = IVBH Berichte.
<https://doi.org/http://doi.org/10.5169/seals-32425>
- LS-Dyna Documentation, 2018. KEYWORD USER'S MANUAL.

- Quinton, B., 2015. Experimental and numerical investigation of moving loads on hull structures. PhD thesis, Memorial University of Newfoundland.
- Quinton, B., 2008. Progressive damage to a Ship's structure due to ice loading. Master thesis, Memorial University of Newfoundland.
<https://doi.org/10.13140/RG.2.1.1395.6562>
- Ruggieri, C., Ferrari, J.A., 2004. Structural Behavior of Dented Tubular Members Under Lateral Loads. *J. Offshore Mech. Arct. Eng.* 126, 191.
<https://doi.org/10.1115/1.1712979>
- Shen, W.Q., Jones, N., 1991. A comment on the low speed impact of a clamped beam by a heavy striker. *J. Struct. Mech.* 19, 527–549.
- Soreide, T.H., Moan, T., Amdahl, J., Taby, J., 1982. Analysis of Ship/Platform Impacts. *Behav. Off-Shore Struct.* 2, 257–278.
- Sriskandarajah, T., Ragupathy, P., Anurudran, G., Wilkins, R., 1999. Fishing Gear Interaction On HP/HT Pipe-in-Pipe Systems. Ninth Int. Offshore Polar Eng. Conf. 30 May-4 June, Brest, Fr. II, 8. <https://doi.org/ISOPE-I-99-141>
- SUH, M.S., 1987. PLASTIC ANALYSIS OF DENTED TUBES SUBJECTED TO COMBINED LOADING (DOCTOR OF PHILOSOPHY).
- Thomas, S.G., Reid, S.R., Johnson, W., 1976. Large deformations of thin-walled circular tubes under transverse loading—I: an experimental survey of the bending of simply supported tubes under a central load. *Int. J. Mech. Sci.* 18, 325in3327-326in6333.

- Wang, Y., Qian, X., Liew, J.Y.R., Zhang, M.H., 2014. Experimental behavior of cement filled pipe-in-pipe composite structures under transverse impact. *Int. J. Impact Eng.* 72, 1–16. <https://doi.org/10.1016/j.ijimpeng.2014.05.004>
- Wierzbicki, T., Suh, M.S., 1988. Indentation of tubes under combined loading. *Int. J. Mech. Sci.* 30, 229–248.
- Zheng, J., Palmer, A., Brunning, P., 2013. Overtrawlability and Mechanical Damage of Pipe-in-Pipe. *J. Appl. Mech.* 81, 031006. <https://doi.org/10.1115/1.4024877>
- Zheng, Jiexin, Palmer, A., Brunning, P., Gan, C.T., 2014. Indentation and external pressure on subsea single wall pipe and pipe-in-pipe. *Ocean Eng.* 83, 125–132. <https://doi.org/10.1016/j.oceaneng.2014.03.028>
- Zheng, J., Palmer, A., Brunning, P., Lim, G., Shu, S., 2014. Method to assess the overtrawlability of pipe-in-pipe. *Proc. Annu. Offshore Technol. Conf.* 1.
- Zheng, J., Palmer, A., Lipski, W., Brunning, P., 2012. Impact Damage on Pipe-in-Pipe Systems, in: *International Offshore and Polar Engineering Conference*. Rhodes, Greece, pp. 152–157.

8 Summary and Conclusions

Throughout the present thesis, the mechanical behaviour of subsea pipelines was investigated where the pipe is subject to an impact event, and the interference load imposes plastic damage on the pipe and induces the damage longitudinally along the pipe. It was demonstrated that the progression of plastic damage along a pipe could significantly lower the structural resistance of the pipe; this reduction is termed as the damage progression effect. As an example, the structural resistance of a subsea pipeline subject to a diagonal interference load could significantly be higher if only the normal component of the interference load is considered. In other words, the tangential component of the diagonal interference load could induce the potential plastic damage along the pipe and lower the structural capacity of the pipe. In conclusion, new mechanical behaviour in subsea pipelines was introduced and investigated, which should be considered in the assessment of failure limit states in pipes against any accidental events where the progression of plastic damage along the pipe is likely.

It was shown that the damage progression effect occurs only if the interference load imposes plastic damage to the pipe. Therefore, there is no damage progression effect during the elastic response. Furthermore, under minimal localized plastic response, this effect is negligible. In addition, the present study showed that the main source of this effect is due to the complex nonlinear behaviour which occurs where the indenter induces the plastic damage along the pipe. By the initiation of damage progression, the resistance

of the pipe in the region, which is in the trailing side of the load, drops promptly and considerably depending on the plastic damage size.

The findings of the present study could be applied to any cylindrical structure where the structure is subject to an interference load, and the load induces the plastic damage longitudinally along the pipe. However, the present thesis is conducted with a focus on the interaction between subsea pipelines and bottom trawl gear. Accordingly, the present study identified and investigated the damage progression associated gaps in the DNV-RP-F111 design guideline, which is the current industry recommended practice for the assessment of subsea pipelines against the trawl gear interference load. As such, first, a hybrid shell beam model is developed to expand the applicability of the current industry recommended finite element model (the BSM model) for pipe sizes smaller than 10 inches. Then the hybrid model is employed to investigate the potential damage progression effect in subsea pipelines where the pipe is subject to a diagonal trawl impact. In addition, a simplified model of a pipe restrained laterally by steel saddle-shaped support was employed to examine the potential damage progression effect in subsea pipelines, where the pipe is subject to repeated trawl impacts at adjacent locations.

With respect to the description provided in Section 3.3.2, the accuracy of the hybrid model was partly validated against the present and previous study physical tests and employed to investigate a 5-inch diameter pipe subject to a perpendicular indentation.

The results obtained from the hybrid model were compared against those by the BSM model (recommended by DNV-RP-F111 (2014)) and the analytical method. It was demonstrated that:

- The finite element approach (with BSM/hybrid model) could significantly reduce the unnecessary conservatism (compared to using the analytical approach) and improve the economy of a project for small pipe sizes
- Using the hybrid model leads to a similar total resulting dent depth with the one obtained from the BSM model for a 10-inch diameter pipe (only 4% difference).
- Using the hybrid model could reduce the conservatism associated with the BSM model for medium pipe sizes (with outer diameter larger than 10 inches). A sensitivity case was conducted for a 14-inch diameter pipe, which showed that using the hybrid model reduces the resulting dent size on a pipe by 15% compared to the case where the BSM model is employed.
- Employing the hybrid model could be a suitable alternative to the BSM model for small pipe sizes (outer diameter less than 10 inches). A sensitivity case was studied for a 5-inch diameter pipe, which showed that the resulting total dent depth obtained from the BSM model is 14% lower than the one derived from the hybrid model.

The discrepancy between results obtained from the BSM versus the hybrid model could be due to a) the shell stiffness implemented in the BSM versus the hybrid model, b) the more realistic contact representation in the hybrid model versus point contact in the BSM

model, c) the coupling effect between the local and global stiffness of the pipe, which is disregarded in the BSM model, d) the difference in the transition time from phase a (mainly local deformation) to phase b (the combination of local and global deformation) in the BSM versus the hybrid model, e) the path-dependency of the pipe response during the plastic indentation, which could not be considered in the BSM model.

The hybrid model was then employed to perform numerical investigations to assess the structural resistance of a pipe subject to a diagonal trawl impact. The main objective was to examine the effect of the tangential component of the diagonal trawl impact on the resulting pipe's dent size. Accordingly, two cases were examined with the same normal velocity component, including case-1) where the pipe is subject to a non-perpendicular trawl impact with 30 degrees angle and the velocity of 2.6 m/sec, and case-2) where the pipe is subject to only the normal component of the diagonal impact in case-1. The results of this study showed that the imposed dent depth on a pipe under case-1 is around 20% higher than the one under case-2. This finding shows the progression of damage, induced by the tangential component of the non-perpendicular impact in case-1, decreases the structural resistance of the pipe, and leads to larger resulting dent size on the pipe, compared to case-2 where the tangential component of the impact is disregarded.

It was concluded that in order to assess a scenario where a subsea pipeline is subject to a diagonal trawl impact, the BSM model should be improved to account for the tangential

component of the impact as well as the progression of damage along the pipe. In this regard, the hybrid shell-beam model, which is developed in the present study, is a suitable and numerically efficient alternative.

Furthermore, another numerical study was conducted to study a scenario where the pipe is subject to several adjacent perpendicular indentations. This scenario represents an idealization of a subsea pipeline, restrained laterally by steel saddle-shaped support, and subjected to repeated trawl impacts. The results showed that by the progression of damage along the pipe, under the same imposed perpendicular loads, the size of dent depth increases by 29%. This result is aligned with the findings of the present study that the progression of damage along a pipe decreases the structural resistance of the pipe. The finite element analyses in this study were conducted under the quasi-static condition. However, the findings of this study show that for scenarios where the pipe is subject to subsequent impacts, applying several impacts at the same location on the pipe may not be the most critical (dominant) scenario, and the effect of damage progression under repeated impacts should be investigated.

A series of experimental investigations were performed on a 5-inch diameter SWP pipe (schedule 40) subject to a lateral interference load to examine the influence of the progression of damage on the pipe's structural resistance. Accordingly, four laboratory tests were conducted, and the effect of friction, boundary condition, and loading condition

were investigated. The tests were conducted under the quasi-static condition with a load path consisting of two phases, including a) phase 1, where the pipe is subject to a perpendicular indentation, and b) phase 2, where the resulting damage on the pipe is pushed along the pipe for 300 mm. The results obtained from the physical tests showed that:

- Due to the damage progression along the pipe in phase 2, the structural resistance of the pipe drops significantly (i.e., 33.5% in Test 1, as presented in Section 6.2.2.1.1).
- The friction between the indenter and the pipe does not change the damage progression effect, at least for the experimental conditions of the present study.
- Due to the damage progression effect, the dent depth in the pipe increases by 52% when the ~ 150 KN perpendicular load translates along the pipe.
- The damage progression effect is significantly larger where the pipe response is based on a pure local deformation versus a combination of local and global deformation.

Furthermore, a novel experimental investigation was performed to assess the damage progression effect in PiP systems. Accordingly, a PiP specimen was examined under the two-phase loading condition where a) in phase 1, the specimen was subject to 75 mm perpendicular indentation, and b) in phase 2, the vertical position of the indenter was maintained; however, the indenter translated longitudinally and pushed the plastic

damage along the specimen. The test data shows that during phase 1, the vertical resistance of the specimen has a sudden jump when the inner and carrier pipes come into contact. However, shortly after the involvement of the inner pipe, the slope of the load-displacement curve declines noticeably. The comparison of these results in the present work with those in the previous physical studies suggests that the structural behaviour of the PiP specimen was affected due to the presence of residual stress in the carrier and inner pipes, induced during the assembly procedure.

A simplified numerical model of the physical test was examined using the finite element method. It was shown that implementing the residual stress on the PiP specimen in the form of an axial force leads to a better numerical prediction; an axial tensile and compressive force were imposed on both ends of the carrier and inner pipes, respectively. Accordingly, the results showed that by increasing the axial force at both ends of the PiP specimen, the finite element results approach the test data, which provides evidence regarding the influence of the residual stress on the PiP structural behaviour. Furthermore, the numerical results showed that the PiP's structural capacity could drop significantly where the inner pipe is subject to a compressive axial force. In other words, the compressive axial force, which is induced in a PiP product (due to, i.e., thermal expansion or internal pressure), could lower the structural capacity of the PiP system against a lateral interference load (i.e., trawl gear impact).

The results obtained from the lab-scale physical test showed a significant drop (10%) in the structural resistance of the PiP specimen by the initiation of phase 2 of loading. In conclusion, the findings of the present study identified, introduced, and investigated a gap in the present design guidelines regarding the considerable effect of damage progression in PiP systems, where the PiP product is subject to a substantial lateral interference load.

9 Future Work

The present thesis studied some aspects of the damage progression effect in pipelines due to the non-rupture type interference loads applied to the pipe in the lateral direction. For future works, the structural response of a pipe under a rupture-type interference load causing damage progression should be investigated. In this regard, the rupture initiation in a ductile structure could be predicted using the stress triaxiality as well as strain intensity (Bao and Wierzbicki, 2004). Therefore, these two factors could be employed to investigate the effect of damage progression on the mechanical behaviour of a pipe, where the pipe is subject to a lateral rupture-type interference load.

The hybrid model is developed for the overtrawlability assessment of small-sized subsea pipelines. However, this model could be used for other impact scenarios in offshore areas to investigate a submerged pipeline subject to a lateral interference load applied by a knife-edge indenter (i.e., dropped object, anchor impact, etc.).

In the present research, the hybrid model was employed to examine a scenario where the pipe is subject to a non-perpendicular trawl impact. To further investigate this topic, more sensitivity studies should be performed on, i.e., pipe size, pipe wall-thickness, pipe-soil interaction, etc. Furthermore, in the present research, only the first phase of the trawl gear interference with a subsea pipeline was investigated (the initial impact phase). However, the pull-over phase where the pipe is dragged by the trawl gear could also result in the

damage progression effect. As such, further research should be conducted to investigate the damage progression effect in a pipe, where the pipe is subject to a trawl pull-over load.

The present thesis also addressed another damage progression effect associated gap in the DNV-RP-F111 design guideline, where the pipe is subject to subsequent trawl impacts. Accordingly, the present work identified, introduced, and examined the damage progression effect in subsea pipelines where the pipe is subject to a particular pattern of repeated indentations at neighboring locations. To further investigate this topic, varied random load patterns should also be examined. Furthermore, the analyses in the present study were conducted under the quasi-static condition. Therefore, similar studies should also be performed under the impact condition.

A series of physical tests were conducted in the present research on SWP and PiP systems to investigate the damage progression effect under the quasi-static condition. The test data on a PiP specimen during the 75 mm perpendicular indentation showed only a small additional strength compared to the exact same test but on the carrier pipe. Using finite element analyses, it was shown that the structural behaviour of the PiP specimen was affected by the residual stress induced during the assembly procedure. Therefore, a further experimental study is required to examine the structural response of the PiP specimen by modifying the test setup to avoid residual stress. Furthermore, the numerical

results of the present study showed that where the inner pipe is subject to a compressive axial force, the overall capacity of the PiP system could decline significantly. Accordingly, lab-scale tests on a PiP specimen subject to a varied range of axial forces accompanied by lateral interference loads, are required to further investigate the effect of combined loading on the PiP's mechanical behaviour.

Reference

- Abaqus Documentation, 2019. Analysis User's Manual.
- Alexander, C., 2007. ASSESSING THE EFFECTS OF IMPACT FORCES ON SUBSEA FLOWLINES AND PIPELINES, in: The 26th International Conference on Offshore Mechanics and Arctic Engineering. San Diego, California USA.
- ASTME8/E8M-13, 2013. Standard Test Methods for Tension Testing of Metallic Materials. <https://doi.org/10.1520/E0008>
- Bai, Y., Bai, Q., 2005. Subsea Pipelines and Risers. Mater. Mech. 1–700. <https://doi.org/10.1016/B978-008044566-3.50023-3>
- Bai, Y., Wierzbicki, T., 2008. A new model of metal plasticity and fracture with pressure and Lode dependence. Int. J. Plast. 24, 1071–1096. <https://doi.org/10.1016/j.ijplas.2007.09.004>
- Bao, Y., Wierzbicki, T., 2004. On fracture locus in the equivalent strain and stress triaxiality space. Int. J. Mech. Sci. 46, 81–98. <https://doi.org/10.1016/j.ijmecsci.2004.02.006>
- Chater, E., Hutchinson, J.W., 1984. on the Propagation of Bulges and Buckles. Am. Soc. Mech. Eng. Press. Vessel. Pip. Div. PVP 84, 123–136.
- Chen, K., Shen, W.Q., 1998. Further experimental study on the failure of fully clamped steel pipes. Int. J. Impact Eng. 21, 177–202. [https://doi.org/10.1016/S0734-743X\(97\)00083-3](https://doi.org/10.1016/S0734-743X(97)00083-3)
- Davaripour, F., Pike, K., Quinton, B.W.T., Persaud, R., 2020a. An Assessment on the

- Overtrawlability of Small Pipe Sizes Using a Hybrid Shell- Beam Model : The Initial Trawl Impact Phase (Revision Requested). Appl. Ocean Res.
- Davaripour, F., Quinton, B., Pike, K., 2020b. A Numerical Investigation on a Pipe Subject to a Non- Perpendicular Trawl Impact Using a Hybrid Shell-Beam Model, in: Offshore Pipeline Conference (OPT 2020). Amsterdam, pp. 1–12.
- Davaripour, F., Quinton, B., Pike, K., 2020c. An Assessment on a Subsea Pipeline Subject to a Diagonal Trawl Impact (Under Review). Appl. Ocean Res.
- Davaripour, F., Quinton, B.W.T., 2018. An Investigation of the Load Carrying Capacity of Pipelines Under Accidental and Longitudinal Moving (Sliding) Loads, in: International Pipeline Conference (IPC). pp. 1–7.
- Davaripour, F., Quinton, B.W.T., C, K.P., 2020d. Effect of Damage Progression on the Plastic Capacity of a Subsea Pipeline (Under Review). Ocean Eng.
- DNV-OS-F101, 2013. Det Norske Veritas - DNV-OS-F101: Submarine pipeline systems. <https://doi.org/DNV-OS-F101>
- DNV-RP-F105, 2006. Det Norske Veritas - Free spanning pipelines 138.
- DNV-RP-F107, 2010. Det Norske Veritas - Risk Assessment of Pipeline Protection. Mater. Technol.
- DNV-RP-F111, 2014. Det Norske Veritas - Interference Between Trawl Gear and Pipelines.
- Ellinas, C.P., Walker, A.C., 1983. Damage on offshore tubular bracing members, IABSE reports = Rapports AIPC = IVBH Berichte.

<https://doi.org/http://doi.org/10.5169/seals-32425>

Emesum, J.C., 2013. Full Scale Trawl Board Impact Testing In Water. University of Stavanger.

Fryba, L., 1999. Vibration of solids and structures under moving loads, Telford, London. Springer.

Fyrileiv, O., Askheim, D.Ø., Verley, R., 2006. PIPELINE-TRAWL INTERACTION: EFFECT OF TRAWL CLUMP WEIGHTS Olav 1–8.

Fyrileiv, O., Spiten, J., 2004. Trawl gear protection within platform safety Zones, in: ASME 2004 23rd International Conference on Offshore Mechanics and Arctic Engineering. American Society of Mechanical Engineers Digital Collection, pp. 217–223.

Hahn, G.D., She, M., Carney, J.F., 1993. Buckle Propagation in submarine Pipelines 45, 177–215.

Hong, L., 2008. Simplified analysis and design of ships subjected to collision and grounding. PhD thesis, Norwegian University of Science and Technology.

Horenberg, J.A.G., Koninklijke, J.G., 1987. An Analytical and Experimental Analysis of Trawl Gear-Pipeline Interaction, in: Offshore Technology Conference.

Jones, N., 2012. Structural impact. Cambridge University Press.

Jones, N., Birch, R.S., 1996. Influence of internal pressure on the impact behavior of steel pipelines. J. Press. Vessel Technol. Trans. ASME 118, 464–471.
<https://doi.org/10.1115/1.2842215>

- Konuk, I., Fredj, A., Yu, S., 2005. 3-Dimensional Bifurcations of Pipe-in-Pipe Structures, in: 24th International Conference on Offshore Mechanics and Arctic Engineering (OMAE 2005). pp. 1–7.
- Kyriakides, S., 1994. Propagating instabilities in structures. *Adv. Appl. Mech.* 30.
- Leis, B.N., Francini, R.B., Mohan, R., Rudland, D.L., Olson, R.J., 1998. Pressure-displacement behavior of transmission pipelines under outside forces - towards a serviceability criterion for mechanical damage. *Proc. Int. Offshore Polar Eng. Conf.* 2, 60–67.
- Liang, H., Zhou, J., Lin, J., Jin, F., Xia, F., Xue, J., Xu, J., 2019. Buckle Propagation in Steel Pipes of Ultra-high Strength: Experiments, Theories and Numerical Simulations. *Acta Mech. Solida Sin.* 1–18.
- LS-Dyna Documentation, 2018. KEYWORD USER’S MANUAL.
- Ng, C.S., Shen, W.Q., 2006. Effect of lateral impact loads on failure of pressurized pipelines supported by foundation. *Proc. Inst. Mech. Eng. Part E J. Process Mech. Eng.* 220, 193–206. <https://doi.org/10.1243/0954408JPME97>
- Palmer, A., Touhey, M., Holder, S., Anderson, M., Booth, S., 2006. Full-scale impact tests on pipelines. *Int. J. Impact Eng.* 32, 1267–1283. <https://doi.org/10.1016/j.ijimpeng.2004.09.003>
- Parkes, E.W., 1958. How to cross an unsafe bridge. *A Divers. Dyn. Plast. Eng.* 186, 606–608.
- Quinton, B., 2015. Experimental and numerical investigation of moving loads on hull

- structures. PhD thesis, Memorial University of Newfoundland.
- Quinton, B., 2008. Progressive damage to a Ship's structure due to ice loading. Master thesis, Memorial University of Newfoundland.
<https://doi.org/10.13140/RG.2.1.1395.6562>
- Quinton, B., Daley, C., Gagnon, R., Colbourne, B., 2017. Guidelines for the nonlinear finite element analysis of hull response to moving loads on ships and offshore structures. *Ships Offshore Struct.* 12, S109–S114.
- Quinton, B., Daley, C.G., Gagnon, R.E., 2012. Realistic moving ice loads and ship structural response, in: *Proceedings of the Twenty-Second International Offshore and Polar Engineering Conference*. pp. 17–22.
- Quinton, B.W.T., Daley, C.G., Gagnon, R.E., 2010. Effect of Moving Ice Loads on the Plastic Capacity of a Ship's Structure, in: *IceTech 2010*. Anchorage, Alaska.
- Quinton, B.W.T., Daley, C.G., Gagnon, R.E., Colbourne, D., 2017. Experimental investigation of accidental sliding loads on the response of hull plating, in: *6th International Conference on Marine Structures (MARSTRUCT 2017)*, 8-10 May. Lisbon, Portugal.
- Ruggieri, C., Ferrari, J.A., 2004. Structural Behavior of Dented Tubular Members Under Lateral Loads. *J. Offshore Mech. Arct. Eng.* 126, 191.
<https://doi.org/10.1115/1.1712979>
- Shen, W.Q., Jones, N., 1991. A comment on the low speed impact of a clamped beam by a heavy striker. *J. Struct. Mech.* 19, 527–549.

- Song, R., Kang, Z., Qin, Y., Li, C., 2009. PIPELINE BUNDLE – A SMART SOLUTION FOR INFIELD TRANSPORTATION Part I : Overview and Engineering Design, in: Proceedings of the ASME 2009 28th International Conference on Ocean, Offshore and Arctic Engineering.
- Soreide, T.H., Moan, T., Amdahl, J., Taby, J., 1982. Analysis of Ship/Platform Impacts. Behav. Off-Shore Struct. 2, 257–278.
- Sriskandarajah, T., Ragupathy, P., Anurudran, G., Wilkins, R., 1999. Fishing Gear Interaction On HP/HT Pipe-in-Pipe Systems. Ninth Int. Offshore Polar Eng. Conf. 30 May-4 June, Brest, Fr. II, 8. <https://doi.org/ISOPE-I-99-141>
- SUH, M.S., 1987. PLASTIC ANALYSIS OF DENTED TUBES SUBJECTED TO COMBINED LOADING (DOCTOR OF PHILOSOPHY).
- Symonds, P.S., Neal, B.G., 1960. Traveling loads on rigid-plastic beams. J. Eng. Mech. Div. 86, 79–90.
- Thomas, S.G., Reid, S.R., Johnson, W., 1976. Large deformations of thin-walled circular tubes under transverse loading—I: an experimental survey of the bending of simply supported tubes under a central load. Int. J. Mech. Sci. 18, 325–333.
- Toridis, T.G., Wen, R.K., 1966. Inelastic response of beams to moving loads. J. Eng. Mech. Div. 92, 43–62.
- Trevor Jee Associates, 1999. Guidelines for the Trenching Design of Submarine Pipelines, Oth 561.
- Wang, Y., Qian, X., Liew, J.Y.R., Zhang, M.H., 2014. Experimental behavior of cement

- filled pipe-in-pipe composite structures under transverse impact. *Int. J. Impact Eng.* 72, 1–16. <https://doi.org/10.1016/j.ijimpeng.2014.05.004>
- Wichtmann, T., Triantafyllidis, T., 2009. On the correlation of “static” and “dynamic” stiffness moduli of non-cohesive soils. *Bautechnik* 86, 28–39. <https://doi.org/10.1002/bate.200910039>
- Wierzbicki, T., Suh, M.S., 1988. Indentation of tubes under combined loading. *Int. J. Mech. Sci.* 30, 229–248.
- Zheng, J., 2014. Overtrawlability and Mechanical Damage of Pipe-in-Pipe, PhD thesis. NATIONAL UNIVERSITY OF SINGAPORE.
- Zheng, J., Palmer, A., Brunning, P., 2013. Overtrawlability and Mechanical Damage of Pipe-in-Pipe. *J. Appl. Mech.* 81, 031006. <https://doi.org/10.1115/1.4024877>
- Zheng, Jiexin, Palmer, A., Brunning, P., Gan, C.T., 2014. Indentation and external pressure on subsea single wall pipe and pipe-in-pipe. *Ocean Eng.* 83, 125–132. <https://doi.org/10.1016/j.oceaneng.2014.03.028>
- Zheng, J., Palmer, A., Brunning, P., Lim, G., Shu, S., 2014. Method to assess the overtrawlability of pipe-in-pipe. *Proc. Annu. Offshore Technol. Conf.* 1.
- Zheng, J., Palmer, A., Lipski, W., Brunning, P., 2012. Impact Damage on Pipe-in-Pipe Systems, in: *International Offshore and Polar Engineering Conference*. Rhodes, Greece, pp. 152–157.

Appendix - Static Analysis

Figure 9-1 shows a view of the swing-arm, indenter, and hydraulic ram. The indenter is connected to the swing-arm and then to the supporting frame. As the connection point between the swing-arm to the test frame resists vertical displacement, the measured vertical load by the MTS load cell varies with the vertical force resisted at the connection point. Accordingly, a static analysis is performed to calculate the vertical load resisted at the connection point. The vertical load measured by the MTS load cell is then adjusted accordingly to provide the vertical load on the indenter.

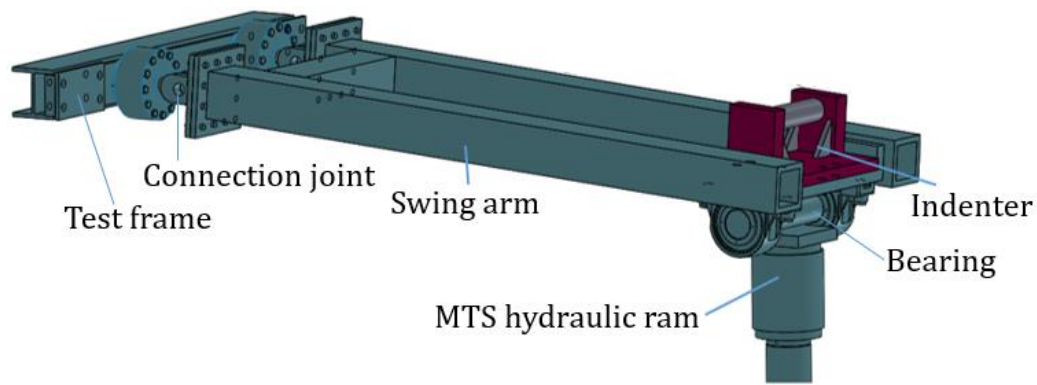


Figure 9-1 A View of the Connection Between the Swing-arm and Indenter

Figure 9-2 shows a schematic view of the indenter, swing-arm, and boundary conditions, where a is the height above the swing-arm to the point of action of the horizontal force on the indenter. b is the length of the swing-arm. B is the joint where the swing-arm is connected to the horizontal load cell. K is where the swing-arm contacts the vertical MTS hydraulic ram. The combination of indenter and the swing-arm is considered as a

continuous beam. Furthermore, a section cut of the beam is provided at joint B to assess the loads and moments.

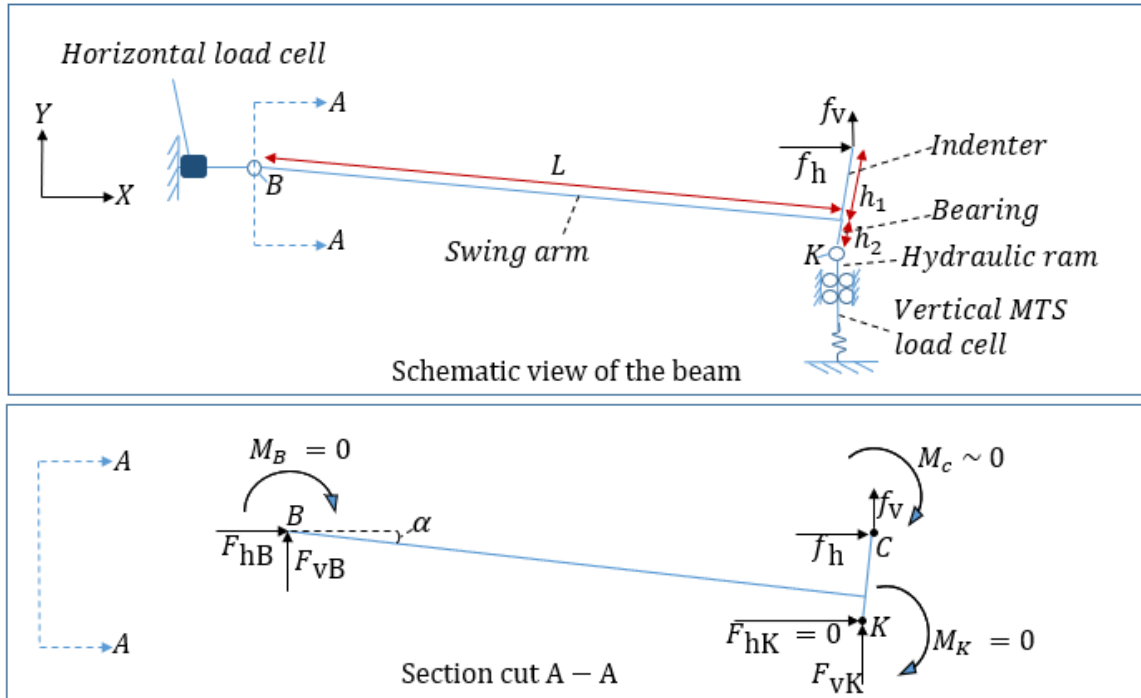


Figure 9-2 Static Analysis of the Load Transferred Along the Indenter and the Swing-Arm

The equilibrium along the beam is assessed via the following equations:

$$\sum f_x = 0 \rightarrow F_{hB} + f_h = 0 \rightarrow F_{hB} = -f_h \quad \text{Equation 9-1}$$

$$\sum M_B = 0 \rightarrow (f_v * \cos(\alpha) + f_h \sin(\alpha) + F_{vk} \cos(\alpha)) * L + (f_v$$

$$* \sin(\alpha) - f_h \cos(\alpha)) * h_1 - F_{vk} \sin(\alpha) * h_2 = 0$$

$$\rightarrow f_v$$

$$= \frac{-(f_h \sin(\alpha) + F_{vk} \cos(\alpha)) * L + f_h \cos(\alpha) * h_1 + F_{vk} \sin(\alpha) * h_2}{\cos(\alpha) * L + \sin(\alpha) * h_1}$$

Accordingly, in Equation 9-1, F_{hB} presents the load recorded by the horizontal load cell; this load is equal to the horizontal load resisted by the specimen (f_h). Also, Equation 9-2 presents the actual vertical load resisted by the specimen, at the joint C. Accordingly, the error developed during the test due to a) the rotation of the swing-arm, and b) the moment along the swing-arm, indenter, and bearing, could be precisely determined using a simple static analysis.